Université de Montréal

Electrospinning and characterization of supramolecular poly(4-vinyl pyridine)-small molecule complexes

par
Xiaoxiao Wang

Département de chimie
Faculté des arts et des sciences

Thèse présentée à la Faculté des études supérieures et postdoctorales
en vue de l'obtention du grade de Philosophiae Doctor (Ph. D.)
en chimie

Décembre 2014

Résumé

La chimie supramoléculaire est basée sur l'assemblage non covalent de blocs simples, des petites molécules aux polymères, pour synthétiser des matériaux fonctionnels ou complexes. La poly(4-vinylpyridine) (P4VP) est l'une des composantes supramoléculaires les plus utilisées en raison de sa chaîne latérale composée d'une pyridine pouvant interagir avec de nombreuses espèces, telles que les petites molécules monofonctionnelles et bifonctionnelles, grâce à divers types d'interactions. Dans cette thèse, des assemblages supramoléculaires de P4VP interagissant par liaisons hydrogène avec de petites molécules sont étudiés, en ayant comme objectifs de faciliter l'électrofilage de polymères et de mieux comprendre et d'optimiser la photoréponse des matériaux contenant des dérivés d'azobenzène.

Une nouvelle approche est proposée afin d'élargir l'applicabilité de l'électrofilage, une technique courante pour produire des nanofibres. À cet effet, un complexe entre la P4VP et un agent de réticulation bifonctionnel capable de former deux liaisons hydrogène, le 4,4'-biphénol (BiOH), a été préparé pour faciliter le processus d'électrofilage des solutions de P4VP. Pour mieux comprendre ce complexe, une nouvelle méthode de spectroscopie infrarouge (IR) a d'abord été développée pour quantifier l'étendue de la complexation. Elle permet de déterminer un paramètre clé, le rapport du coefficient d'absorption d'une paire de bandes attribuées aux groupements pyridines libres et liées par liaisons hydrogène, en utilisant la 4-éthylpyridine comme composé modèle à l'état liquide. Cette méthode a été appliquée à de nombreux complexes de P4VP impliquant des liaisons hydrogène et devrait être généralement applicable à d'autres complexes polymères.

La microscopie électronique à balayage (SEM) a révélé l'effet significatif du BiOH sur la facilité du processus d'électrofilage de P4VP de masses molaires élevées et faibles. La concentration minimale pour former des fibres présentant des perles diminue dans le N, N'-diméthylformamide (DMF) et diminue encore plus lorsque le nitrométhane, un mauvais solvant pour la P4VP et un non-solvant pour le BiOH, est ajouté pour diminuer l'effet de rupture des liaisons hydrogène causé par le DMF. Les liaisons hydrogène dans les solutions et les fibres de P4VP-BiOH ont été quantifiées par spectroscopie IR et les résultats de rhéologie ont démontré la capacité de points de réticulation effectifs, analogues aux enchevêtrements physiques, à augmenter la viscoélasticité de solutions de P4VP pour mieux résister à la formation de gouttelettes. Cette réticulation effective fonctionne en raison d'interactions entre le BiOH bifonctionnel et deux chaînes de P4VP, et entre les groupements hydroxyles du BiOH complexé de manière monofonctionnelle. Des études sur d'autres agents de réticulation de faible masse molaire ont montré que la plus forte réticulation effective est introduite par des groupes d'acide carboxylique et des ions de zinc (II) qui facilitent le processus d'électrofilage par rapport aux groupements hydroxyles du BiOH. De plus, la sublimation est efficace pour éliminer le BiOH contenu dans les fibres sans affecter leur morphologie, fournissant ainsi une méthode élégante pour préparer des fibres de polymères purs dont le processus d'électrofilage est habituellement difficile.

Deux complexes entre la P4VP et des azobenzènes photoactifs portant le même groupement tête hydroxyle et différents groupes queue, soit cyano (A_{CN}) ou hydrogène (A_H), ont été étudiés par spectroscopie infrarouge d'absorbance structurale par modulation de la polarisation (PM-IRSAS) pour évaluer l'impact des groupements queue sur leur performance lors de l'irradiation avec de la lumière polarisée linéairement. Nous avons constaté que A_{CN} mène à la photo-orientation des chaînes latérales de la P4VP et des azobenzènes, tandis que A_H mène seulement à une orientation plus faible des chromophores. La photo-orientation des azobenzènes diminue pour les complexes avec une teneur croissante en chromophore, mais l'orientation de la P4VP augmente. D'autre part, l'orientation résiduelle après la relaxation thermique augmente avec la teneur en A_{CN}, à la fois pour le A_{CN} et la P4VP, mais la tendance opposée est constatée pour A_H. Ces différences suggèrent que le moment dipolaire a un impact sur la diffusion rotationnelle des chromophores. Ces résultats contribueront à orienter la conception de matériaux polymères contenant des azobenzène efficaces.

Mots-clés: Chimie supramoléculaire, poly(4-vinylpyridine), électrofilage, azobenzène, photo-orientation, spectroscopie infrarouge.

Abstract

Supramolecular chemistry is based on the non-covalent assembly of simple building blocks, from small molecules to polymers, to synthesize functional or complex materials. Poly(4-vinyl pyridine) (P4VP) is one of the most used supramolecular components because its side-chain pyridine rings can interact with many species, such as monofunctional and bifunctional small molecules, through various types of interactions. In this thesis, supramolecular assemblies of P4VP hydrogen-bonded with various small molecules are studied with the objectives of facilitating the electrospinning of polymers and to better understand and optimize the photoresponse of azobenzene-containing materials.

A new approach is proposed to widen the applicability of electrospinning, a common technique to produce thin nanofibers. To this end, a complex between P4VP and a bifunctional hydrogen bond crosslinker, 4,4'-biphenol (BiOH), is prepared to increase the electrospinnability of P4VP solutions. To better understand this complex, a new infrared (IR) spectroscopy method is first developed to quantify the extent of complexation. The method allows determining a key parameter, the absorption coefficient ratio of a pair of bands due to free and hydrogen-bonded pyridine rings, by using 4-ethylpyridine as a liquid model compound. This method is applied to many hydrogen-bonded P4VP complexes and should be generally applicable to other polymer complexes.

Scanning electron microscopy (SEM) reveals the significant effect of BiOH on the electrospinnability of P4VP with high and low molecular weights. The minimum concentration for the formation of beaded fibers decreases in N,N'-dimethylformamide (DMF) and to a greater extent when nitromethane, a poor solvent for P4VP and a non-solvent for BiOH, is added to decrease the hydrogen bond breaking effect of DMF. Hydrogen bonding in P4VP-BiOH solutions and fibers is quantified by IR spectroscopy and rheology results demonstrate the capability of the effective crosslinks, as analogs to physical entanglements, of increasing the viscoelasticity of P4VP solutions to better resist the formation of droplets. This effective crosslinking works due to bifunctional interactions of BiOH with two P4VP chains and between the hydroxyl groups of monofunctionally complexed BiOH. Studies of other small crosslinkers show that the stronger effective crosslinking introduced by carboxylic acid groups and zinc (II) ions leads to better electrospinnability than the hydroxyl groups of BiOH. Additionally, sublimation is found to be effective to remove BiOH from fibers without affecting their morphology, providing a smart method for preparing fibers of pure polymers with limited electrospinnability.

Two complexes between P4VP and photoactive azobenzenes bearing the same hydroxyl head group and different tail groups, either cyano (A_{CN}) or hydrogen (A_H), are studied by polarization modulation infrared structural absorbance spectroscopy (PM-IRSAS) to investigate the impact of the tail groups on their performance upon irradiation with linearly polarized light. We find that A_{CN} leads to photo-orientation of both P4VP side-chains and azobenzenes, while A_H only leads to a weaker orientation of the chromophores. Photo-orientation of the azobenzenes decreases for both complexes with increasing chromophore content, but the orientation of P4VP increases. On the other hand, the residual orientation after thermal relaxation increases with increasing A_{CN} content, for both A_{CN} and P4VP, but the opposite trend is found for A_H. Such differences suggest the impact of the dipole moment on the rotational diffusion of chromophores. These findings will contribute to directing the design of efficient azobenzene-containing polymer materials.

Keywords: Supramolecular chemistry, poly(4-vinyl pyridine), electrospinning, azobenzene, photo-orientation, infrared spectroscopy.

Table of contents

List of tables

List of schemes

List of figures

List of abbreviations

α	Angle between a transition dipole moment and a molecular axis of interest
ΔA	Dichroism
Δn	Birefringence
ε_b	Absorption coefficient of hydrogen-bonded pyriding ring band
ε_f	Absorption coefficient of free pyriding ring band
η	Viscosity
$[\eta]$	Intrinsic viscosity
η_0	Zero shear rate viscosity
η_{sp}	Specific viscosity
λ	Wavelength
ρ	Density
a	Ratio of band absorption coefficients
A	Absorbance
A_0	Structural absorbance
$\mathrm{A_{CN}}$	4-hydroxy-4’-cyanoazobenzene
$\mathrm{A_H}$	4-phenylazophenol
A_p	Absorbance parallel to the reference direction
A_s	Absorbance perpendicular to the reference direction
ATR	Attenuated total reflection
BiOH	4,4'-biphenol
c	Concentration
c^*	Critical overlap concentration
c_D	Critical concentrated concentration
CD	Cyclodextrin
c_e	Critical entanglement concentration
c_f	Critical beaded fiber formation concentration

CH_3NO_2	Nitromethane
$CHCl_3$	Chloroform
CN	Cyano
c_p	Critical uniform fiber formation concentration
D	Diameter of fiber
DMF	N,N'-dimethylformamide
E	*trans* isomer
EtPy	4-ethylpridine
F_A	Mole percent of azobenzenes relative to the pyridine rings
f_b	Percentage of the hydrogen-bonded pyridine rings
F_{OH}	Mole percent of hydroxyl groups relative to the pyridine rings
FTIR	Fourier transform infrared
HBCA	4-hydroxy-4'-biphenyl carboxylic acid
HOACOOH	4-hydoxyazobenzene-4'-carboxylic acid
HOAOH	4,4'-Dihydroxyazobenzene
I	Intensity
I_b	Intensity of hydrogen-bonded pyridine ring
I_f	Intensity of free pyridine ring
IR	Infrared
I_{ref}	Intensity of the reference band
k	Slope
m	Mass
MeOH	Methanol
MIX	Mixed solvent of N,N'-dimethylformamide and nitromethane
M_w	Weight-average molecular weight
n	Molar amount
N_a	Avogadro number
NM	Nitromethane
OH	Hydroxyl group
p	Parallel

pKa	Acid dissociation constant at logarithmic scale
$<P_2>$	Orientation parameter
PM-IRLD	Polarization modulation infrared linear dichroism
PM-IRSAS	Polarization modulation infrared structural absorbance spectroscopy
R_g	Radius of gyration
R_h	Hydrodynamic radius
s	Perpendicular
SCLCP	Side chain liquid crystalline polymer
SEM	Scanning electron microscopy
SMs	Small molecules
SRG	Surface relief grating
T	Temperature
t	Time
T_g	glass transition temperature
UV	Ultraviolet
UV-vis	Ultraviolet-visible spectroscopy
V	Volume of the liquid blend
W	Weight fraction
wt %	Weight percent
X	Molar ratio of hydroxyl groups to pyridine
Z	*cis* isomer
$ZnCl_2$	Zinc chloride

Acknowledgements

I attribute my opportunity of pursuing the research on supramolecular chemistry to my two supervisors: Prof. Christian Pellerin and Prof. C.Geraldine Bazuin. I would like to thank sinerely for their patient discussions about my projects and their detailed corrections for my manuiscripts and thesis. I must also be grateful to all jury members of my thesis committee. I deeply appreciate the efforts from all these professors, which led to the final success of my thesis defense.

Many acknowledgements go to my office colleagues in Prof. Pellerin's group and all group members in Prof. Bazuin's lab. Hearfelt thanks go to Mr. Damien Mauran from Prof. Pellerin's group, who trained me for using all the infrared instruments, and Dr. Qian Zhang from Prof. Bazuin's group, who supervised my research during the semester of my Ph. D study. I thank both of them for their generous help.

I would also like to thank Sylvain Essiembre for his valuable support for using DSC, TGA and XRD and Pierre Ménard-Tremblay for using microscopy. Very special thanks go to Prof. Nanci Antonio and his group for SEM characterization. I also extend another gratitude to Prof. Xiaoxia Zhu for his selfless help to the access to using Rheometer and Zetasizer in his lab.

Far too numerous to list, but grateful thanks must go to all my friends in Pavillon J. A. Bombardier for your genuine support and encouragement. Thank you for all the good memories there.

Finally, I must say a huge thank you to my family from the bottom of my heart for all they have done for me.

Chapter 1: Introduction

1.1 Supramolecular polymers

"Supramolecular chemistry", defined as a field focusing on the directed assembly of multiple components through non-covalent interactions, such as van der Waals' forces, hydrophobic interactions, π-π stacking, hydrogen bonding, electrostatic forces, and metal coordination, has received persistent attention since it was developed by Donald J. Cram, Jean-Marie Lehn and Charles J. Pedersen, who shared the Nobel Prize in Chemistry in 1987 (Fig. 1.1).[1] Pedersen first synthesized crown ethers, which can complex with metal salts.[2-3] This work was expanded by Cram to the synthesis of crown ethers with various three dimensional structures, which allows selective interactions with different metal ions.[4-7] Jean-Marie Lehn also synthesized cage-like molecules which can trap other molecules inside and further defined the concept of "supramolecular chemistry".[8]

Figure 1.1. The winners of the 1987 Nobel Prize in Chemistry: Donald J. Cram (left), Jean-Marie Lehn (middle) and Charles J. Pedersen (right).[1]

Due to the relatively weak and very often reversible characteristics of non-covalent interactions, supramolecular assemblies with dynamic structure and smart stimuli sensitivity can easily be prepared, enabling the preparation of large groups of new materials, with shapes from fibers to films to spheres and with numerous potential applications. For example, as shown in Fig. 1.2a, a molecular hydrogel in the form of a network of nanofibers can be self-assembled from small molecular hydrogelators with amphiphilic structures.[9] When these hydrogelators are modified with a more hydrophilic group, like a phosphate group, as precursors, the correct balance of amphiphilic interactions is broken and no gelation takes place. As shown in Fig. 1.2b, these precursors can convert back to hydrogelators by removing the phosphate group through enzymatic catalysis, which allows many potential applications like detecting enzymes, screening enzyme inhibitors and drug delivery.[9] These hydrogels can also be used for maintaining high stability and activity of enzymes in organic solvents by embedding them inside a network of amino acid derivatives, and for the mimicry of enzymes by using enclosed artificial active centers in the peptide network.[10]

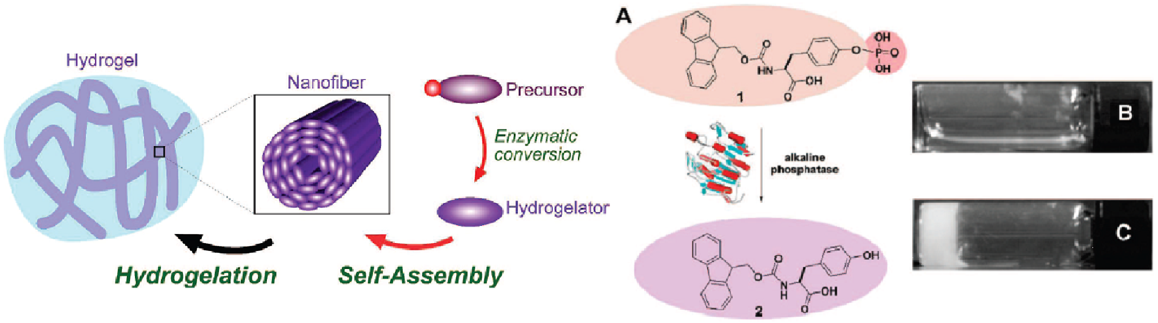

(a) (b)

Figure 1.2. (a) Hydrogels formed by nanofibers self-assembled from amphiphilic hydrogelators, and (b) enzymatic conversion (indicated by the arrow) from hydrogelator precursors (left) and the corresponding transition from solution to gel (right). Adapted with permission from Ref. 9, © 2008 American Chemical Society.

Multiple-layered thin films can be fabricated, as shown in Fig. 1.3, through layer-by-layer assembly, which is a technique of alternately depositing a sequence of monolayered films on a substrate, where the layers are held together by non-covalent interactions like hydrogen bonding, hydrophobic interactions, electrostatic interactions and metal coordination.[11] If these films are loaded with enzymes, antibodies, proteins, DNA, etc, biosensors to probe bio-related species or processes can be prepared.[12] One example is the use of electrodes fabricated with thin films of oxyreductase enzymes to detect substrates that are specifically responsive to these enzymes in solution. As shown in Fig. 1.3b, due to the catalysis of oxyreductases, substrates are transformed from type I (reduced or oxidized state) to type II (oxidized or reduced state), while oxyreductases also change from type I (oxidized or reduced state) to type II (reduced or oxidized state). Type II oxyreductases can then react with the electronic mediators to be converted back to type I, allowing the redox changes of the mediators to be detected and enabling the calculation of the substrate concentration.[12]

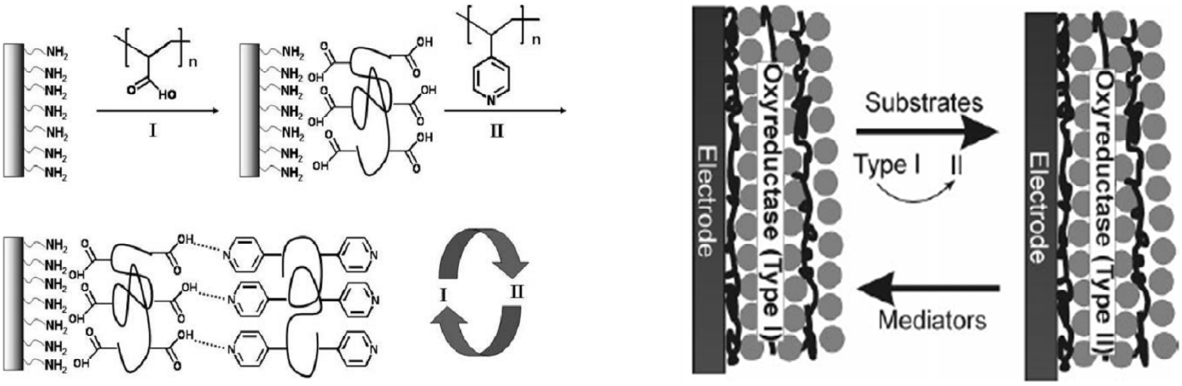

(a) (b)

Figure 1.3. (a) Layer-by-layer assembly based on hydrogen bonding. Reproduced with permission from Ref. 11, © 2007 The Royal Society of Chemistry. (b) Mechanism of detection of oxyreductase biosensor. Reproduced with permission from Ref. 12, © 2006 Wiley-VCH Verlag GmbH & Co. KGaA, Weinheim.

Self-assembled micelles have been prepared from many amphiphilic block copolymers in aqueous solution and have been shown to be responsive to various environmental stimuli like light, temperature, pH, and specific cations.[13] For example, as shown in Fig. 1.4a, poly(*p*-methoxyphenacyl methacrylate)-*b*-poly((oligoethylene glycol)methacrylate) (PMPMA-*b*-POEGMA) has a hydrophilic POEGMA block and a hydrophobic PMPMA block, so that in water it forms micelles with a PMPMA core and a POEGMA corona. These micelles disaggregate under light irradiation, which changes PMPMA to a hydrophilic poly(methacrylic acid) (PMAA). The obtained PMAA-*b*-POEGMA can be converted to a new micellar structure with a PMAA core and a POEGMA corona by reducing the pH or introducing Ca^{2+}, a process that is reversible by increasing the pH or adding ethylenediaminetetraacetic acid sodium salt (EDTA). PMAA-*b*-POEGMA can also form micelles with a POEGMA core and a PMAA corona by increasing the temperature above the LCST of POEGMA or by adding PO_4^{3-}. The process is reversible by decreasing temperature or using dialysis to eliminate the PO_4^{3-}. This phenomenon has potential application in photoresponsive drug delivery, as illustrated in Fig. 1.4b.[14]

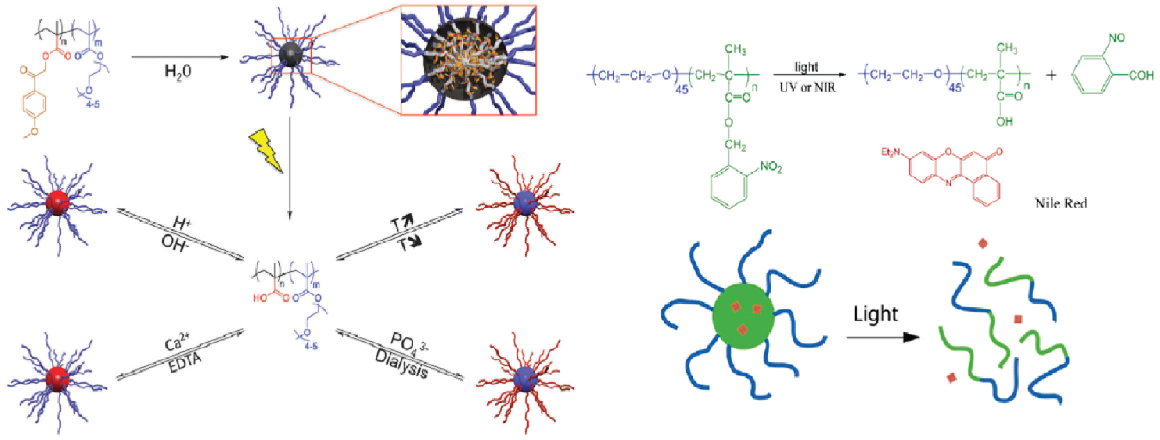

(a) (b)

Figure 1.4. (a) A multi-responsive micellar system based on poly(p-methoxyphenacyl methacrylate)-block-poly((oligo ethylene glycol)methacrylate) diblock copolymers. Reproduced with permission from Ref. 15, © 2012 American Chemical Society. (b) photocontrolled release of an encapsulated agent as a result of the photoinduced dissociation of the polymer micelle. Reproduced with permission from Ref. 14, © 2006 American Chemical Society.

Apart from the examples described above, which are all based on building blocks of a single type of low molar mass molecule or of polymer, a large number of supramolecular materials have been assembled from a combination of small molecules and polymers. Such materials have advantages of high stability, high strength, large flexibility and easy machinability, due to their polymer component. For instance, poly(ethylene oxide) has been used to form inclusion compounds with urea,[16-19] thiourea[19-20] and cyclodextrin.[20-21] Similar inclusion complexes have been prepared from the assembly between cyclodextrin and other linear main-chain polymers, such as poly(propylene oxide), poly(oxytetramethylene), poly(oxytrimethylene), polyesters, and polyamides.[22] Another extensively investigated class is based on the assembly between polymers with side-chain functional groups and appropriately functionalized small molecules, which allows for a much wider variety of supramolecular compositions compared with linear main chain-polymers.[23-24] Among them, poly(4-vinyl pyridine) (P4VP) is often used as the polymer component.

1.1.1 P4VP

According to a paper by Fitzgerald and Fuoss published in 1950, which is also the earliest report, to my knowledge, that describes the synthesis of P4VP, polymerization of vinyl pyridine began with its use as a comonomer with butadiene in synthetic rubber research during World War II.[25] Various methods, like bulk,[25] emulsion,[25] living anionic[26-27] and living radical[28-29] polymerizations could be used to synthesize P4VP. As shown in Fig. 1.5, the pyridine ring of P4VP contains two free electrons on the N atom. Because the lone electron pair does not participate in the conjugation of the pyridine ring, it is weakly basic (pKa = 5.25±0.01)[30] and can complex with many other species through ionic complexation, metal coordination, hydrogen bonding and halogen bonding.

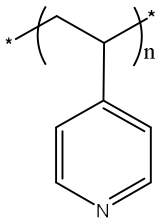

Figure 1.5. Chemical structure of P4VP.

1.1.2 Side-chain P4VP-small molecule complexes

Ionic complexation with P4VP can be achieved by its conversion into a polycation. This occurs upon acid-base interactions with inorganic acids (Fig. 1.6a)[31-32] and organic sulfonic acids (Fig. 1.6b),[33-34] or upon quaternization with alkyl halogen compounds (Fig. 1.6c).[35-38]

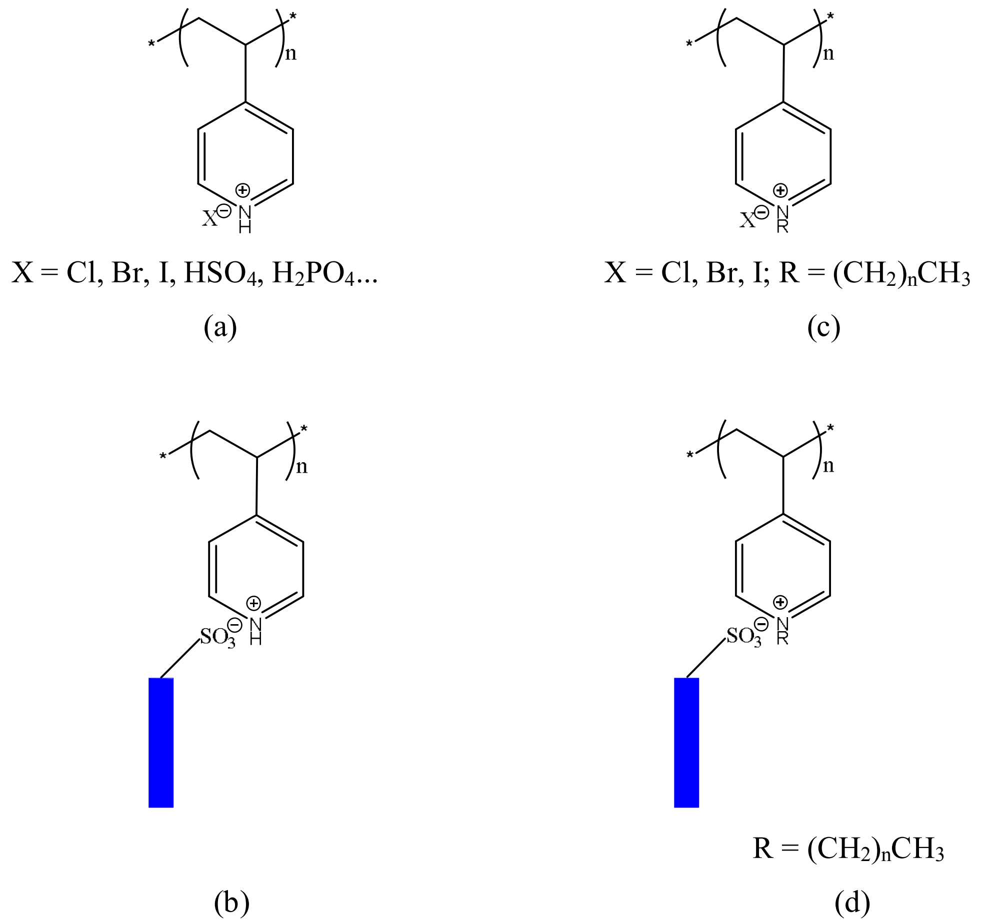

Figure 1.6. Chemical structures of P4VP protonated by (a) simple inorganic acids, (b) mesogenic sulfonic acids, (c) P4VP quaternized with alkyl halides and (d) quaternized P4VP complexed with mesogenic sulfonic acid salts. The blue bar in (b) and (d) indicates a rigid rod-like mesogenic part.

Polycations of P4VP protonated by HCl, H_2SO_4, H_3PO_4, etc., can be used as immobilized catalysts for organic reaction,[31] and as polycationic coatings in humidity sensors due to their water solubility.[32] Such humidity sensors were also prepared from quaternized P4VP.[35-36] Quaternized P4VP can be further modified into photosensitive side chain liquid crystalline polymers (SCLCPs) by ion exchange procedures with molecules containing a rigid rod-like azobenzene-based mesogenic part and a sodium sulfonate group (Fig. 1.6d). One of the simplest of these complexes has been made by Zhang et al. with a commercially available dye, methyl orange, which has no alkyl spacer in its structure, leading to excellent photoactive properties.[37-38] Zhu et al. prepared complexes between P4VP and wedge-shaped mesogenic sulfonic acids that form a supermolecular material with cylindrical morphology, as shown in Fig. 1.7.[33] Ikkala et al. investigated an ionic complex with ordered lamellar structure between P4VP and *p*-dodecylbenzenesulfonic acid.[34]

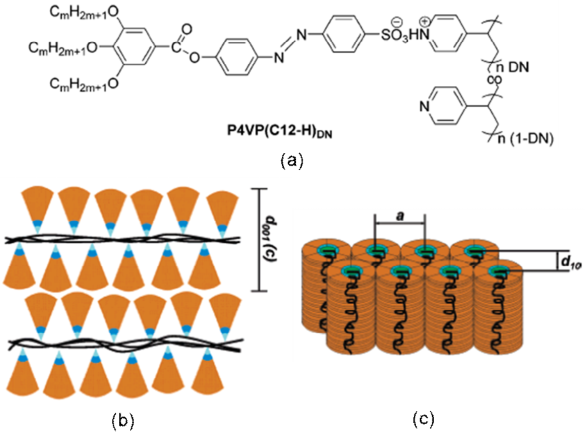

Figure 1.7. (a) Chemical structure of P4VP complexes with wedge-shaped sulfonic acid (P4VP(C12-H)$_{DN}$), m = 12, where DN refers to the degree of neutralization. Proposed packing model (b) in the lamellar phase (0.8 ≥ DN ≥ 0.5) and (c) in the hexagonal cylindrical phase (DN ≥ 0.8) of P4VP(C12-H)$_{DN}$. Adapted with permission from Ref. 33, © 2006 American Chemical Society.

P4VP can coordinate with metal cations, like Zn^{2+}, Ca^{2+}, Cu^{2+}, Co^{2+} and Ni^{2+},[39-40] making it useful for removing heavy metals from waste water.[41] Metal coordination allows the preparation of metallosupramolecular P4VP systems with, for example, various liquid crystalline structures. For instance, a mesomorphic liquid crystal was obtained in a complex of P4VP and zinc dodecyl benzene sulfonate,[42] and a hexagonal structured multicomb polymeric supramolecules was achieved by using 2,6-bis(octylaminomethyl)pyridine as an intermediate to link each P4VP repeating unit and two dodecylbenzenesulfonate counterions.[43] Besides, comblike complexes were also formed between P4VP and zinc salts of carboxylic acid-functionalized alkoxybiphenyl mesogens whose structure changes from amorphous form to liquid crystalline as spacer length increases.[44]

The most often used supramolecular interaction with P4VP is hydrogen bonding. Compared with other interactions, hydrogen bonding can facilitate tuning the properties and the internal structure of complexes in a more controllable and dynamic fashion, for example to form supramolecular SCLCPs. An early attempt was made by Bazuin and Brandys, who blended a mesogenic dialkoxy biphenyl derivative functionalized by carboxylic acid with P4VP to obtain an ordered smectic phase, but they found that phase separation and crystallization of the mesogen occurred when the complex contained over 20 mol% mesogen and was heated above its glass transition temperature.[45-46] Kato et al. reported that a copolymer of poly(4-vinylpyridine-co-styrene) with 10 mol% styrene can form a homogeneous complex with a stoichiometric amount of a carboxylic acid-functionalized mesogen, 6-[(4-octylpheylazo)phenoxyl]hexanoic acid, and that this complex exhibits an ordered smectic phase over a wider temperature range (93-132 °C) than that of the pure mesogen (130-139 °C).[47] Ikkala and coworkers reported a complex between a carboxylic acid-functionalized cholesterol (CholHS) and P4VP (Fig. 1.8) that has a smectic A structure over a full range of degree of complexation, and stable liquid crystallinity at low degree of complexation.[48]

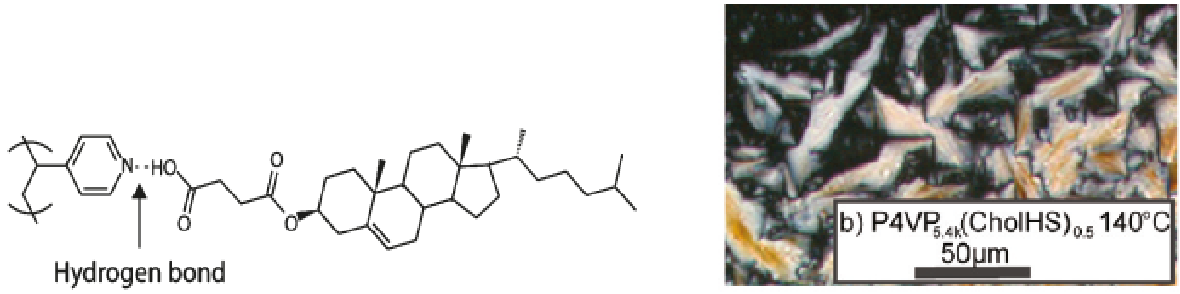

(a) (b)

Figure 1.8. (a) Schematic of a P4VP-CholHS complex, and (b) Polarized optical micrograph of P4VP-CholHS (at a molar amount of CholHS to P4VP repeat unit of 0.5) at 140 °C showing bâtonnets during cooling from the isotropic state. Reproduced with permission from Ref. 48, © 2010 American Chemical Society.

Supramolecular P4VP complexes have been used recently in designing photosensitive materials. Examples based on ionic interactions between protonated or quaternized P4VP and ionic azobenzene-containing small molecules have been given above. There are also numerous examples based on hydrogen bonding with photosensitive molecules. A film of P4VP complexed with 9-anthracene carboxylic acid can undergo reversible photo-controlled deformation upon UV irradiation. This can be enhanced by the addition of LC molecules.[49] Photoinduced birefringence was achieved and investigated in P4VP complexes with hydroxyl-functionalized azobenzene chromophores.[50-51] Surface relief gratings (SRGs) were achieved and investigated with P4VP complexes with azobenzene functionalized with hydroxyl[52] and carboxylic acid[53] groups. Priimagi and coworkers further showed that SRGs can also be obtained from complexes between P4VP and hydroxyl-functionalized bisazobenzene.[54-55] Further discussion about the photoreactivities of P4VP/azobenzene complexes is given in section 1.3.

Very recently, halogen bonding, which is more directional than hydrogen bonding,[56] has been shown to be effective for forming supramolecular complexes. In one of the earliest reports, Bertani et al. prepared comb-like crystals from the complexes between P4VP and iodoperfluorohexanes with various lengths.[57] Priimagi et al. found that films of P4VP complexed with halogen-functionalized azobenezene molecules can be inscribed with SRGs under irradiation more efficiently than analogous hydrogen-bonded complexes.[58]

Other applications of supramolecular complexes involve the development of tunable internal structures. For example, the complex of P4VP and 3,4,5-tris(dodecyloxy)benzoic acid (TDBA) contains a layered internal structure at low TDBA content that enlarges and then changes to a cylindrical structure with increasing TDBA content.[59] However, as the interaction between the pyridine ring and the carboxylic acid group competes with the interactions between carboxylic acid groups, the complexation extent is usually low, especially when the mesogen content is high, though never quantified, limiting the applications. ten Brinke, Ikkala and coworkers first noticed that the complexation between P4VP and nonmesogenic alkylphenols, like 1-dodecyl 3,4,5-trihydroxybenzoate and 4-nonadecylphenol, can lead to a homogeneous blend with mesomorphic structures (see Fig. 1.9a).[60-61] Similar comb-like structures based on nanophase separation were found in complexes between P4VP and 4-(4'-alkylphenyl)azophenols,[62] 4-(4'-alkoxylphenyl)azophenols,[62] and 3-pentadecylphenol (PDP) (see Fig. 1.9b).[63] PDP in particular was studied in detail and used subsequently by many research groups. Hydrogen bonding between PDP and P4VP allowed the tuning of many properties; for instance, the order of the lamellar structure and the thermal properties by changing the PDP content, and the level of the structural hierarchy by changing the P4VP block fraction in poly(styrene-block-(4-vinylpyridine)) (PS-b-P4VP), as will be discussed below.[64-65]

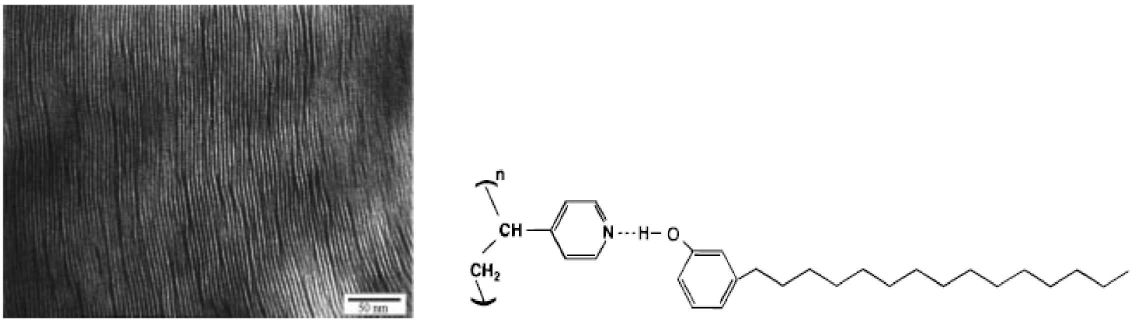

(a) (b)

Figure 1.9. (a) TEM micrograph of a P4VP-(4-nonadecylphenol) equimolar complex. Reproduced with permission from Ref. 61, © 1998 American Chemical Society. (b) Schematic of the P4VP-PDP complex. Reproduced with permission from Ref. 63, © 1996 American Chemical Society.

Hierarchical structures – i.e. different structures at different length scales – can be formed in block copolymers of P4VP and a second block of a nonpolar (noninteracting) polymer such as polystyrene (PS). For example, in the complexes of CholHS with PS-*b*-P4VP, morphologies of smectic P4VP-CholHS structures form inside a larger scaled cylindrical or layered PS-*b*-P4VP structure, when the volume fraction of the two blocks varies.[48] Complexes of PS-P4VP with PDP were investigated in different applications by various research groups. For example, Bazuin and coworkers used the Langmuir-Blodgett (LB) technique to fabricate monolayered films of PS-*b*-P4VP(PDP). They showed that, in general, the morphologies evolve from planar structure to nanostrands and to nanodots (see Fig. 1.10) with increasing polar block content, the precise block content depending on the nature of the blocks and, for PS-*b*-P4VP the presence or not of PDP.[66-67] The nanostrand pattern itself was dependent on the spreading solution concentration and the spreading solvent.[68-69] Moreover, the dot morphology order shows a transition from quasi-hexagonal to quasi-square as a function of compression pressure.[70] Such monolayered films with nanopatterns have potential as the templates for gold deposition,[71] leading to ordered gold nanoparticle films.

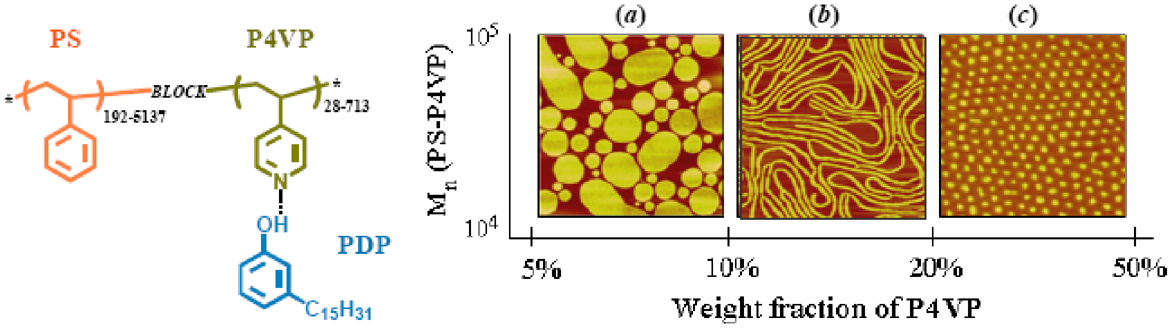

Figure 1.10. Left: PS-*b*-P4VP/PDP complex. Right: AFM height images showing the dependence of the morphology on the P4VP block content: (a) planar aggregates, (b) nanostrands, and (c) nanodots. Reproduced with permission from Ref. 69, © 2010 American Chemical Society.

Stamm and coworkers showed that internal structures of PS-*b*-P4VP could also be obtained from the complexes with much smaller molecules like 2-(4'-hydroxy-phenylazo)benzoic acid (HABA). They used the dip-coating method to obtain films exhibiting cylindrical morphology, the axis of which selectively orients either in horizontal or vertical direction relative to the substrate depending on the solvent used.[72-73] One advantage of small molecules is that they can be very easily removed, so that ordered porous structures can be obtained for further use (see Fig. 1.11). A similar strategy was applied by Bazuin and coworkers, based on the complexes of PS-*b*-P4VP with various small molecules like 1,5-dihydroxynaphthalene (DHN),[74] naphthol[75-77] and naphthoic acid,[75-77] to obtain films with different morphologies from nanocylinders to nanodots.

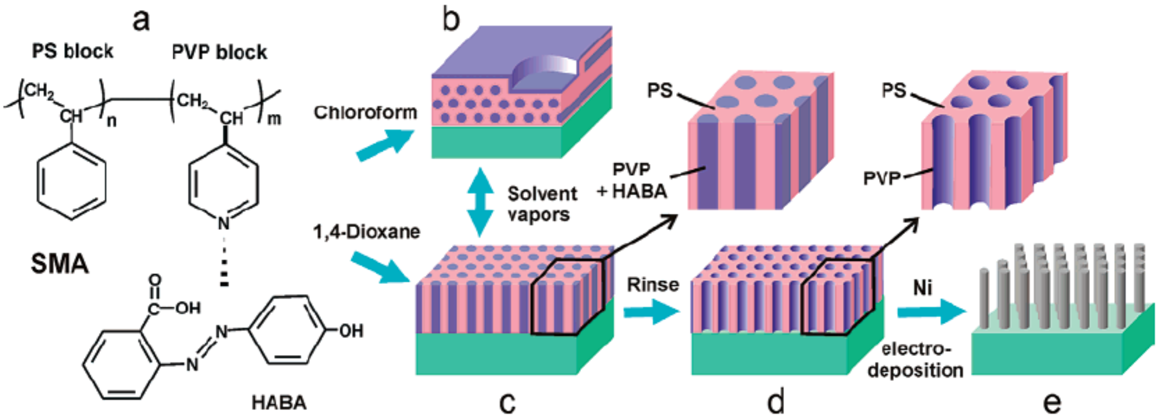

Figure 1.11. Schematic of the fabrication of nanotemplate from PS-*b*-P4VP(4'-hydroxyazobenzene-2-carboxylic acid). Reproduced with permission from Ref. 73, © 2003 American Chemical Society.

1.1.3 Crosslinked P4VP-small molecule complexes

Compared with small molecules with monofunctional groups, P4VP complexed with small molecules with bifunctional groups have been reported less often.[78-80] However, since they potentially can physically crosslink P4VP chains directly, bifunctional small molecules can facilitate the formation of polymer networks. Shibata et al. reported that, by using 1,5-naphthalenedisulfonic acid (NDS) and 1,3-propanedisulfonic acid (PDS) as hydrogen-bond crosslinkers, complexes of P4VP/NDS and P4VP/PDS show both higher glass transition temperatures and decomposition temperatures, which increase with increasing crosslinking density.[79] Craig et al. investigated P4VP networks formed in DMSO using metal coordination with bisfunctional Pd(II) and Pt(II) organometallic crosslinkers, and found that, due to the different dissociation rates of pyridine-metal coordination controlled by the crosslinker structure, both the dynamic viscosity and the elastic storage modulus of the solution could be tailored quantitatively.[78, 80]

1.2 Electrospinning and electrospinnability

Since its development in ancient China, as early as 3500 BC based on the earliest finding of fragments of silk fabric, cloth woven from silk have been popular in high class societies of the ancient world. This has led to an international trade route called the "*silk road*". As great profit was gained from the silk trade, its secret was carefully kept by Chinese emperors until around 550 BC, when Europeans finally discovered that silk was produced by a domesticated worm, called *bombyx mori* or silk worm, as shown in Fig. 1.12a.

(a)

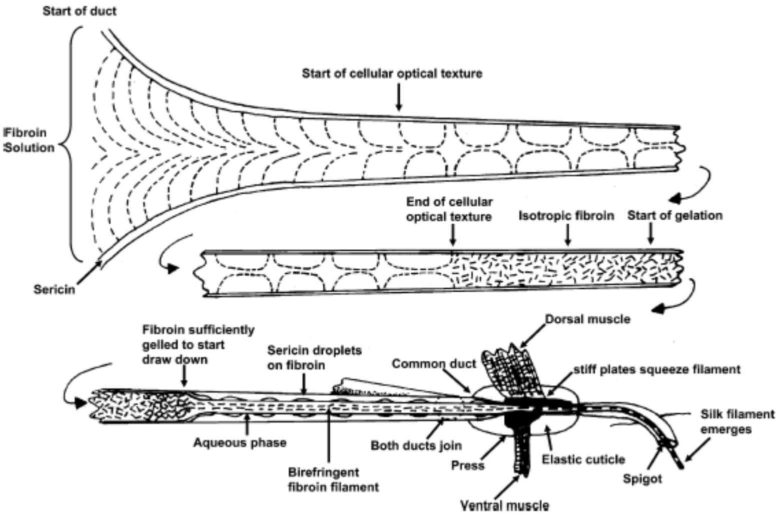

(b)

Figure 1.12. (a) Photo of a Chinese silkworm spinning silk.[81] (b) Mechanism of the spinning of spider silk. Reproduced with permission from Ref. 82, © 2007 American Chemical Society.

The process of silk production by silk worms, by spiders, and by other insects like bees, flies and ants, always involves the extrusion of the proteins from the silk glands through a spinneret, as shown in Fig. 1.12b. Based on the great need for silk in the fabric industry, artificial “silks” were created based on techniques like wet spinning, dry spinning, melt spinning, and gel spinning, which also involve extrusion of polymer solutions through a spinneret with a tiny opening, thus resembling the production of spider silk. Compared with all these techniques based on the extrusion and drawing of fibers by mechanical forces, a new method, called electrospinning, rather applies an electrical field as a driving force for fiber formation.

1.2.1 Electrospinning

Electrospinning is a technique enabling drawing micro- or nano-scaled fibers from polymer solutions or melts under the application of an electrical field. The history of electrospinning before 1990 was summarized by Tucker et al.[83] A milestone in the early 1900s was the submission of patents by Cooley[84-85] and Morton[86] that opened the gate to the industrial use of electrospinning. Another breakthrough in the industrial practice happened in 1938 when Fuchs, Petryanov-Sokolov and Rosenblum used electrospun fibers of cellulose acetate as filter materials, which were called “Petryanov filters” and led to the manufacture of gas masks.[83] A booming period of research about electrospinning started in the early 1990s, based on the pioneering work in Reneker’s group.[87]

A typical electrospinning setup used in the lab is shown in Fig. 1.13a. A semidilute or concentrated polymer solution is stored in a syringe equipped with a needle. The solution is pumped through the needle and forms a drop at the tip. When an electrical field is applied between the needle and the collector, the drop deforms and takes the shape of a cone, called the Taylor Cone,[88] and then ejects as a straight jet. Since the jet is charged, the electrostatic repulsion forces on the surface stretch the jet, leading to a large surface/volume ratio which enables fast evaporation of the solvent. Due to this, the density of the charges on the jet surface increases quickly, leading to a much stronger electrostatic repulsion effect which causes bending instabilities. This leads to the bending of the straight jet which now adopts a large scale whipping motion. During the propagation, the jet becomes thinner with the evaporation of solvent until reaching the collector as fibers. Fig. 1.13b shows the setup used in our lab.

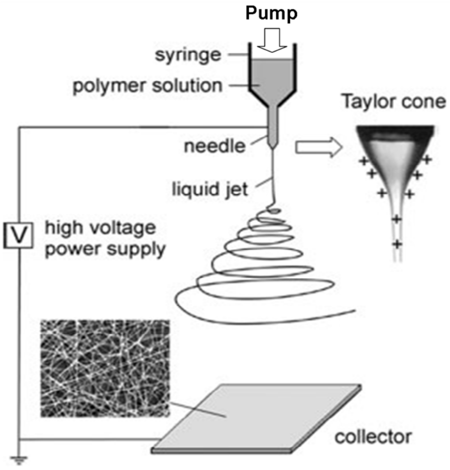

(a)

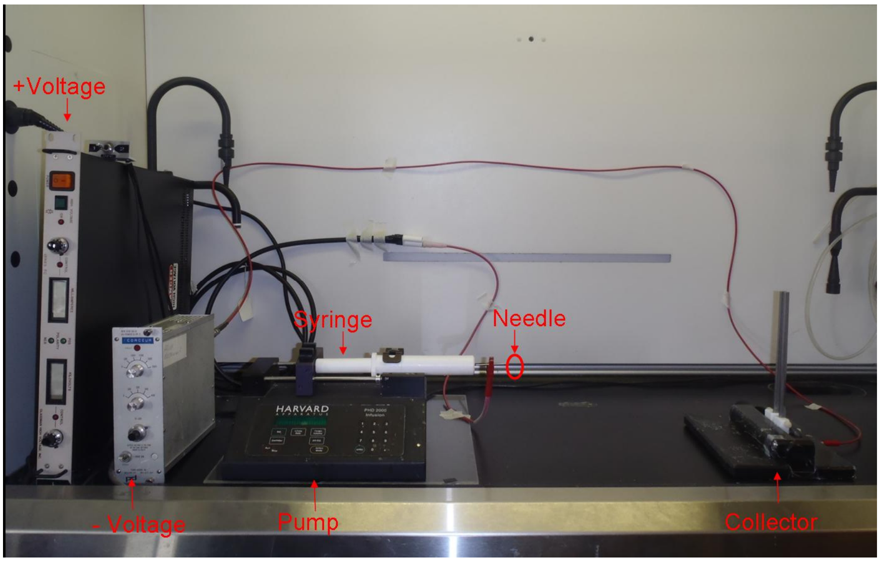

(b)

Figure 1.13. (a) Schematic representation of electrospinning setup. Reproduced with permission from Ref. 89, © 2004 WILEY-VCH Verlag GmbH & Co. KGaA, Weinheim. (b) Electrospinning setup used in our lab.

1.2.2 Electrospinnability and effective crosslinking

Polymer solutions can be electrospun into fibers with the precondition that they possess "electrospinnability", the lack of which leading to the production of droplets via electrospray. As shown in Fig. 1.14, the formation of different morphologies depends on the competition between three forces acting on the jet: electrostatic repulsive stretching, surface tension, and a viscoelastic force which acts in response to the former two. Electrostatic repulsive stretching tends to thin the jet. In contrast, surface tension initiates the shrinkage of the jet, causing the formation of beads and the thinning of jet between beads. Both forces can lead to the breakage of jet, while the viscoelastic force always resists the effect of the other two forces. A polymer system with high inner viscoelasticity is therefore an advantage to avoid electrospray. Many factors like entanglements, hydrogen bonding, hydrophobic interactions and electrostatic interactions facilitate the formation of a network in the solution, thus increasing the viscoelastic forces; then we call the resulting entity as "effective crosslinking" (also known as "physical crosslinking" or "temporary crosslinking").

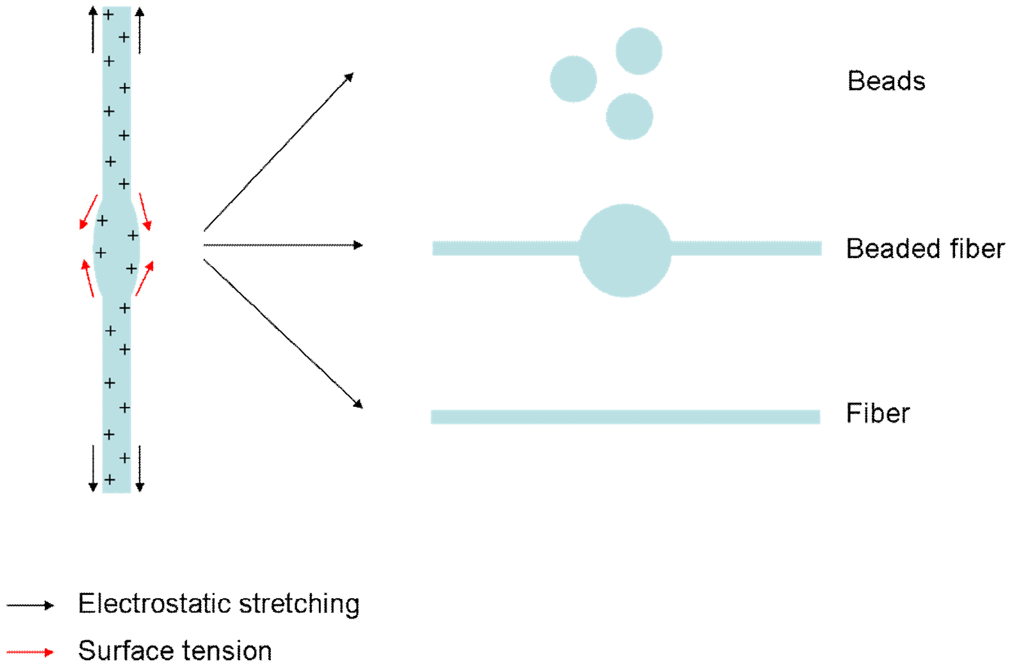

Figure 1.14. Scheme of the formation of beads, beaded fiber and fiber.

1.2.2.1 Entanglement

It is well known that polymer solutions of high concentration and high molecular weight facilitate the production of fibers, demonstrating that the entanglement of polymer chains is a key factor leading to the electrospinnability. The entanglement level of the polymer solution is related to its rheological properties. It is well known that the viscosity of polymer solutions increases with increasing concentration as shown by the Huggins Equation in Eq. 1.1:

$$\eta_{sp} = [\eta]c + k^{'}[\eta]^{2}c^{2} + k^{''}[\eta]^{3}c^{3}\ldots\ldots \qquad (1.1)$$

where η_{sp}, $[\eta]$ and c are the specific viscosity, the intrinsic viscosity and the polymer concentration, respectively, and k' and k'' are constants. η_{sp} represents the contribution of the polymer to the solution viscosity, which is calculated as:

$$\eta_{sp} = \frac{\eta - \eta_{s}}{\eta_{s}} \qquad (1.2)$$

where η and η_s are the viscosities of the solution and of the pure solvent, respectively. Eq. 1.1 indicates that the viscosity increases with concentration in a non-linear fashion ($\eta_{sp} \sim c^{n}$, $n > 1$)

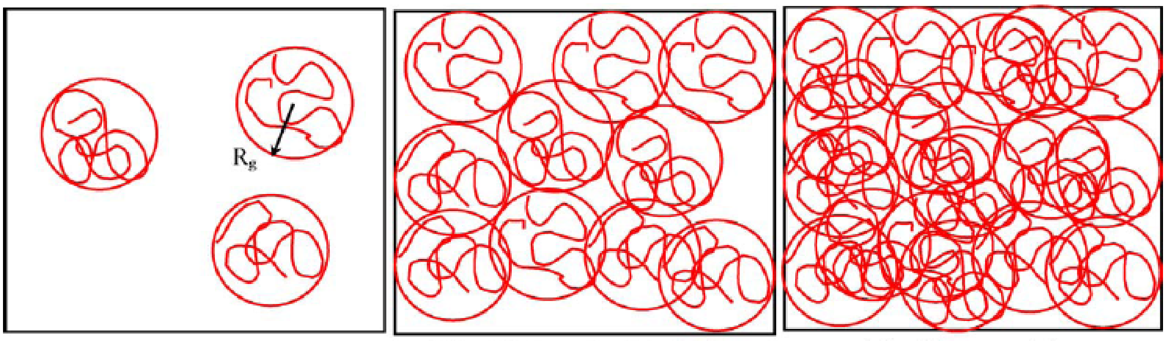

a) Dilute, $c < c^*$ b) Semidilute unentangled, $c^* < c < c_e$ c) Semidilute entangled, $c > c_e$

Figure 1.15. Physical representation of three solution regimes: (a) Dilute regime, (b) Semidilute unentangled regime, and (c) Semidilute entangled regime. Adapted with permission from Ref. 90, © 2005 Elsevier Ltd.

Colby and coworkers have classified polymer solutions into three regimes with the increase of c: dilute regime, semidilute unentangled regime and semidilute entangled regime (see Fig. 1.15).[91] A concentrated regime has also been reported.[92-94] These regimes are separated by three critical concentrations: c^*, c_e and c_D.

c^* is defined as the critical concentration at which the overlap of the individual polymer coils starts to happen. Several methods can be applied to estimate c^*. When $c < c^*$, the polymer solution is in the dilute regime, where no overlap among polymer coils exists and for which the concentration dependence of the specific viscosity is given by $\eta_{sp} \sim c^1$. According to Frisch and Simha, $c[\eta]$, also called the Simha parameter or Berry number,[95] is a measure of the degree of coil overlap in solutions.[96] It is usually accepted that the critical overlap point is approached when $c[\eta] \approx 1$,[97] such that

$$c^* \propto \frac{1}{[\eta]} = \frac{1}{KM^a} \tag{1.3}$$

where K and a are the Mark-Houwink-Sakurada constants and M is the viscosity-average molecular weight. Eq. 1.3 can be applied to estimate the value of c^*. Another way to calculate c^* is using Eq. 1.4, based on the definition that c^* is the concentration at which the polymer concentration inside an individual polymer coil is equal to the solution concentration:[90]

$$c^* = \frac{3M}{4\pi \left(R_g\right)^3 N_a} \tag{1.4}$$

where N_a is the Avogadro number and R_g is the radius of gyration.

c_e is defined as the critical concentration over which entanglements start to form between the polymer coils. When $c^* < c < c_e$, the polymer solution is in the semidilute unentangled regime in which overlap among coils increases but is not high enough for the formation of an entanglement network in the solution. According to Graessley, c_e can also be calculated with Eq. 1.5,

$$c_e = \frac{\rho M_c}{M_w} \tag{1.5}$$

in which ρ, M_c and M_w represent the density of the pure polymer, the critical entanglement molecular weight and the molecular weight of polymer, respectively.[98] M_c is defined as the minimum molecular weight to form entanglements for polymers in the melt state and can be determined from the turning point in a logarithmic plot of viscosity *vs*. molecular weight: $\eta \sim M^1$ when $M_w < M_c$ and $\eta \sim M^{3.4}$ when $M_w > M_c$.

When $c_e < c < c_D$, the polymer solution is in the semidilute entangled regime, in which an entanglement network forms. Finally, when $c > c_D$, the polymer solution is in the concentrated regime, in which the chain dimensions become independent of concentration.[98] According to Graessley, c_D can be estimated by Eq. 1.6:

$$c_D = c^* \left(\frac{R^2{}_0}{R^2{}_\theta} \right)^4 \tag{1.6}$$

in which $R^2{}_0$ is the mean-square end-to-end distance at zero concentration and $R^2{}_\theta$ is the unperturbed dimensions of the polymer coil.

The link between electrospinnability and rheological properties was first illustrated in a pioneering work from Koski et al.,: fiber formation from poly(vinyl alcohol) (PVA)/water solutions was only observed when $c > 5c^*$.[99] McKee, Long and coworkers have tried to establish the relationship between the rheological properties and the electrospinnability. They concluded that fibers of neutral polymers could only be electrospun from semidilute entangled solutions ($c > c_e$).[94, 100]

Shenoy et al. attempted to predict the formation of fibers based on the solution entanglement number ($N_{e(solu)}$), which could be calculated with Eq. 1.7:

$$N_{e(solu)} = \frac{\phi_p M_w}{M_e} \tag{1.7}$$

where ϕ_p is the polymer volume fraction in the solution and M_e is the apparent average molecular weight between two entanglement points of the polymer in the melt state.[101] M_e can be determined using Eq. 1.8:

$$M_e = \frac{\rho R T}{G_N^0} \tag{1.8}$$

in which ρ, R, T, and $G^0{}_N$ are the density of the pure polymer, the ideal gas constant, temperature, and the plateau modulus, which can be obtained from creep compliance measurements.[97] Shenoy et al. further pointed out that the number of entanglements per chain is equal to $N_{e(solu)} - 1$ and that, for linear polymers without specific polymer-polymer interactions in a good solvent, beaded fibers can only be electrospun when the number of entanglements per chain is over 1 ($N_{e(solu)} > 2$) while uniform fibers can be produced when the entanglement number per chain is over 2.5 ($N_{e(solu)} > 3.5$) in the solution.

Eqs 1.5 and 1.7 indicate that when $M_w > M_c$, increasing the molecular weight of the polymer increases the number of entanglements and facilitates fiber formation. Eq. 1.7 also indicates that increasing the polymer concentration leads to entangled solutions, thus leading to the formation of fibers. This is consistent with the experimental observation that, as mentioned before, either increasing polymer concentration or polymer molecular weight can improve the electrospinnability.

1.2.2.2 Hydrogen bonding

Long and coworkers have reported a strategy for improving the electrospinning through the effect of self-complementary multiple hydrogen bonds. One example is by introducing 5 mol% of 2-ureido-4[1H]-pyrimidone pendant groups on the poly(methyl methacrylate) (PMMA) backbone, c_e is lowered by 1-2 wt% as compared with that of pure PMMA with a similar molecular weight.[100] Another example: by introducing 35 mol% of 9-vinlybenzyladenine as comonomer with protonated 2-(dimethylamino)ethyl methacrylate (DMAEMA·HCl), the hydrogen bonding among adenine pendant groups leads to the decrease of c_e by 1.9 wt% and of c_D by 7.3 wt% in water, as compared with pure PDMAEMA·HCl.[102] Tan et al. reported that the addition of 0.5 wt% of graphene oxide, which has many hydroxyl, carbonyl and carboxylic acid groups that can hydrogen-bond in a PVA/water solution, decreases the minimum concentration for fiber formation from 8.5 wt% to 5 wt%.[103] Hermida-Merino et al. showed that, in tetrahydrofuran (THF), 42 wt% polyurethane linked with hydroxyl end-groups acts like a high molecular weight polymer and thus leads to electrospun fibers.[104] In contrast, only droplets were obtained from 47 wt% polyurethane (with a similar molecular weight) terminated with morpholine groups, whose self-binding constant is only 10% of that of hydroxyl groups.[104]

1.2.2.3 Non-polar interactions

Talwar et al. prepared fibers, rather than droplets, from 3 wt% poly(ethylene oxide) (PEO) solutions in water, by blending them with a 0.2 wt% alkali-soluble emulsion polymer with hydrophobic side chains (C_{22} alkyl chains) that leads to the formation of a network based on hydrophobic interactions in aqueous solutions.[105-106] Wu et al. also reported the positive effect of non-polar interchain interactions. They showed that adding 10 wt% of small molecule liquid crystals (4'-cyanobiphenyl-4-yl 4'-propylbi(cyclohexane)-4-carboxylate) enables to form electrospun fibers from a solution of 33 wt% poly((methyl-(4-propoxybenzoic acid cholesterol ester)siloxane)-co-(methyl-(4-acetoxyphenyl-4-propoxybenzoate)siloxane)) in $CHCl_3$, which originally only led to thin beaded fibers.[107]

1.2.2.4 Electrostatic interactions

Long et al. first reported that the effect of zwitterionic aggregation resembles the effect of entanglements and facilitates the electrospinning of poly(n-butyl acrylate-co-sulfobetaine methacrylamide) (P*n*BA-*co*-PSBMAm) in $CHCl_3$/ethanol.[108] They found that, with the same total number of repeat units, the c_e of P*n*BA-*co*-PSBMAm with 10 mol% of zwitterionic SBMAm units is 1.5 wt% while c_e is 5 wt% for pure P*n*BA.[108] According to Shi et al., plasma treatment on poly(ethylene oxide) (PEO) solutions can lead to charged PEO in the solution and improve the electrospinning. As an example, 4 wt% plasma-treated PEO in water leads to much more beadless fibers than a 4 wt% untreated PEO solution.[109] An attempt to use Ca^{2+} for facilitating the fiber formation of alginate, although it only transited from droplets into more elongated shapes, was reported by Fang et al.[110]

1.2.2.5 Electrospinning of low molecular weight species

Based on these various effective crosslinking strategies, many low molecular weight species have been electrospun. For example, phospholipids are small molecules with a hydrophilic head and a hydrophobic tail, so their amphiphilic interactions drive the formation of spherical micelles above the critical micelle concentration (CMC, 0.1-0.5 wt%) in the solution. When increasing the concentration over 43 wt%, these micelles can further aggregate as cylindrical assemblies, leading to fibers by electrospinning.[111] Cyclodextrins (CDs) are a group of small molecules composed of sugar molecules linked in a ring and featuring multiple hydroxyl groups. Based on their strong intermolecular hydrogen bonding in highly concentrated solutions, electrospinning was successfully applied to β-CD in a mixed solvent of an ionic liquid and DMF,[112] and to 57.9 wt% methylated β-CD[113] and 140 wt% hydroxypropyl-β-CD in DMF.[114] Melts of both 1,3,5-cyclohexane- and 1,3,5-benzene-trisamides were successfully electrospun by Singer et al.,[115] due to the self-assembly made possible by the strong hydrogen bonds of three amides and by the non-polar interaction of the three alkyl groups.

1.2.3 Electrospinning of P4VP

Reports about the electrospinning of pure P4VP are very rare. The only two published works, to the best of my knowledge, are about using electrospun P4VP fibers to absorb $HAuCl_4$ and CdTe nanoparticles.[116-117] All other electrospinning reports involving P4VP are based on using P4VP as one block of a block copolymer or as one component in blends. For example, Xu et al. reported the electrospinning of block copolymers of 4-vinyl pyridine (4VP) and pentachlorophenyl acrylate (PCPA) (P4VP-b-PCPA) from THF/DMF as substrates for antibacterial application.[118] ten Brinke, Ikkala and coworkers were the first to prepare hierarchically structured electrospun fibers from PS-b-P4VP(PDP)/DMF solutions.[119-120] The preparation of gold nanowires from plasma-treated PS-b-P4VP(Au) fibers from PS-b-P4VP($HAuCl_4$)/DMF solutions was reported by Park et al.[121] Finally, in an article not included in this thesis, I have prepared light-responsive fibers by electrospinning blends of PMMA and an azobenzene-containing SCLCP complex between methyl orange and methylated P4VP.[122]

1.3 Photoinduced orientation of P4VP-azobenzene complexes

Azobenzene and its derivatives (structures are shown in Fig. 1.16a-c) are the most widely used dyes in industry and have been attracting attention from researchers persistently. These dyes have π-π* and n-π* bands in their UV-Vis spectra, the latter originating from the non-bonding pairs of electrons carried by -N=N-. The UV-vis absorptions of azobenzene derivatives are greatly affected by the nature of the substituent,[123-124] leading to their characteristic colors. According to this, azobenzene can be categorized into three types: unsubstituted azobenzenes with yellow color, aminoazobenzenes with orange color, and pseudo-stilbenes (azobenzene with an electron-donating and an electron-withdrawing group in 4 and 4' positions) with red color, as shown by their representative compounds in Fig. 1.16a, b and c, respectively.[125] This change of color from yellow to red indicates the red shift of the dominant absorption band from the UV to the visible region, as shown in Fig. 1.16d.[126]

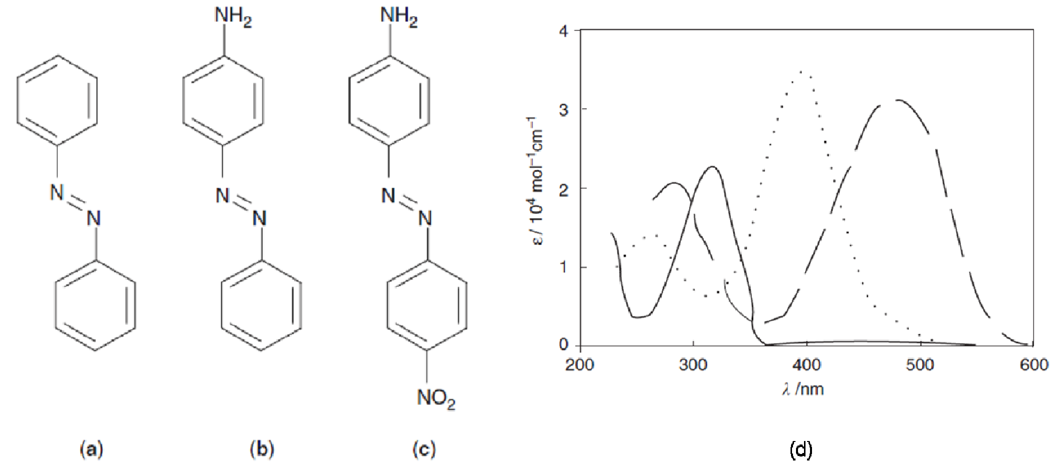

Figure 1.16. (a) Unsubstituted azobenzene, (b) aminoazobenzene, (c) pseudo-stilbene, and (d) typical absorbance spectra for *trans*-azobenzenes of unsubstituted azobenzene (solid line), aminoazobenzene (dotted line) and pseudo-stilbene (dashed line). Reproduced with permission from Ref. 126, © 2009 John Wiley & Sons, Inc.

A well known property of the azobenzene compounds is their reversible photoisomerization between *trans* and *cis* geometric forms, as shown in Fig. 1.17. The *trans* (*E*) form can switch to *cis* (*Z*) form with the absorption of light (usually UV light) and the *cis* form can switch back to *trans* form by the absorption of visible blue light or by thermal relaxation. *E* and *Z* are distinguishable in structures, physical properties and spectral characteristics. For example, the distance between the carbons at the 4 and 4' positions is 0.9 nm for *E* and 0.55 nm,[127] and the n-π* absorption intensity increases for *Z* in UV-Vis spectra. Compared with *Z*, *E* is more stable by about 50 kJ/mol,[123] making *E* the predominant form at room temperature.

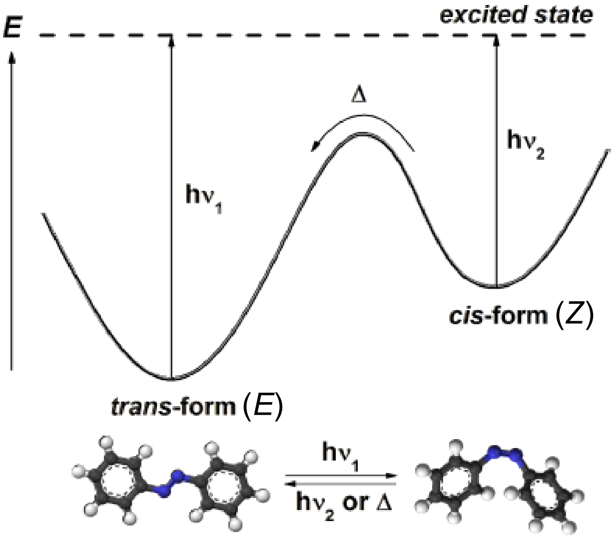

Figure 1.17. Photoisomerization of azobenezene between *trans* and *cis* forms. Reproduced with permission from Ref. 128, © 2012 García-Amorós and Velasco; licensee Beilstein-Institut.

E→*Z* photoisomerization in solution usually happens as fast as 0.7-14 picoseconds at 30 °C[129] or 14±3 picoseconds at room temperature,[130] while the thermal relaxation of *Z*→*E* occurs much more slowly on a timescale from milliseconds to years, depending on the azobenzene structure and the surrounding environment like the solvent, temperature, etc.[128, 131-132] Generally, the lifetime of *Z* is from milliseconds[133] to deciseconds[134] for pseudo-stilbenes, seconds[134] to minutes[135] for aminoazobenzenes, and hours or longer[135] for unsubstituted azobenzenes. For some azobenzenes in a polymer matrix or with conformational constraint, this lifetime could even be as long as days or years. For example, Lamarre and Sung reported that the azobenzene unit in the main chain of polyurethanes has a *Z* lifetime of 4 days,[136] and Rau and Rötger reported that the half-life of azobenzenophanes is around one year.[137] Therefore, isolated Z can be obtained for azobenzenes with high *Z*→*E* activation energy (E_a). For example, Talaty and Fargo reported the isolation in the *Z* form of a series of aminoazobenzenes whose E_a are as high as 85-100 kJ/mol in chloroform,[138] and Aronzon et al. reported an isolated liquid crystal, which is a mixture of two-thirds of *p*-*n*-butyl-*p*-

methoxyazoxybenzene and one-third of *p*-*n*-butyl-*p*-heptanoylazoxybenzene with E_a of 66±7 kJ/mol.[139]

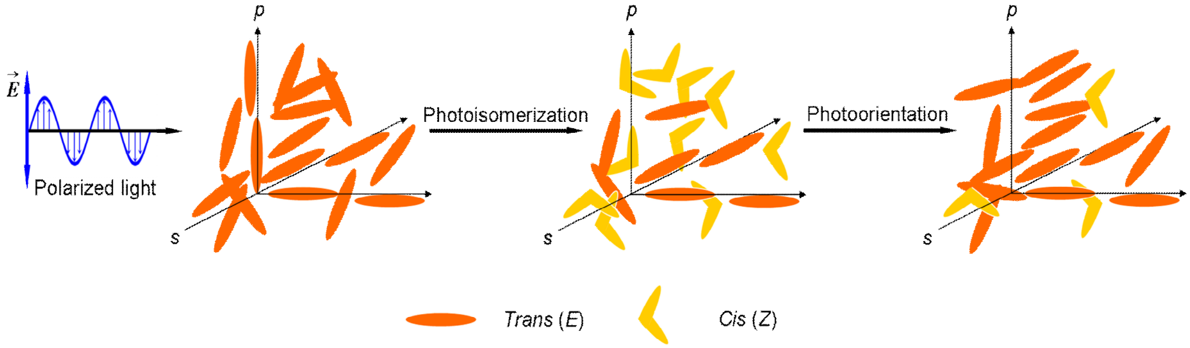

Figure 1.18. Scheme of the photoisomerization of azobenezenes upon irradiation of a linearly-polarized light. *p* and *s* represent the directions parallel and perpendicular to the electric field polarization of the pump beam, respectively.

If the irradiation is linearly polarized, only azobenzenes whose long axis (or a projection of the long axis vector) is aligned parallel (*p*) to the direction of the electric field ($\vec{E}$) of the pump beam light can absorb a photon since the absorption probability is proportional to the cosine square of the angle between the long axis and the light polarization. This selective absorption and the following $E \rightarrow Z$ isomerization thus induces an initial anisotropy of the distribution of both *E* and *Z*, called angular hole burning.[140] After several cycles of $E \rightarrow Z \rightarrow E$ isomerizations, azobenzene molecules have the tendency to orient perpendicular (*s*) to the polarization of the pump light, as shown in Fig. 1.18, because *E* isomers that have relaxed with their transition dipole moment along the *s* direction cannot absorb photons anymore. Therefore, the whole photo-orientation process involves a fast mode (angular hole burning) and a slow mode (angular reorientation) simultaneously, appearing as a biexponential function of orientation against irradiation time.[141] A similar behavior is also found for the reversed thermal relaxation process.[141] The angular reorientation process involves a rotational diffusion of the excited molecules, which can even induce the cooperative motion of polymer segments or even main chains in azobenzene-containing polymeric systems.[142] Therefore, such phenomenon of photoisomerization and photo-orientation provides opportunities for applications like photo-driven mechanics,[143-144] photo-induced change of the surface wetting properties,[145-146] surface relief grating,[142, 147] non-linear optical materials[148] and information storage.[149]

1.3.1 Photoinduced orientation of azobenzene-containing polymers measured by polarized Fourier transform infrared (FT-IR) spectroscopy

As described by Natansohn and Rochon, ("*By far the most popular and informative spectral method to analyze the photoinduced motion is FTIR*"[142]) polarized Fourier transform infrared (FT-IR) spectroscopy is very informative to follow the photoinduced orientation, as it clearly distinguishes the contribution of bands due to specific functional groups, in contrast with the usual spectral methods, like polarized UV-Vis, which only reflects the orientation of the chromophores, and optical methods, like birefringence, which only measures the overall orientation of all components.

Photoinduced orientation in a sample can be quantitatively characterized by its birefringence (Δn), which is the difference between the refractive indices in the p and s directions, by using Eq. 1.9:

$$I = I_0 \sin^2\left(\frac{\pi|\Delta n|d}{\lambda}\right) \tag{1.9}$$

where I_0 the intensity of the incident light, I is the intensity transmitted through the sample between crossed polarizers, d the thickness of the sample, and λ the wavelength of the probe beam.[52]

For spectral methods, the absorbance of the band of interest (A) is proportional to the square of the scalar product of the band transition dipole moment ($\vec{M}$) and the electric field amplitude ($\vec{E}$), $A \propto (\vec{M} \bullet \vec{E})^2$, which is equal to $M^2 \times E^2 \cos^2\theta$, where M and E are the absolute values of $\vec{M}$ and $\vec{E}$ respectively, and θ the angle between the transition dipole moment and the electric field of the linearly-polarized light. A normalized linear dichroism, $<T_2>$, can be defined by using Eq. 1.10:

$$\langle T_2 \rangle = \frac{A_p - A_s}{A_p + 2A_s} = \frac{\Delta A}{3A_0} \tag{1.10}$$

where A_p and A_s are the absorbance of the band of interest with the probe beam polarized parallel (p) and perpendicular (s) to the pump beam polarization, respectively, ΔA the dichroic difference, and A_0 the structural absorbance.[150]

Using these optical and spectral methods, Hvilsted and coworkers have studied a series of side-chain liquid crystalline polyesters with different numbers of methylene units in the main chain between two ester groups, and in the spacer linking the main chain with a functional group-tailed azobenzene.[151-155] They found that cyano and hydrogen tails lead to higher activities upon irradiation compared with nitro and methoxy tails,[155] and that both cyanoazobenzene mesogen and side-chain methylene segments tend to orient perpendicular to the laser polarization for all polyesters investigated.[151-154] In contrast, orientation of main-chain methylene groups occurs only for polyesters with long main-chain methylene segment (poly(tetradecanedioates) and poly(dodecanedioates)).[152-154] Such cooperative orientation, however, was not observed in a polymethacrylate with a 6 methylene units side chain linked to a cyano-tailed azobenzene, suggesting again the influence of the main chain flexibility.[153] Further FT-IR evidence of such cooperative orientation was found from the main chain of epoxy-based polymers with azobenzene side chain tailed with cyano and carboxylic acid groups,[156] and from the biphenylene unit in nunchaku-like molecules containing an azobenzene tailed with cyano or carboxylic acid groups, a biphenylene unit and a five carbons spacer.[157]

By using polarized FT-IR spectroscopy, Tawa et al. have conducted a series of studies on the photoinduced orientation of azobenzene-doped polymers[158-159] and of polymers with covalently bonded azobenzene side chains.[160-161] They found that the mobility of substituents depends on their relative volume during photoisomerization. In PMMA doped with dispersed orange 3 (DO3, NO_2-C_6H_4-N=N-C_6H_4-NH_2), for example, the p-NO_2-C_6H_4 group is less mobile than the p-NH_2-C_6H_4 group due to the larger relative volume of the former.[158-159] Another example is a covalently bonded system of polyurethane and azobenzene with a NO_2 tail, for which the p-NO_2-C_6H_4 group is more mobile than the p-dialkylamino-C_6H_4 group.[161] Besides, Tawa et al. found that, for doped systems, the free volume of the polymer and the local polarity are also important. For example, the motion of the azobenzene can be restricted by the small free volume of the polymer and by the large local polarity of the environment when polymers have large free volumes.[159] They also found that, compared with systems of polymers doped with azobenzene, polymers linked covalently with the azobenzene exhibit larger photoinduced orientation.[161]

As introduced in section 1.1.2, Priimagi and coworkers have investigated many polymeric hydrogen-bonded azobenzene-containing complexes, including P4VP-azobenzene. They found that photoinduced orientation is greatly influenced by the content in azobenzene chromophores and that such influence varies depending on the type of azobenzene used.[50-52] For P4VP/4-nitro-4'-hydroxylazobenzene, both photoinduced birefringence in the photostationary state and the residual birefringence after thermal relaxation increase with increasing chromophore concentration.[50] In contrast, for poly(4-vinyl phenol)/4-(2-pyridylazo)-N,N-dimethylaniline, photoinduced orientation decreases with increasing azobenzene content.[51] Such contrast is clearer for complexes between the same molecular weight P4VP and 4-hydroxyl azobenzenes whose 4' position is substituted with different tails. They found that, with increasing chromophore concentration, the photoinduced birefringence contribution per azobenzene unit increases when the tail is hydrogen, and decreases when tails are dimethyl amino and cyano groups.[52] Such different influences of azobenzenes are certainly related to the difference in chromophore-chromophore interactions, as suggested by the authors. However, as only polarized UV-vis and birefringence were applied to characterize the photoactivity in these works, there is an interest to investigate the impact of the structural difference of azobenzenes by more informative tools based on vibrational spectroscopy.

1.3.2 Photoinduced orientation of azobenzene-containing polymers measured by polarization modulation infrared linear dichroism (PM-IRLD)

For traditional polarized FT-IR spectroscopy, the polarization of the IR beam can only be changed manually or mechanically with a polarizer in a time scale of seconds, which limits its application for recording accurate information on the structure and conformation during some dynamic processes, like fast deformation of films and photoinduced orientation and thermal relaxation. Besides, when ΔA is very small, traditional polarized FT-IR spectroscopy cannot provide sufficient sensitivity since A_p and A_s are measured from two separate spectra successively.[162] To overcome this limitation, polarization modulation infrared linear dichroism (PM-IRLD) was developed by Nafie and Diem,[163] providing high sensitivity[162-163] and a time resolution as high as 200 ms.[164]

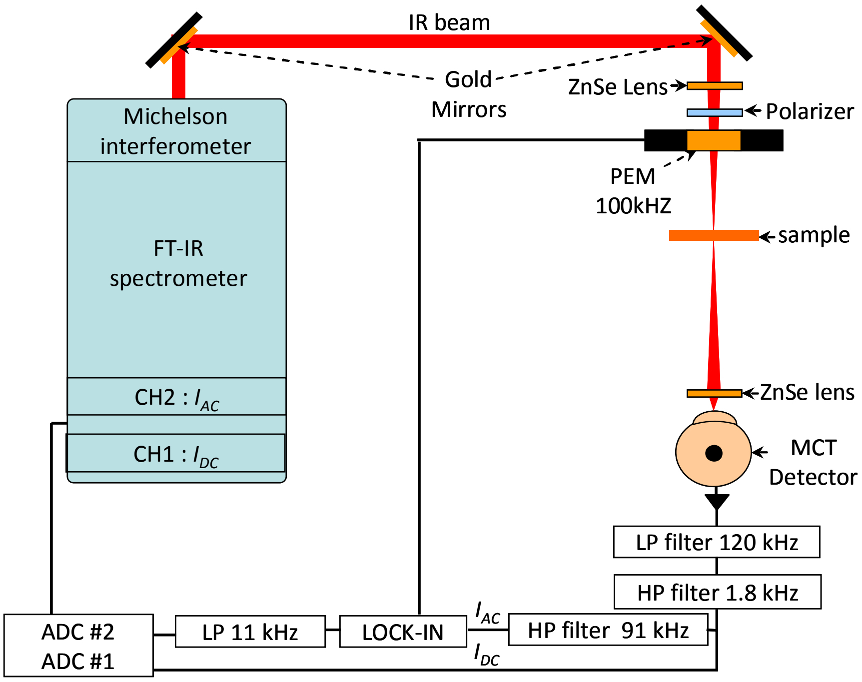

Figure 1.19. Scheme of the PM-IRLD setup. CH1: channel 1, CH2: channel 2, ADC: analog-to-digital converter, LP: low-pass filter, HP: high-pass filter, MCT: mercury cadmium telluride, PEM: photoelastic modulator.

Fig. 1.19 shows the scheme of the PM-IRLD setup and the related procedures to quantify the dichroic difference, as first illustrated by Buffeteau, Pézolet and coworkers.[165-167] First, the output IR beam of a standard FT-IR interferometer is linearly polarized via a holographic polarizer. The polarization state of the beam is then modulated by a photoelastic modulator (PEM), which contains a ZnSe crystal cyclically stretched and compressed by piezoelectric transducers, from parallel to perpendicular, with respect to the reference direction of the pump beam, with a frequency of 100 kHz. After this modulation, as shown in Eq. 1.11, the signal (I) received by the mercury cadmium telluride detector (MCT) can be expressed as the sum of two signals, I_{AC} and I_{DC}:

$$I = I_{AC} + I_{DC} \tag{1.11}$$

where I_{DC} is the signal modulated only by the FT-IR interferometer (at low Fourier frequencies) and I_{AC} is the signal modulated by both the interferometer and by the PEM (at 100 kHz).

The I_{AC} signal is filtered to remove the low frequency components and is then demodulated with a lock-in amplifier referenced to the PEM modulation frequency, followed by another filtration through a low-pass filter. After that, both I_{AC} and I_{DC} interferograms are sampled by two analog-to-digital converters (ADC) and are recorded as signals in channel 2 and channel 1, respectively. After Fourier transformation, the I_{AC} and I_{DC} can be given by Eqs. 1.12 and 1.13:

$$I_{AC} = 2CI_0 g''\left[\left(T_p - T_s\right)J_2\left(\phi_0\right)\right] \tag{1.12}$$

$$I_{DC} = CI_0 g'\left[\left(T_p + T_s\right) + \left(T_p - T_s\right)J_0\left(\phi_0\right)\right] \tag{1.13}$$

where C is a constant for the transmittance of the optical setup and for the detection yield, I_0 the light intensity after the polarizer, g' and g" the amplification and filtering constants for I_{DC} and I_{AC}, respectively, T_p and T_s the parallel and perpendicular transmittances of the sample, respectively, J_n the Bessel functions of order n, and ϕ_0 the maximum dephasing introduced by the PEM. These two signals can be ratioed, yielding the experimental spectrum S, as seen in Eq. 1.14:

$$S = \frac{I_{AC}}{I_{DC}} = \frac{2G\left(T_p - T_s\right)J_2\left(\phi_0\right)}{\left[\left(T_p + T_s\right) + \left(T_p - T_s\right)J_0\left(\phi_0\right)\right]} \tag{1.14}$$

where G is the ratio of g'' to g'.

In Eq. 1.14, $J_0(\phi_0)$ and $J_2(\phi_0)$ can be determined through calibration measurements by replacing the sample with a second polarizer and measuring spectra with its polarization parallel and perpendicular to the first polarizer in front of the PEM, simulating a sample perfectly anisotropic in the parallel and perpendicular directions, respectively. In this case, two calibration spectra, C_{pp} and C_{ps}, can be obtained, as shown in Eq. 1.15 and 1.16, respectively:

$$C_{pp} = \frac{2G'J_2(\phi_0)}{1+J_0(\phi_0)} \tag{1.15}$$

$$C_{ps} = \frac{2G'J_2(\phi_0)}{1-J_0(\phi_0)} \tag{1.16}$$

where G' is the gain and filtering constant for the calibration measurements. Finally, based on Eqs. 1.14, 1.15, 1.16 and the relation of $A = -\log T$, ΔA could be calculated as in Eq. 1.17.

$$\Delta A = A_p - A_s = \log\left[\frac{C_{ps}\left(\frac{G}{G'}C_{pp} - S\right)}{C_{pp}\left(\frac{G}{G'}C_{ps} + S\right)}\right] \tag{1.17}$$

Buffeteau and Pézolet first applied PM-IRLD to covalently bonded azobenzene-containing polymers and have observed the cooperative orientation of the azobenzene and C=O ester groups of the main chain in Disperse Red 1-containing amorphous azopolymer (pDR1A),[165] and of phenylene diacrylate groups of the main chain in Disperse Red 19-containing semicrystalline azopolymer (pDR19T).[168] In contrast, only the azobenzene moieties were found to be oriented for azobenzene-containing side chain liquid crystalline polymers with various spacer lengths.[169]

1.3.3 Polarization modulation infrared structural absorbance spectroscopy (PM-IRSAS)

As illustrated in section 1.3.2, PM-IRLD provides ΔA with a high sensitivity and a high time resolution, but it does not allow recording A_0, which is the structural absorbance. A_0 can be calculated by using A_p and A_s, as shown in Eq. 1.10, if the samples are uniaxially oriented, but these individual polarized spectra are not directly measured by standard PM-IRLD. Pellerin and coworkers first developed a new method, named polarization modulation infrared structural absorbance spectroscopy (PM-IRSAS), to calculate A_p and A_s based on PM-IRLD measurement.[170] Their method combines Eqs. 1.12 to 1.16 to express T_p and T_s as Eqs. 1.18 and 1.19, respectively:

$$T_p = \frac{I_{DC}}{2I_0Cg'}\left[1+\left(\frac{G'}{G}\right)\left(\frac{S}{C_{ps}}\right)\right] \tag{1.18}$$

$$T_s = \frac{I_{DC}}{2I_0Cg'}\left[1-\left(\frac{G'}{G}\right)\left(\frac{S}{C_{pp}}\right)\right] \tag{1.19}$$

These two equations show that T_p and T_s can be calculated if I_0 is known. Unfortunately, measuring I_0 is impossible for two reasons: first, there is not enough space between the first polarizer and the PEM to insert a detector; second, I_0 changes when the IR beam passes through other optical elements before reaching the sample. However, in the ideal scenario where the sample is perfectly isotropic, like an empty "background", the $T_p - T_s$ term in Eq. 1.13 should be zero. If we assume that the systematic anisotropy caused by the optical devices is negligible compared with $T_p + T_s$ in Eq. 1.13, I_0 can be determined by recording the I_{DC} of the background (I_{DCbk}) by Eq. 1.13. This enables calculating A_p and A_s, expressed as:

$$A_p = -\log\left[\frac{I_{DC}}{2I_{DCbk}}\left(1+\frac{G'S}{GC_{ps}}\right)\right] \tag{1.20}$$

$$A_s = -\log\left[\frac{I_{DC}}{2I_{DCbk}}\left(1-\frac{G'S}{GC_{pp}}\right)\right] \tag{1.21}$$

Eqs. 1.20 and 1.21 further allow calculating the orientation function, $<P_2>$ of the molecular axis of interest ,which could be the polymer main chain during the deformation of a polymer film[170-175] or the long axis of the azobenzene molecules upon irradiation,[158-161] as shown in Eq. 1.22:

$$\left\langle P_2(\cos\theta)\right\rangle = \left(\frac{2}{3\cos^2\alpha - 1}\right)\left(\frac{\Delta A}{3A_0}\right), \quad \frac{\Delta A}{3A_0} = \left\langle P_2(\cos\gamma)\right\rangle = \frac{\left\langle 3\cos^2\gamma - 1\right\rangle}{2} \tag{1.22}$$

where, as shown in Fig. 1. 20, Z is the axis parallel to the laser polarization, θ the angle between the molecular axis of interest and Z, α the angle between the transition dipole moment of the selected band and the molecular axis of interest, and γ the angle between the transition dipole moment of the selected band and the Z axis.

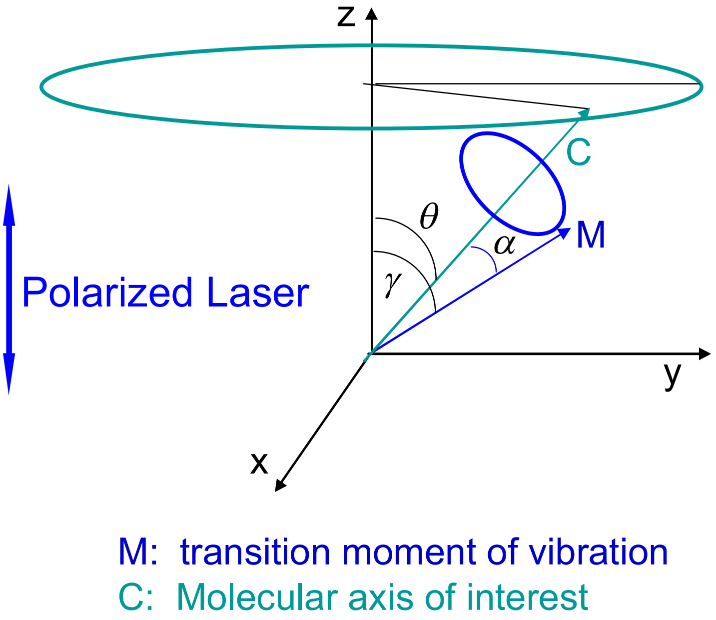

Figure 1.20. Axis system for calculating the orientation function.

The validation of PM-IRSAS can be seen in Fig. 1.21, which shows that the spectra of A_p, A_s and A_0 obtained from PM-IRSAS are very close to those obtained from traditional polarized FT-IR for drawn poly(ethylene terephthalate). Up to now, PM-IRSAS has been applied to measure simultaneously the orientation of the fluorophores (4,4′-bis(2-benzoxazolyl)stilbene or 2,5-bis(5-*tert*-butyl-benzoxazol-2-yl)thiophene) and of the crystalline phase of poly(1,4-butylene)succinate in their blends during the stretching of the film.[176] The results show that the fluorophores orient much less than the crystalline phase of the polymer, indicating that measuring the dye orientation by fluorescence spectroscopy cannot be used as a means to estimate the polymer orientation, as previously done in the literature.

These examples clearly show two advantages of PM-IRSAS associated with the dynamic measurement *in situ* of A_p, A_s and A_0: 1) it leads to more accurate calculation of the dynamic orientation function by using real time A_0, compared with PM-IRLD which requires using the initial A_0 (such as the A_0 of the unirradiated azobenzenes for photoirradiation studies)[150, 165, 168-169] or an adjusted A_0 (for instance by assuming the sample thinning based on the draw ratio for an affine deformation).[171-175] This can lead to large errors if the samples does not behave as predicted, for instance in the case of stress-induced crystallization or if the A_0 of an azobenzene band decreases due to $E \rightarrow Z$ isomerization. 2) it can provide additional information like the crystallization[170, 172] of *E* and *Z* fractions. Because of this, it becomes very interesting to use PM-IRSAS to study the hydrogen-bonded P4VP-azobenzene complexes, as discussed in Sections 1.1.2 and 1.3.1, so that the impact of the chromophore structures on the photoactivity of the complexes could be more clearly interpreted to facilitate the rational design of the photosensitive systems.

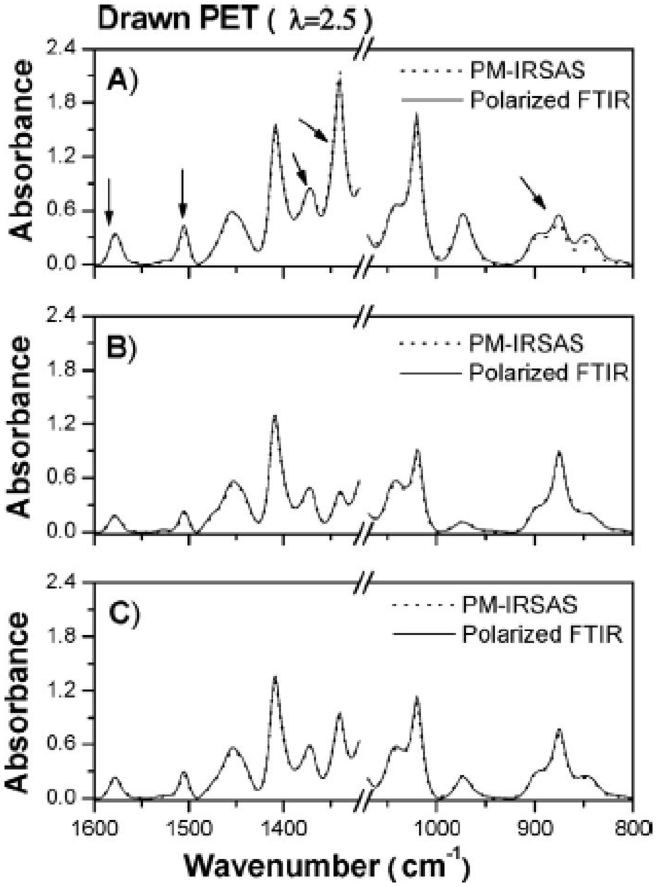

Figure 1.21. Comparison of (A) A_p, (B) A_s, and (C) A_0 recorded by static polarized FT-IR (solid line) and by PM-IRSAS (dotted line) for a uniaxially drawn poly(ethylene terephthalate) film. Reproduced with permission from Ref. 170, © 2008 Society for Applied Spectroscopy.

1.4 Objectives of the thesis

Although electrospinning is a powerful tool to produce fibers from solutions of many polymers, there are still several challenges in the application of this technique, including two that are related to a lack of electrospinnability. The first is that many species are not or poorly electrospinnable. These include the vast majority of small molecules, rigid polymers like polyelectrolytes and some biomacromolecules that do not readily entangle, and polymers with a molecular weight below M_c. The second is that some polymers, even if they can be electrospun, possess a high critical fiber formation concentration. Thus, the solutions suitable for electrospinning are very viscous, making solution transfer from vials to syringes difficult and the needles become easily clogged. Such high viscosity also presents a challenge in view of the larger-scale commercial implementation of electrospinning. These challenges initiated our first motivation, which is to develop a method to improve the electrospinnability of these species based on the strategy of increasing effective crosslinking, as discussed in Section 1.2.2, by introducing supramolecular crosslinks in their solutions.

To establish this strategy, we selected P4VP as a model polymer and used 4,4'-biphenol (BiOH) as a model small molecule hydrogen-bonding crosslinker. Therefore, the first task is to quantitatively determine the extent of crosslinking between P4VP and BiOH in solution and in the bulk state. To this end, a key is to obtain the ratio (a) of the band absorption coefficients of a free pyridine band to that of a hydrogen-bonded pyridine band. However, the previously reported values for a were not reliable, leading to the need of developing a universal method to determine it. The second task is to investigate the effect of BiOH on the electrospinnability of P4VP (with M_w = 200 kg/mol), with the goal of lowering the minimum P4VP concentration needed for fiber formation, based on the concept that the effective crosslinks formed between pyridine rings and hydroxyl groups of BiOH can enhance the viscoelasticity of the P4VP solutions. The third task is to further apply this strategy to systems of lower molecular weight P4VP (M_w = 50 kg/mol) and to other small crosslinkers to investigate the influence of the strength of the crosslinking interaction on the electrospinnability.

The second motivation of this thesis is to study photoactive complexes based on hydrogen bonding between P4VP and hydroxy azobenzene molecules with different tail substituents, with the goal of understanding the influence of the tail group on the photoinduced orientation. In the current literature, the photo-orientation of such systems was only characterized by birefringence,[52] which only reflects the overall contribution of all components in the complexes. We therefore hope to measure the photo-orientation of certain bands using time-resolved infrared spectroscopy and to further understand the impact of tail groups at a molecular level. To reach this goal, the polarization modulation infrared structural absorbance spectroscopy (PM-IRSAS) method, developed in our group,[170] was applied to study the films of such complexes upon irradiation, allowing the *in situ* measurement of the orientation function and of the structural absorbance of the bands of interest.

1.5 Content of the thesis

This thesis consists of four result chapters, each of them addressing one of the four objectives described in the previous section. Chapter 2 describes a new infrared spectroscopy method developed to determine the complexation extent in electrospun fibers of P4VP/BiOH. First, the a ratio of the free pyridine band (993 cm^{-1}) to that of the hydrogen-bonded pyridine band (1008 cm^{-1}) was determined. Our method consists in analyzing a liquid blend of BiOH with a model compound, 4-ethylpyridine (EtPy) by using the attenuated total reflection (ATR) mode. Then, the percentage of the hydrogen-bonded pyridine rings (f_b) in P4VP/BiOH was further calculated using the value determined for a. This method was later applied in Chapters 3, 4 and 5 to determine the values of a for different supramolecular P4VP complexes and from there, their f_b. This chapter was published as a full paper in Vibrational Spectroscopy (Wang, X.; Bazuin, C. G.; Pellerin, C., *Vib. Spectrosc.* **2014,** 71, 18-23).

In Chapter 3, the effect of the addition of BiOH on the electrospinnability of P4VP (200 kg/mol) in N,N-dimethylformamide (DMF) and in a mixed solvent (MIX) of DMF and nitromethane (CH_3NO_2) was investigated. Scanning electron microscopy (SEM) was used to characterize the morphology of the electrospun products from the four systems of P4VP/DMF, P4VP-BiOH/DMF, P4VP/MIX and P4VP-BiOH/MIX, providing the critical concentrations of fiber formation (c_f) and of pure fiber formation (c_p) for each system. To reveal the link between electrospinning and solution properties, the coil dimensions, the extent of complexation in solution and the viscosities were measured. Both the expansion of coil dimensions with addition of BiOH and the ATR results confirm the formation of hydrogen-bonded complexes in the solutions. The rheological results provide the critical concentration of the semidilute entangled (c_e) and concentrated regimes (c_D) of each system, which are close to c_f and c_p, respectively. This work was published as a full paper in Polymer (Wang, X.; Bazuin, C. G.; Pellerin, C., *Polymer* **2015,** 57, 62-69).

Chapter 4 extends the strategy of using BiOH to increase the electrospinnability of P4VP solutions to a lower molecular weight P4VP (50 kg/mol), where the impact is shown to be greater. In this chapter, other small crosslinkers, 4-hydroxy-4'-biphenyl carboxylic acid (HBCA) and $ZnCl_2$, with stronger interactions with pyridine rings, are shown to induce larger improvements of electrospinnability for P4VP in DMF. A sublimation method was successfully used to remove BiOH from P4VP/BiOH fibers, leading to pure P4VP fibers without damage. This chapter will soon be submitted for publication.

In Chapter 5, PM-IRSAS and UV-vis spectroscopy were used to investigate photo-orientation in films of P4VP with 4-phenylazophenol (P4VP/A_H) and 4-hydroxyl-4'-cyanoazobenzene (P4VP/A_{CN}) upon irradiation with a linearly polarized 488-nm laser light. Both photo-orientation and residual orientation of azobenzene bands (from C-N and C≡N groups) and P4VP bands (from pyridine rings) were calculated from the PM-IRSAS results. The impact of the azobenzene content on the azobenzene orientation and on the polymer orientation differs for the two complexes. Such differences in trends were related to the relative contributions of angular hole burning and of rotational diffusion, resulting from cycles of *trans-cis-trans* isomerization, which is higher for A_{CN} than for A_H because of its relatively larger transition dipole moment. This work, conducted in collaboration with postdoctoral fellow Jaana Vapaavuori, who contributed to the UV-vis and birefringence measurements and their related data analysis, will soon be submitted for publication. Finally, Chapter 6 presents the general conclusions of this thesis and perspectives for future work.

1.6 References

1. "The Nobel Prize in Chemistry 1987". http://www.nobelprize.org/nobel_prizes/chemistry/laureates/1987/.
2. Pedersen, C. J., *Org. Syn.* **1972,** 52, 66-74.
3. Pedersen, C. J., *J. Amer. Chem. Soc.* **1967,** 89, 7017-7036.
4. Cram, D. J., Multiheteromacrocycles that Complex Metal Ions. Second Progress Report, 1 May 1975 -- 30 April 1976. Energy, U. S. D. o., Ed. 1976.
5. Cram, D. J., Multiheteromacrocycles that Complex Metal Ions. Fourth Progress Report, 1 May 1977 -- 30 April 1978. Energy, U. S. D. o., Ed. 1978.

6. Cram, D. J., Multiheteromacrocycles that Complex Metal Ions. Sixth Progress Report, 1 May 1979-30 April 1980. Energy, U. S. D. o., Ed. 1980.
7. Cram, D. J., Multiheteromacrocycles that Complex Metal Ions. Ninth Progress Report (includes results of last three years), 1 May 1980 -- 30 April 1983. Energy, U. S. D. o., Ed. 1982.
8. Lehn, J.-M., Supramolecular Chemistry: Concepts and Perspectives. Wiley-VCH: New York: 1995.
9. Yang, Z.; Liang, G.; Xu, B., *Acc. Chem. Res.* **2008,** 41, 315-326.
10. Gao, Y.; Zhao, F.; Wang, Q.; Zhang, Y.; Xu, B., *Chem. Soc. Rev.* **2010,** 39, 3425-3433.
11. Zhang, X.; Chen, H.; Zhang, H., *Chem. Commun.* **2007**, 1395-1405.
12. Tang, Z.; Wang, Y.; Podsiadlo, P.; Kotov, N. A., *Adv. Mater.* **2006,** 18, 3203-3224.
13. Gohy, J. F.; Zhao, Y., *Chem. Soc. Rev.* **2013,** 42, 7117-7129.
14. Jiang, J.; Tong, X.; Morris, D.; Zhao, Y., *Macromolecules* **2006,** 39, 4633-4640.
15. Bertrand, O.; Fustin, C.-A.; Gohy, J.-F., *ACS Macro Lett.* **2012,** 1, 949-953.
16. Liu, Y.; Pellerin, C., *Macromolecules* **2006,** 39, 8886-8888.
17. Liu, Y.; Antaya, H.; Pellerin, C., *J. Polym. Sci., Part B: Polym. Phys.* **2008,** 46, 1903-1913.
18. Liu, Y.; Pellerin, C., *Polymer* **2009,** 50, 2601-2607.
19. Bailey, F. E., Jr.; France, H. G., *J. Polym. Sci.* **1961,** 49, 397-406.
20. Liu, Y.; Antaya, H.; Pellerin, C., *J. Phys. Chem. B* **2010,** 114, 2373-2378.
21. Harada, A.; Li, J.; Kamachi, M., *Nature* **1992,** 356, 325-327.
22. Wenz, G.; Han, B.-H.; Muller, A., *Chem. Rev.* **2006,** 106, 782-817.
23. Pollino, J. M.; Weck, M., *Chem. Soc. Rev.* **2005,** 34, 193-207.
24. Weck, M., *Polym. Int.* **2007,** 56, 453-460.
25. Fitzgerald, E. B.; Fuoss, R. M., *Ind. Eng. Chem.* **1950,** 42, 1603-1606.
26. Varshney, S. K.; Zhong, X. F.; Eisenberg, A., *Macromolecules* **1993,** 26, 701-706.
27. Creutz, S.; Teyssié, P.; Jerôme, R., *Macromolecules* **1997,** 30, 1-5.
28. Bohrisch, J.; Wendler, U.; Jaeger, W., *Macromol. Rapid Commun.* **1997,** 18, 975-982.
29. Xia, J.; Zhang, X.; Matyjaszewski, K., *Macromolecules* **1999,** 32, 3531-3533.
30. Linnell, R., *J. Org. Chem.* **1960,** 25, 290-290.
31. Borah, K. J.; Dutta, P.; Borah, R., *Bull. Korean Chem. Soc.* **2011,** 32, 225-228.

32. Gu, B.; Yin, M.; Zhang, A. P.; Qian, J.; He, S., *Opt. Express* **2011,** 19, 4140-4146.

33. Zhu, X.; Beginn, U.; Moller, M.; Gearba, R. I.; Anokhin, D. V.; Ivanov, D. A., *J. Am. Chem. Soc.* **2006,** 128, 16928-16937.

34. Ikkala, O.; Ruokolainen, J.; Tenbrinke, G.; Torkkeli, M.; Serimaa, R., *Macromolecules* **1995,** 28, 7088-7094.

35. Li, Y.; Yang, M. J.; She, Y., *Sens. Actuators, B* **2005,** 107, 252-257.

36. Sakai, Y.; Sadaoka, Y.; Matsuguchi, M.; Kanakura, Y.; Tamura, M., *J. Electrochem. Soc.* **1991,** 138, 2474-2478.

37. Zhang, Q.; Wang, X.; Barrett, C. J.; Bazuin, C. G., *Chem. Mater.* **2009,** 21, 3216-3227.

38. Zhang, Q.; Bazuin, C. G.; Barrett, C. J., *Chem. Mater.* **2008,** 20, 29-31.

39. Belfiore, L. A.; McCurdie, M. P.; Das, P. K., *Polymer* **2001,** 42, 09995-10006.

40. Zander, N. E.; Orlicki, J. A.; Rawlett, A. M., *Polym. Prepr. (Am. Chem. Soc., Div. Polym. Chem.)* **2009,** 50, 710-711.

41. Viel, P.; Palacin, S.; Descours, F.; Bureau, C.; Le Derf, F.; Lyskawa, J.; Sallé, M., *Appl. Surf. Sci.* **2003,** 212-213, 792-796.

42. Ruokolainen, J.; Tanner, J.; ten Brinke, G.; Ikkala, O.; Torkkeli, M.; Serimaa, R., *Macromolecules* **1995,** 28, 7779-7784.

43. Valkama, S.; Lehtonen, O.; Lappalainen, K.; Kosonen, H.; Castro, P.; Repo, T.; Torkkeli, M.; Serimaa, R.; ten Brinke, G.; Leskelae, M.; Ikkala, O., *Macromol. Rapid Commun.* **2003,** 24, 556-560.

44. Benouazzane, M.; Bravo-Grimaldo, E.; Bissessur, R.; Bazuin, C. G., *Macromolecules* **2006,** 39, 5364-5370.

45. Bazuin, C. G.; Brandys, F. A., *Chem. Mater.* **1992,** 4, 970-972.

46. Brandys, F. A.; Bazuin, C. G., *Chem. Mater.* **1996,** 8, 83-92.

47. Kato, T.; Hirota, N.; Fujishima, A.; Frechet, J. M. J., *J. Polym. Sci., Part A: Polym. Chem.* **1996,** 34, 57-62.

48. Korhonen, J. T.; Verho, T.; Rannou, P.; Ikkala, O., *Macromolecules* **2010,** 43, 1507-1514.

49. Kondo, M.; Takemoto, M.; Fukae, R.; Kawatsuki, N., *Polym. J.* **2012,** 44, 410-414.

50. Priimagi, A.; Vapaavuori, J.; Rodriguez, F. J.; Faul, C. F. J.; Heino, M. T.; Ikkala, O.; Kauranen, M.; Kaivola, M., *Chem. Mater.* **2008,** 20, 6358-6363.

51. Priimagi, A.; Kaivola, M.; Rodriguez, F. J.; Kauranen, M., *Appl. Phys. Lett.* **2007,** 90, 121103/121101-121103/121103.
52. Vapaavuori, J.; Valtavirta, V.; Alasaarela, T.; Mamiya, J.-I.; Priimagi, A.; Shishido, A.; Kaivola, M., *J. Mater. Chem.* **2011,** 21, 15437-15441.
53. Gao, J.; He, Y.; Liu, F.; Zhang, X.; Wang, Z.; Wang, X., *Chem. Mater.* **2007,** 19, 3877-3881.
54. Koskela, J. E.; Vapaavuori, J.; Hautala, J.; Priimagi, A.; Faul, C. F. J.; Kaivola, M.; Ras, R. H. A., *J. Phys. Chem. C* **2012,** 116, 2363-2370.
55. Vapaavuori, J.; Priimagi, A.; Kaivola, M., *J. Mater. Chem.* **2010,** 20, 5260-5264.
56. Priimagi, A.; Cavallo, G.; Metrangolo, P.; Resnati, G., *Acc. Chem. Res.* **2013,** 46, 2686-2695.
57. Bertani, R.; Metrangolo, P.; Moiana, A.; Perez, E.; Pilati, T.; Resnati, G.; Rico-Lattes, I.; Sassi, A., *Adv. Mater.* **2002,** 14, 1197-1201.
58. Priimagi, A.; Cavallo, G.; Forni, A.; Gorynsztejn-Leben, M.; Kaivola, M.; Metrangolo, P.; Milani, R.; Shishido, A.; Pilati, T.; Resnati, G.; Terraneo, G., *Adv. Funct. Mater.* **2012,** 22, 2572-2579.
59. Wang, S.-J.; Xu, Y.-S.; Yang, S.; Chen, E.-Q., *Macromolecules* **2012,** 45, 8760-8769.
60. Ruokolainen, J.; Torkkeli, M.; Serimaa, R.; Vahvaselkae, S.; Saariaho, M.; ten Brinke, G.; Ikkala, O., *Macromolecules* **1996,** 29, 6621-6628.
61. Ruokolainen, J.; Tanner, J.; Ikkala, O.; ten Brinke, G.; Thomas, E. L., *Macromolecules* **1998,** 31, 3532-3536.
62. de Wit, J.; van Ekenstein, G. A.; Polushkin, E.; Kvashnina, K.; Bras, W.; Ikkala, O.; ten Brinke, G., *Macromolecules* **2008,** 41, 4200-4204.
63. Ruokolainen, J.; ten Brinke, G.; Ikkala, O.; Torkkeli, M.; Serimaa, R., *Macromolecules* **1996,** 29, 3409-3415.
64. Ikkala, O.; ten Brinke, G., *Chem. Commun.* **2004**, 2131-2137.
65. ten Brinke, G.; Ikkala, O., *Chem. Rec.* **2004,** 4, 219-230.
66. Lu, Q.; Bazuin, C. G., *Nano Lett.* **2005,** 5, 1309-1314.
67. Perepichka, I. I.; Badia, A.; Bazuin, C. G., *ACS Nano* **2010,** 4, 6825-6835.
68. Perepichka, I. I.; Lu, Q.; Badia, A.; Bazuin, C. G., *Langmuir* **2013,** 29, 4502-4519.

69. Perepichka, I. I.; Badia, A.; Bazuin, C. G., *Polym. Prepr. (Am. Chem. Soc., Div. Polym. Chem.)* **2010,** 51, 253-254.
70. Perepichka, I. I.; Borozenko, K.; Badia, A.; Bazuin, C. G., *J. Am. Chem. Soc.* **2011,** 133, 19702-19705.
71. Perepichka, I. I.; Chen, X.; Bazuin, C. G., *Sci. China Chem.* **2012,** 56, 48-55.
72. Tokarev, I.; Krenek, R.; Burkov, Y.; Schmeisser, D.; Sidorenko, A.; Minko, S.; Stamm, M., *Macromolecules* **2005,** 38, 507-516.
73. Sidorenko, A.; Tokarev, I.; Minko, S.; Stamm, M., *J. Am. Chem. Soc.* **2003,** 125, 12211-12216.
74. Laforgue, A.; Bazuin, C. G.; Prud'homme, R. E., *Macromolecules* **2006,** 39, 6473-6482.
75. Roland, S.; Pellerin, C.; Bazuin, C. G.; Prud'homme, R. E., *Macromolecules* **2012,** 45, 7964-7972.
76. Roland, S.; Prud'homme, R. E.; Bazuin, C. G., *ACS Macro Lett.* **2012,** 1, 973-976.
77. Roland, S.; Gaspard, D.; Prud'homme, R. E.; Bazuin, C. G., *Macromolecules* **2012,** 45, 5463-5476.
78. Loveless, D. M.; Jeon, S. L.; Craig, S. L., *Macromolecules* **2005,** 38, 10171-10177.
79. Shibata, M.; Kimura, Y.; Yaginuma, D., *Polymer* **2004,** 45, 7571-7577.
80. Yount, W. C.; Loveless, D. M.; Craig, S. L., *J. Am. Chem. Soc.* **2005,** 127, 14488-14496.
81. "Spider know-how could cut future energy costs". http://www.ox.ac.uk/media/news_stories/2011/111123.html.
82. Asakura, T.; Umemura, K.; Nakazawa, Y.; Hirose, H.; Higham, J.; Knight, D., *Biomacromolecules* **2007,** 8, 175-181.
83. Tucker, N.; Stanger, J. J.; Staiger, M. P.; Razzaq, H.; Hofman, K., *J. Eng. Fibers Fabr.* **2012,** 7, 63-73.
84. Cooley, J. F., Apparatus for electrically dispersing fluids. Google Patents: 1902.
85. Cooley, J. F., Electrical method of dispersing fluids. Google Patents: 1903.
86. Morton, W. J., Method of dispersing fluids. Google Patents: 1902.
87. Doshi, J.; Reneker, D. H., *J. Electrost.* **1995,** 35, 151-160.
88. Taylor, G., *Proc. R. Soc. London, Ser. A Math. Phys. Sci.* **1964,** 280, 383-397.

89. Li, D.; Xia, Y., *Adv. Mater.* **2004,** 16, 1151-1170.
90. Gupta, P.; Elkins, C.; Long, T. E.; Wilkes, G. L., *Polymer* **2005,** 46, 4799-4810.
91. Colby, R. H.; Rubinstein, M.; Daoud, M., *J. Phys. II* **1994,** 4, 1299-1310.
92. Colby, R. H.; Fetters, L. J.; Funk, W. G.; Graessley, W. W., *Macromolecules* **1991,** 24, 3873-3882.
93. McKee, M. G.; Hunley, M. T.; Layman, J. M.; Long, T. E., *Macromolecules* **2006,** 39, 575-583.
94. McKee, M. G.; Wilkes, G. L.; Colby, R. H.; Long, T. E., *Macromolecules* **2004,** 37, 1760-1767.
95. Hager, B. L.; Berry, G. C., *J. Polym. Sci., Polym. Phys. Ed.* **1982,** 20, 911-928.
96. Frisch, H. L.; Simha, R., *Rheology*. Academic Press 1956: New York, 1956; Vol. 1.
97. Graessley, W. W., *Advances in Polymer Science, Vol. 16: The Entanglement Concept in Polymer Rheology*. Springer: 1974; p 179 pp.
98. Graessley, W. W., *Polymer* **1980,** 21, 258-262.
99. Koski, A.; Yim, K.; Shivkumar, S., *Mater. Lett.* **2003,** 58, 493-497.
100. McKee, M. G.; Elkins, C. L.; Long, T. E., *Polymer* **2004,** 45, 8705-8715.
101. Shenoy, S. L.; Bates, W. D.; Frisch, H. L.; Wnek, G. E., *Polymer* **2005,** 46, 3372-3384.
102. Hemp, S. T.; Hunley, M. T.; Cheng, S.; DeMella, K. C.; Long, T. E., *Polymer* **2012,** 53, 1437-1443.
103. Tan, Y.; Song, Y.; Zheng, Q., *Nanoscale* **2012,** 4, 6997-7005.
104. Hermida-Merino, D.; Belal, M.; Greenland, B. W.; Woodward, P.; Slark, A. T.; Davis, F. J.; Mitchell, G. R.; Hamley, I. W.; Hayes, W., *Eur. Polym. J.* **2012,** 48, 1249-1255.
105. Talwar, S.; Hinestroza, J.; Pourdeyhimi, B.; Khan, S. A., *Macromolecules* **2008,** 41, 4275-4283.
106. Talwar, S.; Krishnan, A. S.; Hinestroza, J. P.; Pourdeyhimi, B.; Khan, S. A., *Macromolecules* **2010,** 43, 7650-7656.
107. Wu, Y.; An, Q.; Yin, J.; Hua, T.; Xie, H.; Li, G.; Tang, H., *Colloid Polym. Sci.* **2008,** 286, 897-905.
108. Brown, R. H.; Hunley, M. T.; Allen, J. M. H.; Long, T. E., *Polymer* **2009,** 50, 4781-4787.

109. Shi, Q.; Vitchuli, N.; Nowak, J.; Lin, Z.; Guo, B.; McCord, M.; Bourham, M.; Zhang, X., *J. Polym. Sci., Part B: Polym. Phys.* **2011,** 49, 115-122.

110. Fang, D.; Liu, Y.; Jiang, S.; Nie, J.; Ma, G., *Carbohydr. Polym.* **2011,** 85, 276-279.

111. McKee, M. G.; Layman, J. M.; Cashion, M. P.; Long, T. E., *Science* **2006,** 311, 353-355.

112. Ahn, Y.; Kang, Y.; Ku, M.; Yang, Y.-H.; Jung, S.; Kim, H., *RSC Adv.* **2013,** 3, 14983-14987.

113. Celebioglu, A.; Uyar, T., *Chem. Commun.* **2010,** 46, 6903-6905.

114. Zhang, W.; Chen, M.; Zha, B.; Diao, G., *PCCP* **2012,** 14, 9729-9737.

115. Singer, J. C.; Giesa, R.; Schmidt, H.-W., *Soft Matter* **2012,** 8, 9972-9976.

116. Lu, L. C.; Wang, W. Q.; Cai, W. J., *J. Polym. Mater.* **2012,** 29, 181-187.

117. Wang, S.; Li, Y.; Li, J.; Du, J.; Bai, J.; Yang, Q.; Chen, X., *J. Appl. Polym. Sci.* **2008,** 108, 281-286.

118. Qun, X. L.; Fang, Y.; Shan, Y.; Fu, G.-D.; Liang, S.; Nie, S.; Zhu, M., *High Perform. Polym.* **2010,** 22, 359-376.

119. Ruotsalainen, T.; Turku, J.; Heikkilä, P.; Ruokolainen, J.; Nykänen, A.; Laitinen, T.; Torkkeli, M.; Serimaa, R.; ten Brinke, G.; Harlin, A.; Ikkala, O., *Adv. Mater.* **2005,** 17, 1048-1052.

120. Ruotsalainen, T.; Turku, J.; Hiekkataipale, P.; Vainio, U.; Serimaa, R.; ten Brinke, G.; Harlin, A.; Ruokolainen, J.; Ikkala, O., *Soft Matter* **2007,** 3, 978-985.

121. Park, S.; Moon, S. C.; Chen, D.; Farris, R. J.; Russell, T. P., *J. Mater. Chem.* **2010,** 20, 1198-1202.

122. Wang, X.; Zhang, Q.; Bazuin, C. G.; Pellerin, C., *Macromol. Symp.* **2014,** 336, 30-38.

123. Rau, H., *Angew. Chem.* **1973,** 85, 248-258.

124. Gore, P. H.; Wheeler, O. H., *J. Org. Chem.* **1961,** 26, 3295-3298.

125. Rau, H., *Photochemistry and Photophysics Volume II*. CRC Press, Inc.: Boca Raton, Florida, USA, 1990.

126. Yager, K. G.; Barrett, C. J., *Smart Light-Responsive Materials: Azobenzene-Containing Polymers and Liquid Crystals*. John Wiley & Sons, INC.: Boca Raton, Florida, USA, 2009.

127. Hrozhyk, U.; Serak, S.; Tabiryan, N.; White, T. J.; Bunning, T. J., *Opt. Express* **2009,** 17, 716-722.

128. Garcia-Amoros, J.; Velasco, D., *Beilstein J. Org. Chem.* **2012,** 8, 1003-1017, No. 1113.

129. Lednev, I. K.; Ye, T.-Q.; Hester, R. E.; Moore, J. N., *J. Phys. Chem.* **1996,** 100, 13338-13341.

130. Kobayashi, T.; Degenkolb, E. O.; Rentzepis, P. M., *J. Phys. Chem.* **1979,** 83, 2431-2434.

131. Merino, E.; Ribagorda, M., *Beilstein J. Org. Chem.* **2012,** 8, 1071-1090, No. 1119.

132. Han, M.; Honda, T., *Sci. China Chem.* **2011,** 54, 1955-1961.

133. Whitten, D. G.; Wildes, P. D.; Pacifici, J. G.; Irick, G., Jr., *J. Amer. Chem. Soc.* **1971,** 93, 2004-2008.

134. Janossy, I.; Szabados, L., *J. Nonlinear Opt. Phys. Mater.* **1998,** 7, 539-551.

135. Yager, K. G.; Barrett, C. J., *J. Photochem. Photobiol., A* **2006,** 182, 250-261.

136. Lamarre, L.; Sung, C. S. P., *Macromolecules* **1983,** 16, 1729-1736.

137. Rau, H.; Rötger, D., *Mol. Cryst. Liq. Cryst. Sci. Technol., Sect. A. Mol. Cryst. Liq. Cryst.* **1994,** 246, 143-146.

138. Talaty, E. R.; Fargo, J. C., *Chem. Commun.* **1967**, 65.

139. Aronzon, D.; Levy, E. P.; Collings, P. J.; Chanishvili, A.; Chilaya, G.; Petriashvili, G., *Liq. Cryst.* **2007,** 34, 707-718.

140. Dumont, M. L.; Sekkat, Z., *Nonconducting Photopolymers and Applications, Proceedings of SPIE* **1992,** 1774, 188-199.

141. Ho, M.-S.; Natansohn, A.; Barrett, C.; Rochon, P., *Can. J. Chem.* **1995,** 73, 1773-1778.

142. Natansohn, A.; Rochon, P., *Chem. Rev.* **2002,** 102, 4139-4175.

143. Yu, Y.; Nakano, M.; Ikeda, T., *Nature* **2003,** 425, 145.

144. Yamada, M.; Kondo, M.; Mamiya, J.-i.; Yu, Y.; Kinoshita, M.; Barrett, C. J.; Ikeda, T., *Angew. Chem., Int. Ed.* **2008,** 47, 4986-4988.

145. Wagner, N.; Theato, P., *Polymer* **2014,** 55, 3436-3453.

146. Ahmad, N. M.; Lu, X.; Barrett, C. J., *J. Mater. Chem.* **2010,** 20, 244-247.

147. Ichimura, K.; Oh, S. K.; Nakagawa, M., *Science* **2000,** 288, 1624-1626.

148. Yesodha, S. K.; Sadashiva Pillai, C. K.; Tsutsumi, N., *Prog. Polym. Sci.* **2004,** 29, 45-74.

149. Liu, Z. F.; Hashimoto, K.; Fujishima, A., *Nature* **1990,** 347, 658-660.

150. Buffeteau, T.; Lagugné Labarthet, F.; Pézolet, M.; Sourisseau, C., *Macromolecules* **1998,** 31, 7312-7320.

151. Hvilsted, S.; Andruzzi, F.; Kulinna, C.; Siesler, H. W.; Ramanujam, P. S., *Macromolecules* **1995,** 28, 2172-2183.

152. Kulinna, C.; Hvilsted, S.; Hendann, C.; Siesler, H. W.; Ramanujam, P. S., *Macromolecules* **1998,** 31, 2141-2151.

153. Han, M.; Kidowaki, M.; Ichimura, K.; Ramanujam, P. S.; Hvilsted, S., *Macromolecules* **2001,** 34, 4256-4262.

154. Zebger, I.; Rutloh, M.; Hoffmann, U.; Stumpe, J.; Siesler, H. W.; Hvilsted, S., *J. Phys. Chem. A* **2002,** 106, 3454-3462.

155. Zebger, I.; Kulinna, C.; Siesler, H. W.; Andruzzi, F.; Pedersen, M.; Ramanujam, P. S.; Hvilsted, S., *Macromol. Symp.* **1995,** 94, 159-170.

156. Wang, Y.; He, Y.; Wang, X., *Polym. Bull.* **2011,** 68, 1731-1746.

157. Wang, Y.; Ye, G.; Wang, X., *J. Mater. Chem.* **2012,** 22, 7614-7621.

158. Tawa, K.; Kamada, K.; Sakaguchi, T.; Ohta, K., *Appl. Spectrosc.* **1998,** 52, 1536-1540.

159. Tawa, K.; Kamada, K.; Sakaguchi, T.; Ohta, K., *Polymer* **2000,** 41, 3235-3242.

160. Tawa, K.; Zettsu, N.; Minematsu, K.; Ohta, K.; Namba, A.; Tran-Cong, Q., *J. Photochem. Photobiol., A* **2001,** 143, 31-38.

161. Tawa, K.; Kamada, K.; Kiyohara, K.; Ohta, K.; Yasumatsu, D.; Sekkat, Z.; Kawata, S., *Macromolecules* **2001,** 34, 8232-8238.

162. Marcott, C., *Appl. Spectrosc.* **1984,** 38, 442-443.

163. Nafie, L. A.; Diem, M., *Appl. Spectrosc.* **1979,** 33, 130-135.

164. Buffeteau, T.; Pézolet, M., Linear Dichroism in Infrared Spectroscopy. In *Handbook of Vibrational Spectroscopy*, John Wiley & Sons, Ltd: 2006.

165. Buffeteau, T.; Pézolet, M., *Appl. Spectrosc.* **1996,** 50, 948-955.

166. Buffeteau, T.; Desbat, B.; Pézolet, M.; Turlet, J. M., *J. Chim. Phys. Phys.-Chim. Biol.* **1993,** 90, 1467-1489.

167. Buffeteau, T.; Desbat, B.; Besbes, S.; Nafati, M.; Bokobza, L., *Polymer* **1994,** 35, 2538-2541.

168. Buffeteau, T.; Pézolet, M., *Macromolecules* **1998,** 31, 2631-2635.

169. Labarthet, F. L.; Freiberg, S.; Pellerin, C.; Pézolet, M.; Natansohn, A.; Rochon, P., *Macromolecules* **2000,** 33, 6815-6823.

170. Liang, Y.; Mauran, D.; Prud'homme, R. E.; Pellerin, C., *Appl. Spectrosc.* **2008,** 62, 941-947.

171. Pellerin, C.; Prud'homme, R. E.; Pézolet, M., *Macromolecules* **2000,** 33, 7009-7015.

172. Pellerin, C.; Rousseau, M.-E.; Prud'homme, R. E.; Pézolet, M., *Appl. Spectrosc.* **2002,** 56, 17-23.

173. Pellerin, C.; Pelletier, I.; Pézolet, M.; Prud'homme, R. E., *Macromolecules* **2002,** 36, 153-161.

174. Pellerin, C.; Prud'homme, R. E.; Pézolet, M., *Polymer* **2003,** 44, 3291-3297.

175. Pellerin, C.; Prud'homme, R. E.; Pézolet, M.; Weinstock, B. A.; Griffiths, P. R., *Macromolecules* **2003,** 36, 4838-4843.

176. Fourati, M. A.; Pellerin, C.; Bazuin, C. G.; Prud'homme, R. E., *Polymer* **2013,** 54, 730-736.

Chapter 2: Quantitative analysis of hydrogen bonding in electrospun fibers of poly(4-vinyl pyridine)/(4,4'-biphenol) complexes by ATR using liquid blends as models[*]

2.1 Résumé

Pour comprendre les caractéristiques des fibres électrofilées de la poly(4-vinylpyridine) (P4VP) qui est potentiellement réticulée par liaison hydrogène lorsqu'elle est mélangée avec de petites molécules comme le 4,4'-biphénol (BiOH), il est nécessaire de déterminer la proportion de pyridines liées par des liaisons hydrogène (f_b) et de la comparer avec F_{OH}, le pourcentage molaire de groupements OH disponibles pour interagir avec ces pyridines. Bien que cela puisse être fait par spectroscopie infrarouge à transformée de Fourier (FTIR), deux difficultés pratiques doivent être surmontées. Tout d'abord, les intensités des bandes de la pyridine libre et de celle liée par liaisons hydrogène qui se chevauchent doivent être obtenues, ce qui est possible en utilisant la dérivée seconde du spectre. De plus, le rapport du coefficient d'absorption des bandes (a) doit être connu. Dans le système P4VP/BiOH, seule la paire formée de la bande pyridine libre et celle liée par liaisons hydrogène à, respectivement, 993 et 1007 cm^{-1} peut être utilisée pour une analyse quantitative. En analysant des mélanges liquides de BiOH ainsi que de phénol avec un composé modèle, la 4-éthylpyridine (EtPy), nous avons déterminé, en utilisant le mode de réflexion totale atténuée (ATR), que a = 0,40. Cela a conduit à des valeurs de $f_b = F_{OH}$, indiquant la complexation complète entre les groupements OH et la pyridine jusqu'à la limite de solubilité du BiOH dans la EtPy (F_{OH} = 60%) et jusqu'à F_{OH} = 100% dans le mélange EtPy/phénol. Dans les fibres électrofilées de P4VP/BiOH préparées à partir de solutions avec un F_{OH} atteignant jusqu'à 120%, f_b correspond en moyenne à 0,76F_{OH} et la complexation complète des groupements pyridines n'est obtenue qu'à environ

---

[*] Published as a full paper in *Vibrational Spectroscopy* **2014**, 71, 18-23 by Xiaoxiao Wang, C. Geraldine Bazuin and Christian Pellerin.

F_{OH} = 160%. Dans les deux mélanges P4VP/BiOH et EtPy/BiOH, la complexation se produit entre une pyridine et un groupement hydroxyle. Ce travail décrit une nouvelle méthode pour quantifier le nombre relatif de pyridines liées par liaisons hydrogène dans la P4VP; cette méthode devrait être applicable à d'autres mélanges de polymères/petites molécules et polymère-polymère ayant des systèmes modèles liquides appropriés.

2.2 Abstract

To understand the characteristics of electrospun fibers of poly(4-vinyl pyridine) (P4VP) that are potentially crosslinked by hydrogen-bonding when blended with small molecules like 4,4'-biphenol (BiOH), it is necessary to determine the proportion of hydrogen-bonded pyridine rings (f_b) and to contrast it with F_{OH}, the mole percent of OH groups available for interacting with the pyridine rings. While this can be done by Fourier transform infrared spectroscopy (FTIR), two practical difficulties must be overcome. First, the correct intensities of the overlapped bands of free and hydrogen-bonded pyridine must be obtained, which is possible using the second derivative spectra. Second, the band absorption coefficient ratio (a) of the pair of bands must be known. In the P4VP/BiOH system, only the pair of free and hydrogen-bonded pyridine ring bands at 993 and 1007 cm^{-1}, respectively, can be used for quantitative analysis. We determined, by analysis of liquid blends of BiOH as well as phenol with a model compound, 4-ethylpyridine (EtPy), using the attenuated total reflection mode (ATR), that a = 0.40. This led to values of $f_b = F_{OH}$, indicative of full complexation of the OH groups to pyridine, up to the BiOH solubility limit in EtPy (F_{OH} = 60%) and up to F_{OH} = 100% in the EtPy/phenol blends. In the electrospun P4VP/BiOH fibers prepared from solutions with F_{OH} up to about 120%, f_b averages $0.76F_{OH}$, and full complexation of the pyridine groups is achieved only at about F_{OH} = 160%. In both P4VP/BiOH and EtPy/BiOH, the complexation occurs between one pyridine ring and one hydroxyl group. This work thus shows a new method to quantify the relative number of hydrogen-bonded pyridine rings in P4VP; it is expected to be applicable to other polymer-small molecule and polymer-polymer blends having suitable liquid models.

2.3 Introduction

Ever since the concept of "supramolecular chemistry" was introduced by Lehn,[1] it has been playing an important role in material design.[2-8] It typically refers to the binding of two or more molecular building blocks by noncovalent interactions to achieve larger supermolecules or supramolecular assemblies. Among these building blocks, functional polymers have been widely used because of their high stability, flexibility and easy machinability, with poly(4-vinyl pyridine) (P4VP) being one of the most popular representatives. The pyridine rings in P4VP, due to the lone electron pair on N that does not participate in the ring conjugation, are weakly basic and can complex with many other species, such as functional small molecules (SMs), through hydrogen-bonding,[9-12] acid-base interactions,[13-14] and ionic complexation,[15-20] to form a variety of side-chain assemblies.

Hydrogen-bonded supramolecular complexes have especially been investigated since the properties and structure of such materials can be controlled in a dynamic fashion and they are easy to prepare. A much studied design is the complex between P4VP and 3-pentadecylphenol (PDP),[21] which, since the 1990s, has been the subject of a large amount of work by Ikkala, ten Brinke and coworkers, as well as other groups, involving not only P4VP homopolymer but also block copolymers of polystyrene-b-poly(4-vinyl pyridine) (PS-b-P4VP) that can lead to hierarchically structured materials.[9-10, 22-24] Hydrogen-bonded (PS-b-P4VP)/SM complexes were further prepared in the form of thin films and used as structure-controllable nanotemplates.[25-29] By using functionalized azobenzene chromophores, photosensitive materials can be prepared,[30-31] a strategy also applied to halogen-bonded P4VP-azobenzene complexes.[32]

Complexes of P4VP with bifunctional SMs, to obtain an effectively crosslinked network, have been much less reported than those with monofunctional SMs. Examples include a P4VP complex ionically crosslinked by disulfonic acid, which increases the glass transition temperature (Tg) and heat resistance of P4VP,[33] and a P4VP network in DMSO formed with bifunctional Pd(II) or Pt(II) organometallic crosslinkers, where the viscoelastic solution properties can be precisely controlled by the dissociation rate constants of different metal-ligand complexes.[34-35]

In our work, we are investigating hydrogen-bonded complexes of P4VP and 4,4'-biphenol (BiOH) prepared by electrospinning. To understand the properties of the electrospun fibers, it is necessary to quantify the number of pyridine rings hydrogen-bonded by the bifunctional SM and thereby evaluate the extent of hydrogen-bonded crosslinking. This can be accomplished by using Fourier transform infrared spectroscopy (FTIR) to analyze the relative intensities of a pair of bands associated with free and hydrogen-bonded groups. This approach has been used by Coleman and coworkers for various polymer blends; for example, poly(vinyl phenol) with poly(ethylene-co-vinyl acetate),[36] poly(ethylene-co-methacrylic acid) (EMAA) with poly(ethylene oxide-co-propylene oxide),[37] and EMAA with poly(2-vinyl pyridine) (P2VP).[38] The level of complexation of the carbonyl groups was determined from the absorbance of the carbonyl stretching band, which shifts to lower frequency upon hydrogen bonding. Similarly, the complexation of the pyridine groups was estimated by measuring the relative intensity of the free and H-bonded ring stretching bands at around 1590 and 1600 cm^{-1}, respectively.

In order to quantify the fraction of complexed units, it is necessary to know the ratio of the absorption coefficients (a) associated with the free and hydrogen-bonded bands. Coleman and coworkers[38] determined that a is close to unity for the 1590/1600 cm^{-1} band pair of P2VP by measuring the transmission spectra of samples containing a known fraction of the interacting units. This value was confirmed by Cesteros et al.[39] and used for quantifying the complexation of P2VP as well as P4VP blended with poly(hydroxymethacrylates), and by Ikkala and coworkers[40-41] for P4VP/cholesteryl hemisuccinate complexes.

A limitation to this method is the frequent overlap of the P4VP bands around 1600 cm^{-1} with aromatic stretching bands originating from the complementary SM. This is the case with BiOH as the SM. A well-known alternative to estimate the hydrogen-bonding is the band pair just below and just above 1000 cm^{-1}, which are due to free and bonded pyridine, respectively.[12, 25, 28-31] However, the a ratio has never been determined for this band pair, restricting its use to semi-quantitative results. A further complication in our study is that the IR spectra of electrospun fibers can only be measured using the attenuated total reflection (ATR) mode because their small size leads to strong spectral distortions (Christiansen effect) when measured in transmission.

Here, we demonstrate a new method to quantify the percentage of hydrogen-bonded pyridine rings in P4VP by ATR spectroscopy. It is based on the use of a liquid model compound, 4-ethylpyridine, which has a spectrum very similar to that of P4VP and which avoids the issue of the quality of the contact with the ATR crystal.

2.4 Experimental

P4VP (M_w = 200,000 g/mol) was obtained from Scientific Polymer Products, 4,4'-biphenol (BiOH, 97%) and 4-ethylpyridine (EtPy, 98%) from Aldrich, phenol (99%) from BDH, and N,N'-dimethylformamide (DMF, 99.8%) from EMD, all used as received. Liquid blends of EtPy/BiOH and EtPy/phenol of various molar ratios were prepared by dissolving the appropriate amounts of BiOH or phenol in EtPy in 10 mL vials. P4VP/BiOH solutions with a series of BiOH contents for electrospinning were prepared by dissolving BiOH and P4VP in DMF in 20 mL vials. The P4VP concentration was always 10.0±0.5 wt %. All blends and solutions were shaken gently for 5 days with a Heidolph UNIMAX 1010 shaker (Rose Scientific) to obtain homogenous samples and were left for 1 day before further spectroscopic measurement or electrospinning. The composition of the complexes, which are nominal for P4VP/BiOH fibers, are indicated as EtPy/BiOH(F_{OH}), EtPy/phenol(F_{OH}) and P4VP/BiOH(F_{OH}), where F_{OH} refers to the content of BiOH or phenol in terms of the mole percent of hydroxyl groups relative to the pyridine rings of P4VP or EtPy. Because of the limited solubility of BiOH in EtPy, the maximum F_{OH} giving a homogeneous blend in this case was 60%.

To prepare electrospun fibers, the P4VP/BiOH solution was transferred to a syringe, mounted on a syringe pump (PHD 2000, Harvard Apparatus), and extruded through a needle (model 91022, Hamilton) at a rate of 0.01 mL/min. A +20 kV potential was applied to the needle using a MFC series 120 W regulated high-voltage DC power supply (Glassman High Voltage). The collector was made of a glass slide covered with aluminum foil and connected to the -2 kV cathode of a Nim Standard HV power supply (Power Design). The distance between the tip of the needle and the collector was 10 cm. The collected fibers were dried in vacuum at 60°C for about a month to remove DMF.

IR spectra of the fibers and liquid blends were recorded using a Tensor 27 FT-IR spectrometer (Bruker Optics) equipped with a HgCdTe detector. A VariGATR accessory (Harrick Scientific) with a Ge crystal was used at an incidence angle of 60° to measure all IR spectra with the exception of those in the OH stretching region, which were obtained with a MIRacle (Pike Technologies) ATR accessory with a silicon element. All spectra were obtained with a resolution of 4 cm^{-1} by averaging 200 scans for the fibers and 100 scans for the liquid blends.

2.5 Results and discussion

Fig. 2.1 compares the IR spectrum of electrospun P4VP/BiOH(92%) fibers with those of pure P4VP and pure BiOH. The literature assignments of the bands below 1700 cm^{-1} are provided in the supplementary information (Fig. 2.S1 and Table 2.S1). The P4VP band at 993 cm^{-1} is assigned to deformation vibrations of the pyridine ring.[42-43] It shifts to 1007 cm^{-1} in the presence of BiOH (shown by the dashed line in Fig. 2.1), thus confirming the formation of hydrogen bonds between the pyridine ring and the hydroxyl group of BiOH. The BiOH band at 1022 cm^{-1} is assigned to C-C stretching and to out-of-plane C-H bending vibrations[44-46] and is shifted to around 1024 cm^{-1} in the complexes. The weak BiOH band at 1003 cm^{-1} is assigned to in-plane bending vibrations of the phenyl ring.[46-47] It is not visible in the absorbance or second-derivative spectra of the EtPy/BiOH complexes, possibly due to a blue shift toward the much more intense 1007 cm^{-1} P4VP band.

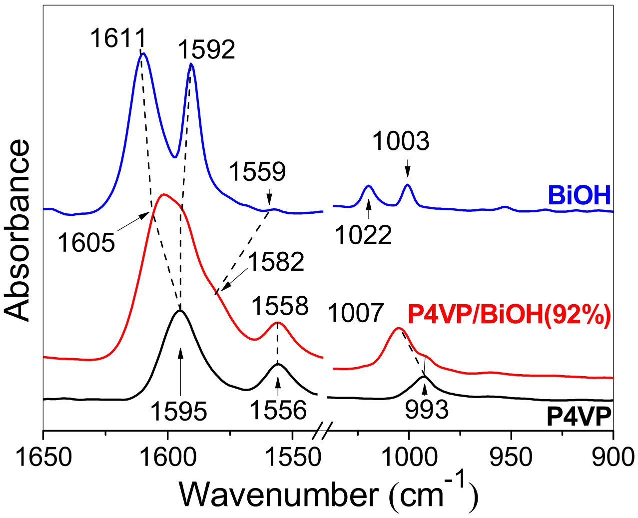

Figure 2.1. Absorbance spectra of pure P4VP powder, pure BiOH powder and electrospun P4VP/BiOH (92%) fibers.

The two bands in the P4VP spectrum at 1595 and 1556 cm^{-1} are assigned to the ν_{8a}[48-49] and ν_{8b}[48] ring stretching modes, respectively. For the P4VP/BiOH(92%) complex, the 1556 cm^{-1} band is shifted slightly to 1558 cm^{-1} and the 1595 cm^{-1} band is shifted to 1605 cm^{-1}, again indicating the formation of hydrogen-bonded pyridine rings.[38-39] In this same region, the spectrum of BiOH shows three bands, located at 1611 cm^{-1}, 1592 cm^{-1} and 1559 cm^{-1}. The 1611 cm^{-1} band is assigned to the ν_{8a} mode[44-47] and shifts toward 1605 cm^{-1} for the complex, overlapping the hydrogen-bonded ν_{8a} P4VP band. The 1592 cm^{-1} band, assigned to the ν_{8b} mode,[44-47] shifts to 1595 cm^{-1} for the complex. Thus, the band around 1600 cm^{-1} for the complexes is composed of four strongly overlapping bands, two from P4VP and two from BiOH, all shifted more closely together by hydrogen bonding. Furthermore, hydrogen bonding causes the BiOH band at 1559 cm^{-1} to shift to 1582 cm^{-1}, forming a weak shoulder on the four-component band around 1600 cm^{-1}.

Due to that strong overlap, quantitative analysis of the extent of hydrogen bonding, which, in principle, can be done by following the relative intensities of the P4VP bands at 1595 and 1605 cm^{-1}, is, in practice, almost impossible. Only the pair of bands at 993 and 1007 cm^{-1} is amenable to quantitative determination of hydrogen-bonded pyridine rings. For this, we use Eq. 2.1,

$$f_b = \frac{I_b}{I_b + I_f / a} \times 100\% \tag{2.1}$$

where f_b is the percentage of hydrogen-bonded pyridine rings, I_b and I_f are the intensity of bands from hydrogen-bonded and free pyridine, respectively, and a is defined as

$$a = \varepsilon_f / \varepsilon_b \tag{2.2}$$

where ε_f and ε_b are the absorption coefficients of the free and the hydrogen-bonded pyridine band, respectively. Determining I_b, I_f and a correctly is critical for obtaining an accurate value for f_b. In a previous work, to evaluate the miscibility of P4VP and a phenolic resin, Kuo et al.[50] calculated f_b by determining I_f and I_b from the areas of the curve-fitted bands at 993 cm^{-1} and 1003 cm^{-1} (the equivalent of the 1007 cm^{-1} band in our case), using a value of 1 for a, with reference to Cesteros et al.[39] However, no value of a for the 993/1003 cm^{-1} band pair was reported by the latter, and, in addition, f_b determined by Kuo et al. for low hydroxyl content was much higher than the theoretical value for maximum complexation, indicating that the value of 1 is overestimated. Therefore, we undertook the necessary work to determine the true value for a.

To do this, spectra must be taken of a series of samples with different BiOH contents. Then, I_f and I_b must be quantified and the plot of I_f vs. I_b must give a straight line of negative slope, from which a can be extracted. This will be valid only if the amount of P4VP probed by the IR beam is constant for each sample. These conditions are not easy to satisfy. In the present case, the samples of interest are solid fibers that must be measured by ATR, where the contact between each sample and the ATR crystal is poorly controlled so that the amount of material detected varies from sample to sample, which makes the plot of I_f vs. I_b meaningless. A similar problem is encountered in transmission mode if the film thickness is not constant.[51] In these situations, choosing an appropriate reference band as an internal standard is essential,[37, 52] in which case a plot of I_f/I_{ref} vs. I_b/I_{ref}, where I_{ref} is the intensity of the reference band, is used to extract a. Three criteria must be satisfied by the reference band: first, it must be isolated; second, its absorption coefficient must remain constant upon complexation; third, it must originate from P4VP. The band at 1068 cm^{-1} (see Fig. 2.S1 and Table 2.S1) appears to be the only one meeting these criteria. However, we found that the plot of I_f/I_{ref} against I_b/I_{ref} had very poor linearity, most likely due to a variation of its absorption coefficient upon complexation with P4VP.

Coleman and coworkers developed a method to determine a without using a reference band,[36-37] notably by casting a hydrogen-bonded polymer blend on an IR window, and calculating a from two spectra recorded at different temperatures. The keys for the success of this method are that the amount of sample in the IR beam must be constant during heating, which is a problem for complexes with small molecules that can evaporate on heating, and the effect of temperature on the band absorption coefficient must be minimal.[37] For the P4VP/BiOH fibers on ATR, this approach is not feasible because the contact between the fibers and the ATR crystal changes significantly with temperature.

An alternative is to analyze a model system, notably the liquid blend EtPy/BiOH. This system is ideal for two reasons. First, as shown in Fig. 2.2, the absorbance and second-derivative spectra of EtPy and EtPy/BiOH are very close to those of P4VP and P4VP/BiOH, respectively, in the region of interest. In particular, the free pyridine ring band at 994 cm^{-1} for EtPy is very close to that at 993 cm^{-1} for P4VP and the hydrogen-bonded pyridine ring band at 1009 cm^{-1} for EtPy/BiOH is close to that of 1007 cm^{-1} for P4VP/BiOH. Second, the distribution of the two components in the liquid is homogeneous, so that an accurate correlation between IR and the chemical ratio of the two components can be obtained. A dilution effect, resulting from the addition of BiOH to EtPy must, however, be taken into account. This can be done straightforwardly, since (1) the precise concentration of EtPy in the EtPy/BiOH liquid blend can be calculated and (2) the contact with the ATR crystal is equally perfect for all samples due to their liquid nature, making the dilution effect the sole correction that needs to be applied. As prior knowledge of the band shapes, widths, etc. for curve-fitting the overlapped bands is not available, a second derivative analysis was done. The latter method has been shown to be a good alternative for obtaining quantitative information on overlapped band components as long as their bandwidth does not change.[53-54]

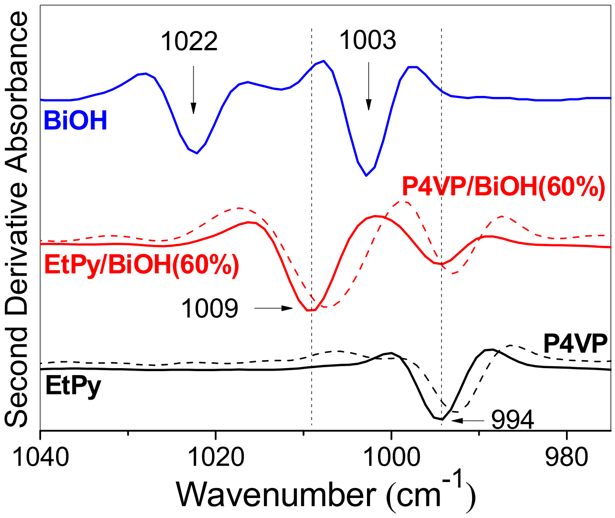

Figure 2.2. Second derivative spectra of (solid lines) pure EtPy liquid, pure BiOH powder and a EtPy/BiOH(60%) liquid blend and of (dashed lines) P4VP powder and electrospun P4VP/BiOH(60%) fibers; all bands are negative.

To determine *a* by this method, the intensities, I_f and I_b, are taken as the absolute values of the negative second derivative bands at the peak positions, 994 and 1009 cm^{-1}, respectively, using the horizontal zero line as the baseline. An error might be introduced by not accounting for a possible contribution from the 1003 cm^{-1} BiOH band, although no evidence for this band is visible in the second derivative spectra of either EtPy/BiOH(60%) or P4VP/BiOH(60%) (Fig. 2.2). An additional contribution around 1005 cm^{-1}, which probably originates from this band, is only discernible in the second derivative spectra of P4VP/BiOH complexes with an excess of BiOH. In any case, any contribution from this band was ignored, and regarded as a possible systematic error in our subsequent analysis. Since the same systematic error, if present, would apply both to the liquid blends and to the P4VP/BiOH fibers, any effect on the final result is considered negligible.

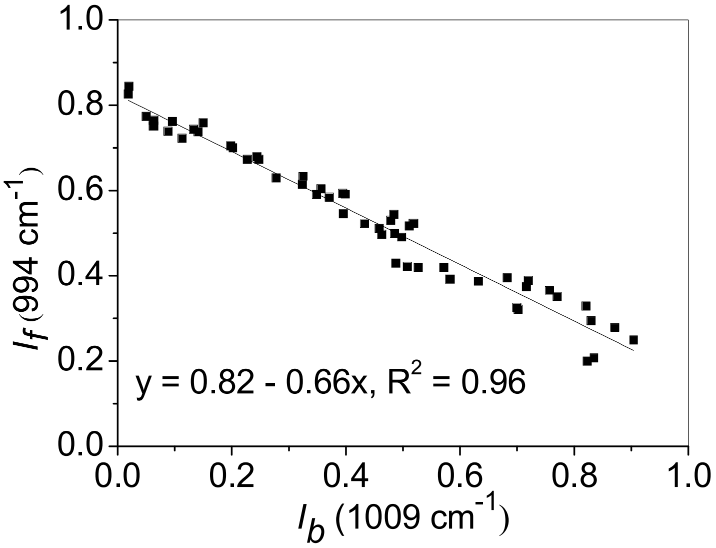

Figure 2.3. The intensity, I_f, of the free pyridine ring band at 994 cm^{-1} versus the intensity, I_b, of the hydrogen-bonded pyridine ring band at 1009 cm^{-1}, as obtained from the second derivative spectra of the EtPy/BiOH(2-60%) liquid blends. The line represents the least-square fit of the data points.

As shown in Fig. 2.3, the plot of I_f vs. I_b determined from the second derivative spectra is linear with a slope of -0.66. To extract a, the value of the slope must be corrected by the dilution factor mentioned above. This can be done as follows. I_f and I_b are related to the absorption coefficients, ε_f and ε_b, whose ratio defines a (Eq. 2.2), by Eqs. 2.3 and 2.4,

$$I_f = \frac{\varepsilon_f n_f}{V} \tag{2.3}$$

$$I_b = \frac{\varepsilon_b n_b}{V} \tag{2.4}$$

where n_f and n_b are the molar amounts of free and hydrogen-bonded pyridine rings detected by ATR and V is the volume of the EtPy/BiOH liquid blend. V can be expressed as the total mass of EtPy/BiOH relative to its density (ρ_{mix}) (Eq. 2.5),

$$V = \frac{M_{EtPy} n_{EtPy} + M_{BiOH} n_{BiOH}}{\rho_{mix}} \tag{2.5}$$

where M_{EtPy} and M_{BiOH} are the molecular weights of EtPy and BiOH, respectively, and n_{EtPy} and n_{BiOH} their molar quantities in the liquid blend.

Extrapolation of the least-squares fit in Fig. 2.3 to the x and y axes provides the intensities for the two extreme situations. In the first, all of the pyridine rings are free, giving $I_{f(pure)}$ (y axis intersect, $I_b = 0$), which occurs for n_{BiOH} equals zero. In the second, all of the pyridine rings are hydrogen-bonded, giving $I_{b(pure)}$ (x axis intersect, $I_f = 0$), which occurs when n_{BiOH} (which contains two OH moieties) is $0.5n_{EtPy}$, assuming that EtPy/BiOH(100%) is fully complexed. In these extreme cases, Eqs. 2.3 and 2.4, with V substituted by Eq. 2.5, are reduced to Eqs. 2.6 and 2.7, respectively.

$$I_{f(pure)} = \frac{\varepsilon_f \rho_{EtPy}}{M_{EtPy}} \tag{2.6}$$

$$I_{b(pure)} = \frac{\varepsilon_b \rho_{mix}}{M_{EtPy} + 0.5M_{BiOH}} \tag{2.7}$$

In Eq. 2.6, which describes pure (liquid) EtPy, ρ_{mix} is simply replaced by ρ_{EtPy}. The hypothesis of full complexation on which Eq. 2.7 is based must be validated experimentally. This is not possible for EtPy/BiOH due to the solubility limit of BiOH in EtPy. However, it can be done with the help of the structurally closely related compound, phenol, which is fully miscible with EtPy over the whole composition range. As shown in Fig. 2.4, the fact that the plot of I_f/I_b against F_{OH} (phenol or BiOH) for EtPy/phenol superposes that for EtPy/BiOH up to 60% F_{OH} shows that their H-bonding behavior in this range is identical. Since the plot for EtPy/phenol continues smoothly to higher F_{OH} and reaches zero at about 100% F_{OH}, as it should for fully hydrogen-bonded complexation, it can be inferred that I_f/I_b should reach 0 for EtPy/BiOH(100%) as well if it were miscible and fully complexed. Therefore, it can be concluded that the assumption that $n_{BiOH}/n_{EtPy} = 0.5$ when $I_f = 0$, leading to Eq. 2.7, is a good approximation.

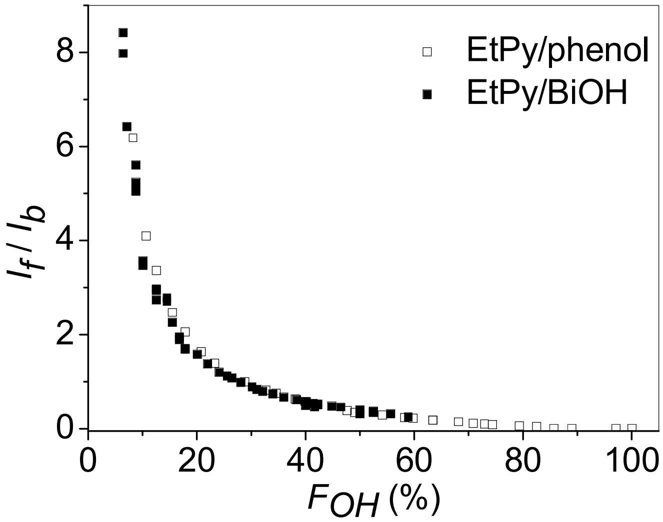

Figure 2.4. The ratio of the intensity of free pyridine rings vs. the intensity of hydrogen-bonded pyridine rings (I_f/I_b) against F_{OH} (mol% OH) obtained from the IR spectra of the EtPy/phenol and EtPy/BiOH liquid blends in the 1040-980 cm^{-1} region.

By substituting ε_f and ε_b in Eq. 2.2 by the rearranged forms of Eqs. 2.6 and 2.7, we arrive at Eq. 2.8, which gives the expression for the corrected value of a.

$$a = \frac{I_{f(pure)}}{I_{b(pure)}} \times \frac{\rho_{mix} M_{EtPy}}{\rho_{EtPy}\left(M_{EtPy} + 0.5 M_{BiOH}\right)} \tag{2.8}$$

Since the ratio, $I_{f(pure)}/I_{h(pure)}$, also corresponds to the slope of the least-squares fit in Fig. 2.3 (value of 0.66), it is clear that the righthand factor in Eq. 2.8 corresponds to the dilution factor that must be used to correct the value for a obtained from the slope. The variable, ρ_{mix}, which is the density of EtPy/BiOH(100%), cannot be measured due to the solubility limit of BiOH in EtPy, but it can be estimated as 1.06 g/mL by mass averaging. This estimated value was validated by measuring the density of EtPy/BiOH(28%), which was 1.01 g/mL and compares very well with the mass averaged density of 0.99 g/mL.

Now a can be calculated using Eq. 2.8, from which a value of 0.40 is obtained, considering that $I_{f(pure)}/I_{h(pure)} = 0.66$, $\rho_{mix} = 1.06$ g/mL, $\rho_{EtPy} = 0.942$ g/mL, $M_{EtPy} = 107.15$

g/mol, and M_{BiOH} = 186.21 g/mol. This allows determining f_b from Eq. 2.1 using the intensities of the 994 and 1009 cm^{-1} bands (determined by the second derivative spectra). Fig. 2.5 shows the plot of f_b as a function of BiOH hydroxyl content from 0 to 60% for the EtPy/BiOH solutions. The agreement with the theoretical curve (red line in Fig. 2.5, representing full complexation) is excellent, indicating that all of the BiOH molecules are hydrogen bonded with both OH functions of each BiOH molecule, in accordance with the analysis related to Fig. 2.4. This is supported by the fact that the IR band at 3350 cm^{-1} for BiOH, which is due to the O-H stretching vibration (ν(OH)) in self-associated BiOH,[55] is not found in the spectra of the liquid blends (see Fig. 2.S3). Therefore, it appears that the supramolecular complex formed in the EtPy/BiOH liquid is composed of a BiOH molecule flanked by an EtPy molecule on each side, thus with the formula $EtPy_2BiOH$, and that each hydrogen bond involves one pyridine ring and one hydroxyl group. This result is in contrast with the hypothesis from Beezer et al. that, in pyridine/phenol blends in CCl_4, a complex can be formed with one OH group interacting with two pyridine rings (pyridine$_2$/phenol) or with one pyridine ring interacting with two OH groups (pyridine/phenol$_2$) when pyridine or phenol is in large excess, respectively.[56]

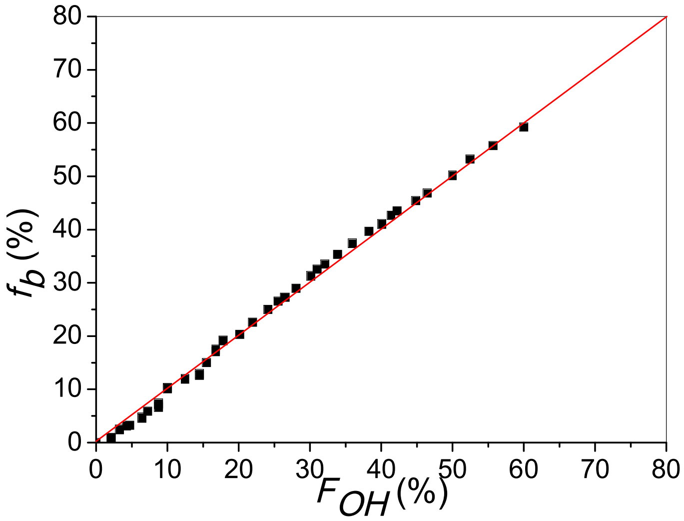

Figure 2.5. Percentage of hydrogen-bonded pyridine rings, f_b (%), as a function of BiOH content, F_{OH} (%), for EtPy/BiOH liquid blends. The red line describes the theoretical values for full complexation of BiOH to EtPy.

We can finally reach our goal, which is to calculate f_b in the electrospun P4VP/BiOH fibers, using Eq. 2.1 and the relative intensities of the 1007 and 993 cm^{-1} bands determined from the second derivative spectra. The results are shown in Fig. 2.6, where it is observed that f_b increases linearly with BiOH content up to more than 100% BiOH. The slope of 0.76, which is lower by 24% than what would be obtained if the BiOH molecules were fully complexed to P4VP (red line in Fig. 2.6), indicates that a fraction of the BiOH hydroxyl groups in the fibers remains free. It is possible that each BiOH molecule is actually complexed with P4VP, but some by only one hydroxyl group, assuming little loss of BiOH during electrospinning and drying of the fibers. This assumption was validated by a nuclear magnetic resonance analysis of P4VP/BiOH(92%) fibers redissolved in deuterated methanol, which showed that the BiOH fraction in the fibers was similar to that in the original solution. The continued linear increase of f_b to about 125% BiOH is followed by a slow approach to the maximum P4VP complexation of 100%, which is only reached in the presence of a large excess of BiOH (F_{OH} $\geq$ 160%).

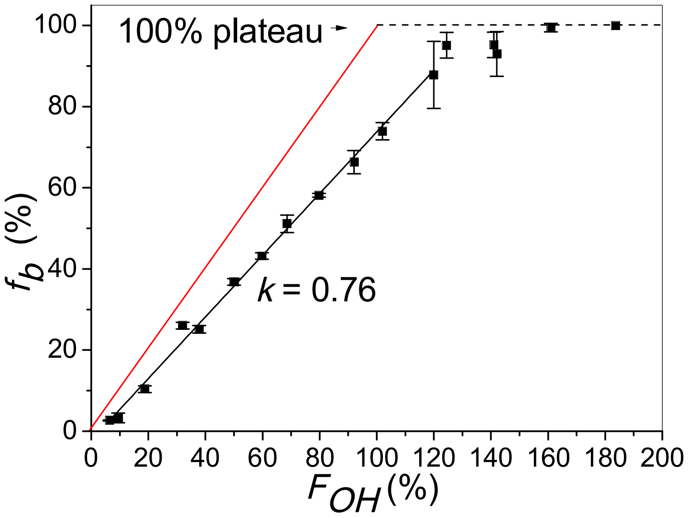

Figure 2.6. Percentage of hydrogen-bonded pyridine rings, f_b (%), as a function of BiOH content, F_{OH} (%) for P4VP/BiOH electrospun fibers. The red line describes the theoretical values for full complexation of BiOH to P4VP.*

* Error bars present the standard deviation of uncertainty.

The incomplete hydrogen-bond complexation in the P4VP/BiOH fibers, compared to full complexation in the EtPy/BiOH and EtPy/phenol liquid blends, can be related, in part, to the electrospinning process. The very fast solvent evaporation rate and the probability that BiOH is largely hydrogen bonded to DMF in solution likely kinetically limits OH-Pyridine complexation. This may be exacerbated by the high Tg of P4VP (about 142 °C), which restricts chain mobility and reorganization to accommodate the double hydrogen bonding per BiOH molecule. In addition, steric effects of polymer chain connectivity might affect the hydrogen bonding interactions of BiOH with the P4VP repeat units.[57] The fact that f_b is always larger than 50% of F_{OH} suggests that, like for EtPy/BiOH, one pyridine is complexed to one hydroxyl group. It also indicates that at least some BiOH molecules are hydrogen bonded to two P4VP repeat units, which is required for BiOH to effectively crosslink the P4VP chains by hydrogen bonding.

Incomplete hydrogen bonding was reported also for polymer blends, notably by Garton[57] and by Kuo et al.[50] In the first case, for a polycaprolactone/phenoxy blend with equimolar carbonyl and hydroxy groups, less than 35% of the carbonyl groups were hydrogen-bonded by OH groups, and this increased to only 50% when the hydroxyls were in 15-fold excess.[57] In the second case, for a P4VP/phenolic blend, the free pyridine band at 993 cm^{-1} was visible as a shoulder in the IR spectra even for a OH/VP molar ratio of four.[50] As mentioned above, a value of $a = 1$ was used to calculate f_b, which means that for a F_{OH} of 25% and I_b/I_f of 0.66, f_b is 40% according to Eq. 2.1. This is much higher than F_{OH}, which is not reasonable. However, if the value of $a = 0.4$, as we determined, is used instead, then f_b is 21%, which is 84% of F_{OH}.

2.6 Conclusion

We determined the proportion of hydrogen-bonded pyridine rings (f_b) in P4VP/BiOH electrospun fibers by IR spectroscopy, using the intensities of the free and hydrogen-bonded pyridine ring bands at 993 and 1007 cm^{-1}, respectively, as determined from the second derivative spectra. To do this, it was necessary to determine the ratio of the absorption coefficients, a, for this pair of bands. This was accomplished by analyzing the ATR spectra of model liquid blends, EtPy/BiOH and EtPy/phenol, leading to $a = 0.40$. The results show that, in P4VP/BiOH electrospun fibers, when the molar percentage of the hydroxyl groups relative to the pyridine rings (F_{OH}) is lower than 100%, f_b is about 76% of F_{OH}. Complete hydrogen bonding of P4VP is reached only for a large excess of BiOH, notably for $F_{OH} \geq 160\%$. In comparison, for the EtPy/BiOH liquid blend, f_b equals F_{OH}, indicating one-to-one complexation between the pyridine ring and the hydroxyl group. The different extents of hydrogen bonding in P4VP/BiOH and EtPy/BiOH is attributed mainly to steric and kinetic effects. We believe that our method, by sidestepping the requirement for an internal reference band, can find use for a broad range of supramolecular complexes and polymer blends as long as a suitable liquid model of the polymer repeat unit is available.

2.7 Acknowledgements

This work was supported by the Natural Sciences and Engineering Research Council of Canada (NSERC) and Fonds de recherche du Québec – Nature et Technologie (FRQNT). X.W. thanks the China Scholarship Council (CSC) and Université de Montréal for financial support.

2.8 Supplementary information

The characteristics of the band assignments in Tables 2.S1 and 2.S2 are indicated as follows: ν: stretching vibration; δ: in-plane bending vibration; γ: out-of-plane bending vibration; τ: torsional vibration; def: deformation; ν_ϕ, δ_ϕ, γ_ϕ and τ_ϕ: simultaneous stretching, in-plane bending, out-of-plane bending and torsional vibration of the ring; γ_w: wagging vibration; γ_r: rocking vibration; as: asymmetric; ν(CX): stretching vibrations of the bond between the pyridine ring and the main chain; *s*: strong; *m*: medium; *w*: weak; *vw*: very weak; *sh*: shoulder; *h*: hidden band; *dh*: deeply hidden band.

P4VP/BiOH

The literature assignments of the P4VP and BiOH bands below 1700 cm^{-1} and the tentative attribution of the bands in the complex spectrum are summarized in Table 2.S1. The position of overlapped bands was determined based on the second derivative spectra (see Fig. 2.S1b); therefore, some bands listed in Table 2.S1 are not clearly visible in Fig. 2.S1.

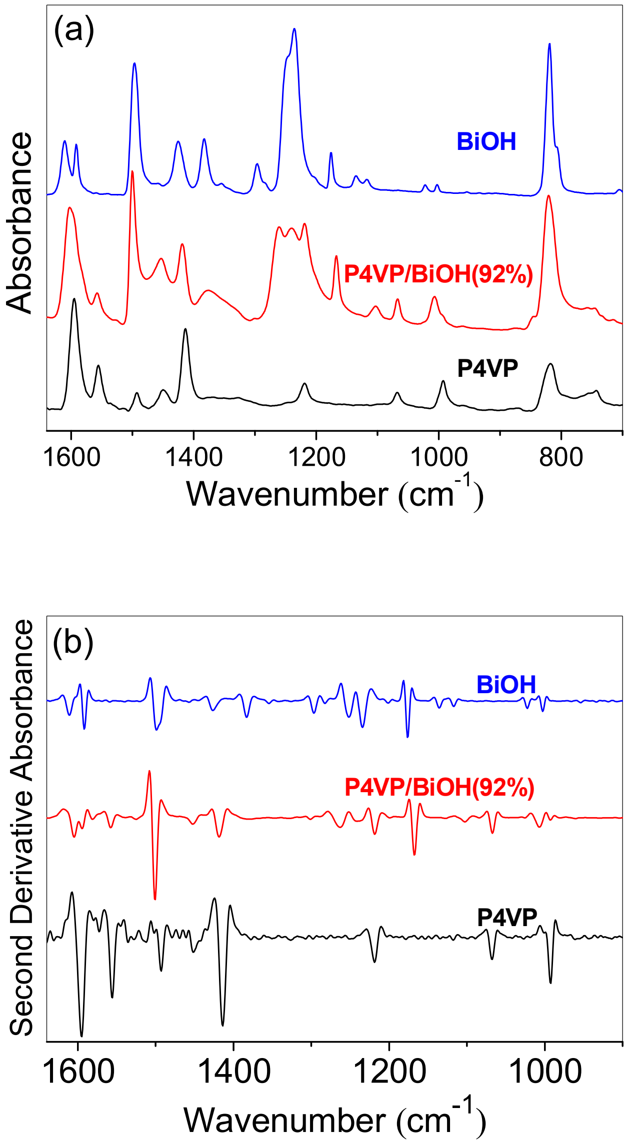

Figure 2.S1. (a) Absorbance spectra and (b) second derivative spectra of pure P4VP powder, pure BiOH powder and electrospun P4VP/BiOH(92%) fibers.

Table 2.S1. Tentative band assignments for P4VP, BiOH and P4VP/BiOH(92%).

Ref	Assignment	P4VP	P4VP/BiOH	BiOH	Assignment	Ref
48	ν_{8a}	1595.3,*s*	1605,*s*	1611,*s*	ν_{8a}	44-47
			1594.5,*sh*	1591.8,*s*	ν_{8b}	44-47
			1581.5,*sh*	1558.9,*w*	753(γ(CH)) +814(ν(CO))	55
48	ν_{8b}	1556,*m*	1558,*m*			
48, 58	ν_{ϕ}	1492.6,*m*	1501,*s*	1499,*s* 1494,*sh*	ν_{ϕ},δ(CH)	45-47
43, 48, 58	$\delta(CH_2)$,$\delta(CH_2)_{as}$	1451.7,*m*	1452.5,*m*			
48, 58	ν_{ϕ}	1413.9,*s*	1418.5,*s*	1426.6,*s*	ν_{ϕ},δ(CH)	45-47
43, 48, 58-59	$\gamma_w(CH_2)$,ν(CX),$\delta(CH_2)$	1378,*vw*	1380,*vw*	1383.5,*s*	416(ring def)+972(γ(CH))	55
48	δ(CH)	1326.6,*w*	1330,*vw*	1326,*sh*	ν(CC),δ(CH)	45, 47, 55
			1301,*w*	1296.6,*m*	δ(CH)	55
42, 59	ν(CN),δ(CH)	1263,*w*	1263,*m*	1251.7,*sh*	ν(CO)	55
			1241.5,*m*	1234.6,*s*	ν(CO),δ(OH),δ(CH),δ(CC)	44-45, 47
42-43, 58-60	δ(CH),ν_{ϕ},ν(CX)	1218.7,*m*	1219,*s*			
42-43, 58-60	δ(CH),ν_{ϕ},$\delta(CH_2)$,$\gamma_r(CH_2)$	1180,*vw*	1167.8,*s*	1176,*s*	δ(CH),ν(CC),δ(OH)	44-45
58-59	δ(CH), $\delta(CH_2)$,$\gamma_r(CH_2)$	1108,*vw*	1102.8,*m*	1135.6,*m*	δ(CH),ν(CC)	44-45
				1117,*m*	ν(CC),δ(CH)	44-47
42-43, 58	ν_{ϕ},$\delta(CH_2)$,δ_{ϕ}	1067.9,*m*	1067.5,*m*			
			1024,*vw*	1022.4,*m*	ν(CC),δ(CH)	44-46
42-43	ν_{ϕ},δ_{ϕ},τ_{ϕ},γ(CH),$\gamma_r(CH_2)$	992.8,*m*	1007,*m*			
			1005,*dh*	1003,*m*	δ_{ϕ},ν(CC)	46-47
42-43, 58, 60	γ(CH),$\gamma_r(CH_2)$	958,*w*	960,*vw*	965,*w* 954,*w*	γ(CH)	45-47
58	γ(CH)	872.4,*vw*	872.70,*vw*			
			847.7,*w*			
58	γ(CH)	826.8,*sh*	823,*s*	818.7,*s*	γ(CH)	44-46
58	γ(CH)	815,*m*	813,*sh*	805.2,*sh*	$\nu(CO)_{as}$,$\nu(CC)_{as}$,δ(CH)	44-45, 47, 61

EtPy/BiOH

Fig. 2.S2 shows that both the absorbance and second-derivative spectra of EtPy and the EtPy/BiOH liquid blend are very close to those of P4VP and of the P4VP/BiOH complex, respectively. The main difference between Tables 2.S1 and 2.S2 is the exact absorption frequencies.

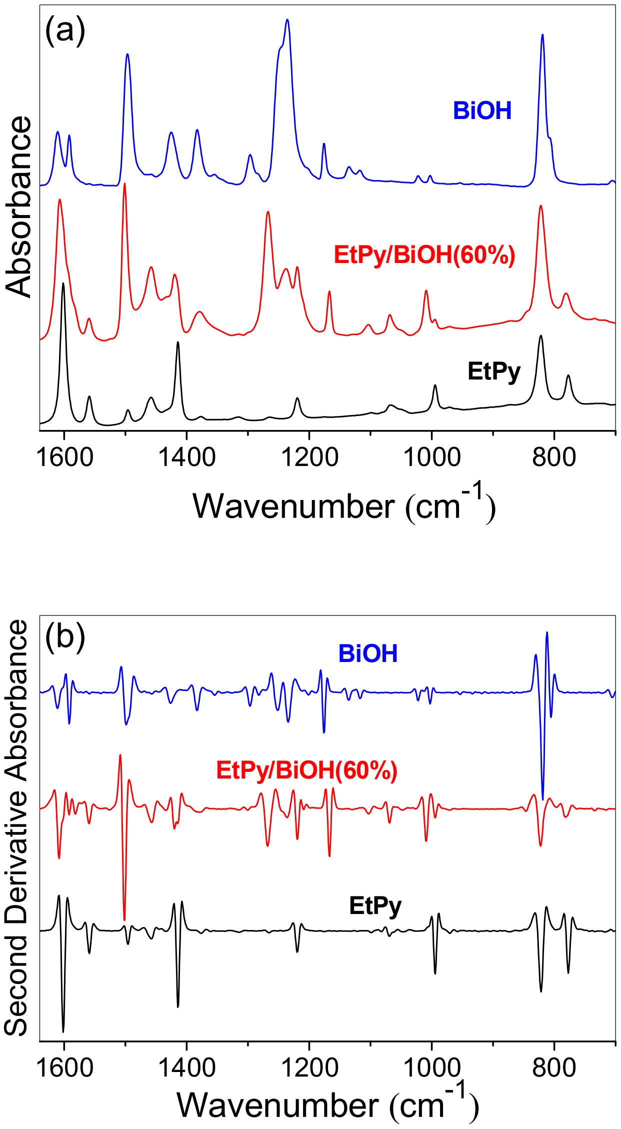

Figure 2.S2. (a) Absorbance spectra and (b) second derivative spectra of pure EtPy liquid, pure BiOH powder and an EtPy-BiOH(60%) liquid blend.

Table 2.S2. Tentative band assignment for EtPy, BiOH and EtPy/BiOH(60%).

Ref	Assignment	EtPy	EtPy/BiOH	BiOH	Assignment	Ref
48	ν_{8a}	1601.7,*s*	1608.5,*s*	1611,*s*	ν_{8a}	44-47
			1592.1,*sh*	1591.8,*s*	ν_{8b}	44-47
			1582,*sh*	1558.9,*w*	753(γ(CH)) +814(ν(CO))	55
48	ν_{8a}	1559.1,*m*	1559,*m*			
48, 58	ν_{ϕ}	1496.1,*m*	1501.8,*s*	1499,*s* 1494,*sh*	ν_{ϕ},δ(CH)	45-47
43, 48, 58	$\delta(\mathrm{CH}_2)$, $\delta(\mathrm{CH}_3)_{as}$	1458,*m*	1458.2,*m* 1434.7,*sh*			
			1421.3,*m*	1426.6,*s*	ν_{ϕ},δ(CH)	45-47
48, 58	ν_{ϕ}	1414.4,*s*	1415,*sh*			
43, 48, 58-59	$\gamma_w(\mathrm{CH}_2)$,ν(CX),$\delta(\mathrm{CH}_3)$,ν_{ϕ}	1376.8,*w*	1383,*w*	1383.5,*s*	416(ring def)+972(γ(CH))	55
43, 48, 58	δ(CH)	1361.3,*vw*	1378,*sh*			
48	δ(CH)	1338.3,*vw*	1344,*vw*	1342,*vw*	814($\nu(\mathrm{CO})_{as}$)+530($\nu(\mathrm{CO})_{as}$)	55
44-45, 48, 58	δ(CH)	1315.3,*w*	1316,*vw*	1326,*sh*	ν(CC),δ(CH)	45, 47, 55
			1300,*vw*	1296.6,*m*	δ(CH)	55
42, 59	ν(CN),δ(CH)	1265.5,*w*	1268.6,*s*	1251.7,*sh*	ν(CO)	55
			1246,*sh* 1236,*m*	1234.6,*s*	ν(CO),δ(OH),δ(CH),δ(CC)	44-45, 47
42-43, 58-60	δ(CH),ν_{ϕ},ν(CX)	1220,*m*	1219,*s*			
42-43, 58-60	δ(CH),ν_{ϕ},$\delta(\mathrm{CH}_3)$,$\gamma_r(\mathrm{CH}_2)$	1175.7,*vw*	1167.9,*s*	1176,*s*	δ(CH),ν(CC),δ(OH)	44-45
58-59	δ(CH),$\delta(\mathrm{CH}_3)$,$\gamma_r((\mathrm{CH}_3))$	1099.3,*vw*	1102,*m*	1135.6,*m* 1117,*m*	δ(CH),ν(CC) ν(CC),δ(CH)	44-45 44-47
42-43, 58	ν_0,$\delta(\mathrm{CH}_3)$,δ_{ϕ}	1068,*m* 1063,*sh*	1069.4,*s*			
42-43, 58-60	$\gamma_r(\mathrm{CH}_3)$	1046.5,*sh*	1047.9,*w*			
				1022.4,*m*	ν(CC),δ(CH)	44-46
42-43	ν_{ϕ},δ_{ϕ},τ_{ϕ},γ(CH),$\gamma_r(\mathrm{CH}_3)$	994.4,*m*	1009.3,*s*			
				1003,*m*	δ_0,ν(CC)	46-47
42-43, 58, 60	γ(CH), $\gamma_r(\mathrm{CH}_3)$	970.6,*vw*	970.87,*w*	965,*w*	γ(CH)	45-47
42-43, 58, 60	γ(CH), $\gamma_r(\mathrm{CH}_3)$	958,*sh*	957.32,*sh*	954,*w*	γ(CH)	45-47
			847,*w*			
58	γ(CH)	821.8,*s*	822.2,*s*	818.7,*s*	γ(CH)	44-46
				805.2,*sh*	$\nu(\mathrm{CO})_{as}$,$\nu(\mathrm{CC})_{as}$,δ(CH)	44-45, 47, 61

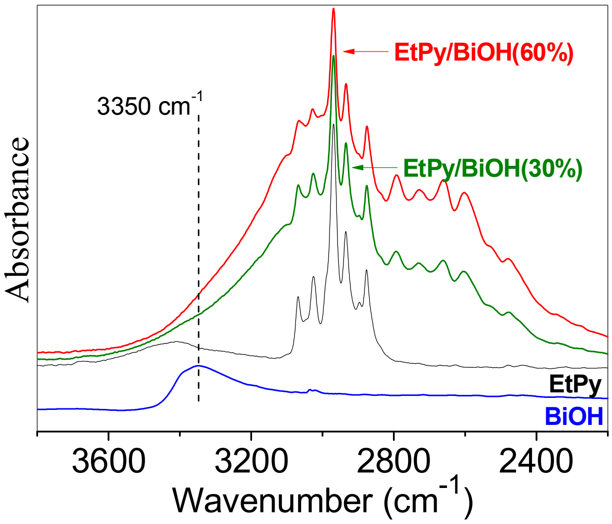

Figure 2.S3. Absorbance spectra of pure BiOH powder, pure EtPy liquid, and EtPy/BiOH(30%) and EtPy-BiOH(60%) liquid blends. The absorption band at around 3400 cm^{-1} in the spectra of EtPy is attributed to water.

2.9 References

1. Lehn, J.-M., *Supramolecular Chemistry: Concepts and Perspectives*. 1st ed.; Wiley-VCH: New York: 1995.
2. Binder, W. H.; Zirbs, R., *Adv. Polym. Sci.* **2007,** 207, 1-78.
3. Bouteiller, L., *Adv. Polym. Sci.* **2007,** 207, 79-112.
4. Lehn, J.-M., *Chem. Soc. Rev.* **2007,** 36, 151-160.
5. McLaughlin, C. K.; Hamblin, G. D.; Sleiman, H. F., *Chem. Soc. Rev.* **2011,** 40, 5647-5656.
6. ten Brinke, G.; Ruokolainen, J.; Ikkala, O., *Adv. Polym. Sci.* **2007,** 207, 113-177.
7. Whitesides, G. M.; Mathias, J. P.; Seto, C. T., *Science* **1991,** 254, 1312-1319.
8. Wuest, J. D., *Chem. Commun.* **2005**, 5830-5837.
9. ten Brinke, G.; Ikkala, O., *Chem. Rec.* **2004,** 4, 219-230.
10. Ikkala, O.; ten Brinke, G., *Chem. Commun.* **2004**, 2131-2137.
11. Ikkala, O.; ten Brinke, G., *Science* **2002,** 295, 2407-2409.

12. Brandys, F. A.; Bazuin, C. G., *Chem. Mater.* **1996,** 8, 83-92.
13. Tiitu, M.; Torkkeli, M.; Serimaa, R.; Makela, T.; Ikkala, O., *Solid State Ionics* **2005,** 176, 1291-1299.
14. Gu, B.; Yin, M.; Zhang, A. P.; Qian, J.; He, S., *Opt. Express* **2011,** 19, 4140-4146.
15. Ikkala, O.; Ruokolainen, J.; ten Brinke, G.; Torkkeli, M.; Serimaa, R., *Macromolecules* **1995,** 28, 7088-7094.
16. Belfiore, L. A.; McCurdie, M. P.; Das, P. K., *Polymer* **2001,** 42, 09995-10006.
17. Benouazzane, M.; Bravo-Grimaldo, E.; Bissessur, R.; Bazuin, C. G., *Macromolecules* **2006,** 39, 5364-5370.
18. Zhu, X.; Beginn, U.; Moeller, M.; Gearba, R. I.; Anokhin, D. V.; Ivanov, D. A., *J. Am. Chem. Soc.* **2006,** 128, 16928-16937.
19. Zhang, Q.; Bazuin, C. G.; Barrett, C. J., *Chem. Mater.* **2008,** 20, 29-31.
20. Zhang, Q.; Wang, X.; Barrett, C. J.; Bazuin, C. G., *Chem. Mater.* **2009,** 21, 3216-3227.
21. Ruokolainen, J.; Torkkeli, M.; Serimaa, R.; Komanschek, E.; ten Brinke, G.; Ikkala, O., *Macromolecules* **1997,** 30, 2002-2007.
22. van Zoelen, W.; Asumaa, T.; Ruokolainen, J.; Ikkala, O.; ten Brinke, G., *Macromolecules* **2008,** 41, 3199-3208.
23. Perepichka, I. I.; Lu, Q.; Badia, A.; Bazuin, C. G., *Langmuir* **2013,** 29, 4502-4519.
24. Huang, W. H.; Chen, P. Y.; Tung, S. H., *Macromolecules* **2012,** 45, 1562-1569.
25. Sidorenko, A.; Tokarev, I.; Minko, S.; Stamm, M., *J. Am. Chem. Soc.* **2003,** 125, 12211-12216.
26. Nandan, B.; Gowd, E. B.; Bigall, N. C.; Eychmueller, A.; Formanek, P.; Simon, P.; Stamm, M., *Adv. Funct. Mater.* **2009,** 19, 2805-2811.
27. Roland, S.; Prud'homme, R. E.; Bazuin, C. G., *ACS Macro Lett.* **2012,** 1, 973-976.
28. Roland, S.; Pellerin, C.; Bazuin, C. G.; Prud'homme, R. E., *Macromolecules* **2012,** 45, 7964-7972.
29. Laforgue, A.; Bazuin, C. G.; Prud'homme, R. E., *Macromolecules* **2006,** 39, 6473-6482.
30. Priimagi, A.; Vapaavuori, J.; Rodriguez, F. J.; Faul, C. F. J.; Heino, M. T.; Ikkala, O.; Kauranen, M.; Kaivola, M., *Chem. Mater.* **2008,** 20, 6358-6363.
31. Vapaavuori, J.; Priimagi, A.; Kaivola, M., *J. Mater. Chem.* **2010,** 20, 5260-5264.

32. Priimagi, A.; Cavallo, G.; Forni, A.; Gorynsztejn-Leben, M.; Kaivola, M.; Metrangolo, P.; Milani, R.; Shishido, A.; Pilati, T.; Resnati, G.; Terraneo, G., *Adv. Funct. Mater.* **2012,** 22, 2572-2579.
33. Shibata, M.; Kimura, Y.; Yaginuma, D., *Polymer* **2004,** 45, 7571-7577.
34. Loveless, D. M.; Jeon, S. L.; Craig, S. L., *Macromolecules* **2005,** 38, 10171-10177.
35. Yount, W. C.; Loveless, D. M.; Craig, S. L., *J. Am. Chem. Soc.* **2005,** 127, 14488-14496.
36. Moskala, E. J.; Howe, S. E.; Painter, P. C.; Coleman, M. M., *Macromolecules* **1984,** 17, 1671-1678.
37. Lee, J. Y.; Painter, P. C.; Coleman, M. M., *Macromolecules* **1988,** 21, 346-354.
38. Lee, J. Y.; Painter, P. C.; Coleman, M. M., *Macromolecules* **1988,** 21, 954-960.
39. Cesteros, L. C.; Meaurio, E.; Katime, I., *Macromolecules* **1993,** 26, 2323-2330.
40. Soininen, A. J.; Tanionou, I.; ten Brummelhuis, N.; Schlaad, H.; Hadjichristidis, N.; Ikkala, O.; Raula, J.; Mezzenga, R.; Ruokolainen, J., *Macromolecules* **2012,** 45, 7091-7097.
41. Korhonen, J. T.; Verho, T.; Rannou, P.; Ikkala, O., *Macromolecules* **2010,** 43, 1507-1514.
42. Arenas, J. F.; Tocon, I. L.; Otero, J. C.; Marcos, J. I., *J. Mol. Struct.* **1997,** 410-411, 443-446.
43. Lopez, T. I.; Woolley, M. S.; Otero, J. C.; Marcos, J. I., *J. Mol. Struct.* **1998,** 470, 241-246.
44. Kubinyi, M.; Billes, F.; Grofcsik, A.; Keresztury, G., *J. Mol. Struct.* **1992,** 266, 339-344.
45. Lampert, H.; Mikenda, W.; Karpfen, A., *J. Phys. Chem. A* **1997,** 101, 2254-2263.
46. Michalska, D.; Bienko, D. C.; Abkowicz-Bienko, A. J.; Latajka, Z., *J. Phys. Chem.* **1996,** 100, 17786-17790.
47. Michalska, D.; Zierkiewicz, W.; Bienko, D. C.; Wojciechowski, W.; Zeegers-Huyskens, T., *J. Phys. Chem. A* **2001,** 105, 8734-8739.
48. Panov, V. P.; Kazarin, L. A.; Dubrovin, V. I.; Gusev, V. V.; Kirsh, Y. E., *Zh. Prikl. Spektrosk.* **1974,** 21, 862-869.
49. Mayo, D. W.; Miller, F. A.; Hannah, R. W., Course Notes on the Interpretation of Infrared and Raman Spectra. John Wiley & Sons: 2004.
50. Kuo, S.-W.; Lin, C.-L.; Chang, F.-C., *Polymer* **2002,** 43, 3943-3949.

51. Liang, Y.; Mauran, D.; Prud'homme, R. E.; Pellerin, C., *Appl. Spectrosc.* **2008,** 62, 941-947.
52. Guevremont, J.; Ajji, A.; Cole, K. C.; Dumoulin, M. M., *Polymer* **1995,** 36, 3385-3392.
53. Dong, A.; Huang, P.; Caughey, W. S., *Biochemistry* **1990,** 29, 3303-3308.
54. Sasic, S.; Ozaki, Y., Raman, Infrared, and Near-Infrared Chemical Imaging. John Wiley & Sons: 2011.
55. Evans, J. C., *Spectrochim. Acta* **1960,** 16, 1382-1392.
56. Beezer, A. E.; Hawksworth, W. A.; Orban, M.; Tyrrell, H. J. V., *J. Chem. Soc., Faraday Trans. 1* **1977,** 73, 1326-1333.
57. Garton, A., *Polym. Eng. Sci.* **1984,** 24, 112-116.
58. Topacli, A.; Bayari, S., *Spectrochim. Acta, Part A* **1999,** 55A, 1389-1394.
59. Shakila, G.; Periandy, S.; Ramalingam, S., *Spectrochim. Acta, Part A* **2011,** 78A, 732-739.
60. Sert, Y.; Ucun, F.; Boeyuekata, M., *Indian J. Phys.* **2012,** 86, 859-869.
61. PoIjansek, I.; Krajnc, M., *Acta Chim. Slov.* **2005,** 52, 238-244.

Chapter 3: Effect of small molecule hydrogen-bond crosslinker and solvent power on the electrospinnability of poly(4-vinyl pyridine)*

3.1 Résumé

La fabrication de fibres électrofilées requiert généralement des solutions relativement concentrées pour obtenir suffisamment d'enchevêtrements agissant comme des points de réticulation physique pendant le processus d'électrofilage. Nous proposons une approche supramoléculaire afin de diminuer la concentration nécessaire. À cette fin, nous avons étudié l'impact d'un agent de réticulation formant de faibles liaisons hydrogène, le 4,4'-biphénol (BiOH), sur le comportement d'électrofilage de la poly(4-vinylpyridine) (P4VP) dans le N,N-diméthylformamide (DMF) et dans un mélange de DMF et de nitrométhane (CH_3NO_2). Puisque la rhéologie de solutions joue un rôle crucial durant le processus d'électrofilage, diverses propriétés de la solution ont été caractérisées. La pelote statistique de polymère a prend de l'expansion suite à l'ajout de BiOH mais se contracte avec l'addition de CH_3NO_2 (un mauvais solvant). La réticulation par liaisons hydrogène dans les solutions de P4VP/BiOH (mélange équimolaire pyridine:hydroxyle) a été quantifiée par spectroscopie infrarouge à réflexion totale atténuée (ATR) et il s'est avéré qu'elle augmente avec la concentration de la P4VP, en particulier dans le mélange de solvants. La réticulation par liaisons hydrogène et l'effet du mauvais solvant améliorent ainsi la formation d'un réseau réticulé. Cette situation conduit à l'apparition du régime semi-dilué enchevêtré à des concentrations moins élevées abaissant ainsi par un facteur deux la concentration critique pour la formation de fibres. Par ailleurs, l'ajout de BiOH mène à un régime concentré apparent qui permet la préparation de fibres uniformes. Sur la base de cette stratégie supramoléculaire qui augmente la réticulation

---

* Published as a full paper in *Polymer* **2015**, 57, 62-69 by Xiaoxiao Wang, C. Geraldine Bazuin and Christian Pellerin.

effective, il est possible de préparer de longues fibres électrofilées alignées sans l'obligation d'utiliser des solutions très visqueuses.

3.2 Abstract

The fabrication of electrospun fibers generally requires relatively concentrated solutions to have sufficient chain entanglements acting as physical crosslinks during the electrospinning process. We propose a supramolecular approach to diminish the necessary concentration. To this end, we investigated the use of a small hydrogen-bond effective crosslinker, 4,4'-biphenol (BiOH), on the electrospinning behavior of poly(4-vinyl pyridine) (P4VP) in N,N-dimethylformamide (DMF) and in a mixture of DMF and nitromethane (CH_3NO_2). Since solution rheology plays a crucial role in the electrospinning process, various solution properties were characterized. Coil dimensions showed expansion with the addition of BiOH and contraction with the addition of CH_3NO_2 (a poor solvent). Hydrogen-bond crosslinking in solutions of P4VP/BiOH (equimolar pyridine:hydroxyl) was quantified by attenuated total reflection (ATR) infrared spectroscopy, and was found to increase with increasing P4VP concentration, especially in the mixed solvent. Hydrogen-bond crosslinking and the effect of the poor solvent thus enhance the formation of an effectively crosslinked network. This leads to an earlier onset of the apparent semidilute entangled regime and, hence, to a lower critical concentration for fiber formation, which decreases by a factor of two. Furthermore, the addition of BiOH leads to the appearance of a clear concentrated regime that enables preparing uniform fibers. Based on this supramolecular strategy for increasing the effective crosslinking network, it is possible to prepare long aligned electrospun fibers without the need for using highly viscous solutions.

3.3 Introduction

Electrospinning is a widely used technique to create continuous polymer fibers with diameters from tens of nm to several μm. A prerequisite for producing continuous fibers and for avoiding droplets caused by capillary instability is the formation of an effective polymer network. Efforts have been made to establish relationships between the rheological behavior of the polymer solution and the electrospinning process. For example, it was shown that the formation of fibers is possible when the product of the polymer concentration and the intrinsic viscosity ($c[\eta]$) exceeds 5.[1] McKee et al. further showed that the formation of beaded fibers is obtained above the entanglement concentration (c_e).[2] Shenoy et al. suggested that beaded fibers can form when the number of entanglements per chain surpasses 1, though this conclusion is only valid for polymers in good solvents without specific polymer-polymer association.[3] These and other works highlight the crucial role of entanglements for the successful electrospinning of polymer solutions. The entanglements are, in fact, responsible for the formation of an effective crosslink network in the timescale of fiber formation in the electrospinning jet. This means, first, that fibers can form only for polymers with molecular weights above the entanglement molecular weight (M_e) and, second, only for solution concentrations that are in the entangled regime (although too high a concentration leads to such high viscosities that electrospinning is impossible even with a high applied voltage).

Increasing the solution entanglement density, either by increasing the polymer molecular weight or the solution concentration, is therefore the most common strategy for facilitating the formation of uniform fibers rather than drops or beaded fibers. An alternative method is to add an easily electrospinnable polymer, usually a high molecular weight polymer with a flexible backbone such as poly(ethylene oxide) (PEO), to less or non fiber-forming polymers like many natural biomacromolecules[4] and polyelectrolytes[5-7] that possess rigid chains. Still another approach is to increase the entanglement density by increasing the flexibility of the polymer chains in solution. This approach was used to overcome the difficulty in electrospinning sodium alginate (SA)/water solutions by adding glycerol as a cosolvent, which interacts more strongly with SA, thereby reducing hydrogen bonding between SA repeat units and leading to a more flexible chain conformation.[8] Similarly, it was found that the addition of NaCl into a poly(2-dimethylamino ethyl methacrylate hydrochloride) aqueous solution, by screening the repulsive electrostatic interactions to make the chains coil-like, leads to fiber formation at a lower concentration than that for the pure aqueous solution.[9]

Two additional strategies to improve the electrospinnability of polymer solutions are to decrease the surface tension and to introduce effective crosslinks (also called physical or temporary crosslinks) in addition to those provided by entanglements. Fong et al. found that beaded fibers are obtained from a 3 wt% PEO/water solution, which has a high surface tension (75.8 mN/m), whereas uniform fibers are obtained when using water/ethanol (57/40 mass ratio) with a lower surface tension of 50.5 mN/m.[10] Similarly, it was shown that fibers can be electrospun at lower concentration from a PEO/ethanol (4 wt%) solution than from a PEO/water (7 wt%) solution.[11] Adding surfactants can also decrease the surface tension and aid in electrospinning, as demonstrated by the addition of TritonX-100 or Pluronic F127 that leads to uniform SA-PEO fibers rather than beaded fibers.[12] The impact of an enhanced effective crosslink network through hydrogen bonding,[13-15] physical gelation[16] and hydrophobic junctions[17] on electrospinnability has also been discussed in the literature, but all of the systems investigated involve self-complementary interactions. Finally, the addition of a poor solvent can also improve electrospinnability by increasing the polymer-polymer interactions, which could be considered in this context as a type of effective crosslinks. For example, it was found that poly[2-methoxy-5-(2'-ethylhexyloxy)-1,4-phenylenevinylene] fibers can be electrospun from a mixture of isopropanol (a poor solvent) and chloroform (a good solvent), whereas electrospinning from a pure chloroform solution leads to droplets.[18]

In this work, we investigate the effect of a small hydrogen-bond crosslinker, 4,4'-biphenol (BiOH), on the rheological and electrospinning behavior of poly(4-vinyl pyridine) (P4VP) solutions (Scheme 3.1), using both pure N,N-dimethylformamide (DMF) and DMF mixed with a poor solvent, nitromethane. The objective is to improve the electrospinnability of P4VP by hydrogen-bond crosslinks that increase the effective crosslink density of the solution. P4VP has been widely used as a functional polymer, since the pyridine ring can be coordinated with metal ions,[19-20] quaternized into a cationic polyelectrolyte for further complexation with ionic molecules,[21] and act as a hydrogen-bond acceptor to enable supramolecular assembly with hydrogen bond donors.[22-23] Hydrogen-bond complexation between polystyrene-b-poly(4-vinyl pyridine) (PS-b-P4VP) and monofunctional amphiphiles has been extensively investigated by ten Brinke, Ikkala and coworkers to generate hierarchical structures.[24-26] Hydrogen-bonded complexes of PS-b-P4VP with small bifunctional molecules have also been used to form films with ordered structure.[27-28] In contrast, very few investigations of the use of PS-b-P4VP complexes[29-30] and of pure P4VP or P4VP complexes[31-32] for preparing electrospun fibers have been undertaken. Furthermore, our work is the first systematic study, to our knowledge, to demonstrate the effect of small hydrogen-bonded crosslinkers on the electrospinnability of a polymer.

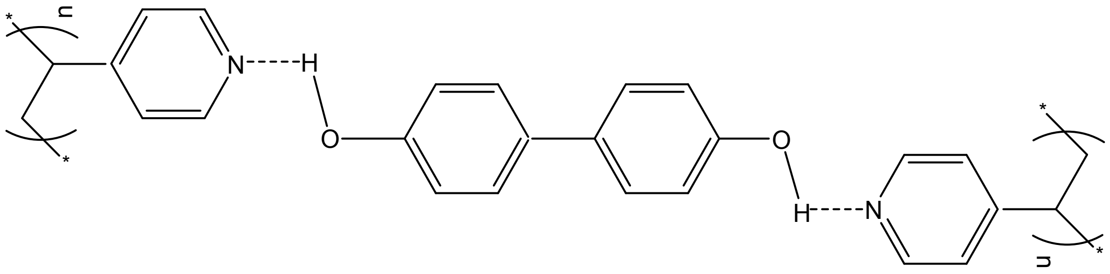

Scheme 3.1. Idealized hydrogen-bonded complex between poly(4-vinyl pyridine) and 4,4'-biphenol (P4VP-BiOH) leading to effective crosslinking.

3.4 Experimental

Poly(4-vinyl pyridine) (P4VP) with a viscosity average molecular weight of 200 kg/mol was obtained from Scientific Polymer Products. 4,4'-Biphenol (BiOH; 97%) and nitromethane (ACS reagent grade $\geq$ 95%) were purchased from Aldrich, and N,N-dimethylformamide (DMF, 99.8%) from EMD. All products were used as received. P4VP was solubilized, with or without BiOH, in pure DMF or in a mixture of DMF and nitromethane (MIX) in 10 ml vials to give solutions of various concentrations. All concentrations are given in terms of wt% P4VP. The MIX solutions were prepared by first mixing the solvents with a 1.7:1.0 DMF:nitromethane volume ratio, which were then added to the solutes, followed by homogenization for two min in an ultrasonic bath (Fisher Scientific FS60). This solvent mixing ratio was selected because it contains the largest volume fraction of the poor solvent (nitromethane) that enables preparing 30wt% solutions. Unless noted otherwise, all P4VP-BiOH solutions were prepared at a 1:1 molar ratio of hydroxyl groups to pyridine rings. For electrospinning, the solution was transferred to a syringe, mounted on a syringe pump (PHD 2000, Harvard Apparatus), and extruded through a needle (Hamilton, 91022) at a rate of 0.01 mL/min. A +20 kV voltage was applied to the needle using a FC series 120 W regulated high-voltage DC power supply (Glassman High Voltage). The collector was composed of a glass slide covered with aluminum foil, and connected to the -2 kV cathode of a Nim Standard HV power supply (Power Design). The distance between the tip of the needle and the collector was 10 cm. The fibers were dried naturally in a fume hood for over one week before scanning electron microscopy (SEM) characterization and were further dried in a vacuum oven at 60 °C before Fourier transform infrared spectroscopy (FT-IR) characterization.

The morphology of the electrospun samples was characterized by SEM, either with a FEI Quanta 200 FEG environmental scanning electron microscope, for which the samples were first coated with gold (Sputter Coater, Agar Scientific), or with a JEOL JSM-7400F high resolution field emission scanning electron microscope without gold coating on the samples. The size of the fibers and droplets was measured using ImageJ. FT-IR spectra were measured on a Tensor 27 spectrometer (Bruker Optics) with a MCT detector and a MIRacle (Pike Technologies) attenuated total reflection (ATR) accessory equipped with a silicon crystal, at 4 cm^{-1} resolution. For liquid samples, FT-IR measurements were made by depositing the solution (50−100 μL) directly on the ATR crystal (fully covered by the drop). A spectrum of the solvent was subtracted using OPUS (Bruker Optics). For fibers, spectra were recorded by pressing a bundle of fibers on the ATR crystal. All spectra were an average of 100 scans for solutions and 400 scans for fibers.

Solution rheology was characterized with an advanced rheometer AR2000 (TA Instruments) using a steel cone (cone angle = 1.59°, cone diameter = 40 mm, truncation = 55 μm). The measurements were performed in continuous ramp mode at 25 °C by applying shear stress from 0 to 200 Pa or more. The zero shear rate viscosity (η_0) was determined from viscosity-shear rate plots following the method of Colby and coworkers.[33] The hydrodynamic radius (R_h) of P4VP (in ~0.5 wt% solution) was measured using a Zetasizer Nanoseries system (Malvern Instruments) at 25 °C, with a non-invasive backscatter detection (NIBS) method at an angle of 173°. The raw data were fitted using the cumulant method and Z-average values were determined.

3.5 Results and discussion

3.5.1 Morphology of electrospun products

As a point of reference, the electrospun products of P4VP/DMF at various concentrations are shown in Fig. 3.1. At low concentrations, 2 to 8 wt%, electrospraying results only in droplets (average diameter ~320 nm). Some of them are decorated with short filaments (140-600 nm in length), while others are elongated or deformed into erythrocyte-like shapes. The 10 wt% solution gives a network-like morphology of droplets interconnected by short fibers (average length ~5 μm) and sometimes beaded fibers. Longer fibers (average length > 12 μm) form for solutions of 12 wt% and above, although they are still mixed with droplets and beads (average diameter ~50 nm), even to a small extent at concentrations of 25 wt%.

The threshold for forming "real" fibers (as opposed to the short "fibers" attached to the droplets at low concentrations) was determined by the ratio of fiber length to droplet size. At a critical concentration, c_f, this ratio increases dramatically from 1-2 to over 10 (Table 3.S1 in Supporting Information) and the average fiber length becomes larger than 5 μm. This concentration, which is 12 wt% for pure P4VP electrospun from DMF, is defined as the onset of beaded fiber formation. Another critical concentration, c_p, not observed for P4VP/DMF in the range of concentrations investigated, is defined as the onset of pure and uniform fibers. The c_f and c_p values for the different systems studied here are summarized in Table 3.1 (see Table 3.S1 for details regarding the determination of c_f).

Table 3.1. Critical concentrations for the formation of beaded fibers (c_f) and uniform fibers (c_p) electrospun from P4VP-based solutions

	c_f (wt%)	c_p (wt%)
P4VP/DMF	12	
P4VP-BiOH/DMF	10	20
P4VP/MIX	8	
P4VP-BiOH/MIX	6	14

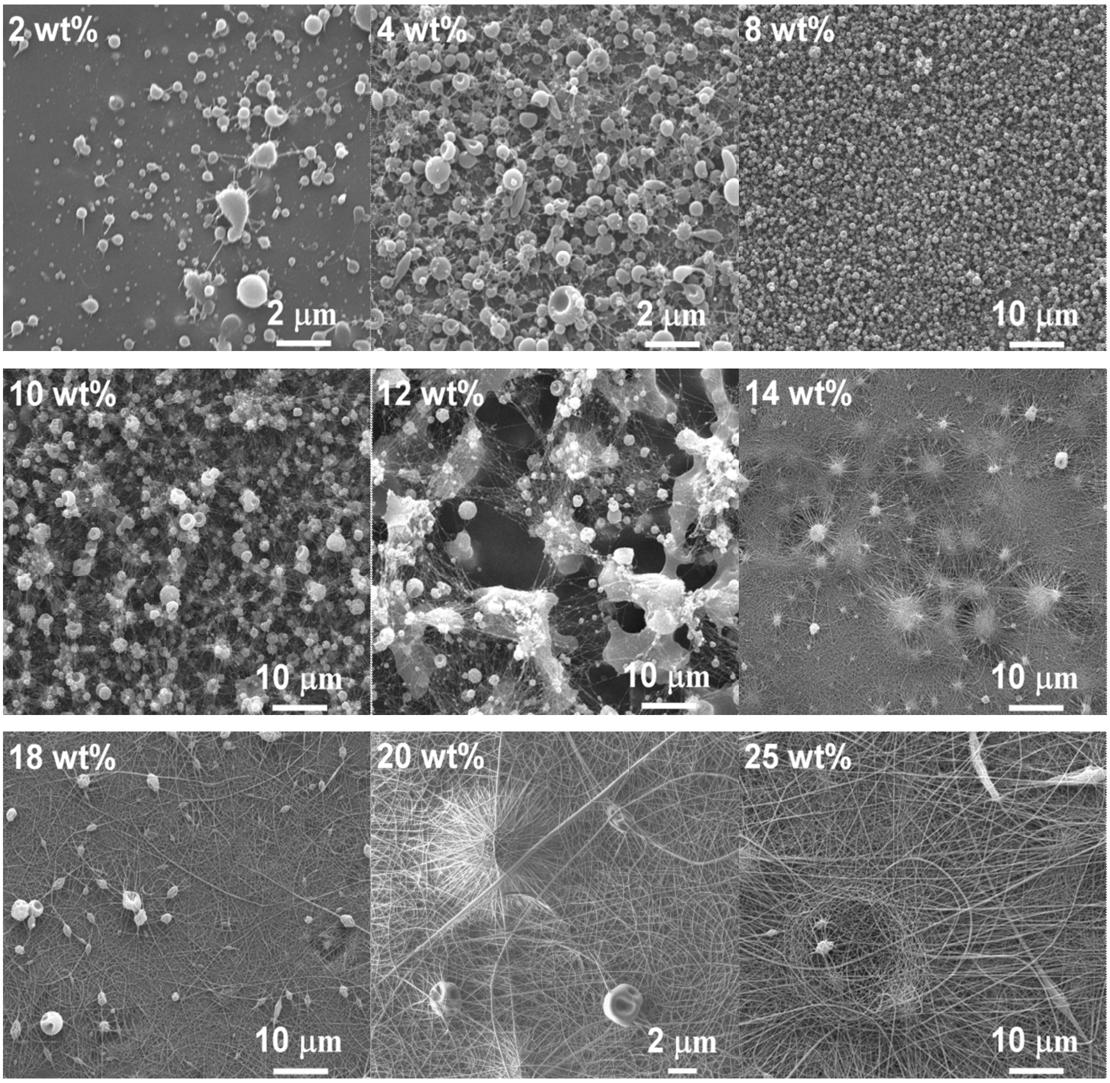

Figure 3.1. SEM images of the electrospun products from P4VP/DMF solutions of different concentrations.

Fig. 3.2 shows that, with the addition of BiOH, c_f is reduced only slightly from 12 wt% for P4VP/DMF solutions to 10 wt%. However, uniform fibers can now be obtained, defining a clear c_p value of 20 wt%. Since DMF can act also as a hydrogen-bond acceptor, the temporary crosslinking effect of BiOH might be improved by using a binary mixture of DMF with a poor solvent that cannot hydrogen bond strongly with either the pyridine rings or the hydroxyl groups.

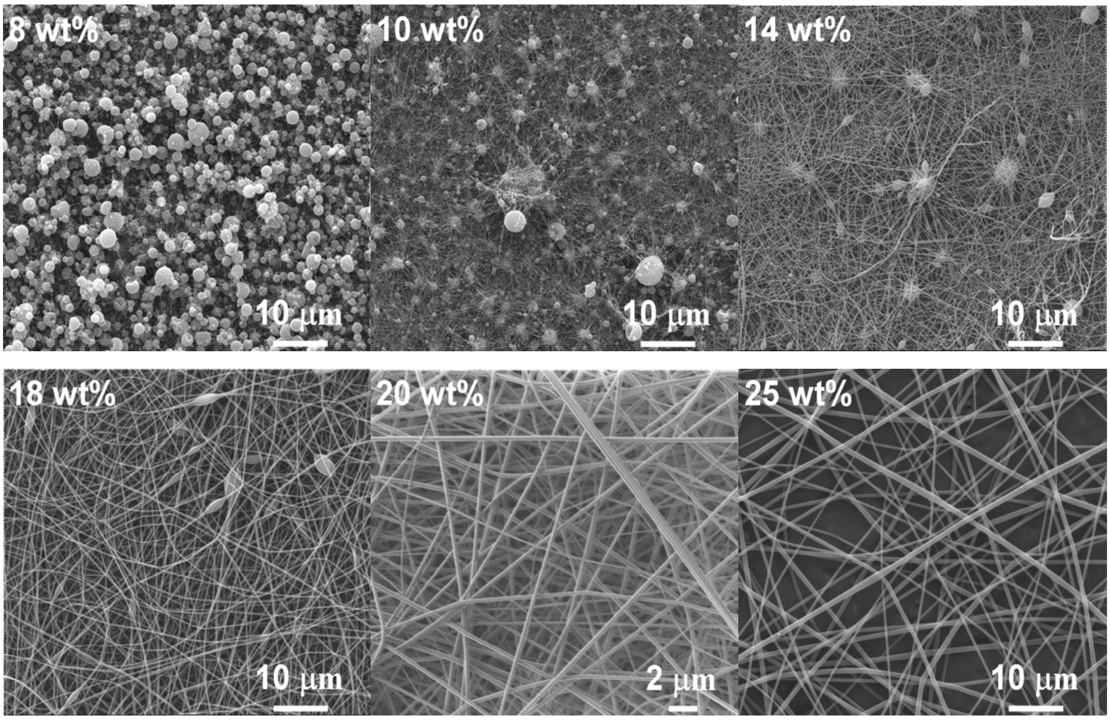

Figure 3.2. SEM images of the electrospun products from P4VP-BiOH/DMF solutions of different concentrations.

To this end, nitromethane (CH_3NO_2), a non-solvent for BiOH and a poor solvent for P4VP, was selected in a DMF:CH_3NO_2 volume ratio of 1.7:1.0. Since pure CH_3NO_2 dissolves P4VP (200 kg/mol) poorly through a weak acid-base interaction ($NH^+ \ldots CH_2NO_2^-$),[34] it is expected that using the DMF-CH_3NO_2 mixture will increase the P4VP-BiOH hydrogen bonding in solution. Fig. 3.3 and Table 3.1 bear out this expectation, showing that c_f and c_p decrease to 6 and 14 wt%, respectively, with P4VP-BiOH/MIX. Furthermore, the fibers thicken as the solution concentration increases. At 20 wt% concentration, the fibers have an average diameter of 800 nm and, above 23 wt%, fused ribbons form. Ribbon-shaped fibers form when a dried skin prevents solvent evaporation from within the core of the fiber, which eventually collapses.[35] The presence of fused fibers can be attributed to their interpenetration, due to presence of residual solvent, after deposition on the collector. This phenomenon is promoted by the use of solvents with high boiling points such as DMF and CH_3NO_2.

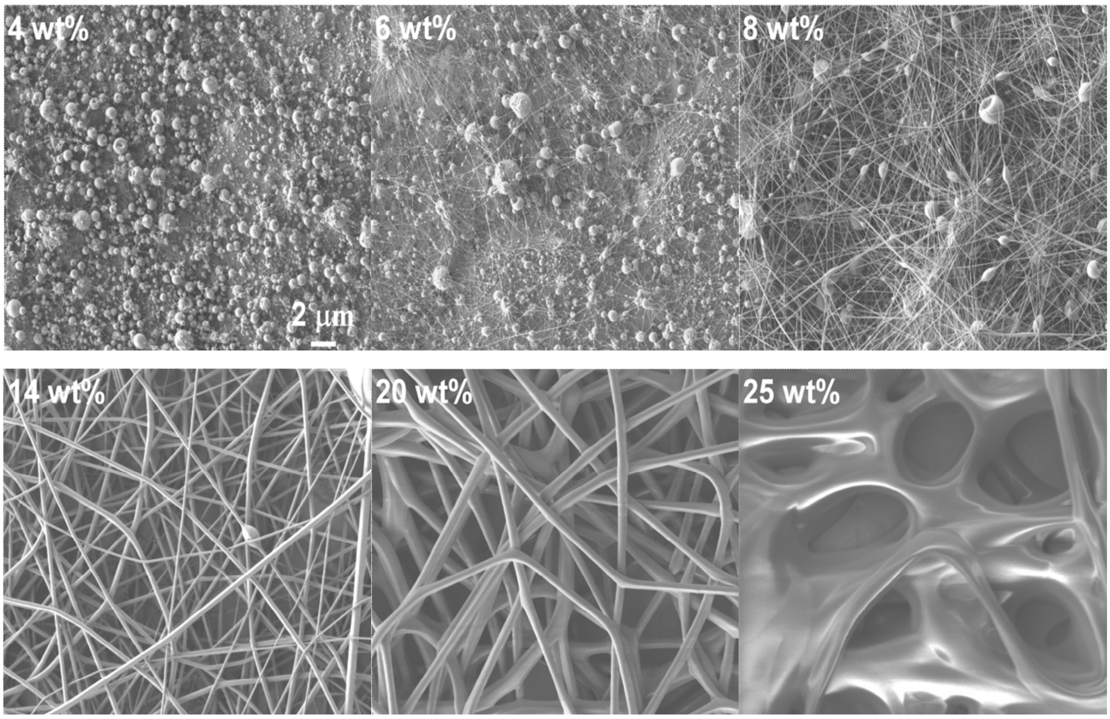

Figure 3.3. SEM images of electrospun products from P4VP-BiOH/MIX solutions of different concentrations. All images have the same scale bar as shown in the first image.

To distinguish the direct effect of the solvent itself from its indirect effect on the electrospinning behavior via its influence on promoting BiOH-P4VP H-bonding, the influence of the mixed solvent on the electrospinning of pure P4VP was verified. Fig. 3.4 and Table 3.1 show that c_f occurs at 8 wt% for P4VP/MIX, which is between the values for P4VP/DMF and P4VP-BiOH/MIX. Fibers become more uniform with an increase in solution concentration, but a few large beads or droplets are still observable at the highest concentrations used. This result suggests that both direct and indirect effects contribute to the behavior in P4VP-BiOH/MIX. It should be mentioned here that a small amount of precipitate was found for most of the P4VP/MIX solutions, but only for the lowest concentrations (below 8 wt%) of P4VP-BiOH/MIX. This implies that the actual c_f and c_p for P4VP/MIX occur at slightly lower concentrations. This phenomenon is further discussed below and in the Supporting Information.

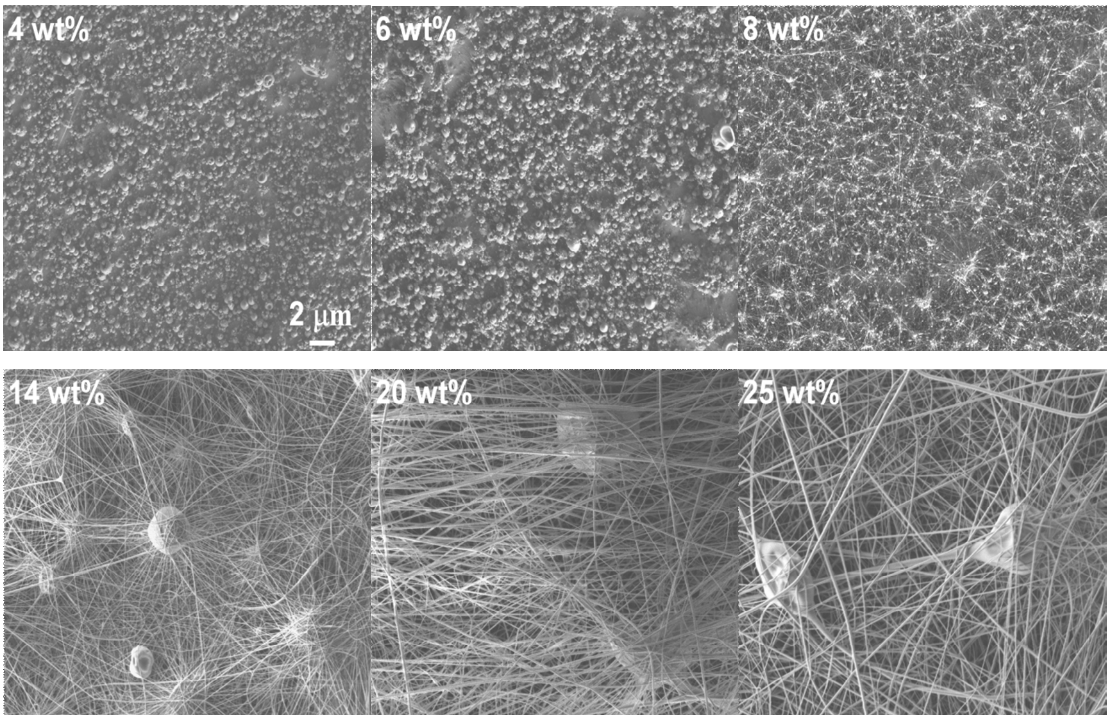

Figure 3.4. SEM images of electrospun products from P4VP/MIX solutions of different concentrations. All images have the same scale bar as shown in the first image.

The average diameters of the electrospun fibers, including the beaded and short fibers, are plotted in Fig. 3.5a. They range from 20 nm to 2 μm, increasing with concentration and depending on the presence of BiOH and CH_3NO_2. Generally, for a given concentration, the average diameter for the different systems decreases as P4VP-BiOH/MIX > P4VP-BiOH/DMF > P4VP/DMF ≥ P4VP/MIX. The correlation between diameter (D) and polymer concentration (c) is expressed as $D \propto c^x$. The scaling exponents range from 1.4 to 3.2, with the BiOH-containing systems possessing the largest values. This is comparable with exponents of 2.6 to 3.1, reported in the literature for poly(methyl methacrylate) (PMMA) with various M_w in DMF,[36] linear and branched poly(ethylene terephthalate-co-ethylene isophthalate) with different M_w in 70/30 w/w chloroform/DMF,[2] and PMMA in chloroform/DMF with various compositions.[15] To account for the fact that different systems have different viscoelastic properties in solution, the diameters are also plotted logarithmically against zero shear rate viscosity (η_0) in Fig. 3.5b. The general trend is similar to that observed in Fig. 3.5a, which is expressed as $D \propto \eta_0^x$. If a linear regression of the four systems together is done (see Fig. 3.S1), an exponent of 0.78 is obtained, similar to corresponding literature values.[2, 36] An additional observation that can be made is that, for solutions leading to electrospun fibers with the same diameter, those containing BiOH are less viscous, which is advantageous for solution transfer from vials to the syringe during the electrospinning process.

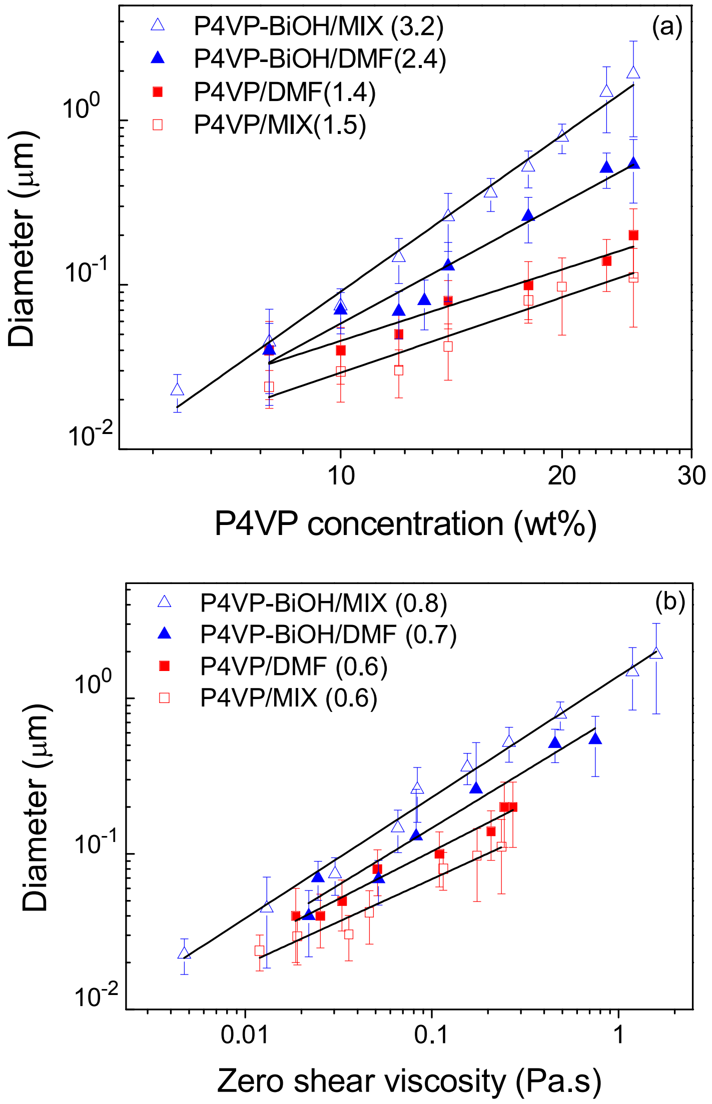

Figure 3.5. Fiber diameters as a function of (a) P4VP concentration and (b) zero shear rate viscosity for solutions of △: P4VP-BiOH/MIX; ▲: P4VP-BiOH/DMF; ■: P4VP/DMF; □: P4VP/MIX. The numbers in the parentheses indicate the scaling exponents (x) in the correlations of $D \propto c^x$ and $D \propto \eta_0^x$ for panels (a) and (b), respectively. The error bars indicate the standard deviations for the diameters (n = 100-200).

3.5.2 Solution properties

Complexation between P4VP and BiOH in solution was confirmed by measuring infrared spectra, as shown in Fig. 3.6a. The 993 cm^{-1} band, assigned to a stretching mode of free pyridine rings of P4VP, shifts to a higher wavenumber (1008 cm^{-1} here) when the pyridine rings are hydrogen-bonded.[28] The intensity ratio of these two bands therefore reveals the extent of complexation in solution. Fig. 3.6a shows that the 993 cm^{-1} band is more intense than the 1008 cm^{-1} band in P4VP-BiOH/DMF solution, indicating that the pyridine rings are only partially complexed with BiOH in the solution. By comparison, the 993 cm^{-1} band is very weak in the spectrum of dried electrospun fibers, indicating almost complete P4VP-BiOH complexation. The percentage of hydrogen-bonded P4VP pyridine rings (f_b) can be calculated from Eq. 3.1, where I_b and I_f are the intensity of the hydrogen-bonded and free pyridine ring bands, respectively, and a is the ratio of the absorption coefficients of the 1008 and 993 cm^{-1} bands. In a previous paper, we described a method to obtain a, determined to be 0.4, and to obtain I_b and I_f through a second-derivative analysis.[32]

$$f_b = \frac{I_b}{I_b + I_f / a} \times 100\%, \quad a = \varepsilon_f / \varepsilon_b \qquad (3.1)$$

As shown in Fig. 3.6b, f_b increases linearly with P4VP concentration for both P4VP-BiOH/DMF and P4VP-BiOH/MIX, as highly concentrated solutions increase the probability that BiOH and pyridine rings interact with each other by diminishing the detrimental effect of DMF as a hydrogen-bond breaker. Furthermore, f_b is always much higher, and shows a greater slope with P4VP concentration, in the mixed solution than in pure DMF. As an example, f_b is around 22% in P4VP-BiOH/MIX and 11% in P4VP-BiOH/DMF for a P4VP concentration of 25 wt%. This clearly supports the supposition made above, that the mixed solvent increases P4VP-BiOH hydrogen-bonding in solution. It is noteworthy that, for P4VP-BiOH/DMF, for example, the maximum f_b is only about 15% for a 35 wt% P4VP concentration. As a consequence, the BiOH-P4VP H-bonding, which is relatively low, is probably dominated by BiOH that is H-bonded by just one of its OH groups to P4VP (monofunctionally attached BiOH). This could give rise to OH-OH H-bonding between two monofunctionally attached

BiOH molecules. Such OH-OH interactions could also lead to an effective crosslinking effect, although it would be significantly weaker than bifunctionally attached BiOH (as shown in Scheme 1), since OH-OH interactions are weaker than OH-pyridine interactions.

As the solution becomes more concentrated, f_b increases linearly (Fig. 3.6b) so that the more effective bifunctionally attached BiOH complex becomes more probable. It is expected that the f_b values continue to increase with concentration (to finally reach the value in the dried fibers), so that, during electrospinning, they must continue to increase as the solution jet becomes more concentrated due to solvent evaporation. Although it is impossible to calculate f_b in the jet during electrospinning, the final f_b in the dried fibers (electrospun from a solution with a 25 wt% P4VP concentration) reached as high as 70%, supporting this hypothesis. Given the equimolar ratio of pyridine rings and BiOH hydroxyl groups, any f_b value above 50% implies that some fraction of P4VP chains are necessarily effectively crosslinked by bifunctionally attached BiOH (which is certainly the case in the dried fibers). This implies that H-bond crosslinking must exist and increase in the jet, enabling to better resist capillary instability and electrical stretching, and thus leading to the observed formation of uniform fibers.

Fig. 3.6b also helps rationalize the observation mentioned earlier regarding the incomplete dissolution of pure P4VP and, more intriguingly, of dilute P4VP-BiOH in the mixed solvent where a non-solvent for P4VP was added. As detailed in the Supporting Information (Fig. 3.S2 and associated text), monofunctional hydrogen bonding of P4VP by BiOH leads to a polymer complex with pendant OH groups that can further hydrogen bond with DMF. The presence of BiOH thereby leads to improved solubility of P4VP in DMF, which can compensate for the presence of the non-solvent. For this to happen, the value of f_b must be sufficiently high, which, as shown in Fig. 3.6b, is not the case for low concentrations of P4VP-BiOH, thus explaining their incomplete dissolution in the mixed solvent.

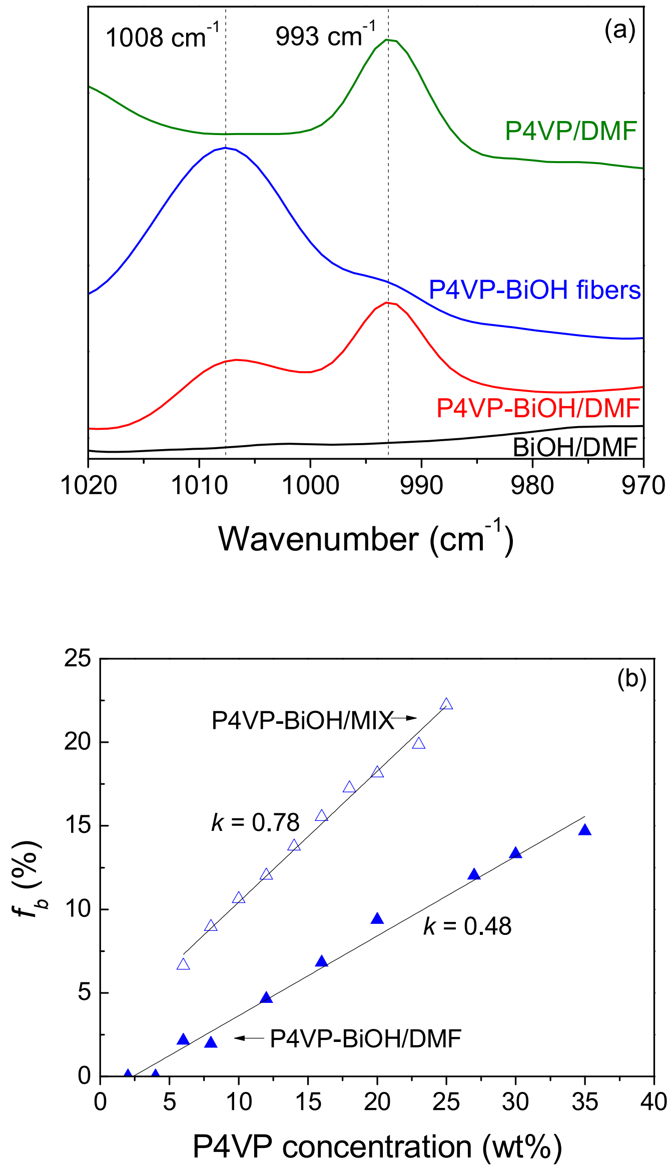

Figure 3.6. (a) Infrared spectra of BiOH/DMF (10 wt%), P4VP-BiOH/DMF (27 wt% P4VP concentration), and dried fibers electrospun from P4VP-BiOH/DMF and P4VP/DMF (25 wt% P4VP concentration). For all solutions, the DMF spectrum was subtracted. (b) Fraction of hydrogen-bonded pyridine rings (f_b) as a function of P4VP concentration (equimolar pyridine:OH).

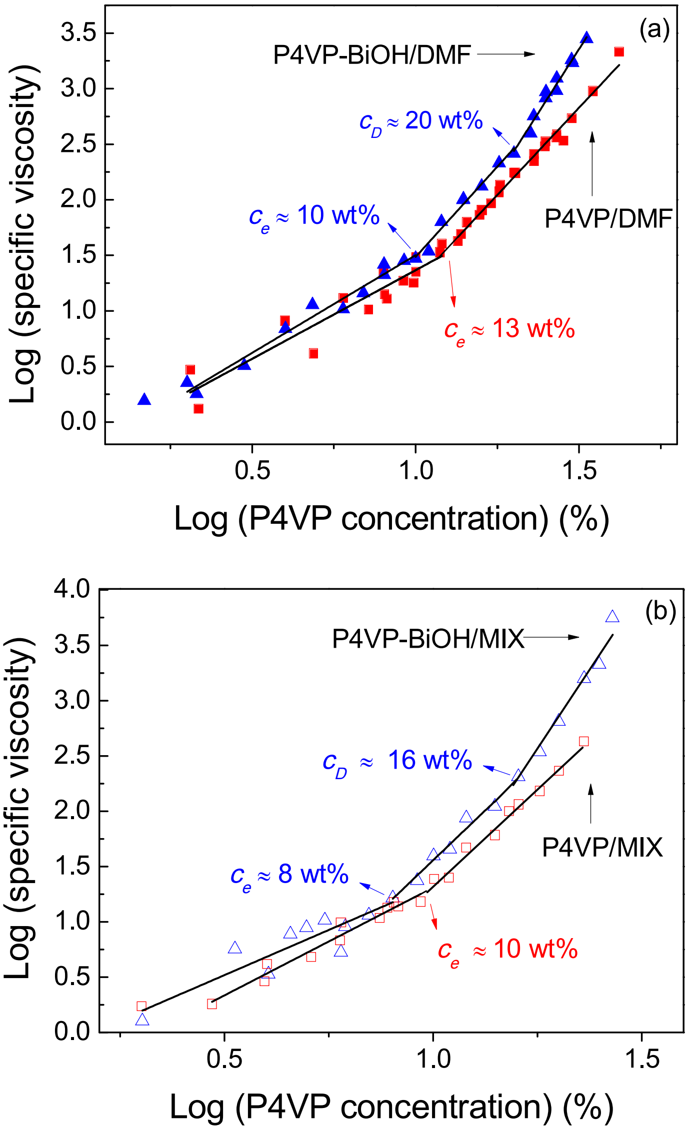

Figure 3.7. Specific viscosity as a function of P4VP concentration in (a) DMF solutions and (b) MIX solutions.

As shown by the plots of specific viscosity, η_{sp}, as a function of P4VP concentration in Fig. 3.7, the presence of BiOH in the P4VP solutions leads also to an increase in viscosity, which is most evident above 10 wt% in DMF and 8 wt% in MIX. The increase in viscosity for a given solvent can be attributed to both bifunctionally attached BiOH hydrogen bonding and

OH-OH hydrogen bonding between monofunctionally attached BiOH, although again the former must be more effective due to its greater strength.

The effect of the addition of nitromethane to DMF was also verified by comparing BiOH-free solutions. It was found that there is a crossover point, at 10% concentration, in the specific viscosity vs. concentration curves, where the viscosity is lower for P4VP/MIX than for P4VP/DMF below this point and the opposite above this point (Fig. 3.S3). The lower viscosity of P4VP/MIX at low concentration can be explained by a shrinkage of the P4VP random coils (R_h = 13.5 nm) caused by the presence of the non-solvent in MIX as compared to P4VP in pure DMF (R_h = 14.2 nm), as shown in Table 3.2. At higher concentration, the poor solvent enhances polymer-polymer association and, therefore, the viscosity. Such a crossover point has also been reported for polystyrene[37] and poly(α-methylstyrene).[38]

Table 3.2. Rheological properties of the electrospinning solutions

Solution	R_h (nm) [a]	Semidilute unentangled regime [b]	c_e (wt%) [c]	Semidilute entangled regime [b]	c_D (wt%) [d]	Concentrated regime [b]
P4VP/DMF	14.2 ± 0.1	1.6	13	3.1		
P4VP-BiOH/DMF	14.6 ± 0.1	1.8	10	3.3	20	4.6
P4VP/MIX	13.5 ± 0.1	1.9	10	3.5		
P4VP-BiOH/MIX	13.7 ± 0.1	1.6	8	3.6	16	5.8

[a] Hydrodynamic radius of P4VP in dilute solutions. [b] Exponent n in the equation, $\eta \propto c^n$, describing the power law dependence between viscosity (η) and P4VP concentration (c). The terms "entangled" and "unentangled" are maintained for convenience although effective crosslinks arising from H-bonding cannot be equated with entanglements. [c] Onset of the semidilute entangled regime. [d] Onset of the concentrated regime.

Furthermore, Table 3.2 shows that the addition of BiOH causes a small increase in the R_h of P4VP (from 14.2 to 14.6 nm in DMF and from 13.5 to 13.7 nm in MIX), indicating that BiOH extends the P4VP coil a little in dilute P4VP solutions. Additional evidence for this is given in Fig. 3.S4, which shows that R_h increases linearly with the addition of increasingly excess amounts of BiOH in both DMF and MIX.

Polymer solutions have been divided into different concentration regimes that can be determined from viscosity plots such as shown in Fig. 3.7 and that have been identified as follows. In the dilute regime, there is no polymer coil overlap[39]. In the semidilute unentangled regime, the coils overlap without forming chain entanglements. The onset of this regime is defined by the overlap concentration, c^*.[39] The semidilute entangled regime is characterized by chain entanglements, and its onset is defined by the entanglement concentration, c_e.[39] Finally, there is the concentrated regime, at an onset of c_D, where the many entanglements give rise to topological constraints for the polymer chains.[40] Each regime shows a different power law dependence between specific viscosity and concentration (or reduced concentration (c/c^*)), $\eta \propto c^n$, where n is different.[39] These regimes are thus distinguished by changes in linear slopes in the logarithmic plot of viscosity with concentration, with the intersections giving the appropriate onset concentrations. These different regimes can also be distinguished in the present system, as shown in Fig. 3.7 and tabulated in Table 3.2. Since topological entanglements and other forms of effective physical crosslinks or interactions all contribute to the viscoelastic properties of polymer solutions, the reported c_e and c_D should be interpreted as the effective (or apparent) values.

The data show that the addition of BiOH and nitromethane each decrease the c_e of P4VP/DMF from 13 to 10 wt%, attributed to the increase in effective crosslinking caused by hydrogen-bonded complexation and increased polymer-polymer association, respectively. The two effects together, which decrease c_e to 8 wt%, appear additive. No concentrated regime can be found for the solutions of pure P4VP in either DMF or MIX, but it appears after the addition of BiOH. In this case, c_D decreases from 20% for P4VP-BiOH/DMF to 16 wt% for P4VP-BiOH/MIX. It can be concluded that the addition of BiOH and of nitromethane have a similar effect on c_e, but that the effect of BiOH is dominant in determining c_D.

The morphology of electrospun polymer fibers is strongly related to the rheological properties of the polymer solutions. Some authors correlate fiber morphology dependence with critical values of $c[\eta]$ (or c/c^*), above which fiber formation occurs.[1, 36] The critical c/c^* value reported for the formation of beaded fibers is variable, ranging from 3 to 5 or even larger, while the critical c/c^* reported for uniform fiber formation ranges from 4 to 10. McKee et al. have also reported that, in neutral polymer solutions, formation of beaded fibers is observed close to or at a concentration of 1.2 or 1.3 times c_e, and that uniform (non-beaded) fiber formation is reached at concentrations 2 to 2.5 times c_e.[2] In our work, both c_f and c_p are found at concentrations close to c_e and c_D, respectively, with c_f/c_e ratios of 0.8-0.9 and c_p/c_D ratios of 0.9-1.0 (Tables 3.1 and 3.2).

In addition to randomly aligned fibers mats, such as those in the SEM images of Figs. 3.1-4, it is also common to use a collector composed of two parallel rods or a rotating drum to obtain long aligned fibers. Preparing such bundles is essential for characterizing the orientation and other properties of electrospun fibers,[41] when the analysis of individual fibers is not possible.[42-43] However, it is often necessary to use quite high solution concentrations, making solution transfer difficult during manipulation. In the present system, it was found that, whereas concentrations above 30 wt% ($\eta_0 \approx 0.45$ Pa.s) are necessary for pure P4VP/DMF to obtain aligned fibers between two rods (inside gap of 2.7 cm), concentrations as low as 13 wt% ($\eta_0 \approx 0.1$ Pa.s) are sufficient for P4VP-BiOH/MIX. This illustrates that long aligned fibers can be prepared using a supramolecular approach to introduce effective crosslinks while avoiding the use of very viscous solutions.

3.6 Conclusion

The addition of 4,4'-biphenol (BiOH) as a hydrogen-bond crosslinker and of nitromethane as a poor solvent for P4VP were shown to be efficient methods to improve the electrospinnability of P4VP solutions. SEM shows that the critical P4VP concentration for the formation of beaded fibers (c_f) decreases from 12 wt% for P4VP/DMF to as little as 6 wt% when combining the effects of adding the BiOH crosslinker and nitromethane (poor solvent) to DMF (good solvent). When using BiOH, pure and uniform fibers could be obtained above P4VP concentrations of 20 and 14 wt% in DMF and the mixed solvent, respectively. Infrared spectroscopy results prove the hydrogen-bonded complexation of P4VP by BiOH in solution, which increases with increasing P4VP concentration and in the presence of nitromethane. The specific viscosity of P4VP solutions also increases with the addition of BiOH in both pure DMF and mixed solvent, and a concentrated regime was found above 20 and 16 wt%, respectively, correlating withthe formation of uniform fibers. We believe that the effective crosslinking caused by hydrogen bonding facilitates the electrospinning of P4VP and that this strategy can pave the way to the electrospinning of low molecular weight polymers and rigid polymers by using appropriate crosslinkers.

3.7 Acknowledgment

This work was supported by the Natural Sciences and Engineering Research Council of Canada (NSERC) and Fonds de Recherche du Québec – Nature etTechnologie (FRQNT). X.W. thanks the China Scholarship Council (CSC) and Université de Montréal for financial support. We thank Prof. X.X. Zhu for providing access to his rheometer and Zetasizer, and A. Laventure for her assistance.

3.8 Supplementary information

Table 3.S1. Ratio of fiber length to droplet size of electrospun fibers

	Fiber length/droplet size						
P4VP concentration (wt%)	2	4	6	8	10	12	14
P4VP/DMF	1.1	1.3	1.0	1.4	4.7	16.0*	14.1
P4VP-BiOH/DMF	0.6	1.6	2.0	1.8	20.8*	10.2	28.6
P4VP/MIX		1.1	1.2	10.5*	7.9	9.9	15.2
P4VP-BiOH/MIX	1.2	2.0	12.8*	25.5	32		

* indicates the critical fiber formation concentration (c_f).

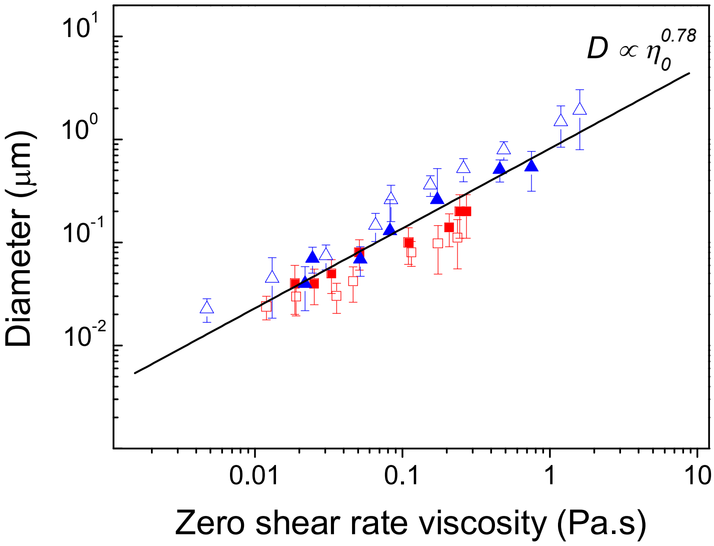

Figure 3.S1. Linear regression of the fiber diameter *vs*. zero shear rate viscosity for the solutions: △, P4VP-BiOH/MIX; ▲, P4VP-BiOH/DMF; ■, P4VP/DMF; and □, P4VP/MIX.

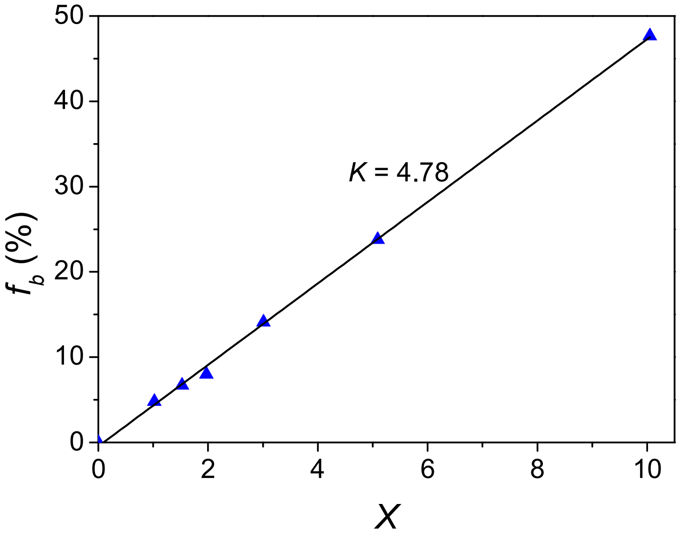

Figure 3.S2. Calculated percentage of hydrogen-bonded pyridine rings (f_b) as a function of BiOH content (expressed as the molar ratio, X, of hydroxyl groups to pyridine) in 1.5:1.0 DMF:nitromethane solutions (P4VP concentration = 4 wt%).

Fig. 3.S2 shows the percentage of hydrogen-bonded pyridine rings, f_b, determined for the P4VP-BiOH complex in the mixed solvent of DMF:CH_3NO_2 (v:v = 1.5:1.0). The P4VP concentration was fixed at 4 wt% and the molar fraction (X) of hydroxyl groups *vs.* pyridine rings varied from 0 to 10. The values of f_b increase linearly with BiOH content, giving a slope of 4.78. Full dissolution of P4VP was observed only for $X \geq 1.5$, that is for $f_b \geq 6.7\%$. This minimum value of f_b corresponds to that obtained for a 16 wt% P4VP concentration in DMF solution for the stoichiometric amount of BiOH (X=1) used throughout the main text. BiOH can either crosslink two pyridine rings or it can H-bond to a single ring, which is most probable when f_b is below 50%, leaving a free hydroxyl group exposed in solution. We believe that an increase in the number of monocomplexed BiOH enables the complete dissolution of P4VP in the mixed solvent system due to the favorable interaction of the exposed hydroxyl groups with DMF. The DMF-nitromethane mixture is therefore a better solvent for the BiOH-decorated P4VP than for P4VP by itself. This can also explain the observation that complete dissolution is possible for P4VP-BiOH/MIX (with X=1) when the concentration is above 8 wt%. As shown in Fig. 3.6b of the main text, the fraction of pyridine rings that are complexed with BiOH increases with concentration. This leads to a larger number of pendant hydroxyl groups on P4VP, which aids its dissolution in MIX.

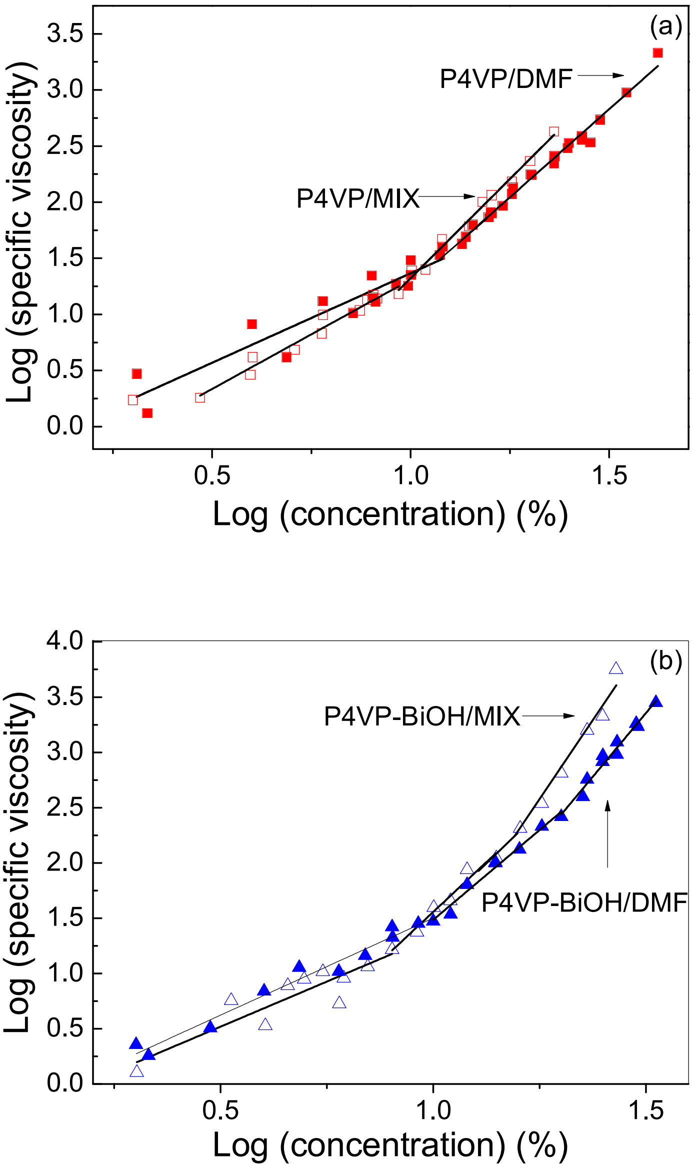

Figure 3.S3. Specific viscosity as a function of P4VP concentration for (a) pure P4VP solutions and (b) P4VP-BiOH solutions.

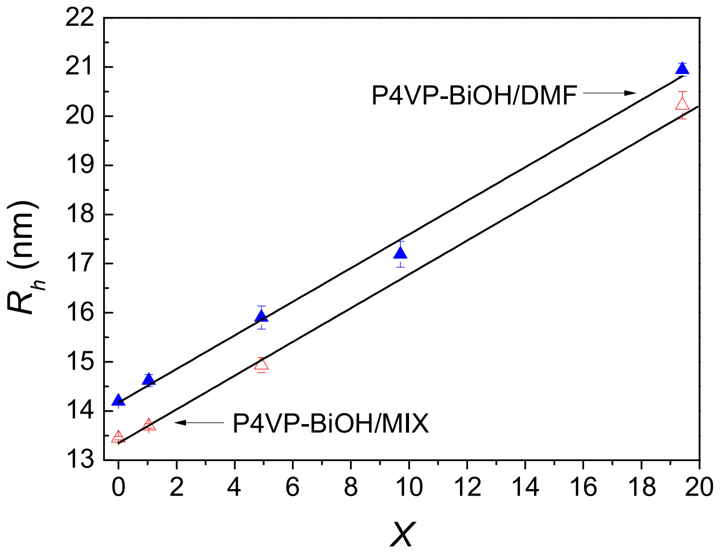

Figure 3.S4. Hydrodynamic radius (R_h) as a function of BiOH content (expressed as the molar ratio, *X,* of hydroxyl groups to pyridine) in 1.7:1.0 DMF:nitromethane solutions (P4VP concentration = 0.5 wt%).

3.9 References

1. Koski, A.; Yim, K.; Shivkumar, S., *Mater. Lett.* **2004,** 58, 493-497.
2. McKee, M. G.; Wilkes, G. L.; Colby, R. H.; Long, T. E., *Macromolecules* **2004,** 37, 1760-1767.
3. Shenoy, S. L.; Bates, W. D.; Frisch, H. L.; Wnek, G. E., *Polymer* **2005,** 46, 3372-3384.
4. Schiffman, J. D.; Schauer, C. L., *Polym. Rev.* **2008,** 48, 317-352.
5. Mincheva, R.; Manolova, N.; Paneva, D.; Rashkov, I., *J. Bioact. Compat. Polym.* **2005,** 20, 419-435.
6. Chen, H.; Snyder, J. D.; Elabd, Y. A., *Macromolecules* **2008,** 41, 128-135.
7. Wang, X.; Zhang, Q.; Bazuin, C. G.; Pellerin, C., *Macromol. Symp.* **2014,** 336, 30-38.
8. Nie, H.; He, A.; Zheng, J.; Xu, S.; Li, J.; Han, C. C., *Biomacromolecules* **2008,** 9, 1362-1365.
9. McKee, M. G.; Hunley, M. T.; Layman, J. M.; Long, T. E., *Macromolecules* **2006,** 39, 575-583.

10. Fong, H.; Chun, I.; Reneker, D. H., *Polymer* **1999,** 40, 4585-4592.
11. Son, W. K.; Youk, J. H.; Lee, T. S.; Park, W. H., *Polymer* **2004,** 45, 2959-2966.
12. Bonino, C. A.; Krebs, M. D.; Saquing, C. D.; Jeong, S. I.; Shearer, K. L.; Alsberg, E.; Khan, S. A., *Carbohydr. Polym.* **2011,** 85, 111-119.
13. Demir, M. M.; Yilgor, I.; Yilgor, E.; Erman, B., *Polymer* **2002,** 43, 3303-3309.
14. McKee, M. G.; Park, T.; Unal, S.; Yilgor, I.; Long, T. E., *Polymer* **2005,** 46, 2011-2015.
15. McKee, M. G.; Elkins, C. L.; Long, T. E., *Polymer* **2004,** 45, 8705-8715.
16. Shenoy, S. L.; Bates, W. D.; Wnek, G., *Polymer* **2005,** 46, 8990-9004.
17. Talwar, S.; Hinestroza, J.; Pourdeyhimi, B.; Khan, S. A., *Macromolecules* **2008,** 41, 4275-4283.
18. Zhong, W.; Li, F.; Chen, L.; Chen, Y.; Wei, Y., *J. Mater. Chem.* **2012,** 22, 5523-5530.
19. Benouazzane, M.; Bravo-Grimaldo, E.; Bissessur, R.; Bazuin, C. G., *Macromolecules* **2006,** 39, 5364-5370.
20. Belfiore, L. A.; McCurdie, M. P.; Das, P. K., *Polymer* **2001,** 42, 09995-10006.
21. Zhang, Q.; Wang, X.; Barrett, C. J.; Bazuin, C. G., *Chem. Mater.* **2009,** 21, 3216-3227.
22. Brandys, F. A.; Bazuin, C. G., *Chem. Mater.* **1996,** 8, 83-92.
23. Kato, T.; Frechet, J. M. J., *J. Am. Chem. Soc.* **1989,** 111, 8533-8534.
24. Ikkala, O.; ten Brinke, G., *Chem. Commun.* **2004**, 2131-2137.
25. ten Brinke, G.; Ikkala, O., *Chem. Rec.* **2004,** 4, 219-230.
26. van Zoelen, W.; Asumaa, T.; Ruokolainen, J.; Ikkala, O.; ten Brinke, G., *Macromolecules* **2008,** 41, 3199-3208.
27. Sidorenko, A.; Tokarev, I.; Minko, S.; Stamm, M., *J. Am. Chem. Soc.* **2003,** 125, 12211-12216.
28. Laforgue, A.; Bazuin, C. G.; Prud'homme, R. E., *Macromolecules* **2006,** 39, 6473-6482.
29. Ruotsalainen, T.; Turku, J.; Heikkila, P.; Ruokolainen, J.; Nykanen, A.; Laitinen, T.; Torkkeli, M.; Serimaa, R.; ten Brinke, G.; Harlin, A.; Ikkala, O., *Adv. Mater.* **2005,** 17, 1048-1052.
30. Ruotsalainen, T.; Turku, J.; Hiekkataipale, P.; Vainio, U.; Serimaa, R.; ten Brinke, G.; Harlin, A.; Ruokolainen, J.; Ikkala, O., *Soft Matter* **2007,** 3, 978-985.
31. Wang, S.; Li, Y.; Li, J.; Du, J.; Bai, J.; Yang, Q.; Chen, X., *J. Appl. Polym. Sci.* **2008,** 108, 281-286.

32. Wang, X.; Bazuin, C. G.; Pellerin, C., *Vib. Spectrosc.* **2014,** 71, 18-23.
33. Boris, D. C.; Colby, R. H., *Macromolecules* **1998,** 31, 5746-5755.
34. Manzur, J.; Zamudio, W., *J. Organomet. Chem.* **1972,** 44, 107-109.
35. Koombhongse, S.; Liu, W.; Reneker, D. H., *J. Polym. Sci., Part B: Polym. Phys.* **2001,** 39, 2598-2606.
36. Gupta, P.; Elkins, C.; Long, T. E.; Wilkes, G. L., *Polymer* **2005,** 46, 4799-4810.
37. Adam, M.; Delsanti, M., *J. Phys.* **1984,** 45, 1513-1521.
38. Isono, Y.; Nagasawa, M., *Macromolecules* **1980,** 13, 862-867.
39. Colby, R. H.; Rubinstein, M.; Daoud, M., *J. Phys. II France* **1994,** 4, 1299-1310.
40. Colby, R. H.; Fetters, L. J.; Funk, W. G.; Graessley, W. W., *Macromolecules* **1991,** 24, 3873-3882.
41. Liu, Y.; Pellerin, C., *Macromolecules* **2006,** 39, 8886-8888.
42. Richard-Lacroix, M.; Pellerin, C., *Macromolecules* **2013,** 46, 9473-9493.
43. Richard-Lacroix, M.; Pellerin, C., *Macromolecules* **2012,** 45, 1946-1953.

Chapter 4: Effect of small effective crosslinkers on the electrospinnability of low molecular weight poly(4-vinyl pyridine)[*]

4.1 Résumé

Nous avons étudié l'effet du 4,4'-biphénol (BiOH) et celui d'autres petites molécules capables de former des liaisons hydrogène sur la facilité du processus d'électrofilage de la poly(4-vinylpyridine) de masse moléculaire faible (M_w = 50 kg/mol). Des mesures de spectroscopie infrarouge et de rhéologie ont montré que l'ajout de BiOH et de nitrométhane (NM, un mauvais solvant) à des solutions de diméthylformamide améliore la réticulation effective en solution,grâce aux liaisons hydrogène entre la P4VP et le BiOH et aux interactions polymère-polymère. Les images de microscopie électronique à balayage (SEM) des produits électrofilés ont révélé la formation de fibres présentant des perles à des concentrations en P4VP de 17 à 53% moins élevée que pour la P4VP pure, et la formation de fibres uniformes sans perles lorsque les deux espèces (BiOH et NM) sont combinées. L'effet de l'acide 4-(4-hydroxyphényl)benzoïque (HBCA) et du $ZnCl_2$, qui peuvent respectivement établir des interactions plus fortes de type liaison hydrogène et de coordination avec les pyridines, a également été examiné. Les résultats de SEM ont montré que le HBCA, dans des conditions de concentrations identiques au BiOH, et avec aussi peu que 1% de $ZnCl_2$ (par rapport aux pyridines), facilite encore plus le processus d'électrofilage que le BiOH, soulignant l'importance de la force des interactions dans l'établissement de la réticulation effective. Finalement, l'élimination des petites molécules par sublimation a été étudiée et le BiOH peut complètement être retiré sans affecter la morphologie des fibres. Ces résultats

---

[*] This chapter will be submitted as a full paper for publication. It is coauthored by C. Geraldine Bazuin and Christian Pellerin.

suggèrent une nouvelle stratégie pour la préparation de nanofibres de polymères purs dont le processus d'électrofilage est difficile.

4.2 Abstract

We investigated the effect of 4,4'-biphenol (BiOH) and other small hydrogen-bonding crosslinkers on the electrospinnability of low molecular weight poly(4-vinyl pyridine) (P4VP with M_w = 50 kg/mol). The addition of BiOH and nitromethane (NM, a poor solvent) in dimethylformamide solutions were shown by infrared spectroscopy and rheology to enhance the effective crosslinking in solution through BiOH-P4VP hydrogen bonding and polymer-polymer interactions. Scanning electron microscopy (SEM) images of the electrospun products revealed the formation of beaded fibers at P4VP concentrations 17-53% lower than for pure P4VP, and of uniform unbeaded fibers when combining both factors. The effect of 4-hydroxy-4'-biphenyl carboxylic acid (HBCA) and $ZnCl_2$, which possess stronger hydrogen-bonded and metal coordination interactions with pyridine rings, respectively, was also explored. SEM showed that HBCA under identical conditions as for BiOH and with only 1% $ZnCl_2$ (with respect to the pyridine rings) leads to much better electrospinnability than BiOH, indicating the importance of strong polymer-crosslinker interactions. Finally, removal of the small molecules by sublimation was investigated and BiOH was found to be completely removable without affecting the fiber morphology. These results provide a new strategy for preparing nanofibers of pure polymers having limited electrospinnability.

4.3 Introduction

Electrospinning is a fast and simple technique to prepare continuous nanofibers from solutions.[1-3] It has gained extensive attention for applications like filtration,[2] drug delivery,[4] wound healing,[5] and tissue engineering.[4, 6] However, its application is limited for solutions of low molar mass polymers and other stiff polymers, like polyelectrolytes[7] and some biomacromolecules,[3] due to a poor electrospinnability caused by an insufficient number of entanglements in solution.

It is well known that using polymers with a relatively high molecular weight or at high concentration facilitates electrospinning. In a pioneering paper by Koski et al., fiber formation was observed when the concentration of poly(vinyl alcohol) (PVA) exceeded 5 times its overlap concentration (c^*) in water.[8] Long and coworkers found that fibers of neutral polymers could be electrospun from solutions in the semidilute entangled regime.[9-10] Shenoy et al. suggested that, for polymers without specific interchain association in a good solvent, beaded fibers can be electrospun when there is more than one entanglement per chain in the solution.[11] These and other works contributed to a deep understanding of the key role of entanglements in electrospinning.

Increasing entanglements is thus the most frequent approach to improve electrospinability.[12-13] A classical way is to blend a non-electrospinnable polymer with an easily-electrospinnable polymer, usually a high molecular weight polymer with flexible chains that can form a well-entangled network at low concentration. For instance, the ionic complex between methyl orange and methylated poly(4-vinyl pyridine) (P4VP) is a completely non-electrospinnable polymer, but it could be electrospun by blending with poly(methyl methacrylate) in N,N-dimethylformamide (DMF).[14] Increasing chain flexibility also leads to an increase of entanglements in solution and thus to a lower minimum concentration needed for fiber formation. Additives can be used to increase the flexibility of polymer chains. For example, glycerol was used as co-solvent in sodium alginate/water solutions,[15] and NaCl was added into a poly(2-dimethylamino ethyl methacrylate hydrochloride) aqueous solution.[16]

In addition to topological entanglements, which are one form of effective crosslinking in solution, other forms based on various self-complementary interactions like hydrogen bonding,[9, 17] electrostatic forces,[18] and hydrophobic interactions,[19] have also been investigated to facilitate electrospinning. It should be noted that there is an increasing number of reports about the electrospinning of non-polymeric species like phospholipids,[20] cyclodextrins,[21-23] 1,3,5-cyclohexanetrisamides and 1,3,5-benzenetrisamides[24] or even low molar mass polymers[25] without electrospinnable polymer carriers. However, these methods are all based on very strong self-complementary interactions, which can only be applied to species with a specific structure.

In the previous chapter, we demonstrated for the first time the strategy of introducing effective crosslinking by adding a small bifunctional hydrogen-bonded crosslinker, 4,4'-biphenol (BiOH). BiOH was shown to improve the electrospinnability of P4VP solutions in DMF with a molecular weight of 200 kg/mol by decreasing the minimum concentration for the fiber formation by 2 wt%.[26] Here, we demonstrate the much larger effect of small molecular crosslinkers (see Scheme 4.1) on the electrospinnability of lower molecular weight P4VP (50 kg/mol). We also show the impact of the strength of the specific interactions by using crosslinkers forming stronger hydrogen bonds and metal coordination interactions, and explore the possibility of removing the small crosslinkers by sublimation.

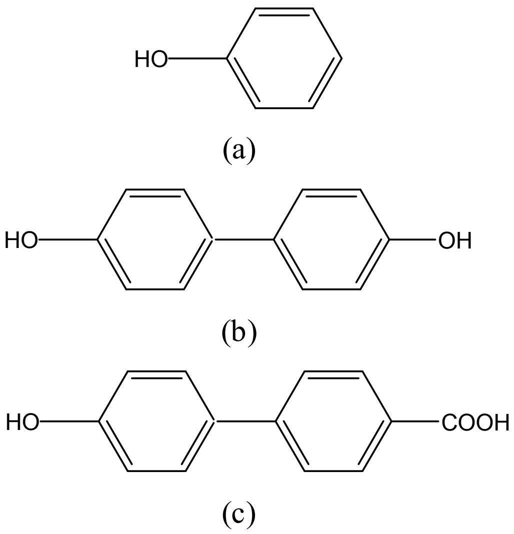

Scheme 4.1. Hydrogen-bonded crosslinkers: (a) phenol; (b) 4,4'-biphenol (BiOH); (c) 4-hydroxy-4'-biphenyl carboxylic acid (HBCA). Zinc chloride was also used as a metal coordination crosslinker.

4.4 Experimental

Poly(4-vinyl pyridine) with a viscosity average molecular weight of 50 kg/mol (P4VP) was obtained from Scientific Polymer Products. 4,4'-biphenol (BiOH; 97%), nitromethane (NM; ACS reagent ≥ 95%), zinc chloride ($ZnCl_2$; 98%) and 4-ethylpyridine (EtPy; 98%) were purchased from Sigma-Aldrich, N,N-dimethylformamide (DMF; 99.8%) from EMD, phenol

(99%) from BDH, 4-hydroxy-4’-biphenyl carboxylic acid (HBCA; 99%) from Alfa Aesar. All compounds were used as received. P4VP was dissolved, with or without crosslinkers, in DMF or in a mixture of DMF and nitromethane (MIX) to give solutions of various concentrations in 10 ml vials. Mixed solvents with a 1.1:1 DMF:NM volume ratio were prepared by adding NM into DMF quickly and were made homogeneous in an ultrasonic bath (Fisher Scientific FS60). Unless otherwise noted, P4VP-BiOH, P4VP-phenol and P4VP-HBCA always refer to complexes with a 1:1 molar fraction of interacting groups (pyridine rings for P4VP and hydroxyl and carboxylic acid groups for the crosslinkers).

To prepare electrospun fibers, each solution was transferred into a syringe, mounted on a syringe pump (PHD 2000, Harvard Apparatus), and extruded through a needle (Hamilton, 91022) at a rate of 0.01 mL/min. A +20 kV voltage was applied to the needle using a FC series 120 W regulated high voltage DC power supply (Glassman High Voltage). The collector, a glass slide covered with aluminum foil, was connected to the -2 kV cathode of a Nim Standard HV power supply (Power Design). The working distance between the tip of the needle and the collector was 10 cm. The fibers were dried in a fume hood for at least one week before scanning electron microscopy (SEM) characterization and further dried in a vacuum oven at 60 ºC for infrared spectroscopy characterization.

The morphology of the electrospun products was characterized by SEM, either with a FEI Quanta 200 FEG environmental scanning electron microscope, for which the samples were first coated with gold (Sputter Coater, Agar Scientific), or with a JEOL JSM-7400F high resolution field emission scanning electron microscope without gold coating on the samples. The size of the fibers and droplets was determined using ImageJ.[27] Fourier transform infrared (FT-IR) spectra were recorded at a 4 cm^{-1} resolution using a Tensor 27 FT-IR spectrometer (Bruker Optics) equipped with a MCT detector. A MIRacle (Pike Technologies) attenuated total reflection (ATR) accessory was used to measure the IR spectra of all fibers and P4VP solutions. For fibers, spectra were recorded by pressing a bundle of fibers on the silicon ATR crystal. For solutions, measurements were made by depositing the solution (50 to 100 μl) directly on the ATR crystal (fully covered by the drop). A spectrum of the solvent was subtracted using OPUS (Bruker Optics). A VariGATR accessory (Harrick Scientific) with a

Ge crystal was used, with an incidence angle of 60°, to measure the IR spectra of the EtPy/small molecules liquid blends. All spectra were an average of 100 scans for solutions and 400 scans for fibers.

Solution rheology was characterized with an advanced rheometer AR2000 (TA Instruments) with a steel cone (cone angle = 1.59°, cone diameter = 40 mm, truncation = 55 μm) geometry. The measurements were performed in continuous ramp mode at 25 °C by applying shear stress from 0 to 200 Pa or more. The zero shear rate viscosity (η_0) was determined from viscosity–shear rate plots following the method of Colby and coworkers.[28]

4.5 Results and discussion

4.5.1 Solution characteristics

The formation of a hydrogen-bonded complex between P4VP and BiOH in DMF solutions was first confirmed using FT-IR, as shown in Fig. 4.1a. The 993 cm^{-1} band in the spectrum of pure P4VP is due to a deformation mode of the free pyridine rings.[29] This band shifts to a higher wavenumber, around 1008 cm^{-1}, when they hydrogen-bond with hydroxyl groups.[20, 28] Both bands are observed in the spectrum of P4VP-BiOH/DMF, indicating a partial hydrogen-bonded complexation even if DMF is a good hydrogen bond breaker. Similar spectra are observed, after solvent subtraction, for solutions in the MIX solvent but the relative intensity of the 1008 cm^{-1} band is larger, indicating a higher extent of hydrogen bonding in the presence of nitromethane (See Fig. 4.S1). The relative intensities of these bands can be used to quantify the percentage of hydrogen-bonded pyridine rings (f_b) with Eq. 4.1:

$$f_b = \frac{I_b}{I_b + I_f / a} \times 100\% \qquad (4.1)$$

where I_f and I_b are the intensities of the 993 cm^{-1} and 1008 cm^{-1} bands, respectively, and a is the ratio their absorption coefficients. I_f and I_b were obtained through a second-derivative analysis of the absorbance spectra and a was determined as 0.4.[29]

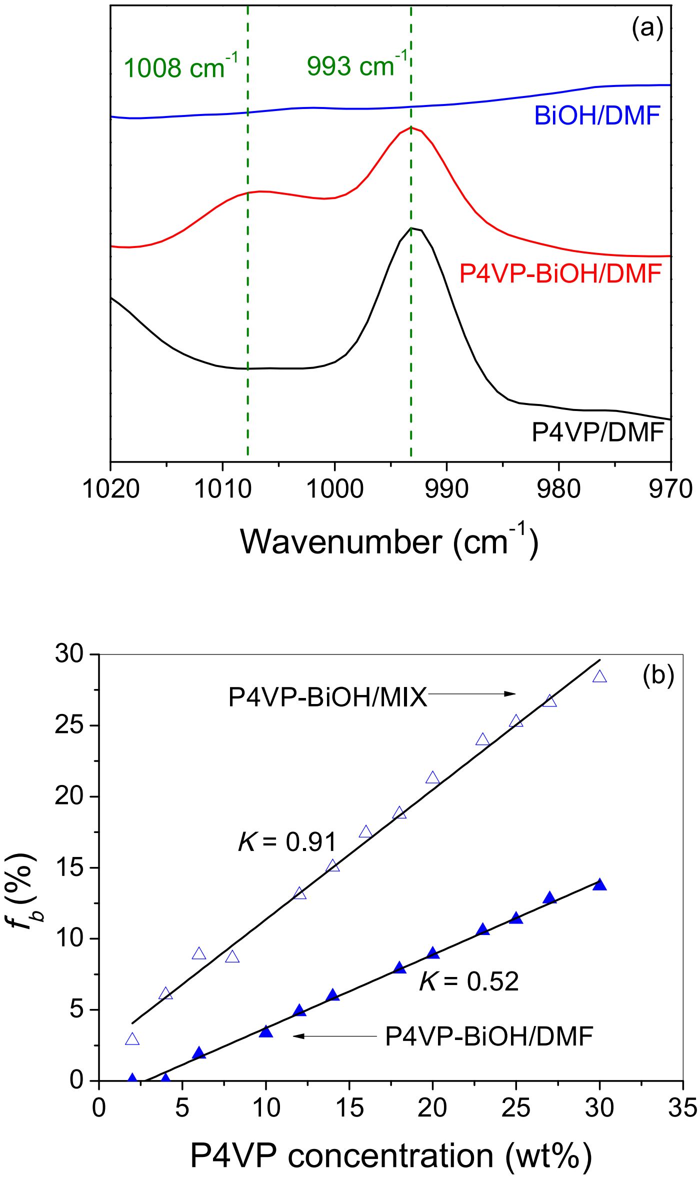

Figure 4.1. (a) ATR spectra of 10 wt% BiOH/DMF (blue), P4VP-BiOH/DMF (P4VP concentration = 20 wt%) (red), and P4VP/DMF (P4VP concentration = 25 wt%) (black). A pure DMF spectrum was subtracted for all solutions. (b) Percentage of hydrogen-bonded pyridine rings (f_b) as a function of P4VP concentration in P4VP-BiOH/DMF and P4VP-BiOH/MIX solutions.

Fig. 4.1b show that f_b increases linearly with P4VP concentration, with slopes of 0.52 and 0.91 in DMF and MIX, respectively. For solutions with the same P4VP concentration, f_b in MIX is around 1.75 times that in DMF, due to the fact that NM is a worse hydrogen bond breaker than DMF.[26] A similar slope of 0.48 was found in DMF solutions for higher molecular weight P4VP200k but a lower slope of 0.78 was measured in mixed solutions.[26] The latter can be explained by the fact that the mixed solvent had a higher DMF:NM volume ratio of 1.7:1 for P4VP200k, as compared with 1.1:1 for P4VP50k, due to the limited solubility of high molecular weight P4VP in nitromethane. As a consequence, using a lower fraction of DMF enables a larger number of hydrogen bonds between P4VP and BiOH in solution and should lead to a greater impact on the rheological properties and to a greater improvement of the electrospinnability for P4VP50k. This advantage should be general since low molecular weight polymers are generally more soluble in poor solvents due to their higher entropy of mixing.

The specific viscosities (η_{sp}) of P4VP solutions are shown in Fig. 4.2 as a function of P4VP concentration. The addition of BiOH increases the viscosity of P4VP solutions in DMF (Fig. 4.2a) and in MIX (Fig. 4.2b) over the full range of concentrations investigated. The influence of BiOH on viscosity may partially originate from effective crosslinking via BiOH molecules interacting with pyridine rings from both hydroxyl groups. However, since Fig. 4.1 shows that the extent of hydrogen bonding is only moderate in solution, the increase in viscosity can also be explained by the monofunctional complexation of BiOH to P4VP, leading to a polymer with pendant OH groups that can further hydrogen bond with DMF or with other OH groups. As expected, the addition of BiOH leads to a larger relative increase in viscosity in MIX than in DMF since the fraction of hydrogen bonded P4VP units is significantly larger.

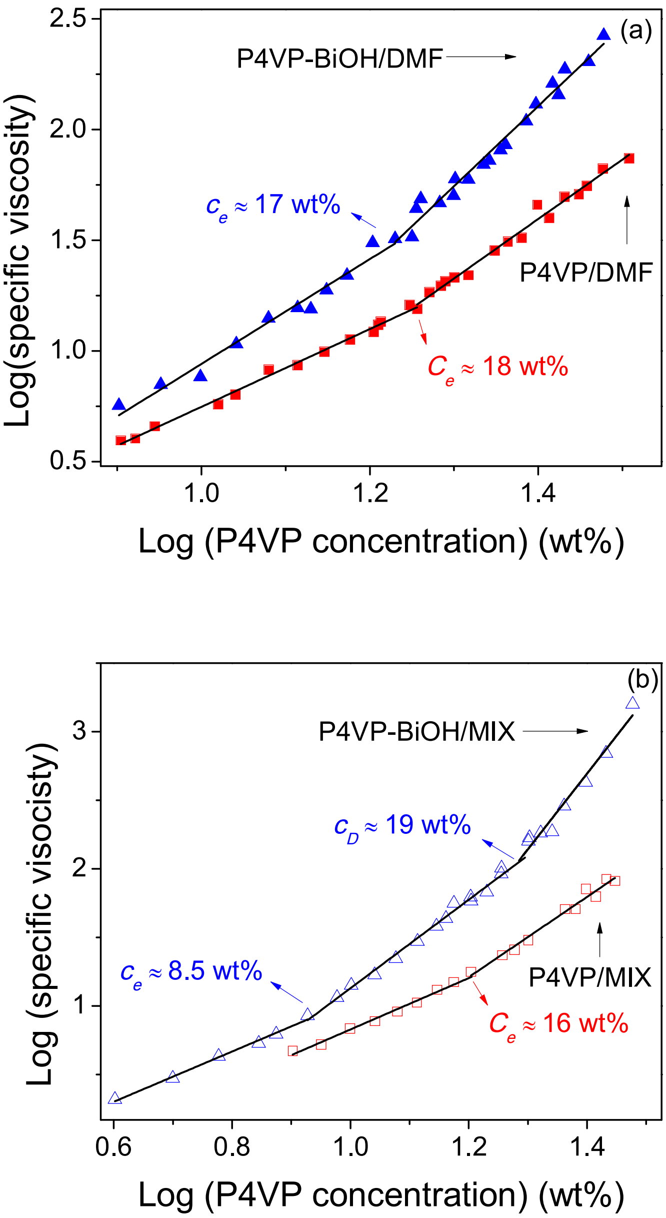

Figure 4.2. Specific viscosity as a function of P4VP concentration for (a) DMF solutions and (b) MIX solutions with (blue data) and without (red data) BiOH.

An increase in viscosity is also found by simply using MIX instead of DMF, even without BiOH, because the poor solvent enhances polymer-polymer association (see Fig. 4.S2), but the influence of adding BiOH is much larger. As an example, for a P4VP concentration of

18 wt%, η_{sp} increases by 175% in the former and only 50% in the latter, indicating the much more important role of hydrogen bonds in increasing the association among polymer chains than pyridine-pyridine interactions. When both MIX and BiOH are used, the viscosity of solutions increases considerably by 400% as compared to the equivalent P4VP/DMF solution.

Fig. 4.2 also shows that each logarithmic plot is composed of 2 or 3 linear ranges with different positive slopes. It is well known that the viscosity of polymer solutions increases exponentially with concentration as $\eta \sim c^n$, where n varies for the different regimes of solution concentrations. These regimes are classified, based on the extent of entanglements in solution, as: the dilute regime (n = 1 in good solvent),[30] in which polymer coils are isolated; the semidilute unentangled regime (n = 1.25-2.0),[31-32] in which polymer coils start to overlap but do not form an entanglement network; the semidilute entangled regime (n = 3.75-4.7),[31] in which significant entanglements form; and the concentrated regime, in which the chain dimensions become independent of concentration. The critical concentrations between the regimes, entanglement concentration (c_e) and concentrated concentration (c_D), are determined as the intersection between two different slopes in the logarithmic plot of viscosity vs. concentration and are reported in Table 4.1 for all systems studied.

Table 4.1. Rheological properties of P4VP solutions

	c_e (wt%)	c_f (wt%)	c_D (wt%)	c_p (wt%)
P4VP/DMF	18	30		
P4VP-BiOH/DMF	17	25		
P4VP/MIX	16	23		
P4VP-BiOH/MIX	8.5	14	19	27

c_e and c_f represent the critical concentration for semidilute entangled regime and fiber formation respectively; c_D and c_p represent the critical concentration for concentrated regime and formation of pure fibers respectively.

As observed in Fig. 4.2, the semidilute unentangled and semidilute entangled regimes appear in all four systems, while only P4VP-BiOH/MIX shows a concentrated regime. For

P4VP/DMF, c_e is around 18 wt%, which is 5 wt% higher than for higher molecular weight P4VP200k.[26] c_e only slightly decreases to around 17 and 16 wt% for P4VP-BiOH/DMF and P4VP/MIX, respectively, indicating their limited individual impact. This was also found for P4VP200K, with c_e only decreasing from 13 wt% to around 10 wt% for both P4VP-BiOH/DMF and P4VP/MIX.[26] In contrast, combining the addition of NM and BiOH significantly increases the apparent entanglements in the solution with c_e decreasing to 8.5 wt%, half of the value for P4VP/DMF. A concentrated regime also becomes observable for these solutions, with a c_D value of 19 wt%. These results suggest that pure and uniform fibers should be electrospinnable for the P4VP-BiOH/MIX system.

4.5.2 Morphology of the electrospun products

Because of the very low molecular weight of P4VP50k, P4VP/DMF solutions cannot be electrospun easily. As shown in Fig. 4.3, only droplets are obtained from solutions below 27 wt%. At 27 wt%, very thin fibers form between the droplets with an average fiber length/droplet size of only 3.2. Solutions at 30 wt% lead to more fibers, including some longer fibers (20-60 μm, see a low magnification SEM image in Fig. 4.S3), with a length 20 to 70 times the average droplet size. The ratio of the average fiber length/droplet size was established in our previous paper as a criterion for defining the formation of beaded fibers.[26] According to this, we regard 30 wt% as the critical concentration of fiber formation (c_f). Although not found for P4VP/DMF, c_p is used to define the critical concentration for forming pure and uniform fibers in the future discussion. Both c_f and c_p for all investigated systems are summarized in Table 4.1.

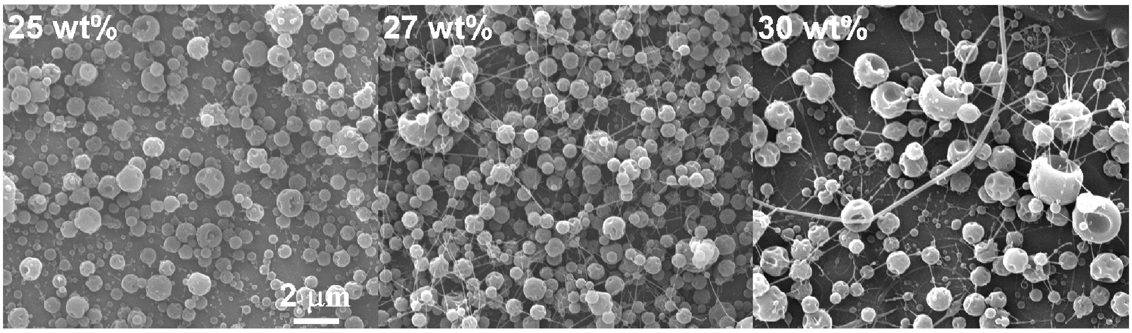

Figure 4.3. SEM images of electrospun products from P4VP/DMF with different P4VP concentrations. All images have the same scale bar as shown in the first image.

As shown in Fig. 4.4, for P4VP-BiOH/DMF, fibers start to form for 23 wt% solution (average fiber length/droplet size ≈ 5) but they are very thin and short (around 4 μm). At 25 wt%, a large amount of longer fibers (> 7 μm) are obtained and meet the criterion to define this concentration as c_f. Thicker and longer beaded fibers were electrospun from solutions with higher P4VP concentration. For P4VP200k, the addition of BiOH into P4VP/DMF led to a decrease of c_f by only 2 wt%,[26] as compared with 5 wt% for P4VP50k. This clearly indicates that BiOH is more effective to increase the electrospinnability of low molecular weight P4VP in absolute terms, but the relative improvement (c_f 17% lower) is very close. This is consistent with the fact that the slopes of the percentage of hydrogen-bonded pyridine rings as a function of P4VP concentration were similar for P4VP200k (0.48) and P4VP50k (0.52). This suggests that the same relative improvement in electrospinnability should be obtained with lower molecular weight polymers.

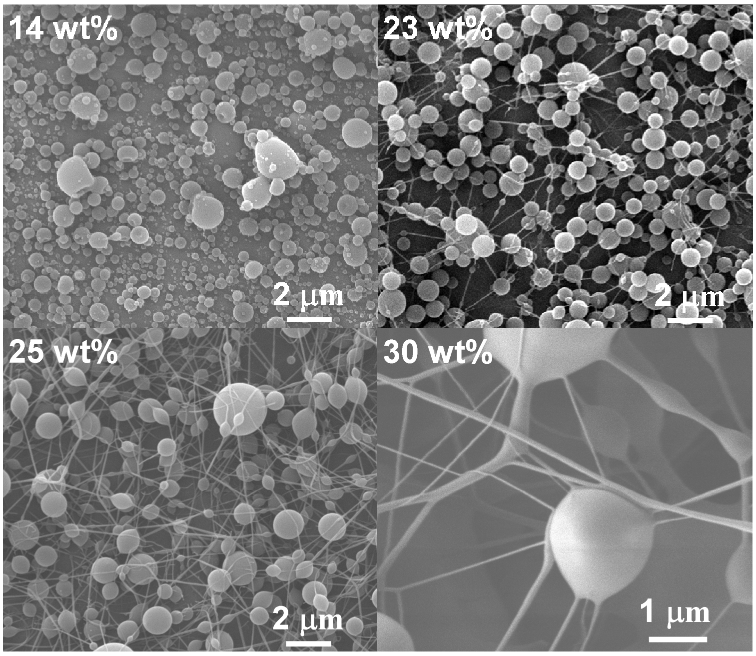

Figure 4.4. SEM images of electrospun products from P4VP-BiOH/DMF with different P4VP concentrations.

Fig. 4.S4 shows that, when MIX is used as a solvent for pure P4VP, traces of very thin beaded fibers appear in 20 wt% solutions but the real fibers respecting the fiber length/droplet size criterion start to form at c_f = 23 wt%. Above 23 wt%, mixtures of long beaded fibers and droplets were electrospun. As discussed above, the MIX solvent increases the solution viscosity and thus improves the electrospinnability by facilitating pyridine-pyridine interactions, which can even lead to the gelation in P4VP/pyridine solutions.[33] A similar effect of using a poor solvent to improve electrospinnability through increased interchain interactions was reported, for example, for poly[2-methoxy-5-(2′-ethylhexyloxy)-1,4-phenylenevinylene] (MEH-PPV) by Zhong et al.[34]

Finally, Fig. 4.5 shows that, when BiOH is added in P4VP/MIX, solutions with a concentration as low as 14 wt% clearly form fibers longer than 20 μm. Interestingly, this c_f value is 1.8 times below that for P4VP-BiOH/DMF, in very good agreement with the 1.75 times increase in the fraction of hydrogen bonded pyridines (f_b) observed by infrared spectroscopy in Fig. 4.2b when changing the solvent from DMF to the mixture containing the non-hydrogen-bond breaker nitromethane. Pure and uniform fibers start to form at 27 wt% P4VP concentration and get thicker at 30 wt%, consistent with the observation of a concentrated regime in the viscosity plot of Fig. 4.3b (with c_D = 19 wt%) above which a well-developed network of effective entanglements exists, leading to a high viscosity and a strong resistance to the electrical stretching and surface tension forces leading to bead formation during the electrospinning process.

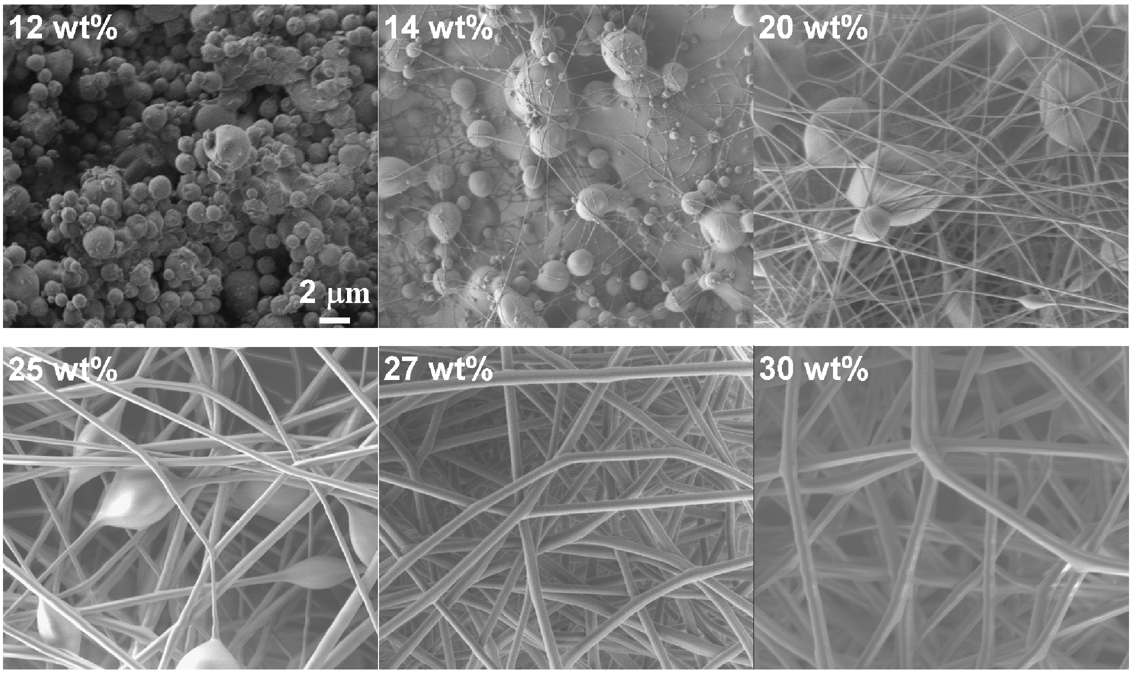

Figure 4.5. SEM images of electrospun products from P4VP-BiOH/MIX with different P4VP concentrations. All images have the same scale bar as shown in the first image.

Generally, the average ratios of c_f to c_e are 1.5-1.6 and the ratio of c_p to c_D is 1.4. This is higher than the 0.8-0.9 and 0.9-1.0 ratios, respectively, observed for P4VP200k.[26] Considering the similar relative improvement in electrospinnability contributed by effective crosslinks, this difference of ratios is mainly due to the low molecular weight of P4VP50k, which does not provide a sufficient number of physical entanglements or effective crosslinks during electrospinning to support the jet formation and prevent droplet formation for concentrations in the early stage of the semidilute entangled regime.

4.5.3 Effect of stronger small molecule crosslinkers

In view of the results with BiOH, we believe that small molecules with stronger interactions with P4VP should give higher stability (or effectiveness) of crosslinking in the solution, especially in pure DMF, and in the jet during electrospinning. For example, molecules with carboxylic acid groups are better hydrogen bond donors compared to those with hydroxyl groups,[35] and metal ions are well known to provide much stronger metal coordination with pyridine rings. Therefore, additional model compounds were blended with P4VP in DMF and their electrospinning behavior explored.

Fig. 4.6 shows SEM images of the electrospun products of 20 wt% P4VP solution, without and with the addition of phenol, BiOH, HBCA (containing hydroxyl and carboxylic acid groups) and $ZnCl_2$. The pure P4VP solution is well below its c_f of 30 wt% and thus only leads to droplets. The addition of phenol does not lead to the formation of fibers either due to the lack of effective crosslinking since hydrogen-bonded phenols have no pendant hydroxyl groups to interact with pyridine or other OH groups. The addition of BiOH only leads to traces of very short and thin fibers since its $c_f = 25$ wt%. In sharp contrast, a large amount of beaded fibers are electrospun from the P4VP-HBCA solution, suggesting that stronger hydrogen-bonded crosslinking facilitates the formation of a stable network during electrospinning. Fig. 4.6 also shows that a similar morphology can be obtained from P4VP-$ZnCl_2$ with a very low content of $ZnCl_2$ (molar ratio of 4VP:Zn^{2+} = 1:0.01). Theoretically, this ratio could lead to a maximum of 4% of crosslinked pyridine rings, according to the tetrahedral coordination between Zn^{2+} and P4VP.[36] This clearly demonstrates that metal coordination is much more effective than hydrogen-bonded crosslinking to improve the electrospinning of P4VP solutions, possibly due to their higher resistance to disruption under deformation. It is noteworthy that such zinc coordination is so strong that a 1:0.1 molar ratio of 4VP:Zn^{2+} can lead to the gelation of P4VP.

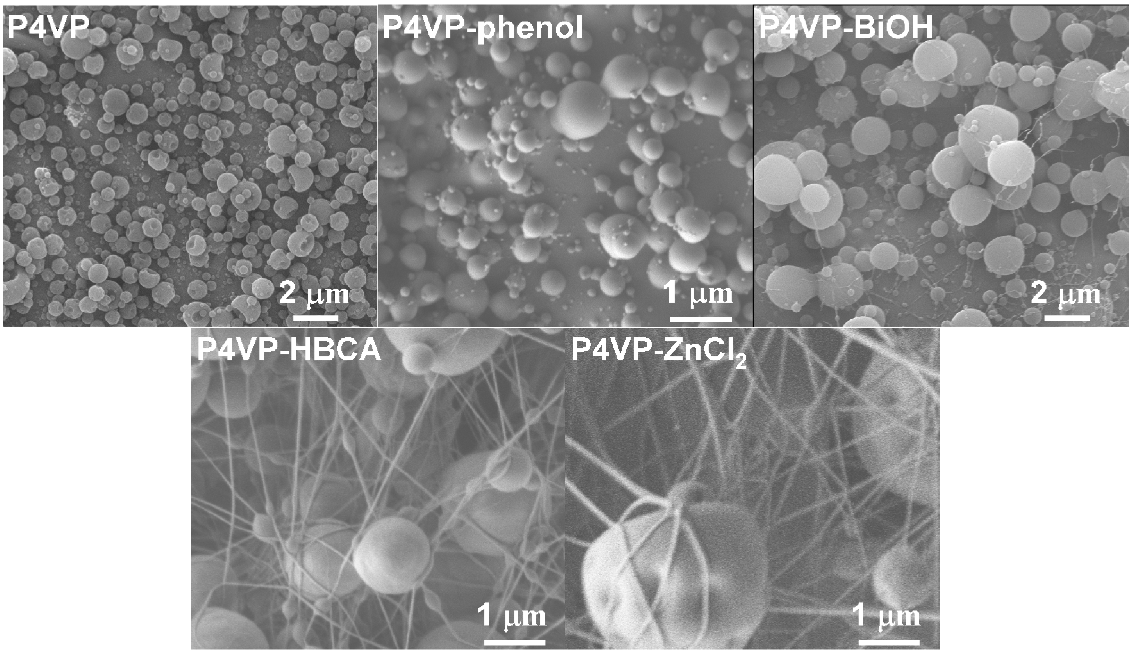

Figure 4.6. SEM images of electrospun products from 20 wt% P4VP solutions in DMF and its complexes with phenol, BiOH, HBCA and $ZnCl_2$.

Table 4.2 shows the fraction of hydrogen-bonded pyridine rings, f_b, in each solution. When introducing phenol, f_b (calculated with $a = 0.62$, see Fig. 4.S5 and Table 4.S1) only reaches 6.6% and leads to a small increase in specific viscosity. In comparison, BiOH leads to a similar f_b of 8.9 % but to a viscosity increase by more than a factor of two. This is due to the presence of the pendant hydroxyl groups in the monofunctionally hydrogen-bonded BiOH, which contribute to the friction between polymer chains and increase viscosity. For P4VP-HBCA, a was determined as 0.56 (see Fig 4.S6) and f_b is calculated as 23.8 % (see Fig 4.S7). This value is almost 3 times that for P4VP-BiOH solutions as stronger hydrogen bonds of the carboxylic acid groups can better resist the breaking effect of DMF. The solution is also almost twice as viscous, leading to the formation of beaded electrospun fibers. The case of $ZnCl_2$ is distinctive since, with a theoretical maximum of 4% of coordinated P4VP rings, it leads to a doubling of the solution viscosity as compared to the pure P4VP solution. Nevertheless, this solution was much less viscous than that with HBCA (and even BiOH), yet its performance in electrospinning was equivalent. This indicates that it is the effectiveness (or strength) of the crosslinked network, especially at extremely high deformation rates, rather than the viscosity at standard shearing rates, that plays the determining role for the electrospinnability.

Table 4.2. Fraction of hydrogen-bonded pyridine rings (f_b) and specific viscosity (η_{sp}) in 20 wt% P4VP solutions

	f_b[a]	η_{sp}
P4VP	---	21.5
P4VP-Phenol	6.6	25.1
P4VP-BiOH	8.9	54.7
P4VP-HBCA	23.8	96.6
P4VP-$ZnCl_2$	---[b]	44.0

a: from infrared analysis of the free and hydrogen-bonded pyridine bands

b: 4 % is the maximum theoretical fraction of metal coordinated pyridine rings

4.5.4 Removal of small molecules

Preparing fibers of pure polymers can be preferable for applications so the removal of additives is often necessary. Usually, additives are removed by using a selective solvent. For example, Gupta et al. used a water soaking method to remove $GaCl_3$ salt from Nylon-6 fibers and obtained porous fibers.[37] Laforgue et al. used methanol to rinse dihydroxynaphthalene (DHN) from thin films of poly(styrene-block-(4-vinylpyridine)) (PS-b-P4VP)/DHN complex.[38] The soaking method is quite easy and quick, but it is not appropriate if keeping the alignment of fibers in bundles or the shape of the mat is important. We thus sublimated the hydrogen bond crosslinkers by holding fibers in a vacuum oven at 120 ºC. For obvious reasons, sublimation of $ZnCl_2$ was not attempted.

As shown in Fig. 4.7, the infrared spectrum of electrospun fibers from P4VP-BiOH is almost identical to that of pure P4VP after sublimation for 2 months, indicating that BiOH was completely removed. The BiOH content, expressed as the percentage of the ratio of the intensity of a BiOH band (1168 cm^{-1}) to a P4VP band (1068 cm^{-1}) to its initial value,[29] was followed in Fig. 4.S9. At 120 ºC, the BiOH content drops by 30% in the first 2 days and then decreases more gradually to 7% in 7 weeks and to 0% after 2 months. It is interesting that at the same time, f_b drops steeply from 68% to 17% in the first 2 days, and then gradually to 0 % even when 15% BiOH remains. For P4VP-HBCA fibers, traces of HBCA remain after sublimation, as seen from the residual HBCA bands at 1182, 1267 and 777 cm^{-1}. Complete removal of HBCA and faster sublimation of BiOH could probably be reached using a pump with a lower base pressure than a standard mechanical pump.

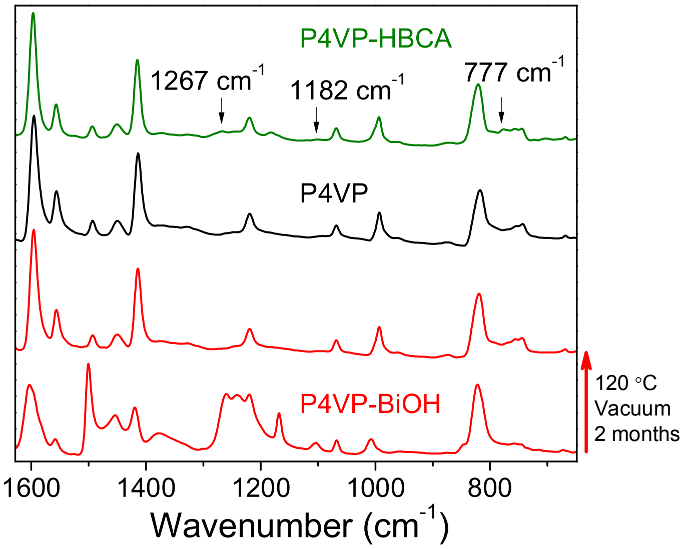

Figure 4.7. Infrared spectra of P4VP powder (black) and fibers electrospun from solutions of P4VP-BiOH (red) before and after sublimation, and of P4VP-HBCA (green) fibers after sublimation in a vacuum oven at 120 ºC for 2 months.

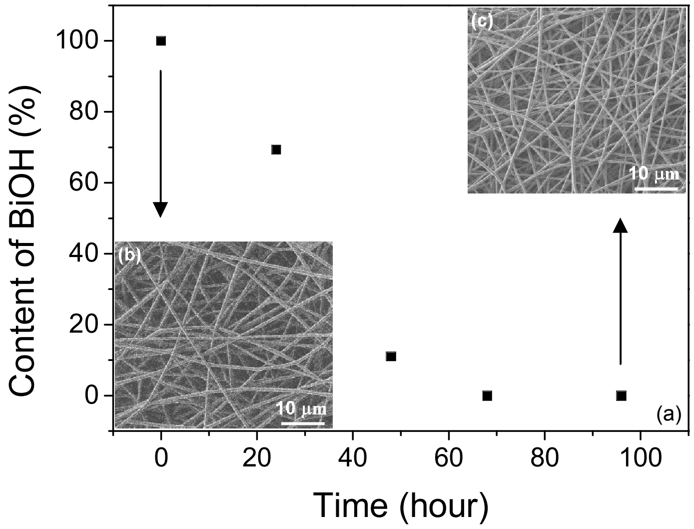

Figure 4.8. (a) Plot of BiOH content in electrospun fibers of P4VP-BiOH/MIX, expressed as the normalized ratio of the intensities of BiOH and P4VP bands at 1168 and 1068 cm^{-1}, respectively, during sublimation at 140 °C. The intensity ratios were normalized with the initial value. The insets are SEM images of fibers (b) before and (c) after sublimation at 140 °C for 78 hours.

Sublimation at 140 °C was also explored with the risk of changing the shape of fibers close to the Tg (142 °C) of P4VP. The BiOH content drops by 89% in 2 days, compared to only 30% at 120 °C, and it is almost completely removed in 3 days, compared with 2 months at 120 °C. The insets of Fig. 4.8 show SEM images of fibers before and after sublimation. A similar morphology, without newly formed beads, indicates that sublimation is an appropriate, although slow, method to remove small molecules inside fibers without affecting their shape.

4.6 Conclusion

In this work, we investigated the effect of 4,4'-biphenol (BiOH), phenol, 4-hydroxy-4'-biphenyl carboxylic acid (HBCA) and zinc chloride ($ZnCl_2$) as small crosslinkers to increase the electrospinnability of low molecular weight P4VP (50 kg/mol) in DMF and a mixed solvent (MIX) consisting of a good (DMF) and a poor (nitromethane) solvent. For the P4VP-

BiOH system, SEM shows that the fiber formation concentration (c_f) decreases when either BiOH or MIX is used, from 30 wt% in P4VP/DMF to 25 and 23 wt%, respectively. The lowest c_f is found at 14 wt% P4VP-BiOH/MIX. Additionally, uniform and pure fibers can be electrospun from P4VP-BiOH/MIX, which is the only system featuring a concentrated regime. The absolute magnitude of the improvement in electrospinnability is much larger than for P4VP50k than previously observed for a higher molecular weight P4VP200k, although the relative improvement is similar. It was also found that the ratio of c_f over c_e, the concentration for forming a semidilute entangled solution, is higher for P4VP50k than for P4VP200k, suggesting that topological entanglements better resist disruption during electrospinning than effective crosslinks by hydrogen bonding.

Due to their stronger hydrogen bonding and metal coordination interactions with pyridine rings, respectively, HBCA and $ZnCl_2$ are more efficient than BiOH at improving the electrospinning of P4VP. In particular, a very low content of $ZnCl_2$ (1 mol% vs. the pyridine rings) enables the formation of fibers at 20 wt% P4VP concentration in DMF. A relative advantage of the more weakly interacting BiOH is that it can be completely sublimated in 2 months at 120 ºC or in around 3 days at 140 ºC (2 ºC below Tg) without affecting the morphology of the fibers. These results suggest that, with proper selection or a bifunctional hydrogen bonding or a metal coordination crosslinker, nanofibers could be electrospun from P4VP below its critical molecular weight for forming an entanglement network, and that uniform fibers of pure P4VP could be obtained after sublimation. We believe this strategy could be expanded to other small molecules and polymers, which could be very useful to overcome a current limitation of electrospinning.

4.7 Acknowledgment

This work was supported by the Natural Sciences and Engineering Research Council of Canada (NSERC) and Fonds de recherche du Québec – Nature et Technologie (FRQNT). X.W. thanks the China Scholarship Council (CSC) and Université de Montréal for financial support. We thank Prof. X.X. Zhu for providing access to his rheometer.

4.8 Supplementary information

Additional infrared spectra, specific viscosity – concentration plots, and SEM images

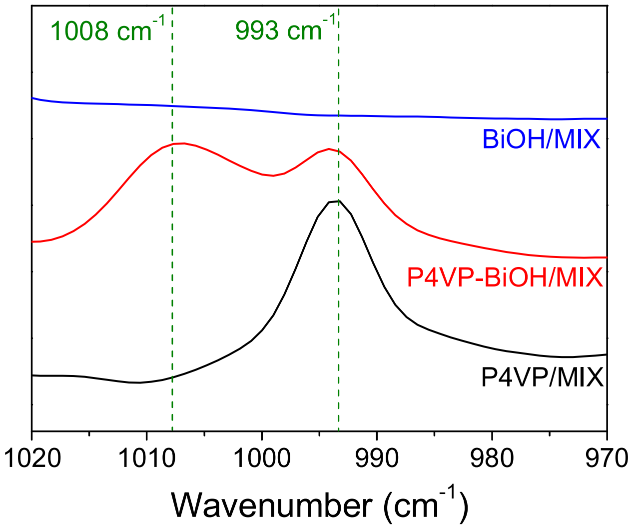

Figure 4.S1. ATR spectra of 10 wt% BiOH/MIX (blue), P4VP-BiOH/MIX (P4VP concentration = 20 wt%) (red), and P4VP/MIX (P4VP concentration = 25 wt%) (black). A MIX spectrum was subtracted for all solutions.

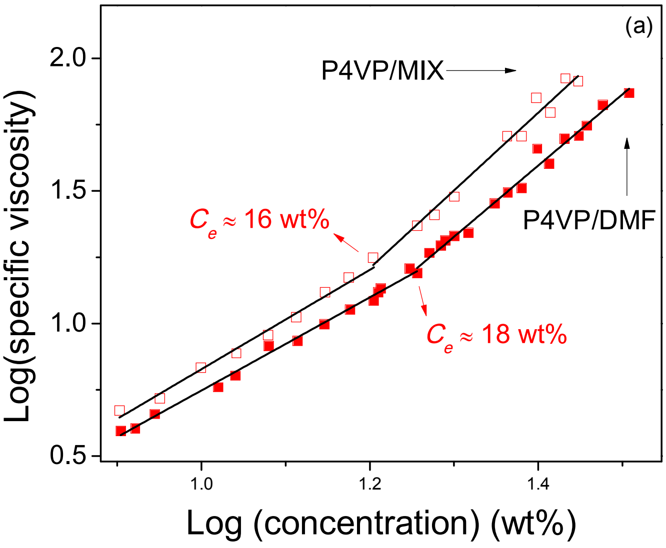

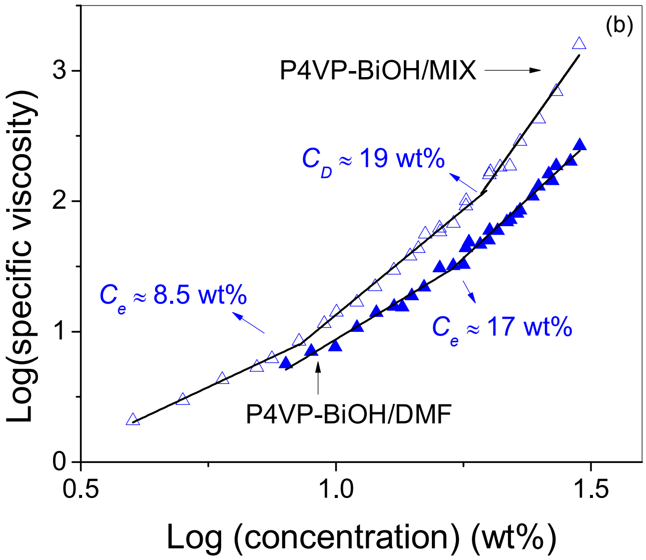

Figure 4.S2. Specific viscosity as a function of P4VP concentration for (a) pure P4VP solutions and (b) P4VP-BiOH solutions.

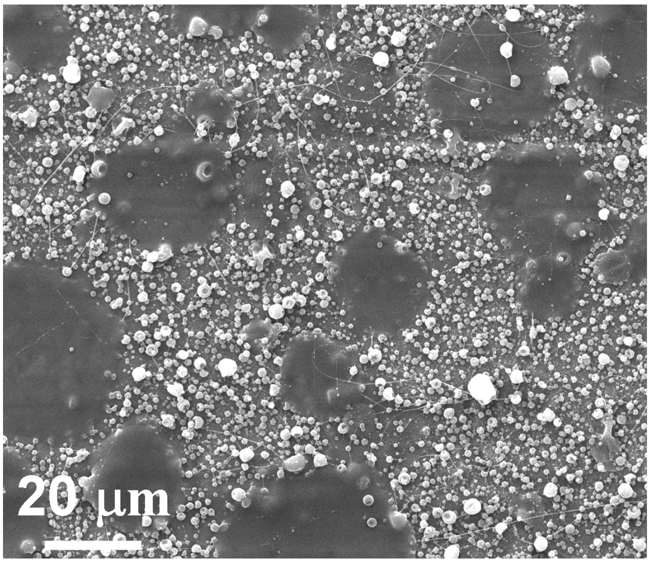

Figure 4.S3. SEM image at low magnification of electrospun products from a 30 wt% P4VP/DMF solution.

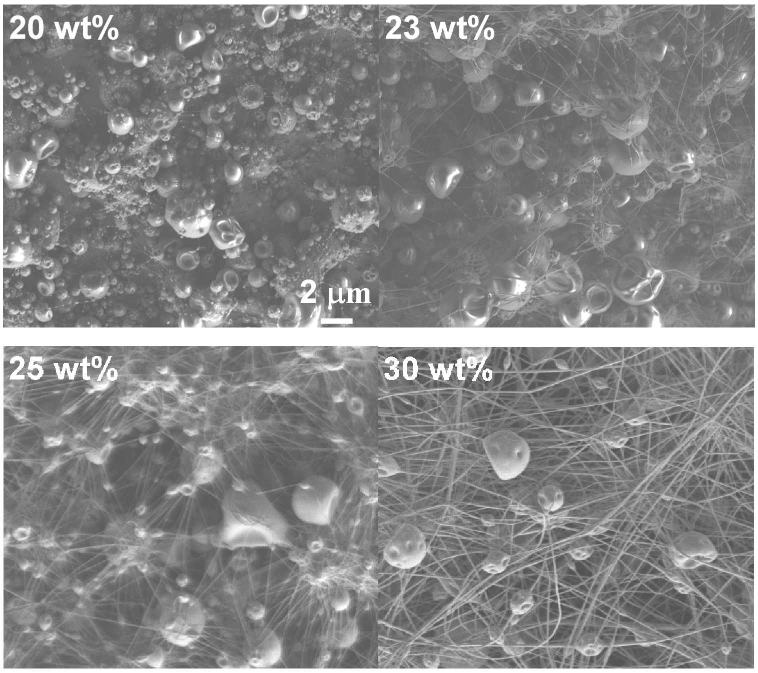

Figure 4.S4. SEM images of electrospun products from P4VP/MIX with different P4VP concentrations. All images have the same scale bar as shown in the first image.

Determination of *a* for P4VP-phenol

To determine the *a* factor, which is necessary to determine the percentage of pyridine-hydroxyl complexation between P4VP and phenol (f_b) using Eq. 4.1 of the main text, a liquid blend model of 4-ethylpyridine (EtPy) and phenol was used, as described in detail in our previous paper.[29] In the liquid blends, F_{OH} represents the nominal molar percentage of hydroxyl groups *vs.* pyridine rings and is noted as EtPy-phenol(F_{OH}).

As shown in Figure S5a, phenol bands at 999.5 and 1024 cm^{-1} were found in the spectra of the complex. The free pyridine band (994.4 cm^{-1}) overlaps with the 999.5 cm^{-1} band from phenol so its apparent position is shifted to around 995 cm^{-1} in EtPy-phenol(60%) and to 998.5 cm^{-1} for F_{OH} = 100% since the free pyridine band has essentially vanished and is only a shoulder on the phenol band. In contrast, the hydrogen-bonded pyridine band at 1009.7 cm^{-1} is not significantly affected by phenol bands. As a consequence, the integration methods used the maximum intensity for the hydrogen-bonded pyridine band (I_b) and the intensity at a fixed frequency (994.4 cm^{-1}) for the free pyridine band (I_f).

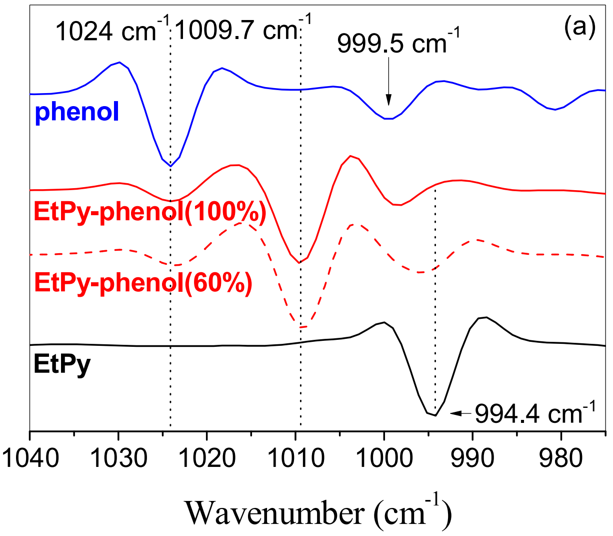

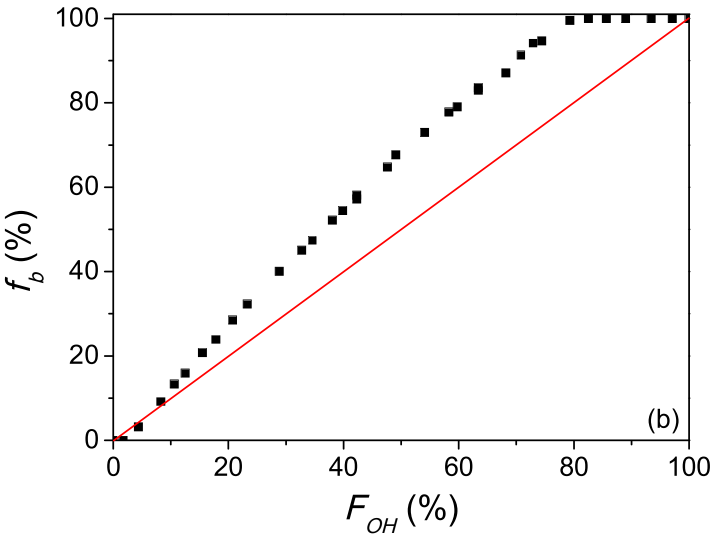

Figure 4.S5. (a) Second-derivative spectra of EtPy, phenol, EtPy-phenol(60%) and EtPy-phenol(100%). All the bands are negative in second-derivative spectra. (b) Percentage of hydrogen-bonded pyridine rings, f_b, as a function of BiOH content, F_{OH}, for EtPy-phenol liquid blends. The red line describes the theoretical values for full complexation of phenol to EtPy.

As described in Eq. 4.1 of the main text, f_b is obtained from I_f, I_b, and a, which is defined as:

$$a = \varepsilon_f / \varepsilon_b \tag{4.S1}$$

where ε_f and ε_b are the absorption coefficients of the free and hydrogen-bonded pyridine bands, respectively. We can express I_f and I_b in terms of the absorption coefficients as:

$$I_f = \frac{\varepsilon_f n_f}{V} \tag{4.S2}$$

$$I_b = \frac{\varepsilon_b n_b}{V} \tag{4.S3}$$

where n_f and n_b are the number of moles of free and hydrogen-bonded pyridine rings in the EtPy-phenol liquid blend whose volume is V. V can further be expressed as:

$$V = \frac{m_{mix}}{\rho_{mix}} \tag{4.S4}$$

where m_{mix} and ρ_{mix} are the mass and density of the prepared EtPy-phenol liquid blend, respectively.

For pure EtPy, Eqs. 4.S2-4.S4 can be reduced to Eq. 4.S5,

$$I_{f(pure)} = \frac{\varepsilon_f \rho_{EtPy}}{M_{EtPy}} \tag{4.S5}$$

where ρ_{mix} is replaced by ρ_{EtPy} and $M_{EtPy} = n_{EtPy} / m_{EtPy}$.

For any EtPy-phenol blend, Eqs. 4.S2 and 4.S3 can be combined to Eq. 4.S6

$$\frac{I_{f(mix)}}{\varepsilon_f} + \frac{I_{b(mix)}}{\varepsilon_b} = \frac{\rho_{mix} n_{EtPy(\mathrm{mix})}}{m_{mix}} \tag{4.S6}$$

where $I_{f(mix)}$, $I_{b(mix)}$ and $n_{EtPy(mix)}$ are I_f, I_b and the total number of moles of EtPy in the liquid blend, respectively. Further, Eq. 4.S7 could be obtained,

$$\varepsilon_b = \frac{I_{b(mix)}}{\rho_{mix} n_{EtPy(\mathrm{mix})} / m_{mix} - I_{f(mix)} \rho_{EtPy} / I_{f(pure)} M_{EtPy}} \tag{4.S7}$$

By rearranging Eqs. 4.S7, 4.S5 and 4.S1, Eq. 4.S8 is obtained:

$$a = \frac{I_{f(pure)} M_{EtPy}}{\rho_{EtPy}} \times \frac{\rho_{mix} n_{EtPy(\mathrm{mix})} / m_{mix} - I_{f(mix)} \rho_{EtPy} / I_{f(pure)} M_{EtPy}}{I_{b(mix)}} \tag{4.S8}$$

can be obtained to calculate a.

Based on the Eq. 4.S8 and by using ρ_{EtPy} = 0.942 g/mL, ρ_{mix} = 0.997 g/mL (estimated according to the method introduced in our previous paper[29]), M_{EtPy} = 107.15 g/mol, $I_{f(pure)}$ = 0.94 and $I_{f(mix)}$ = 0, serials of a could be calculated, as shown in Table 4.S1, leading to an averaged value of 0.62. Fig. 4.S5b shows the plot of f_b as a function of phenol hydroxyl content. The fact that f_b is larger than F_{OH} indicates that one hydroxyl group might complex with more than one pyridine rings.

Table 4.S1. Calculating a with series of liquid blends*

sample	F_{OH} (%)	$I_{b(mix)}$	$n_{EtPy(mix)}$(mol)	m_{mix}(g)	a
1	99.26	0.839	0.0184	3.741	0.625
2	99.26	0.846	0.0184	3.741	0.620
3	99.26	0.843	0.0184	3.741	0.622
4	98.77	0.863	0.0186	3.788	0.609
5	98.77	0.848	0.0186	3.788	0.620
6	98.38	0.837	0.0189	3.842	0.629
7	98.38	0.839	0.0189	3.842	0.628
8	98.38	0.842	0.0189	3.842	0.626

*: ρ_{mix} = 0.997 g/ml, $I_{f(mix)}$ = 0.

Determination of *a* for P4VP-HBCA

The determination of *a* for the P4VP-HBCA system was made, using the method described in our previous paper,[29] by using liquid blends of EtPy and 4-hydroxy-4'-biphenyl carboxylic acid (HBCA) as a model. Figure S6a shows the second-derivative spectra of EtPy, HBCA, and the complex EtPy-HBCA(10.8%). Compared with the spectrum of pure HBCA powder, the band at 1003 cm^{-1} becomes very weak and the band at 1021 cm^{-1} is not found in the spectrum of the complex. As for phenol and BiOH, the free pyridine band of EtPy at 994.4 cm^{-1} partially shifts to a higher wavenumber, at 1014 cm^{-1}, upon hydrogen-bond complexation in the spectrum of EtPy-HBCA(10.8%). This position is higher than for phenol and BiOH (1008-1009 cm^{-1}) due to the stronger hydrogen bonding interaction of the carboxylic acid group of HBCA with the pyridine rings.

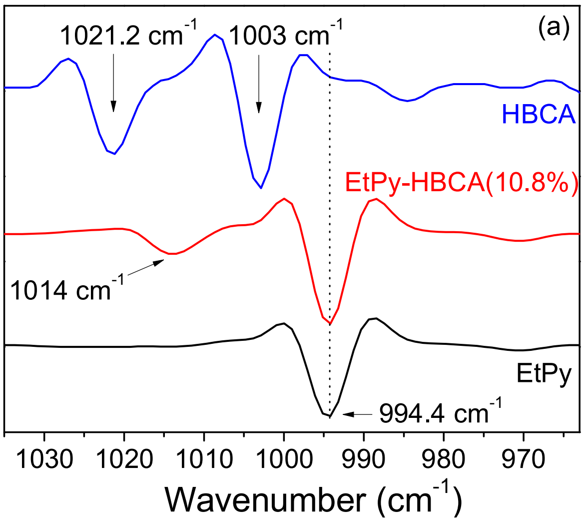

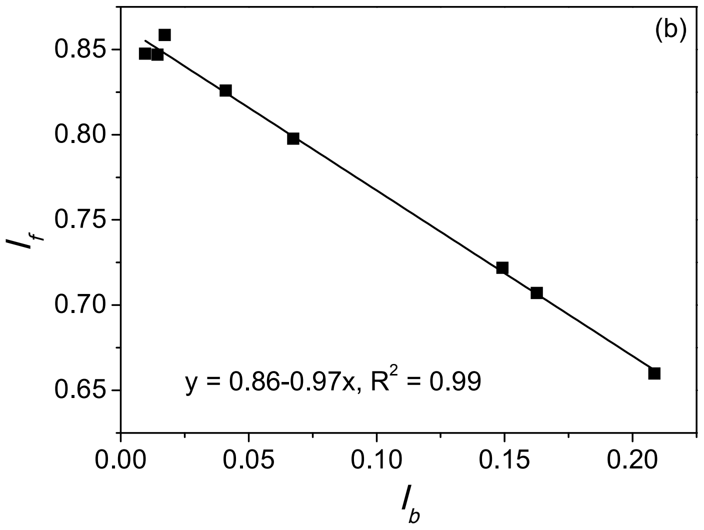

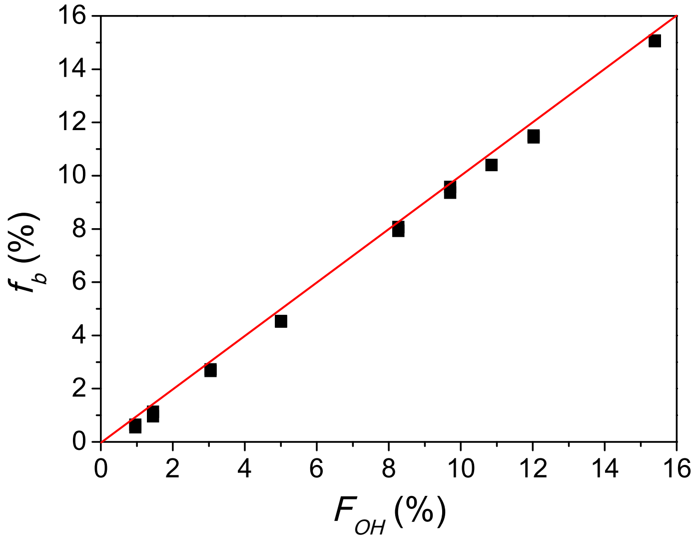

Figure 4.S6. (a) Second-derivative spectra of EtPy, HBCA and the EtPy-HBCA(10.8%) complex. (b) The intensity, I_f, of the free pyridine ring band at 994.4 cm^{-1} versus the intensity, I_b, of the hydrogen-bonded pyridine ring band at 1014 cm^{-1}, as obtained from the second-derivative spectra of the EtPy-HBCA(0.97-15.4%) liquid blends. The line represents the least-square fit of the data points. (c) Percentage of hydrogen-bonded pyridine rings, f_b, as a function of HBCA content, F_{OH}, for EtPy-HBCA liquid blends. The red line shows the theoretical values for full complexation of EtPy by HBCA.

Because of the limited solubility of HBCA in EtPy, such complex could only be prepared with F_{OH} from 0.97% to 15.4%. It should be noted that F_{OH} represents the nominal content of both OH and COOH groups present in solution. From these complexes, the correlation of the intensity of the second-derivative intensities of the bands at 1014 and 994.4 cm^{-1} was obtained and is shown in Figure 4.S6b as a linear line. The slope (k), which is expressed as the ratio of $I_{f(pure)}$ over $I_{b(pure)}$, was obtained as 0.97. According to our previous paper, k should be corrected by a dilution factor to determine the real a using Eq. 4.S9.[29]

$$a = \frac{I_{f(pure)}}{I_{b(pure)}} \times \frac{\rho_{mix} M_{EtPy}}{\rho_{EtPy}\left(M_{EtPy} + 0.5M_{HBCA}\right)} \tag{4.S9}$$

Finally a was determined as 0.56 using ρ_{mix} (assumed density of EtPy-HBCA(100%)) = 1.09 g/mL and M_{HBCA} = 214.22 g/mol. The f_b values agree very well with F_{OH}, as shown in Fig 4.S6c.

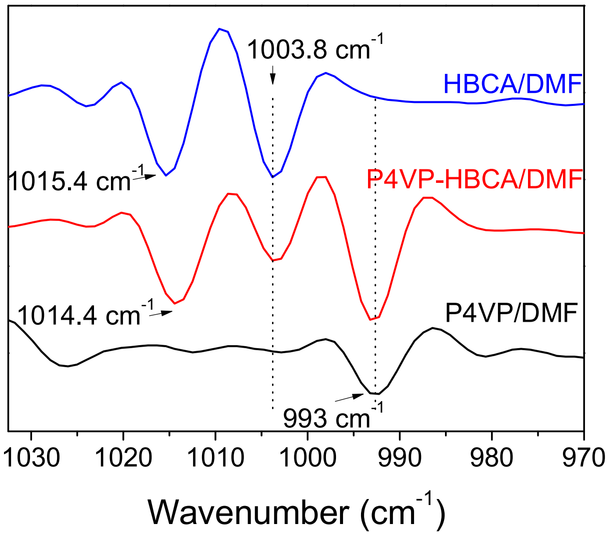

Figure 4.S7. Second-derivative ATR spectra of black: P4VP/DMF; red: P4VP-HBCA/DMF, F_{OH} = 100%; blue: HBCA/DMF; Concentration of P4VP = 20 wt%, and for all the solutions, a DMF spectrum has been subtracted

Figure 4.S7 shows the second-derivative spectra of P4VP/DMF, P4VP-HBCA/DMF and HBCA/DMF. For P4VP/DMF and P4VP-HBCA/DMF, the P4VP concentration was 20 wt% and F_{OH} was 100% for P4VP-HBCA/DMF. Compared with the spectrum of HBCA in liquid EtPy, the band at 1003.8 cm^{-1} remains present in HBCA/DMF and the 1021.2 cm^{-1} band is shifted to 1015.4 cm^{-1}. As a consequence, it overlaps with the hydrogen-bonded P4VP band at 1014.4 cm^{-1} and contribution must be considered in calculating f_b in P4VP-HBCA/DMF. We assumed that the intensity ratio (1.23) of the HBCA bands at 1003.8 and 1015.4 cm^{-1} in HBCA/DMF remained unchanged in P4VP-HBCA/DMF, so that the contribution of 1015.4 cm^{-1} band from HBCA to the 1014.4 cm^{-1} band could be subtracted based on the intensity of 1003.8 cm^{-1} band. Finally, f_b in P4VP-HBCA/DMF (P4VP concentration equal to 20 wt%) was calculated as 23.8 %.

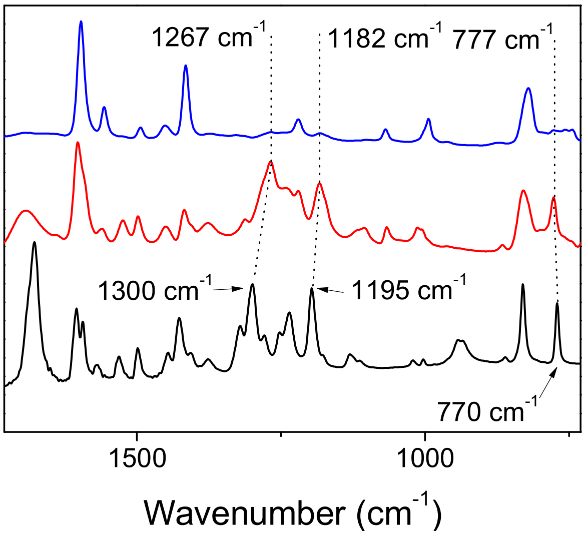

Figure 4.S8. ATR spectra of HBCA powder (black) and of electrospun fibers of P4VP-HBCA before (red) and after (blue) sublimation in a vacuum oven at 120 °C for 2 months.

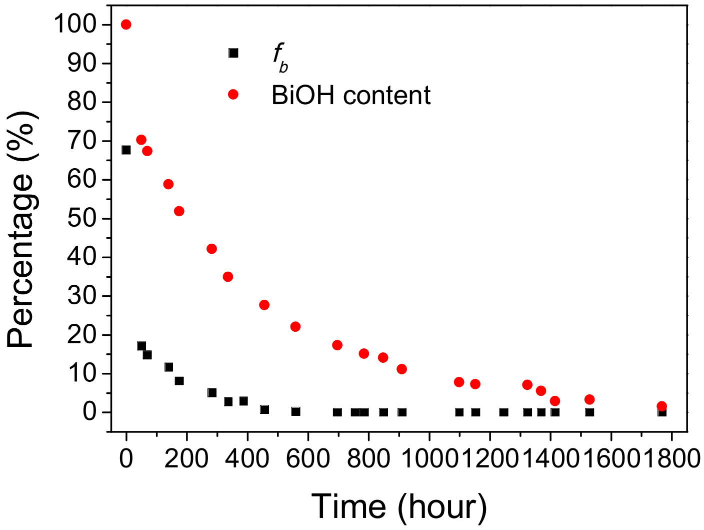

Figure 4.S9. Molar fraction of hydrogen-bonded pyridine rings (f_b) (black) and content in BiOH (red, expressed as the normalized ratio of the intensity of the 1168 cm^{-1} BiOH and 1068 cm^{-1} P4VP bands) in electrospun fibers of P4VP-BiOH/DMF during sublimation at 120 °C.

4.9 References

1. Reneker, D. H.; Yarin, A. L., *Polymer* **2008,** 49, 2387-2425.
2. Greiner, A.; Wendorff, J. H., *Angew. Chem., Int. Ed.* **2007,** 46, 5670-5703.
3. Schiffman, J. D.; Schauer, C. L., *Polym. Rev.* **2008,** 48, 317-352.
4. Sill, T. J.; von, R. H. A., *Biomaterials* **2008,** 29, 1989-2006.
5. Rieger, K. A.; Birch, N. P.; Schiffman, J. D., *J. Mater. Chem. B* **2013,** 1, 4531-4541.
6. Pham, Q. P.; Sharma, U.; Mikos, A. G., *Tissue Eng.* **2006,** 12, 1197-1211.
7. Chen, H.; Snyder, J. D.; Elabd, Y. A., *Macromolecules* **2008,** 41, 128-135.
8. Koski, A.; Yim, K.; Shivkumar, S., *Mater. Lett.* **2003,** 58, 493-497.
9. McKee, M. G.; Elkins, C. L.; Long, T. E., *Polymer* **2004,** 45, 8705-8715.
10. McKee, M. G.; Wilkes, G. L.; Colby, R. H.; Long, T. E., *Macromolecules* **2004,** 37, 1760-1767.
11. Shenoy, S. L.; Bates, W. D.; Frisch, H. L.; Wnek, G. E., *Polymer* **2005,** 46, 3372-3384.

12. Bonino, C. A.; Krebs, M. D.; Saquing, C. D.; Jeong, S. I.; Shearer, K. L.; Alsberg, E.; Khan, S. A., *Carbohydr. Polym.* **2011,** 85, 111-119.
13. Son, W. K.; Youk, J. H.; Lee, T. S.; Park, W. H., *Polymer* **2004,** 45, 2959-2966.
14. Wang, X.; Zhang, Q.; Bazuin, C. G.; Pellerin, C., *Macromol. Symp.* **2014,** 336, 30-38.
15. Nie, H.; He, A.; Zheng, J.; Xu, S.; Li, J.; Han, C. C., *Biomacromolecules* **2008,** 9, 1362-1365.
16. McKee, M. G.; Hunley, M. T.; Layman, J. M.; Long, T. E., *Macromolecules* **2006,** 39, 575-583.
17. Shenoy, S. L.; Bates, W. D.; Wnek, G., *Polymer* **2005,** 46, 8990-9004.
18. Brown, R. H.; Hunley, M. T.; Allen, M. H.; Long, T. E., *Polymer* **2009,** 50, 4781-4787.
19. Talwar, S.; Hinestroza, J.; Pourdeyhimi, B.; Khan, S. A., *Macromolecules* **2008,** 41, 4275-4283.
20. McKee, M. G.; Layman, J. M.; Cashion, M. P.; Long, T. E., *Science* **2006,** 311, 353-355.
21. Ahn, Y.; Kang, Y.; Ku, M.; Yang, Y.-H.; Jung, S.; Kim, H., *RSC Adv.* **2013,** 3, 14983-14987.
22. Celebioglu, A.; Uyar, T., *Chem. Commun.* **2010,** 46, 6903-6905.
23. Zhang, W.; Chen, M.; Zha, B.; Diao, G., *Phys. Chem. Chem. Phys.* **2012,** 14, 9729-9737.
24. Singer, J. C.; Giesa, R.; Schmidt, H.-W., *Soft Matter* **2012,** 8, 9972-9976.
25. Hermida-Merino, D.; Belal, M.; Greenland, B. W.; Woodward, P.; Slark, A. T.; Davis, F. J.; Mitchell, G. R.; Hamley, I. W.; Hayes, W., *Eur. Polym. J.* **2012,** 48, 1249-1255.
26. Wang, X.; Bazuin, C. G.; Pellerin, C., *Polymer* **2015,** 57, 62-69.
27. http://imagej.nih.gov/ij/.
28. Boris, D. C.; Colby, R. H., *Macromolecules* **1998,** 31, 5746-5755.
29. Wang, X.; Bazuin, C. G.; Pellerin, C., *Vib. Spectrosc.* **2014,** 71, 18-23.
30. Gupta, P.; Elkins, C.; Long, T. E.; Wilkes, G. L., *Polymer* **2005,** 46, 4799-4810.
31. Colby, R. H.; Rubinstein, M.; Daoud, M., *J. Phys. II France* **1994,** 4, 1299-1310.
32. Raspaud, E.; Lairez, D.; Adam, M., *Macromolecules* **1995,** 28, 927-933.
33. Vaganova, E.; Rozenberg, M.; Yitzchaik, S., *Chem. Mater.* **2000,** 12, 261-263.
34. Zhong, W.; Li, F.; Chen, L.; Chen, Y.; Wei, Y., *J. Mater. Chem.* **2012,** 22, 5523-5530.
35. Gilli, P.; Pretto, L.; Bertolasi, V.; Gilli, G., *Acc. Chem. Res.* **2009,** 42, 33-44.

36. Zander, N. E.; Orlicki, J. A.; Rawlett, A. M., *Polym. Prepr. (Am. Chem. Soc., Div. Polym. Chem.)* **2009,** 50, 710-711.
37. Gupta, A.; Saquing, C. D.; Afshari, M.; Tonelli, A. E.; Khan, S. A.; Kotek, R., *Macromolecules* **2009,** 42, 709-715.
38. Laforgue, A.; Bazuin, C. G.; Prud'homme, R. E., *Macromolecules* **2006,** 39, 6473-6482.

Chapter 5: Molecular level study of the photo-orientation of hydrogen-bonded poly(4-vinyl pyridine)-azobenzene complexes*

5.1 Résumé

Pour optimiser les propriétés des matériaux polymères contenant des azobenzènes pour différentes applications, telles que des guides d'ondes réinscriptibles et des dispositifs de stockage de données holographiques, il est primordial de comprendre l'influence de la structure de l'azobenzène sur la photoréponse du matériau. Les matériaux supramoléculaires, dans lesquels un azobenzène photoactif complexé contrôle le mouvement ou d'autres propriétés d'un polymère passif, sont particulièrement utiles pour étudier l'impact de modifications chimiques subtiles. Ici, nous utilisons la spectroscopie infrarouge d’absorbance structurale par modulation de la polarisation (PM-IRSAS) pour révéler l'impact du changement de la nature du groupement queue de l'azobenzène dans les complexes supramoléculaires formés par liaisons hydrogène avec la poly (4-vinylpyridine) (P4VP). Nous montrons qu’en changeant le groupement queue hydrogène (A_H) en queue cyano (A_{CN}), une augmentation de la photo-orientation des chromophores est induite, et, fait remarquable, provoque la réorientation des groupements pyridines de la P4VP via leurs liaisons hydrogène. En augmentant le degré de complexation, l'orientation maximale de A_H et de A_{CN} diminue, mais l'orientation de la P4VP augmente dans le complexe P4VP/A_{CN}, et l'orientation résiduelle des deux composés augmente. Au meilleur de notre connaissance, ces travaux constituent la première démonstration de transfert de mouvement induit par la lumière d'un azobenzène à un polymère photopassif au travers de liaisons supramoléculaires.

---

* This chapter will be submitted as a full paper for publication. It is coauthored by Jaana Vapaavuori, C. Geraldine Bazuin and Christian Pellerin.

5.2 Abstract

To optimize azobenzene-containing polymer materials for different applications, such as rewritable waveguides and holographic data storage, it is imperative to understand the effect of the azobenzene structure on the photoresponse of the material. Supramolecular materials, in which a complexed photoactive azobenzene controls the motion or other properties of a non-absorbing passive polymer, are uniquely convenient to study the impact of subtle chemical modifications. Here, we use polarization modulation infrared structural spectroscopy (PM-IRSAS) to reveal the impact of changing the tail-group of the azobenzene in hydrogen-bonded supramolecular complexes with poly(4-vinyl pyridine) (P4VP). We show that by changing the tail-group from hydrogen (A_H) to cyano (A_{CN}), an increased photo-orientation of the chromophores is induced and, remarkably, is converted into rotation of the pyridine groups of P4VP through their hydrogen bond. When increasing the complexation extent, the saturated orientation of both A_H and A_{CN} decreases but, interestingly, the orientation of P4VP increases for P4VP/A_{CN}, and the residual orientation of both components increases. To our knowledge, this is the first demonstration of transfer of light-induced rotational motion from an azobenzene to a photo-passive polymer over such supramolecular bonds.

5.3 Introduction

Azobenzene and its derivatives undergo photo-isomerization between *trans* and *cis*-isomers upon irradiation and various phenomena emerge from this clean and efficient photoreaction.[1-2] Upon illumination of linearly-polarized light, the azobenzenes tend to rotate into a direction in which their transition dipole moment is perpendicular to the polarization of the incident light. This photoinduced orientation is of particular interest for many optoelectronic and photonic applications like surface liquid crystal displays,[3] waveguide couplers,[4-5] and rewritable holographic data storage.[6-7] A larger, macroscopic motion can be induced by light into azobenzene-containing materials,[1, 8] enabling the design of photosensitive devices like artificial muscle[9] and light-driven motor.[10]

To date, the majority of materials studied for applications of photo-orientation are polymers with azobenzene covalently bonded in the main chain,[11-12] as side chain,[1, 4, 6-10] or even crosslinked between chains[8, 10]. Supramolecular azo-containing polymer complexes are gaining increasing attention due to their adjustable material properties and their easier preparation procedure as compared to the synthesis required for covalent polymers. For example, ionic bonding between azobenzene-bearing sulfonate groups and alkylated poly(4-vinyl pyridine) (P4VP),[13-15] poly(dimethylaminoethyl methacrylate)[15] and poly(ferrocenylethylmethylsilane-co-ferrocenylaminomethylsilane)[16] all showed remarkable photoinduced birefringence and formed surface-relief gratings (SRGs). Similar results were also obtained for hydrogen-bonded[17-23] and halogen-bonded[24-25] complexes between P4VP and functionalized azobenzenes with various structures.

Several studies have revealed that both the structure and the content of the supramolecularly-attached azobenzene have significant impact on the efficiency of SRG formation[17, 19] and on their photo-orientation, as measured by the photoinduced birefringence.[18, 20-21, 23] For example, changing only one functional group in hydrogen-bonded P4VP/azobenzene complexes can tune the intermolecular interactions between chromophores and P4VP, and these interactions can then be used to promote the photo-orientation efficiency. By increasing azobenzene content, a large increase in photoinduced birefringence, normalized by the number density of chromophores, was observed for P4VP complexes with nitro-tailed or cyano-tailed azobenzenes, whereas a simple hydrogen tail group resulted in a decreasing trend as a function of increasing chromophore content.[21, 23] More specifically, the saturated birefringence rises with increasing azobenzene content for both chromophores (see Fig. 5.S1), but the contribution per azobenzene unit to the birefringence increases with cyano-tailed azobenzene content but decreases for H-tailed chromophore.[23] This dramatic influence of the tail group of the chromophores calls for further investigations on what makes these very similar systems behave in opposite ways.

As birefringence only provides the overall orientation in the system, it is of interest to employ infrared spectroscopy because it can differentiate between the behaviors of different molecular groups. Indeed, polarized Fourier transform infrared spectroscopy (FT-IR) is a powerful and informative tool to investigate the orientation of azobenzene and polymer selectively in azobenzene-containing systems. Traditional static polarized FT-IR has been applied to study polymers covalently-bonded[26-32] and doped[33-35] with azobenzenes, but it low time resolution limits its use to slow processes. Buffeteau and Pézolet were the first to use polarization modulation infrared linear dichroism (PM-IRLD),[36] a method coupling IR with polarization modulation to enable a time resolution as good as 200 ms, to probe the time-resolved photo-orientation of a disperse red 1-containing amorphous azopolymer.[37] A shortcoming of PM-IRLD is that it only measures the dichroic difference (ΔA) between the spectra parallel (A_p) and perpendicular (A_s) to the laser polarization direction so that the structural absorbance (A_0) information is missing. Liang et al. developed a method called polarization modulation infrared structural absorbance spectroscopy (PM-IRSAS) to overcome this limitation and to improve the accuracy of the calculated orientation parameters.[38]

Here, we employ PM-IRSAS to follow the photo-orientation of the complexes, upon illumination with linearly-polarized light, of light-active azobenzenes with a cyano (A_{CN}) and hydrogen (A_H) tail group and of the photopassive polymer shown in Scheme 5.1. We show that A_{CN} orients more than A_H , under identical conditions, and that it is capable of driving a photo-induced orientation of the pyridine groups of P4VP through their hydrogen-bond. The evolution of the saturated and residual orientation of the azobenzenes and of P4VP, when changing the azobenzene content, enables understanding their contrasting behavior when studied by birefringence. To our knowledge, this is the first report of the transfer of light-induced rotational motion from an azobenzene to a photo-passive polymer over such supramolecular bonds.

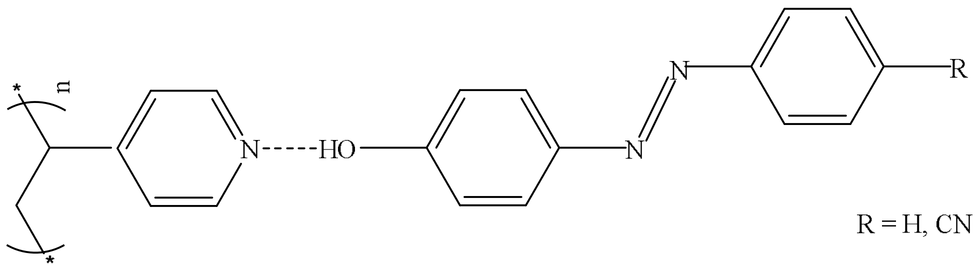

Scheme 5.1. Supramolecular complex between poly(4-vinyl pyridine) (P4VP) and 4-phenylazophenol (A_H, R = H) and 4-hydroxy-4'-cyanoazobenzene (A_{CN}, R = CN).

5.4 Experimental

5.4.1 Materials and samples

Poly(4-vinyl pyridine) (P4VP) with a viscosity average molecular weight of 200 kg/mol was obtained from Scientific Polymer Products. 4-phenylazophenol (A_H, 97%) was purchased from Sigma-Aldrich and 4-hydroxyl-4'-cyanoazobenzene (A_{CN}) from Beamco. Chloroform ($CHCl_3$, HPLC grade) and N,N-dimethylformamide (DMF, 99.8%) were purchased from EMD and methanol (MeOH, HPLC grade) from Fisher Scientific. All products were used as received.

P4VP was dissolved, with or without azobenzenes, in pure $CHCl_3$, DMF or in a mixed solvent of $CHCl_3$ and MeOH in 10 ml vials to give solutions of various concentrations. The solutions in the $CHCl_3$/MeOH solvent mixture were prepared by first mixing the solvents with a 6:1 $CHCl_3$:MeOH mass ratio, which was then added to the solutes, followed by homogenization for 2 min in an ultrasonic bath (Fisher Scientific FS60). All solutions were shaken gently for 3 days with a Heidolph UNIMAX 1010 shaker (Rose Scientific) to obtain homogenous samples and were left for 1 day before further characterization. The composition of the P4VP-azobenzene complexes is indicated as P4VP/A_H(F_A) and P4VP/A_{CN}(F_A), where F_A refers to the mole percent of azobenzene molecules relative to the pyridine rings of P4VP.

For static FT-IR characterization, samples were prepared by casting 5 μL solutions of P4VP/A_H or P4VP/A_{CN} in $CHCl_3$, with a P4VP concentration of 0.1-0.5 wt%, on BaF_2 windows, followed by drying in a hood for 3 days. For PM-IRSAS measurements, samples were prepared by casting 50 μL solutions of the P4VP/A_H or P4VP/A_{CN} in $CHCl_3$/MeOH, with a 1 wt% P4VP concentration, on BaF_2 windows, followed by drying in a hood for 5 days.

For birefringence and UV-Vis spectroscopy experiments, the samples were spin-coated on clean glass substrates. For UV-Vis, the samples were left to dry in a hood for 24 h, whereas for birefringence the samples were baked at 70 °C. The optical density of birefringence samples was set between 0.05-0.1 at 457 nm to ensure that the differences in absorbance have a negligible effect to photo-orientation reached. For azobenzene UV-Vis spectra in solution, the dyes were dissolved in DMF to give a concentration of 0.01 M.

5.4.2 Measurements

Static FT-IR measurements were performed on a Bruker Vertex 70 spectrometer with a deuterated L-alanine triglycine sulfate (DLATGS) detector. All spectra were obtained with a resolution of 4 cm^{-1} by averaging 512 scans. PM-IRSAS measurements were recorded with the same spectrometer and the external setup shown in Scheme 5.2. The optical setup includes a 488 nm laser (20 mW, JDSU FCD488-020) with a beam diameter of 0.7 mm expanded to 7 mm, using a 10X beam expander (Thorlabs INC BE10M), to fully cover the sample. The PM-IRSAS setup includes a liquid-nitrogen-cooled mercury cadmium telluride (MCT) detector (Kolmar Technologies), two ZnSe lens, a KRS-5 wire-grid polarizer (Optometrics), and a photoelastic modulator (PEM-90, type II/ZS50, Hinds Instruments) operating at 100 kHz ($2f_m$). The detected signal is processed to generate the dichroic difference (ΔA) and the individual polarized spectra, following the method described by Liang et al.,[38] using a lock-in amplifier (Stanford Research Systems, SR830) with a 30 μs time constant and two dual-channel electronic filters (Frequency Devices, 90TP/90IPB).

During the PM-IRSAS measurements, photo-orientation was induced by irradiating samples with a vertically-polarized 488 nm diode laser (20 mW/cm^2) for 30 min. All spectra were obtained with a resolution of 4 cm^{-1} by averaging 400 scans for the initial state, 20 scans for the first 1 min of the fast orientation (with laser on) and relaxation (with laser off) processes, and 320 scans for the photostationary/residual relaxation stage. As the size of the samples for PM-IRSAS measurements was usually over 1 cm of diameter, larger than that of the IR beam (~1 mm), the local chemical composition, expressed as the mole percentage of azobenzenes molecules relative to the pyridine rings (F_A), was determined by a calibration method described in Supporting Information to eliminate any potential effect of chemical heterogeneities.

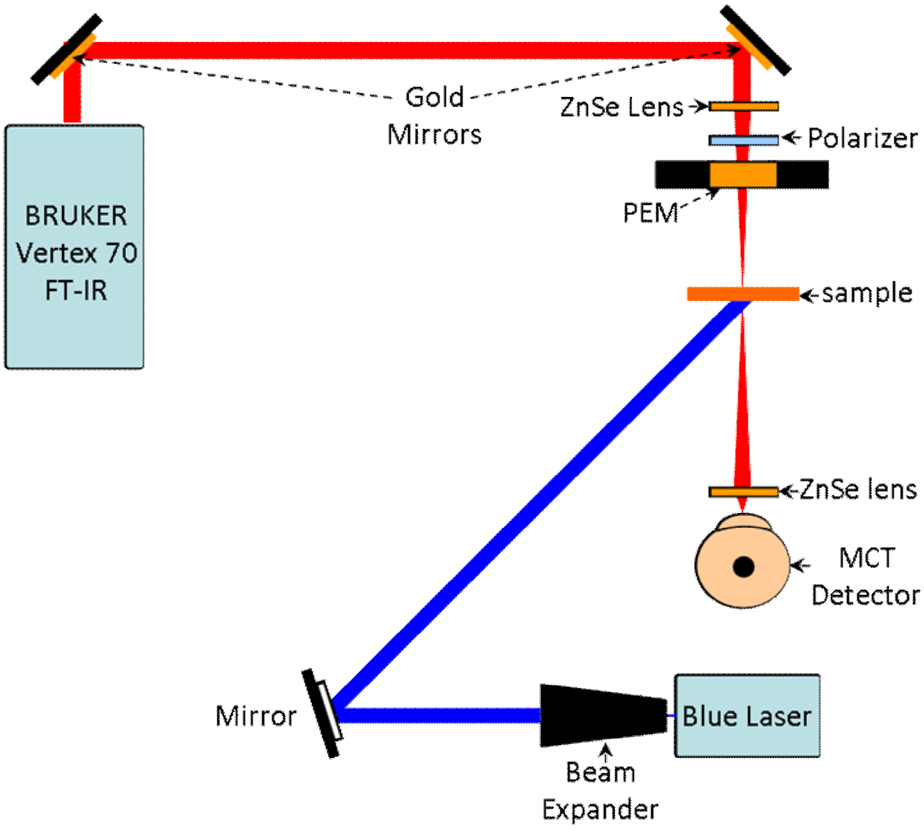

Scheme 5.2. Experimental setup for the polarization modulation infrared structural absorbance spectroscopy (PM-IRSAS) *in situ* study of the photo-orientation of azobenzene-containing supramolecular complexes.

The orientation parameter ($\langle P_2 \rangle$) of the molecular axis of interest, which could be the long axis of the azobenzene or the pyridine ring, was calculated using Eq. 5.1, in which ΔA is the dichroic difference, A_0 is the structural absorbance, and α is the angle between the transition dipole moment of the vibration and the molecular axis of interest. More details about this equation is described in Section 1.3.3 of Chapter 1.

$$\langle P_2 \rangle = \left(\frac{2}{3\cos^2\alpha - 1} \right) \left(\frac{\Delta A}{3A_0} \right) \tag{5.1}$$

For photo-induced birefringence measurements, a vertically-polarized 457 nm laser beam with an intensity of 150 mW/cm^2 was used to induce photo-orientation. Birefringence was measured with a low-power 820 nm laser probe whose transmission was measured through a polarizer/sample/analyzer configuration. The transmission directions of the polarizer and analyzer were set to ± 45° with respect to the polarization direction of the writing beam, and the birefringence (Δn) values were calculated using Eq. 5.2:

$$I = I_0 \sin^2 \left(\frac{\pi |\Delta n| d}{\lambda} \right) \tag{5.2}$$

where d is the thickness of the film, λ the wavelength of the probe beam, I the transmitted photodiode signal through the birefringent sample (polarizer and analyzer perpendicular) and I_0 the signal in the setup prior to the writing process (polarizer and analyzer parallel). The thickness of the samples was measured by usng a DEKTAK 6M profilometer.

The UV-vis measurements were performed with a fiber-coupled spectrometer (Ocean Optics, USB 2000+) and a DH-mini light source, combined with the 488 nm laser to pump the azobenzenes to the photostationary state. A clean glass substrate was used as a reference.

5.5 Results and discussion

The formation of hydrogen-bonded complexes between the azobenzenes and P4VP was confirmed by analyzing the IR spectra upon mixing the two constituents, as shown in Fig. 5.1. The band at 993 cm^{-1} in the spectrum of pure P4VP is due to a deformation vibration of the free pyridine ring. This band shifts to higher frequency upon hydrogen bonding with hydrogen bond donors.[39] In the spectrum of both complexes, a new band appears at 1010 cm^{-1} with a relative intensity, compared with band 993 cm^{-1}, that increases with a higher content of azobenzene. This is a typical evidence of the formation of hydrogen-bonded complex between P4VP and either A_{CN} or A_H.[39]

The coexistence of the bands at 1010 and 993 cm^{-1} for F_A = 100% indicates an incomplete complexation, which is related with steric effects and the restricted mobility of P4VP chains (T_g = 142 °C).[39-40] Therefore, the extent of complexation (f_b), which is the percentage of the hydrogen-bonded pyridine rings in P4VP, can be calculated by Eq. 5.3 as:

$$f_b = \frac{I_b}{I_b + I_f / a} \times 100\% \qquad (5.3)$$

in which I_f and I_b are intensities of the free and hydrogen-bonded pyridine bands at 993 and 1010 cm^{-1}, respectively, and a is defined as the ratio of their band absorption coefficients (ε_f and ε_b, respectively). Because of a partial overlap between the P4VP bands and band due to the azobenzene, a second-derivative method was used to obtain I_b and I_f. It is noteworthy that the spectra of A_H contain two bands, one at 1021 cm^{-1} which shifts to 1019 cm^{-1} in the complex, and one at 999 cm^{-1} which is not visible in either absorbance or second-derivative spectra of the complexes. The a parameters in Eq. 5.3 were determined as 0.39 and 0.35 for P4VP/A_{CN} and P4VP/A_H, respectively, following the method developed in our previous paper.[39] Details of this determination are provided in the Supporting Information.

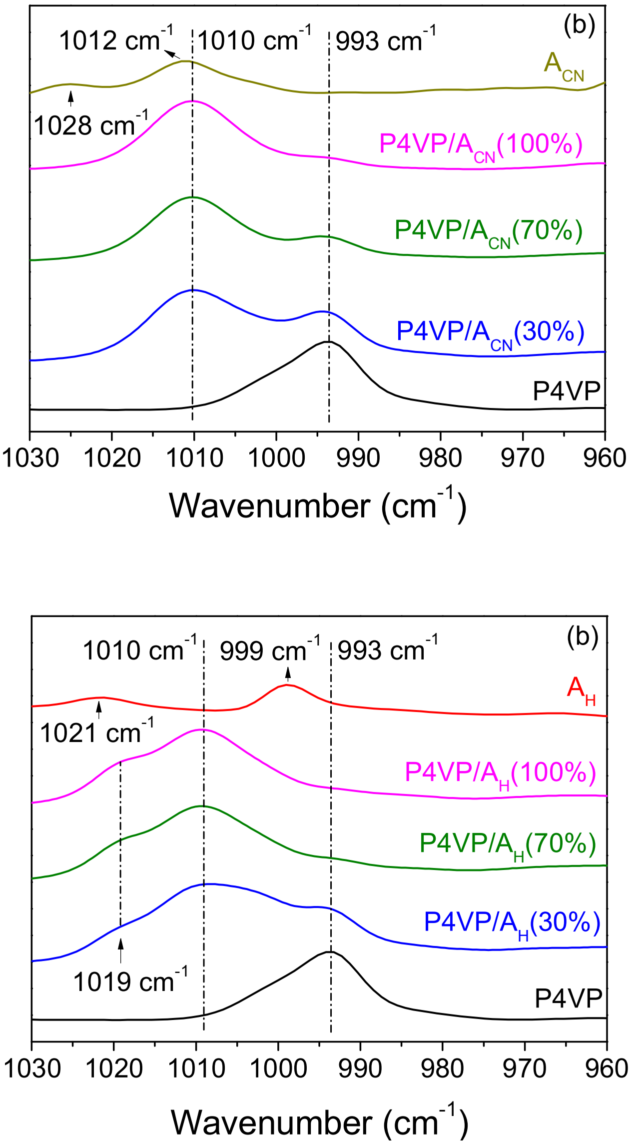

Figure 5.1. Infrared spectra of a pure P4VP film, of the pure azobenzene powder, and of drop-casted films of the P4VP complexes with (a) A_{CN} and (b) A_H powder with azobenzene molar percentage with respect to the P4VP repeat units (F_A) of = 30%, 70% and 100%.

Fig. 5.2 shows that, for both complexes, f_b increases almost linearly with F_A with the same slope of 0.86, 14% below the value that would have been obtained if the chromophores were fully complexed to P4VP (indicated by red line). This indicates that P4VP/A_H and

P4VP/A$_{CN}$ have the same extent of complexation over the full range of F_A, despite their different chemical structures, and thus that a different level of complexation does not explain their different behavior upon irradiation.[21, 23]

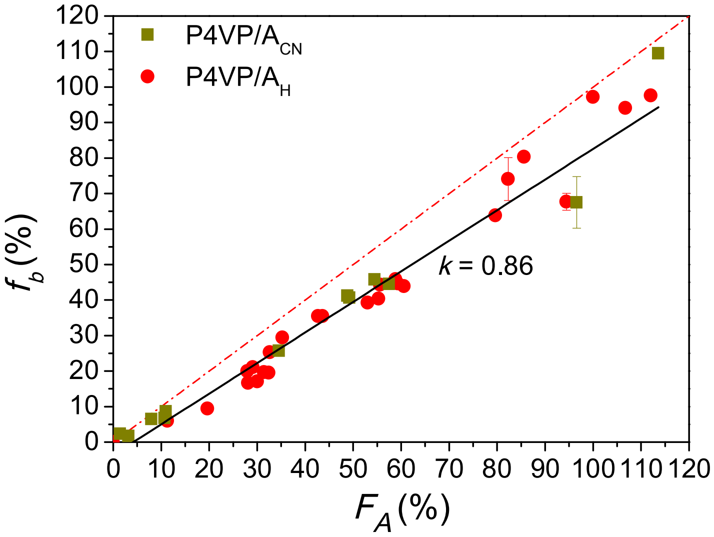

Figure 5.2. Percentage of hydrogen-bonded pyridine rings, f_b (%), as a function of azobenzene content, F_A, for P4VP/A$_{CN}$ and P4VP/A$_H$ complexes. The red line describes the theoretical values for full complexation of the azobenzenes to P4VP.

Fig. 5.3 shows the UV-vis spectra of P4VP/A$_{CN}$ and P4VP/A$_H$ films with different F_A before and after irradiation with linearly-polarized 488 nm diode laser. The spectra feature an intense band with a maximum absorption (λ_{max}) at 345 nm and 349 nm for P4VP/A$_{CN}$ and P4VP/A$_H$, respectively, when F_A is 100%. The absorption band, which is attributed to π-π* absorption,[30, 41] red-shifts when F_A decreases (as indicated by the arrows), suggesting an enhanced chromophore excitonic coupling effect and π-π interaction in the complexes with large F_A.[42] The red shift induced by each 10% decrease in F_A is around 3.6 nm for P4VP/A$_{CN}$, significantly larger than that of around 1 nm for P4VP/A$_H$. This is consistent with the larger dipole moment of A$_{CN}$ as compared to A$_H$. During irradiation with 488 nm light, the intensity of the π-π* band decreases for both P4VP/A$_{CN}$ and P4VP/A$_H$ without change of λ_{max}, indicating firstly the occurrence of *trans-cis* isomerization and secondly that the chromophore-chromophore interactions between the chromophores remaining in *trans* state are not affected by the isomerization.[30, 41] The n-π* absorbance of *cis* isomer under photostationary state (PSS) appears in the spectra of P4VP/A_H as a weak band at around 460 nm.[43] A similar n-π* band appears around 480 nm in the spectra of P4VP/A_{CN} as a shoulder overlapped with the intense π-π* band.

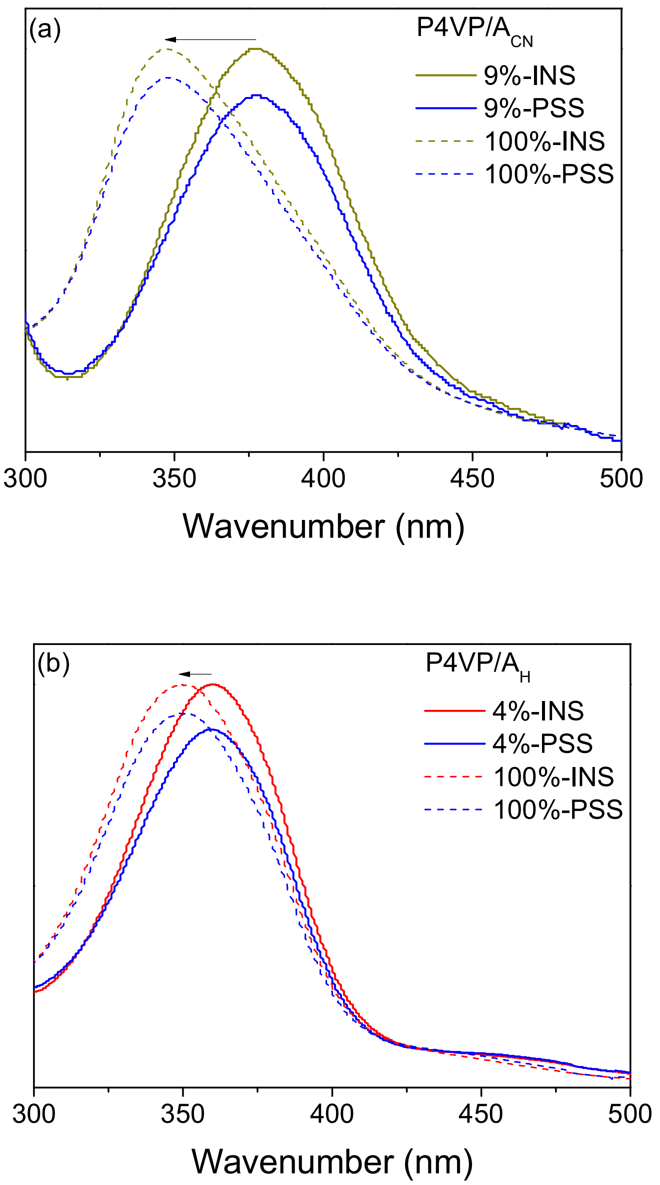

Figure 5.3. Normalized UV-Vis spectra of (a) P4VP/A_{CN} and (b) P4VP/A_H with different nominal F_A, before irradiation (INS) and under irradiation at the photostationary state (PSS).

The decrease of the intensity of the π-π* bands in photostationary state can be used to calculate the loss of *trans* isomers (and thus *cis* isomer formation), which is around 6-7% when F_A is 100% and around 11-13% when F_A is below 10% for both complexes, as shown in Fig. 5.S2. This gradual decrease in photoisomerization efficiency, when F_A increases, is a sign of decreased free volume around the azobenzene molecules.[21] Fig. 5.S2 further shows that the remaining *trans* isomer content in the photostationary state is extremely similar for both complexes, eliminating this factor as an explanation for the different photoresponse behaviors of P4VP/A_{CN} and P4VP/A_H.

Fig. 5.4 compares the dichroic difference (ΔA) and the structural absorbance (A_0) IR spectra of both complexes with the spectra of the pure components. After 30 min of irradiation with a linearly-polarized 488 nm light, many negative bands appear in the ΔA spectra, indicating that the photo-orientation occurs for these bands and that their transition dipole moments are orienting perpendicular to the polarization of the irradiation. To further distinguish the photo-orientation of the azobenzene and of the polymer, the orientation parameter, $\langle P_2 \rangle$, of appropriate individual bands must be quantified using Eq. 5.1. For proper quantification, the selected bands should be isolated, in both the A_0 and ΔA spectra, to avoid contributions from either P4VP or azobenzene and be of sufficient intensity to provide an acceptable signal-to-noise ratio for dynamic studies.

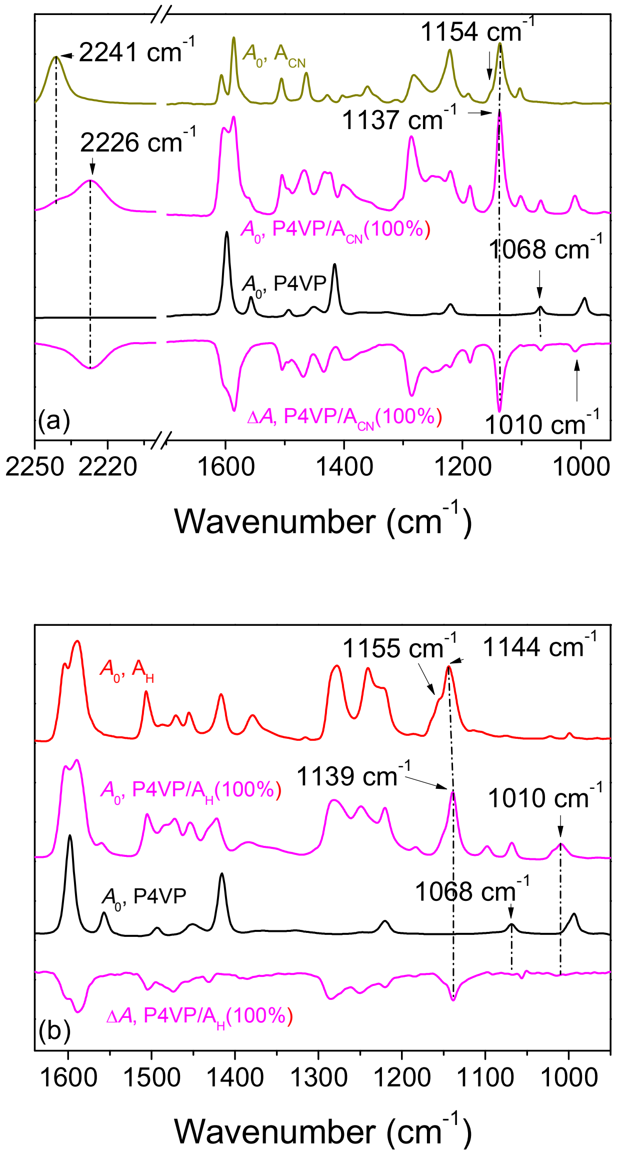

Figure 5.4. Infrared structural absorbance spectra (A_0) and dichroic difference spectra (ΔA) of (a) P4VP/A$_{CN}$(100%) and (b) P4VP/A$_H$(100%) after 30 min of irradiation. The spectra of pure P4VP powder (black) and of the powder of the appropriate pure azobenzene (green for A$_{CN}$ and red for A$_H$) are shown to highlight the isolated bands used for quantification of molecular orientation.

The bands at 1137 and 1144 cm^{-1} in the spectra of pure A_{CN} and A_H, respectively, which are assigned to a symmetric C-N stretching mode of the azobenzene group,[44-45] partially overlap with shoulders at 1154 and 1155 cm^{-1}, respectively, which are due to an in-plane C-H bending in the phenyl rings.[45-46] These shoulder bands become weak in both A_0 and ΔA for the two complexes so that their contribution to the intensity of the 1137 or 1139 cm^{-1} (shifted from 1144 cm^{-1}) bands in the complexes is negligible. Most importantly, these bands are well isolated from any P4VP contribution and are therefore good choices for quantifying the azobenzene orientation. The A_{CN} band at 2241 cm^{-1} is assigned to the C$\equiv$N stretching vibration of the cyano tail group and is very well isolated in all spectra.[47] It shifts to 2226 cm^{-1} in both A_0 and ΔA of P4VP/A_{CN}, with a weak band at 2241 cm^{-1} only appearing when F_A is close to 100%. The C$\equiv$N band was also used to validate the azobenzene orientation in P4VP/A_{CN}.

For P4VP, the band at 1068 cm^{-1}, which can be assigned to a deformation of the pyridine ring,[39] is well isolated from azobenzene bands in the A_0 of the two complexes and meets the criteria mentioned before for calculating $\langle P_2 \rangle$. Interestingly, this band is clearly visible in the ΔA spectrum of P4VP/A_{CN} under irradiation, indicating a quantifiable orientation of the P4VP pyridine rings, but not for P4VP/A_H. Besides, the 1010 cm^{-1} P4VP band also shows negative dichroism in ΔA of P4VP/A_{CN}, indicating the orientation of hydrogen-bonded pyridine rings. This band was also selected, although it overlaps with the 993 cm^{-1} P4VP band in the A_0 spectra, causing an inaccuracy in calculating its $\langle P_2 \rangle$. It should to be noted that there is no clear evidence of bands from the main chain of P4VP, like the in-plane bending vibration of -CH_2- at 1452 cm^{-1},[39] in the ΔA spectra, suggesting that only the side chains of P4VP orient upon irradiation.

For all the selected azobenzene bands, the transition dipole moment of the vibration is parallel to the long axis of the azobenzene, so $\alpha = 0°$ was applied in Eq. 5.1 when calculating $\langle P_2 \rangle$. For the selected P4VP bands, $\alpha = 0°$ was also used because their transition dipole moment is along the long (N-C4) axis of the pyridine ring, which should be more or less parallel to the hydrogen-bonded azobenzene (see Scheme 5.1). As a consequence, these orientation values refer to the orientation of the pyridine side-chains, not to that of the P4VP main chain.

Fig. 5.5a shows the plots of $<P_2>$ *vs*. time for different bands of P4VP/A_{CN}(100%). The curves all contain a photo-orientation stage, where $<P_2>$ increases (toward negative values because the orientation is perpendicular to the laser polarization direction) upon the irradiation, and a thermal relaxation stage, where orientation decreases with the removal of the irradiation to a residual $<P_2>$. Both stages consist of a fast and a slow process, with a relative importance that depends on the specific system and azobenzene content F_A. For most of P4VP/A_{CN} complexes with various F_A, the maximum $<P_2>$ under irradiation (which did not saturate under the experimental conditions) and the residual $<P_2>$ (observed after 30 min of thermal relaxation at room temperature) are approximately the same for the two selected azobenzene bands, and for the two selected polymer bands. As a consequence, only the bands around 1140 cm^{-1} for the azobenzene and 1068 cm^{-1} for P4VP were used in the following figures since they are available for both P4VP/A_{CN} and P4VP/A_H. It is also clearly observed that A_{CN} bands have higher $<P_2>$ and residual $<P_2>$ than P4VP bands, indicating that the driving force of the azobenzene can convert light energy into the orientation of the pyridine rings but that this process is not fully efficient.

Fig. 5.5b shows that, for P4VP/A_H with various F_A, the photo-orientation and thermal relaxation of A_H also follow the biexponential behavior noted for A_{CN}. Significantly higher $<P_2>$ values are obtained when F_A is lower, indicating the importance of the content of the azobenzenes. Besides, several other differences can be observed in the plots of $<P_2>$ *vs*. time as compared with those of P4VP/A_{CN}. First, a photostationary state appears during the photo-orientation for high F_A above around 30%, but not for samples with low F_A. A photostationary state was never observed for the P4VP/A_{CN} complexes. Second, the fast process contributes more to the change of the orientation, during photo-orientation and during relaxation, again in particular for high F_A. In fact, the slow process is barely observable for P4VP/A_H with F_A = 100%. Third, both the maximum and residual $<P_2>$ values are lower for P4VP/A_H with the same F_A, which will be further discussed below.

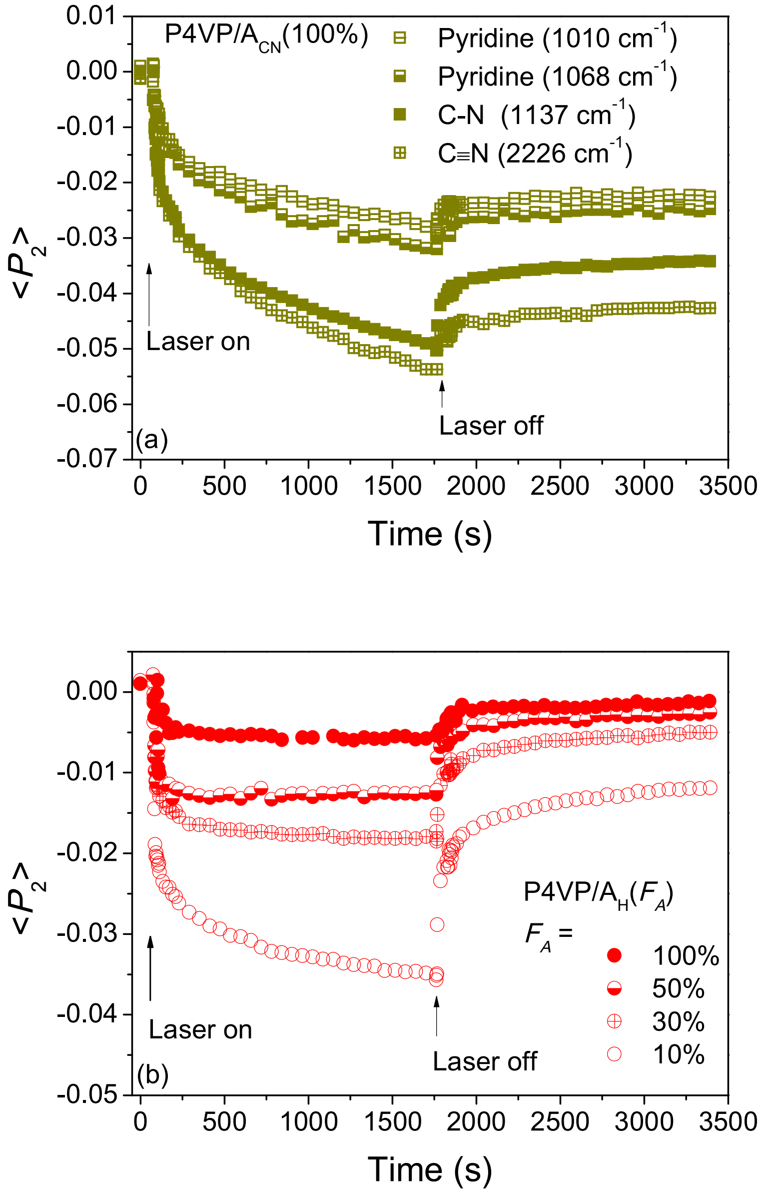

Figure 5.5. Photoinduced orientation (<P_2>) as a function of time for (a) different bands of P4VP/A$_{CN}$(100%) and (b) the 1139 cm^{-1} A$_H$ band in P4VP/A$_H$ with different F_A.

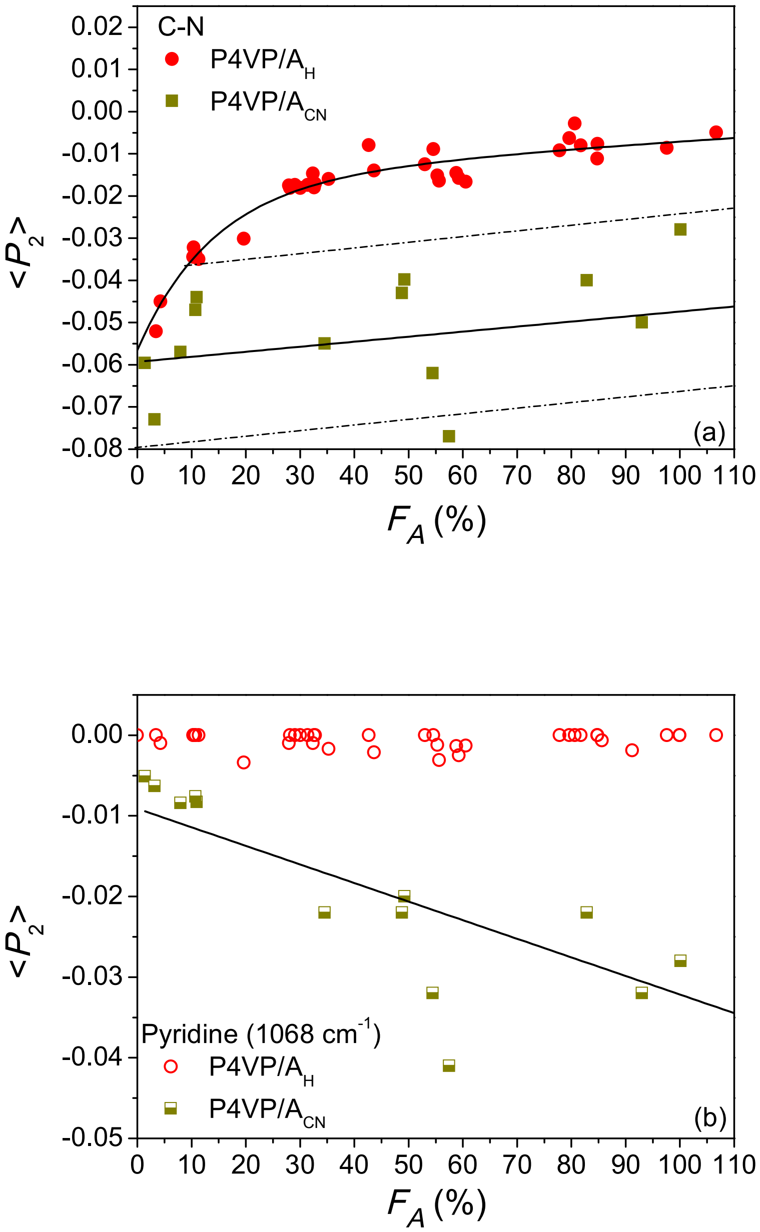

Figure 5.6. Evolution of the maximum <P_2> as a function of F_A for (a) the azobenzene and (b) P4VP in the P4VP/A$_{CN}$ and P4VP/A$_H$ complexes after 30 min of irradiation.

Fig. 5.6 shows the plots of the maximum $<P_2>$ of the C-N azobenzene band and of the pyridine band (1068 cm^{-1}), after 30 min irradiation, as a function of F_A. As mentioned above, results from the C≡N band in P4VP/A_{CN} and hydrogen-bonded pyridine rings (1010 cm^{-1}) in both complexes are not shown because their photoresponse behavior is very close, in the full range of F_A, to that of the C-N band in P4VP/A_{CN} and of the 1068 cm^{-1} pyridine band in both complexes, respectively. Fig. 5.6a shows that the maximum $<P_2>$ of A_H decreases in an exponential fashion with increasing F_A. The orientation of A_{CN} also decreases, although less rapidly, with increasing F_A, as indicated by the dash-dot contour. Interestingly, the maximum $<P_2>$ for the azobenzene in both complexes is very close when F_A is below 4%, that is when the molecules are well isolated from one another, but A_{CN} reaches a much higher $<P_2>$ (on average ~4 times higher when F_A is over 35%) than A_H.

Fig. 5.6b shows that, for P4VP/A_{CN}, the maximum $<P_2>$ of the P4VP pyridine groups increases almost linearly with F_A, which is opposite to the trend observed for A_{CN} in the same complex. The orientation values range from -0.005 to -0.04, which is lower than for A_{CN} (-0.03 to -0.08). For P4VP/A_H, the $<P_2>$ measured from the P4VP bands is essentially zero for all F_A.

The results of Fig. 5.6 help understanding the saturated photoinduced birefringence results in the work of Vapaavuori et al. As shown in Fig. 5.S1, the absolute birefringence increases for both complexes with increasing F_A but much more importantly for the P4VP/A_{CN} complex. This is consistent with the fact that A_{CN} orients more than A_H for the same F_A, in addition to the fact that only A_{CN} leads to a significant orientation of P4VP. The results also justify the divergent trends in the photoinduced birefringence contribution per azobenzene with increasing F_A, which was observed to increase for P4VP/A_{CN} and to decrease for P4VP/A_H.[23] Birefringence measurements reveal the average orientation of the whole system and are therefore affected by the orientation of both the azobenzene and P4VP components. As P4VP barely orients in P4VP/A_H, the overall birefringence is essentially due to the photo-orientation of A_H, explaining its decrease with A_H content based on the decreasing $<P_2>$ values observed in Fig. 5.6a. In contrast, the overall birefringence for P4VP/A_{CN} is the result of the opposing factors: the decreasing orientation of A_{CN} (Fig. 5.6a) and the increasing orientation of P4VP (Fig. 5.6b) with increasing F_A. Fig. 5.S5 shows that, although the absolute values cannot be compared because different irradiation conditions were used, combining the $<P_2>$ values of both components to estimate the birefringence response of P4VP/A_{CN} leads to the expected increasing trend with increasing A_{CN} content.

Fig. 5.7 shows that the residual orientation after 1600 s of thermal relaxation, calculated as the percentage of the residual $<P_2>$ relative to the maximum $<P_2>$ at the end of the irradiation stage, as a function of F_A. As shown in Fig. 5.7a, the residual orientation of both A_{CN} and pyridine rings for P4VP/A_{CN} increases from 40% to 80% with increasing F_A. In contrast, the residual orientation of A_H shows the opposite trend, with the highest value (40%) at very low F_A and the lowest, close to 0% when F_A is 100%. The residual orientation of pyridine rings is meaningless for P4VP/A_H since they barely oriented, as shown in Fig. 5.6b.

Fig. 5.7b shows the residual birefringence, which is the percentage of the residual birefringence, 300 s after removal of the irradiation, relative to the maximum birefringence, as the function of F_A. For both complexes, it starts from 40-50% at low F_A, close to the values observed by infrared spectroscopy in Fig. 5.7a, then increases for P4VP/A_{CN} and decreases for P4VP/A_H with increasing F_A, respectively. Such trends are similar to those shown in Fig. 5.7a.

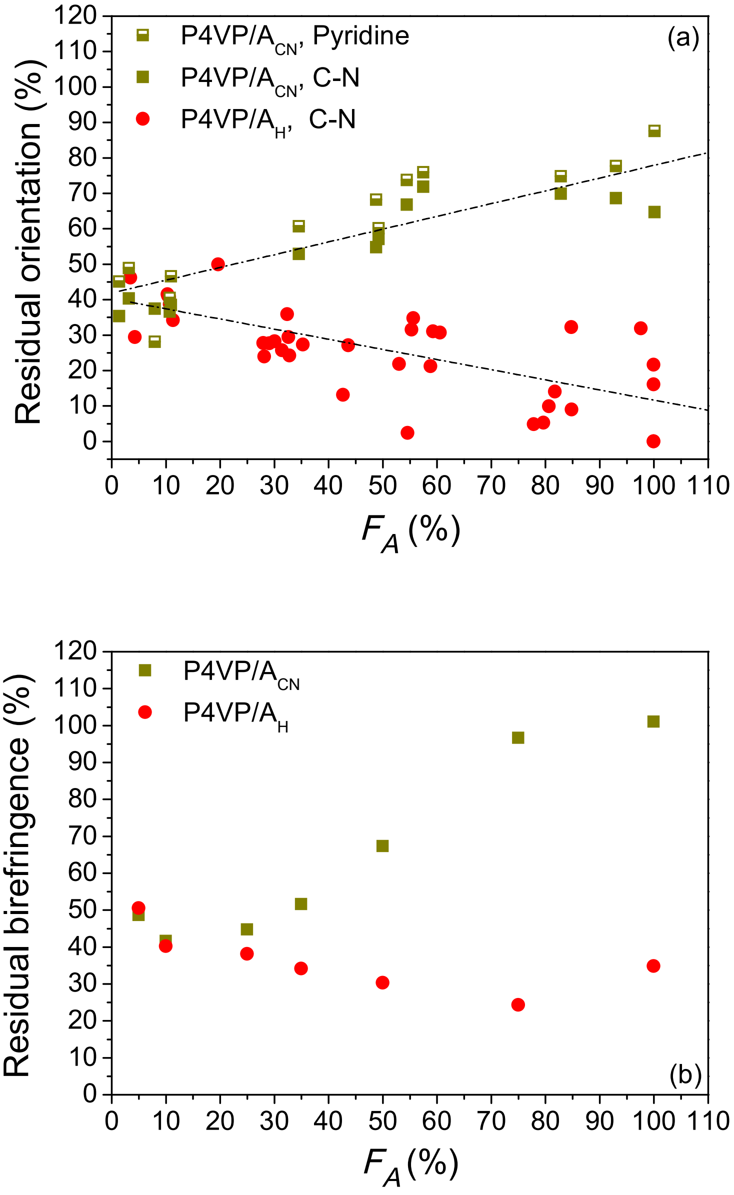

Figure 5.7. (a) Residual orientation, after 1600 s of thermal relaxation, as a function of F_A for the A_{CN} and P4VP in the P4VP/A_{CN} complex and for A_H in the P4VP/A_H complex. The residual orientation is expressed as the percentage of the residual $<P_2>$ relative to the maximum $<P_2>$ at the end of irradiation. (b) Residual birefringence, after 300 s of thermal relaxation, as a function of the nominal F_A for the P4VP/A_{CN} and P4VP/A_H complexes. The percentage of residual birefringence is relative to the saturated birefringence.

It is very clear that A_{CN} and A_H lead to different photoresponse performance in their complexes with P4VP upon irradiation. A prominent molecular difference between these compounds is that A_{CN} is a typical push-pull azobenzene, while A_H only has an electrodonating hydroxyl group. Therefore, the dipole moment of the *trans* isomer of A_{CN} (6.9 D) is much larger than that of A_H (1.7 D), leading to a much stronger dipole-dipole interaction between A_{CN}. As mentioned before, the photoinduced orientation and thermal relaxation curves each contain a fast and a slow process. The fast mode is related with the *trans-cis-trans* isomerization and the slow mode involves the reorientation of the long axis of the chromophores.[48-49] Both modes are affected by the interaction strength between polymer and chromophores and by the molecular environment of the chromophores.[49] In our case, both complexes have exactly the same frequency for the hydrogen-bonded pyridine ring band (1010 cm^{-1}), which indicates a very similar hydrogen bonding strength, and the same complexation extent (f_b) at any F_A, as shown in Fig. 5.2. Furthermore, as shown in Fig. 5.S2, they reach a very similar percentage of *trans* isomers over the full range of F_A under irradiation.

Fig. 5.8 shows the evolution of the absorbance of the azobenzene C-N band, normalized to the absorbance before irradiation, during the photo-orientation and thermal relaxation processes, with the IR beam parallel (A_p) and perpendicular (A_s) to the laser polarization. This band has been shown to be due to *trans* conformers so that its absorbance decreases when photogenerating *cis* isomers. For both complexes, upon irradiation, A_p drops steeply in the first 10 s, indicating the initial angular hole burning process that leads to the depletion of the *trans* isomers due to the formation of *cis* isomers. An increase in bands associated with the *cis* conformers is simultaneously observed in the IR spectra (not shown). A_s also decreases steeply at the same time, although to a smaller extent compared with A_p due to the selective absorption of azobenzene molecules with a component of their electronic transition dipole moment aligned parallel to the electric field direction of the pump laser beam. After this, for P4VP/A_{CN}(80%), A_p continues to decrease significantly, at a much slower rate, while A_s rises, as indicated by the arrow in Fig. 5.8a, and continues increasing. A similar trend is observed for P4VP/A_{CN}(10%), in Fig. 5.8b, although the increase of A_s with time is less obvious.

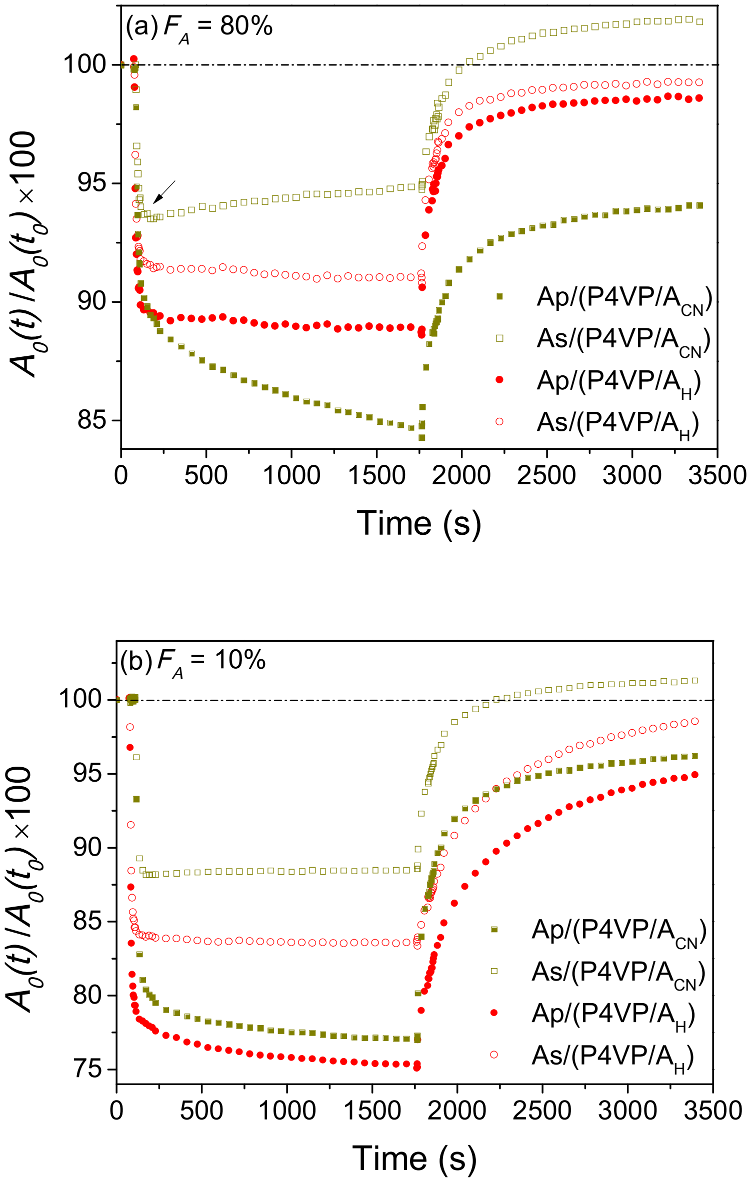

Figure 5.8. Evolution of the normalized IR absorbance, expressed as the percentage of the real time absorbance, $A_0(t)$, relative to the initial absorbance, $A_0(t_0)$, of the azobenzene C-N band parallel (A_p) and perpendicular (A_s) to the polarization direction of laser, during the photo-orientation and thermal relaxation processes, when F_A is (a) 80% and (b) 10%.

The increase of A_s after the fast initial angular hole burning has also been reported for cyano-tailed azobenzenes covalently bonded as the side chain of polyurethane,[50] and for 1-naphthyl-azomethoxybenzene in glassy *o*-terphenyl,[51] and is due to the slow rotational diffusion of azobenzenes. Rotational diffusion originates from the repeated *trans-cis-trans* cycles, leading to the reorientation of the chromophores to the *s* direction and to the observed increase in orientation, as expressed by the <*P2*> values. In P4VP/A_{CN}, cycles of *trans-cis-trans* isomerization disrupt the equilibrium of the strong dipole-dipole interactions among A_{CN}, especially when the A_{CN} content is high, so a new equilibrium is reset quickly, thus accelerating the rotational diffusion and orienting more *trans*-isomers in *s* direction. Comparably, such strong acceleration effect does not exist for A_H, between which π-π interaction dominants, which is weaker compared with dipole-dipole interaction. Considering the similar efficiency of angular hole burning for the same F_A, as shown in Fig. 5.S2, the different performance to accelerate the rotational diffusion between A_{CN} and A_H plays the key role in determine their final photoinduced anisotropy, as shown in Fig. 5.6a.

For P4VP/A_H(80%), upon irradiation, both A_p and A_s decrease steeply first, followed by a slower decrease before reaching an slightly inclined plateau, in which *trans-cis-trans* isomerization reaches a balance, as shown in Fig. 5.8a. The incline of the plateau indicates a reorientation of A_H due to rotational diffusion even during the photostationary state. Such reorientation is more obvious when F_A is low, as shown from P4VP/A_H(10%) in Fig. 5.8b, that the photostationary plateau of A_p is more inclined. This indicates a more effective rotational diffusion, due to the less hindrance induced by chromophore-chromophore interaction as compared with P4VP/A_H with high F_A.

Such effect of hindrance also leads to different efficiencies of *trans-cis* isomerization varied with F_A, as shown in Fig. 5.S2, that the percentage of the remaining *trans*-isomers in the photostationary stage is lower in both complexes with high F_A. This and the more effective rotational diffusion process in low F_A, as concluded above, can explain the trend of P4VP/A_H in Fig. 5.6a, that <P_2> increases with decreasing F_A, because both angular hole burning and the chromophore reorientation contribute to the photoinduced anisotropy. For P4VP/A_{CN}, decreasing F_A leads to both higher efficiency of *trans*-*cis* isomerization and weaker effect of accelerating the rotational diffusion. Although these two lead to the opposite trends of $<P_2>$ with F_A, Fig. 5.6a shows that the former determines that $<P_2>$ of P4VP/A_{CN} increases with decreasing F_A. However, the effect of accelerating the rotational diffusion of A_{CN} is strong enough to induce the cooperative motion of the pyridine rings, which was not found in P4VP/A_H, explaining the difference of $<P_2>$ of P4VP band shown in Fig. 5.6a.

Fig. 5.8 also shows that during thermal relaxation, in both complexes, both A_p and A_s increase fast, followed by a gradually slower increase, indicating a fast *cis*-*trans* isomerization and a slow reorientation process, respectively. For P4VP/A_{CN}, A_s even recovers to a value over the original value and this phenomena was not found when A_{CN} content is very low ($F_A <$ 10%). This is related with the oriented pyridine rings, which are more obvious with higher F_A, as shown in Fig. 5.6b, and their residual orientation, which is also higher with higher F_A, as shown in Fig. 5.7a. For the hydrogen-bonded A_{CN}, some are orientated in *s* direction in *cis*-form. During the thermal relaxation, they can go back to *trans*-form and keep oriented in *s* direction with their complexed pyridine rings. We also found such secondary orientation mostly occurs for P4VP/A_{CN} with high F_A, which means high amount of H-bonded pyridine rings. For P4VP/A_H, as shown in Fig. 5.8b, with low F_A, $<P_2>$ has higher contribution from the reorientation, which is hard to be recovered due to the lack of the *trans*-*cis*-*trans* cycles, so there are higher remains of $<P_2>$ in the complexes, as shown in Fig. 5.7a.

5.6 Conclusion

In this contribution, we used polarization modulation infrared structural absorbance spectroscopy (PM-IRSAS) to investigate the influence of the tail group of azobenzene, from cyano (A_{CN}) to hydrogen (A_H), on the photoactivity of their complexes with poly(4-vinyl pyridine) (P4VP). Upon irradiation with a linearly-polarized 488 nm laser light, the photo-orientation ($<P_2>$) of the azobenzene decreases with increasing chromophore content for both P4VP/A_{CN} and P4VP/A_H. On average, a higher $<P_2>$ is reached for P4VP/A_{CN}. The orientation of the photopassive pyridine rings only occurs in P4VP/A_{CN} and increases with

A_{CN} content, in contrast with the behavior of the photoactive azobenzene. This indicates that the stronger chromophore-chromophore interactions, when the azobenzene is high, decreases the efficiency of *trans-cis-trans* isomerization and that A_{CN} is active enough to drive the alignment of the pyridine rings of P4VP. After stopping irradiation, the residual orientation of both A_{CN} and P4VP increases with A_{CN} content from 40% to 80%. For P4VP/A_H, the residual orientation of A_H decreases with A_H content from 40% to 0%.

We found that this significant difference in the photoresponse of P4VP/A_{CN} and P4VP/A_H is related with the different chromophore-chromophore interactions in these two complexes. Due to the different dipole moment of A_{CN} and A_H, dipole-dipole and π-$\pi*$ interactions dominate in P4VP/A_{CN} and P4VP/A_H, respectively. Because of this, the strong dipole-dipole interactions facilitate the rotational diffusion after the ultrafast *trans-cis* or *cis-trans* isomerization, in either photo-orientation or thermal relaxation processes, and further drive the angular reorientation of the azobenzene, leading to higher photo-orientation and residual orientation. This strong rotational diffusion effect further induces the cooperative movement of P4VP, leading to the orientation of pyridine rings.

5.7 Supplementary information

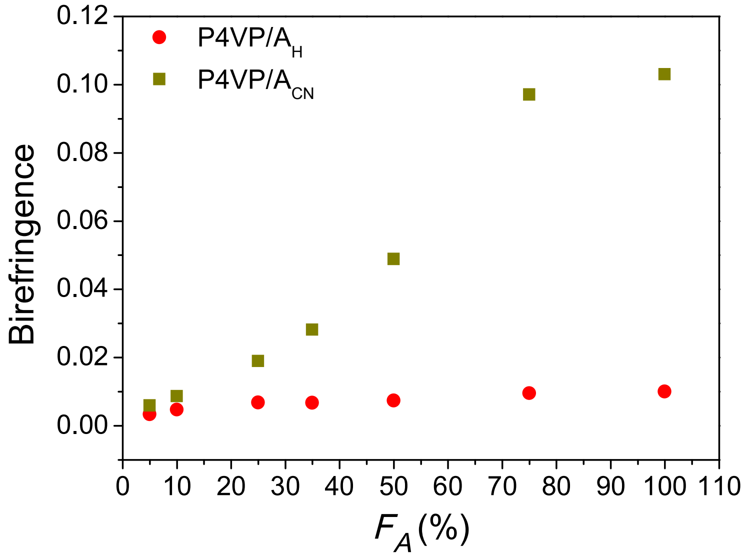

Figure 5.S1. Photoinduced birefringence as a function of nominal azobenzene content, F_A, for P4VP/A_H and P4VP/A_{CN}.

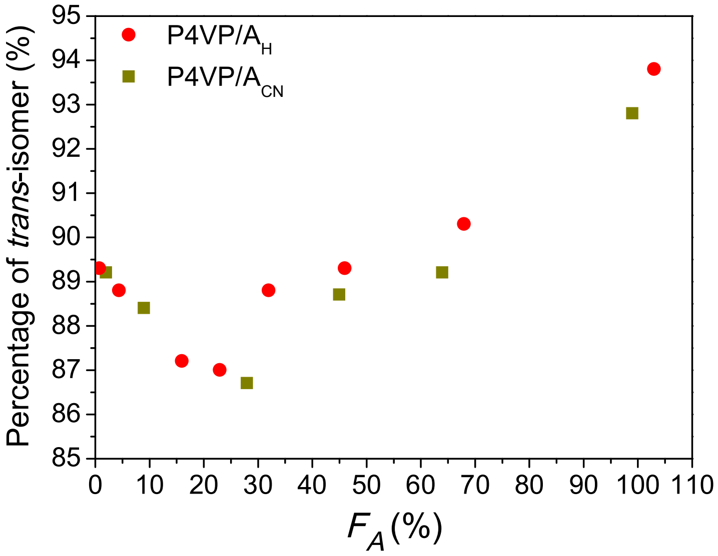

Figure 5.S2. Percentage of *trans*-isomer in the photostationary state as a function of nominal azobenzene content, F_A, for P4VP/A_H and P4VP/A_{CN}.

Determination of F_A

The local F_A was determined for each sample using the absorbance ratio of the bands around 822 cm^{-1}, which is assigned to an out-of-plane C-H bending vibration (γ(CH)) of the pyridine ring, and another γ(CH) band from the aromatic rings of the azobenzenes (around 842 cm^{-1} and 847 cm^{-1} for A_H and A_{CN}, respectively, as shown in Fig. 5.S3).[52]

To obtain a valid calibration curve, IR spectra of a series of standard P4VP/azobenzene films with accurate F_A were recorded. These films were very thin to avoid saturating IR bands, especially induced by the thickness of coffee ring, could be avoided, and small-sized (<5 mm diameter) to be fully localized within the IR beam (6 mm). Thin films were prepared from diluted $CHCl_3$ solutions (P4VP concentration of 0.17%-1.26%) and using P4VP with a lower molecular mass (50 kg/mol instead of 200 kg/mol) to decrease the viscosity of solutions and avoid formation of thick films during the drop-casting. A small volume of solution (2 μL) was dropped on a BaF_2 window followed by natural drying in the hood for two days. The local F_A of these standard samples is regarded as the same as that of their mother solutions. The calibration curves for P4VP/A_H and P4VP/A_{CN} are shown in Fig. 5.S4. Finally, the actual F_A of samples used for PM-IRSAS studies was corrected based on the calibration curves. Fig. 5.S4 shows that the calibrated F_A is in good agreement with the nominal content of the mother solutions, especially when the azobenzene content is low, indicating the validity of calibration curves.

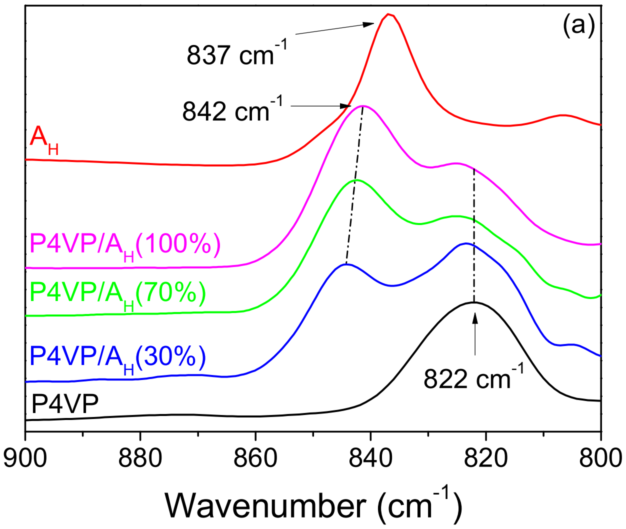

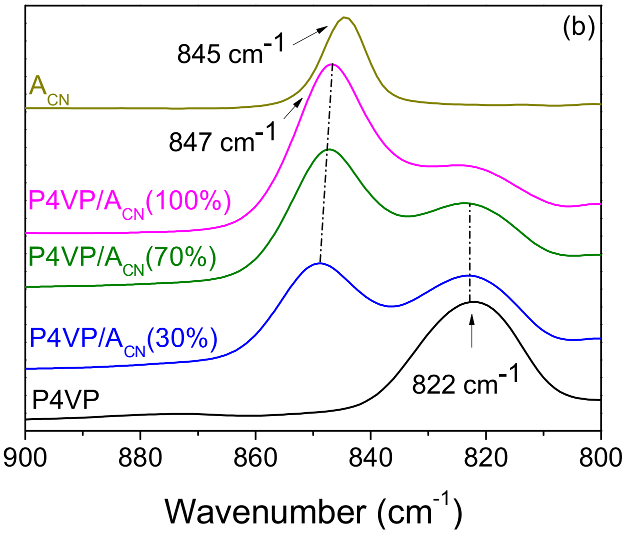

Figure 5.S3. Infrared spectra of pure P4VP powder, pure azobenzene powder and drop-casted P4VP/Azobenzene complexes with nominal F_A of 30%, 70% and 100% for (a) A_H and (b) A_{CN} systems.

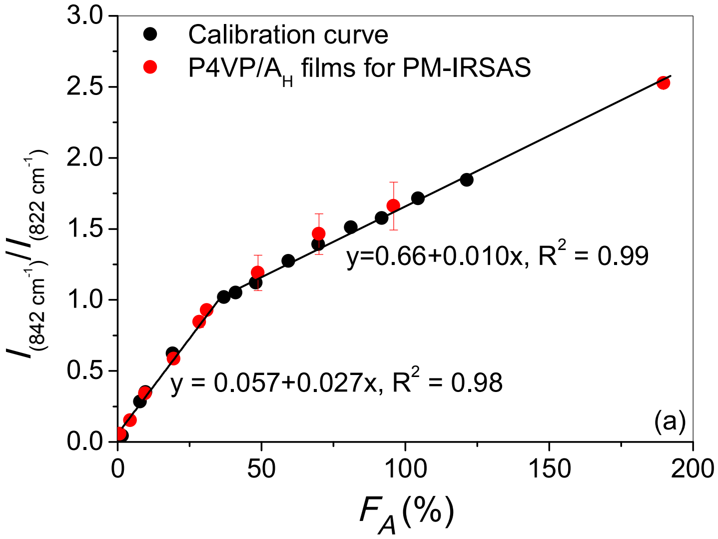

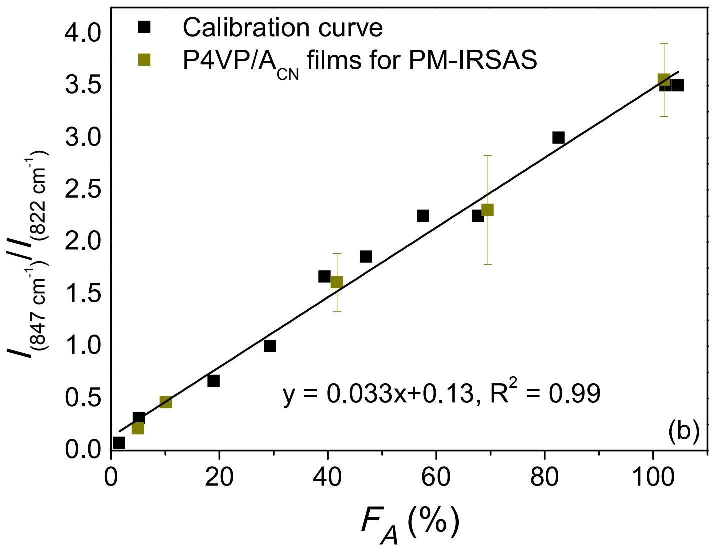

Figure 5.S4. Calibration curves for determining the molar fraction of azobenze in (a) P4VP/A$_H$ and (b) P4VP/A$_{CN}$ complexes. Examples of band ratios for PM-IRSAS samples validate the calibration curves.

Estimation of birefringence from <P2> for P4VP/ACN

Eq. 5.S1 was used to estimate the birefringence (Δn) that would have resulted from the $<P_2>$ values measured under photostationary conditions using the 1137 cm^{-1} band from A_{CN} and the 1068 cm^{-1} band from P4VP. The intrinsic birefringence (Δn) of A_{CN} and P4VP were roughly estimated as 0.2 and 0.1, respectively. W_{ACN} and W_{P4VP} are the weight fraction of A_{CN} and P4VP, respectively. The calculated birefringence against F_A is shown in Fig. 5.S5:

$$\Delta n = \Delta n^o_{A_{CN}} \left|\langle P_2 \rangle_{A_{CN}}\right| \times W_{A_{CN}} + \Delta n^o_{P4VP} \left|\langle P_2 \rangle_{P4VP}\right| \times W_{P4VP} \qquad (5.S1)$$

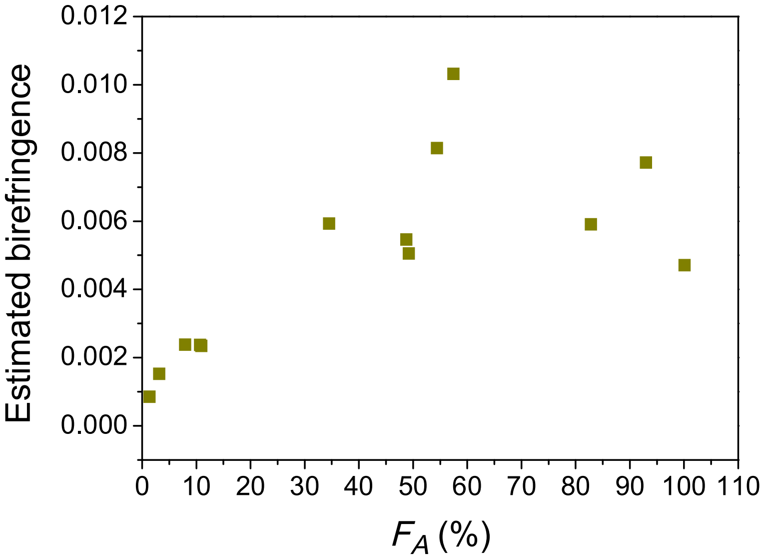

Figure 5.S5. Estimated photoinduced birefringence for P4VP/A_{CN} as a function of F_A.

Determination of the fraction of hydrogen-bonded pyridine rings (f_b)

As described in the main text, the fraction of hydrogen-bonded pyridine rings, f_b, can be calculated by using Eq. 5.3, as shown in the main text, which involves the intensities of the second-derivative bands at 1011 cm^{-1} (hydrogen-bonded pyridine ring, I_b) and 994 cm^{-1} (free pyridine ring, I_f) and a, which represents the ratio of their band absorption coefficients. To determine a for hydroxyl-pyridine complexation between P4VP and A_H, a model of liquid blend of 4-ethylpyridine (EtPy) and A_H was used. EtPy was selected as model compound because of the similarities between: 1) structures of EtPy and that of P4VP; 2) IR spectra of EtPy and that of P4VP; 3) IR spectra of complex EtPy/A_H and that of P4VP/ A_H, as clearly shown in Fig. 5.S6.

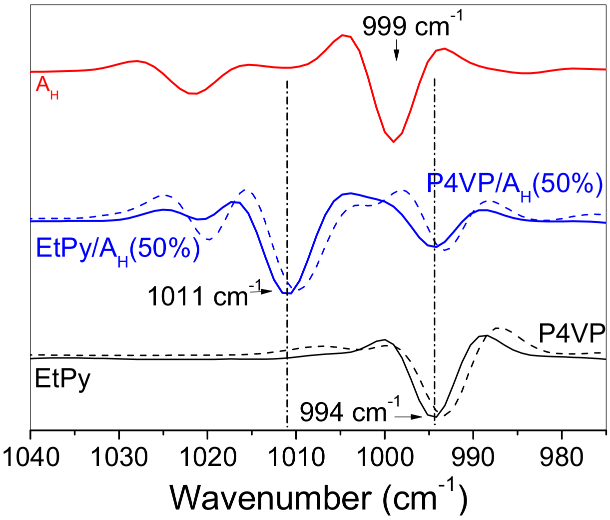

Figure 5.S6. Second derivative spectra of (solid lines) pure EtPy liquid, pure A_H powder and a EtPy/A_H (50%) liquid blend and of (dashed lines) P4VP powder and P4VP/A_H (50%) film; all bands are negative.

Although, as shown in Fig. 5.S7, the plot is composed of two linear sections, $(I_f)_p$ and $(I_b)_p$, which are the intensities when all of the pyridine rings are free and hydrogen-bonded, could be obtained by extrapolating this plot to the y and x axis, respectively.

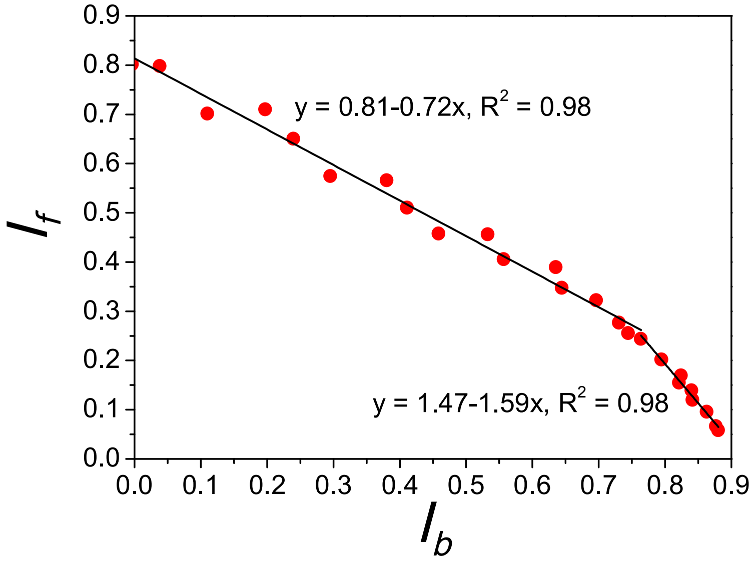

Figure 5.S7. The intensity, I_f, of the free pyridine ring band at 994 cm^{-1} versus the intensity, I_b, of the hydrogen-bonded pyridine ring band at 1011 cm^{-1}, as obtained from the second derivative spectra of the EtPy/A$_H$ liquid blends. The lines represent the least-square fits of the data points.

According to our previous paper, a is calculated by Eq. 5.S2, as the product of $(I_f)_p/(I_b)_p$ and a dilution factor.[39] In Eq. 5.S2, M_{EtPy} and M_{AH} represent the molecular weight of EtPy and A$_H$, respectively, and ρ_{EtPy} and ρ_{mix} represent the density of EtPy and EtPy/A$_H$(100%), respectively. ρ_{mix} cannot be measured due to the solubility limit of A$_H$ in EtPy, but it can be estimated as 1.06 g/mL by mass averaging.

$$a = (I_f)_p / (I_b)_p \times \frac{M_{EtPy}\rho_{mix}}{(M_{EtPy} + M_{A_H})\rho_{EtPy}} \tag{5.S2}$$

From Fig. 5.S7, $(I_f)_p/(I_b)_p$ was obtained as 0.88, and the dilution factor in the right side of Eq. 5.S2 was calculated as 0.394, based on values of M_{EtPy} (107.15 g/mol), M_{AH} (198.22 g/mol), ρ_{EtPy} (0.942 g/ml) and ρ_{mix} (1.06 g/ml). a was finally calculated as 0.35 and was applied in Eq. 5.3, as shown in the main text, to calculate f_b. The calculated f_b are plotted against F_A of EtPy/A_H in Fig. 5.S8, which shows the excellent agreement with the theoretical curve (black line), indicating the accuracy of a. Based on the same method, $a = 0.39$ was determined for A_{CN}.

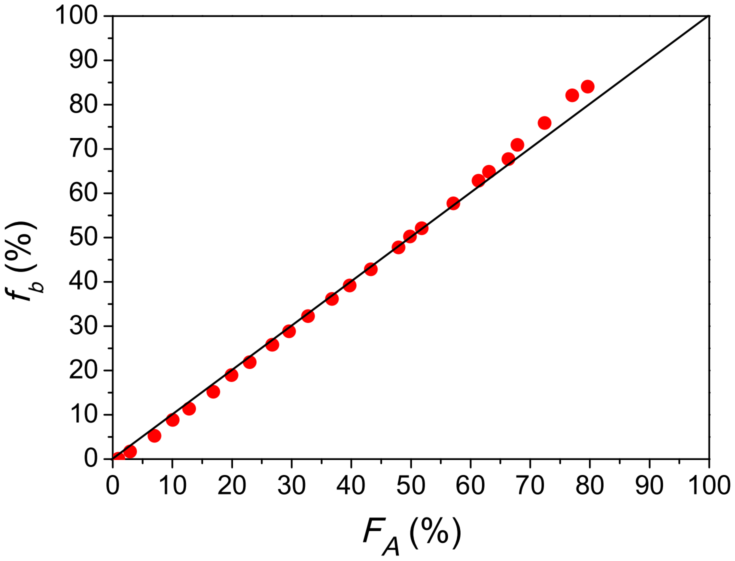

Figure 5.S8. Percentage of hydrogen-bonded pyridine rings, f_b(%), as a function of A_H content, F_A, for EtPy/A_H liquid blends. The black line describes the theoretical values for full complexation of A_H to EtPy.

5.8 References

1. Natansohn, A.; Rochon, P., *Chem. Rev.* **2002,** 102, 4139-4175.
2. Bandara, H. M. D.; Burdette, S. C., *Chem. Soc. Rev.* **2012,** 41, 1809-1825.
3. O'Neill, M.; Kelly, S. M., *J. Phys. D: Appl. Phys.* **2000,** 33, R67-R84.
4. Bang, C.-U.; Shishido, A.; Ikeda, T., *Macromol. Rapid Commun.* **2007,** 28, 1040-1044.
5. Paterson, J.; Natansohn, A.; Rochon, P.; Callender, C. L.; Robitaille, L., *Appl. Phys. Lett.* **1996,** 69, 3318-3320.
6. Shishido, A., *Polym. J.* **2010,** 42, 525-533.
7. Hvilsted, S.; Sánchez, C.; Alcalá, R., *J. Mater. Chem.* **2009,** 19, 6641.

8. Ube, T.; Ikeda, T., *Angew. Chem., Int. Ed.* **2014,** 53, 10290-10299.
9. Takashima, Y.; Hatanaka, S.; Otsubo, M.; Nakahata, M.; Kakuta, T.; Hashidzume, A.; Yamaguchi, H.; Harada, A., *Nat. Commun.* **2012,** 3, 1270.
10. Yamada, M.; Kondo, M.; Mamiya, J.-i.; Yu, Y.; Kinoshita, M.; Barrett, C. J.; Ikeda, T., *Angew. Chem., Int. Ed.* **2008,** 47, 4986-4988.
11. Xue, X.; Zhu, J.; Zhang, Z.; Zhou, N.; Tu, Y.; Zhu, X., *Macromolecules* **2010,** 43, 2704-2712.
12. Fang, L.; Zhang, H.; Li, Z.; Zhang, Y.; Zhang, Y.; Zhang, H., *Macromolecules* **2013,** 46, 7650-7660.
13. Xiao, S.; Lu, X.; Lu, Q.; Su, B., *Macromolecules* **2008,** 41, 3884-3892.
14. Zhang, Q.; Bazuin, C. G.; Barrett, C. J., *Chem. Mater.* **2008,** 20, 29-31.
15. Zhang, Q.; Wang, X.; Barrett, C. J.; Bazuin, C. G., *Chem. Mater.* **2009,** 21, 3216-3227.
16. Ahmed, R.; Priimagi, A.; Faul, C. F.; Manners, I., *Adv Mater* **2012,** 24, 926-931.
17. Gao, J.; He, Y.; Liu, F.; Zhang, X.; Wang, Z.; Wang, X., *Chem. Mater.* **2007,** 19, 3877-3881.
18. Priimagi, A.; Kaivola, M.; Rodriguez, F. J.; Kauranen, M., *Appl. Phys. Lett.* **2007,** 90, 121103/121101-121103/121103.
19. Priimagi, A.; Lindfors, K.; Kaivola, M.; Rochon, P., *ACS Appl. Mater. Interfaces* **2009,** 1, 1183-1189.
20. Priimagi, A.; Shevchenko, A.; Kaivola, M.; Rodriguez, F. J.; Kauranen, M.; Rochon, P., *Opt. Lett.* **2010,** 35, 1813-1815.
21. Priimagi, A.; Vapaavuori, J.; Rodriguez, F. J.; Faul, C. F. J.; Heino, M. T.; Ikkala, O.; Kauranen, M.; Kaivola, M., *Chem. Mater.* **2008,** 20, 6358-6363.
22. Vapaavuori, J.; Priimagi, A.; Kaivola, M., *J. Mater. Chem.* **2010,** 20, 5260-5264.
23. Vapaavuori, J.; Valtavirta, V.; Alasaarela, T.; Mamiya, J.-I.; Priimagi, A.; Shishido, A.; Kaivola, M., *J. Mater. Chem.* **2011,** 21, 15437-15441.
24. Priimagi, A.; Cavallo, G.; Forni, A.; Gorynsztejn-Leben, M.; Kaivola, M.; Metrangolo, P.; Milani, R.; Shishido, A.; Pilati, T.; Resnati, G.; Terraneo, G., *Adv. Funct. Mater.* **2012,** 22, 2572-2579.
25. Priimagi, A.; Cavallo, G.; Metrangolo, P.; Resnati, G., *Acc. Chem. Res.* **2013,** 46, 2686-2695.

26. Tawa, K.; Kamada, K.; Kiyohara, K.; Ohta, K.; Yasumatsu, D.; Sekkat, Z.; Kawata, S., *Macromolecules* **2001,** 34, 8232-8238.
27. Tawa, K.; Zettsu, N.; Minematsu, K.; Ohta, K.; Namba, A.; Tran-Cong, Q., *J. Photochem. Photobiol., A* **2001,** 143, 31-38.
28. Zebger, I.; Rutloh, M.; Hoffmann, U.; Stumpe, J.; Siesler, H. W.; Hvilsted, S., *J. Phys. Chem. A* **2002,** 106, 3454-3462.
29. Zebger, I.; Kulinna, C.; Siesler, H. W.; Andruzzi, F.; Pedersen, M.; Ramanujam, P. S.; Hvilsted, S., *Macromol. Symp.* **1995,** 94, 159-170.
30. Han, M.; Kidowaki, M.; Ichimura, K.; Ramanujam, P. S.; Hvilsted, S., *Macromolecules* **2001,** 34, 4256-4262.
31. Hvilsted, S.; Andruzzi, F.; Kulinna, C.; Siesler, H. W.; Ramanujam, P. S., *Macromolecules* **1995,** 28, 2172-2183.
32. Kulinna, C.; Hvilsted, S.; Hendann, C.; Siesler, H. W.; Ramanujam, P. S., *Macromolecules* **1998,** 31, 2141-2151.
33. Tawa, K.; Kamada, K.; Ohta, K., *J. Photochem. Photobiol., A* **2000,** 134, 185-191.
34. Tawa, K.; Kamada, K.; Sakaguchi, T.; Ohta, K., *Appl. Spectrosc.* **1998,** 52, 1536-1540.
35. Tawa, K.; Kamada, K.; Sakaguchi, T.; Ohta, K., *Polymer* **2000,** 41, 3235-3242.
36. Marcott, C., *Appl. Spectrosc.* **1984,** 38, 442-443.
37. Buffeteau, T.; Pézolet, M., *Appl. Spectrosc.* **1996,** 50, 948-955.
38. Liang, Y.; Mauran, D.; Prud'homme, R. E.; Pellerin, C., *Appl. Spectrosc.* **2008,** 62, 941-947.
39. Wang, X.; Bazuin, C. G.; Pellerin, C., *Vib. Spectrosc.* **2014,** 71, 18-23.
40. Garton, A., *Polym. Eng. Sci.* **1984,** 24, 112-116.
41. Kojima, M.; Nebashi, S.; Ogawa, K.; Kurita, N., *J. Phys. Org. Chem.* **2005,** 18, 994-1000.
42. Tang, Z.; Johal, M. S.; Scudder, P.; Caculitan, N.; Magyar, R. J.; Tretiak, S.; Wang, H.-L., *Thin Solid Films* **2007,** 516, 58-66.
43. Gabor, G.; Frei, Y. F.; Fischer, E., *J. Phys. Chem.* **1968,** 72, 3266-3272.
44. Minisini, B.; Fayet, G.; Tsobnang, F.; Bardeau, J. F., *J. Mol. Model.* **2007,** 13, 1227-1235.

45. Tecklenburg, M. M. J.; Kosnak, D. J.; Bhatnagar, A.; Mohanty, D. K., *J. Raman Spectrosc.* **1997,** 28, 755-763.

46. Stepanic, V.; Baranovic, G.; Smrecki, V., *J. Mol. Struct.* **2001,** 569, 89-109.

47. Getahun, Z.; Huang, C.-Y.; Wang, T.; De Leon, B.; DeGrado, W. F.; Gai, F., *J. Am. Chem. Soc.* **2003,** 125, 405-411.

48. Brown, D.; Natansohn, A.; Rochon, P., *Macromolecules* **1995,** 28, 6116-6123.

49. Ho, M.-S.; Natansohn, A.; Barrett, C.; Rochon, P., *Can. J. Chem.* **1995,** 73, 1773-1778.

50. Sekkat, Z.; Yasumatsu, D.; Kawata, S., *J. Phys. Chem. B* **2002,** 106, 12407-12417.

51. Grebenkin, S. Y.; Bol'shakov, B. V., *J. Photochem. Photobiol., A* **2006,** 184, 155-162.

52. Topacli, A.; Bayari, S., *Spectrochim. Acta, Part A* **1999,** 55A, 1389-1394.

Chapter 6: Conclusion

6.1 Conclusion

Hydrogen-bonded supramolecular P4VP-small molecule complexes are the core topic in this thesis. The degree of complexation can strongly affect the properties and its knowledge is therefore of primary importance, making its quantification highly desirable. This can be done by using FT-IR spectroscopy to measure the relative intensities of a pair of free and hydrogen-bonded P4VP bands. However, due to the different absorption coefficient of each band, correct quantification can only be achieved when the value of the ratio, a, of these two coefficients is known. In the literature, this ratio for the 1590/1600 cm^{-1} band pair of poly(2-vinyl pyridine) (P2VP) was reported to be unity,[1-2] and was subsequently used for P4VP complexes[3-4] and blends,[5] even for other band pairs. However, this is not appropriate, since, as we showed (see below), a varies with different band pairs and with different systems. We therefore, for the first time, developed a method to determine a, which was the subject of Chapter 2. The value determined was used to quantify the extents of hydrogen-bonding in the following chapters.

The method was developed for the pair of bands at 993 (free pyridine) and 1007 (H-bonded pyridine) cm^{-1} in poly(4-vinyl pyridine/4,4'-biphenol) (P4VP/BiOH), using a liquid small molecule, 4-ethyl pyridine (EtPy), as a model compound for P4VP, due to its structural and infrared spectral similarities to that of the P4VP repeat unit. The prepared model blends of EtPy/BiOH were measured by ATR and the results were analyzed by a second-derivative method to obtain the intensities of free pyridine band (I_f) and H-bonded pyridine band (I_b). The plot of I_f *vs.* I_b obtained is linear with a negative slope. Importantly, a correction factor was calculated and applied to the value of this slope to take into account the dilution of the pyridine groups by addition of BiOH.

The keys to the success of this method are: 1) EtPy/BiOH blends are an ideal model for P4VP/BiOH fibers as they have almost the same infrared spectra; 2) the chemical composition of the liquid blends can be precisely controlled and can be related to the theoretical extent of complexation; 3) the distribution of the two components in the liquid is homogenous, so an accurate correlation between IR spectra and the chemical composition can be established; 4) the contact with the ATR crystal is equally perfect for all samples, making the dilution effect the sole factor needed to correct the value of the slope of the I_f-I_b plot.

Using the value of a thus determined, 0.40, the percentage of hydrogen-bonded pyridines, f_b, in EtPy/BiOH could be calculated and was found to be in agreement with the theoretical value, confirming the validity of our approach. Measurements on electrospun P4VP/BiOH fibers showed that f_b is about 76% of F_{OH}, which is the percentage of the hydroxyl groups relative to the pyridine rings, indicating that a significant fraction of the pyridine groups (and as a consequence the BiOH hydroxyl groups) remain free. Full hydrogen-bonded complexation was found only for fibers containing a large excess of BiOH. The incomplete complexation of P4VP, in contrast with full complexation for liquid EtPy, is related to the low mobility and steric effects of the polymer chains.

Our method has two advantages compared with the previously reported method,[2] which involves IR measurements of films of the investigated polymer blends at different temperatures. First, our method makes use only of the intensities of the band pair of interest, avoiding the difficulty (and in some cases the impossibility) of selecting a proper reference band. Second, it gives a more accurate value as it is based solely on measurements at room temperature, is contrast to the previously reported method,[2] which requires heating of the films and is thus affected by temperature-induced changes in the band absorption coefficients.

Besides BiOH, this method was used to determine an a value of 0.62 for P4VP/phenol, 0.56 for P4VP/4-hydroxyl-4'-biphenyl carboxylic acid (HBCA), 0.39 for P4VP/4-hydroxyl-4'-cyano azobenzene (A_{CN}) and 0.35 for P4VP/4-phenylazophenol (A_H). These results indicate for the first time that a varies for different systems, even if using the same pyridine band pair. Thus, it is wrong to use the value of $a = 1$ for different supramolecular P4VP complexes and blends.[1-5] Our results also show that a can be determined accurately using our method if a suitable liquid model of the polymer repeat unit is available, or else it can be estimated based on the different values we determined.

The second objective of this thesis was to investigate if the addition of a bifunctional small molecule with potential to physically crosslink polymer chains by hydrogen bonding can improve the electrospinning of that polymer, and further to establish the link between effective crosslinking and electrospinnability. This was studied using P4VP solutions to which BiOH was added, in Chapter 3 for high molecular weight P4VP (P4VP200k, M_w = 200 kg/mol) and in Chapter 4 for low molecular weight P4VP (P4VP50k, M_w = 50 kg/mol). SEM showed that, for P4VP200k in DMF, adding BiOH with equimolar hydroxyl groups relative to the pyridine rings decreases the critical P4VP concentration for the formation of beaded fibers (c_f) from 12 to 10 wt%, and more substantially from 30 to 25 wt% for P4VP50k. When a mixed solvent (MIX) of DMF with nitromethane, which is a bad solvent for P4VP and a non-solvent for BiOH and thus can also induce effective crosslinking by enhancing pyridine-pyridine interactions, was used, a similar addition of BiOH results in a decrease of c_f from 10 to 8 wt% for P4VP200k and from 23 to 14 wt% for P4VP50k. Two conclusions can be drawn from these results: first, a small hydrogen-bonding crosslinker and a bad solvent have an equivalent effect at increasing the electrospinnability of P4VP/DMF and their combination leads to a synergistic effect; second, the effect of BiOH is more obvious in absolute terms for P4VP50k than for P4VP200k, although the relative improvement is very similar.

IR analysis proved that there is hydrogen-bond complexation between P4VP and BiOH in the solutions, and that it increases with increasing P4VP concentration and in the presence of nitromethane. This correlation between f_b and P4VP concentration suggests the existence of extensive complexation in the electrospun jet, which can effectively resist the forces of electrical stretching and surface tension to prevent the formation of droplets. Our rheological results show that both adding BiOH and using a worse solvent increase the specific viscosity of P4VP and decrease the onset of the semidilute entangled regime (c_e). A concentrated regime was only found above 20, 16 and 19 wt% for P4VP200k-BiOH/DMF, P4VP200k-BiOH/MIX and P4VP50k-BiOH/MIX, respectively, correlating with the formation of pure and uniform fibers. These results indicate that the effective crosslinking introduced by the addition of BiOH and the bad solvent, which is based on hydrogen bonding and enhanced pyridine-pyridine interactions, respectively, is a key to increasing the electrospinnability. This is further proved by the fact that the relative improvement of c_f is consistent with hydrogen-bonded complexation (f_b) in the solutions.

We also compared the effect of BiOH with other small molecule crosslinkers which have stronger interactions with pyridine rings. For 20 wt% P4VP50k, the extent of complexation (f_b) and specific viscosity of P4VP-HBCA in DMF are 2.7 and 1.8 times that of P4VP-BiOH. SEM shows that P4VP-BiOH only leads to the formation of droplets, while beaded fibers were electrospun from P4VP-HBCA. More interestingly, similar fibers were obtained by adding a very low concentration of $ZnCl_2$ to a P4VP solution, namely a 1.0:0.01 molar ratio of pyridine rings to Zn^{2+}. These results show that the stronger the effective crosslinking, the greater the extent of crosslinking, and the better the electrospinnability.

The small molecules added to the electrospinning solution may not always be desirable in the final fibers. To address this, a sublimation method, where fibers were placed in a vacuum oven at high temperature, was successfully used to remove HBCA and BiOH. IR analysis showed that BiOH can be removed more easily, which is consistent with its weaker hydrogen bonding interaction with pyridine rings. The complete removal of BiOH, without breakage or fusing of the fibers, was achieved after about 2 months at 120 °C (22 °C below the Tg of pure P4VP) and after 3 days at 140 °C (near the Tg of 142 °C). This indicates a potential application for obtaining pure fibers from some nonelectrospinnable polymers, like low molecular weight polymers, by introducing small crosslinkers before electrospinning, followed by their removal through sublimation after electrospinning. This is especially interesting for preparing well-aligned fibers while preserving the alignment, for instance in view of measuring orientation or anisotropic properties of the fiber bundle. The choice of appropriate crosslinker depends on the application and the quality of the working conditions. For example, BiOH can be preferred if a high standard of fiber purity is required. HBCA can be a better choice if an ultrahigh-vacuum oven is available. $ZnCl_2$ is ideal if a low amount of additives is tolerable.

We were also interested in studying photoactive supramolecular complexes between P4VP and azobenzenes. In Chapter 5, polarization modulation infrared structural absorbance spectroscopy (PM-IRSAS) was used to investigate the photo-orientation and orientation relaxation of the complexes upon irradiation of a 488-nm linearly polarized light. Two simple azobenzene molecules, having an identical interacting hydroxyl head group but a different tail, either cyano (A_{CN}) or hydrogen (A_H), were selected to compare the influence of the tail groups on the two processes.

These two complexes had been investigated previously by Vapaavuori et al.,[6] who found that their saturated birefringence per azobenzene unit with increasing azobenzene content were quite different. It increases with increasing A_{CN} content and decreases with increasing A_H content, indicating different photoactivities upon irradiation. However, the underlying mechanism was unclear, as birefringence measures only the overall orientation of all components in the system. This initiated our interest in using PM-IRSAS, which provides information on the orientation of each individual component and band, to unveil this mechanism.

In Chapter 5, we found that both photo-orientation and orientation relaxation include a fast mode, related to *trans-cis* isomerization, and a slow mode, related to reorientation of the chromophores. The photo-orientation of both A_{CN} and A_H decreases with increasing F_A and, generally, a higher photo-orientation was obtained from A_{CN}. This trend is related to the effect of lower free volume, when F_A is high, which decreases the efficiency of *trans-cis* isomerization. This effect of free volume is present in both complexes, regardless of the structural difference between azobenzenes. Photo-orientation of the passive pyridine rings of P4VP only occurs in P4VP/A_{CN} and increases with F_A, in contrast to the behaviour of the photoactive azobenzene molecule. After removing the irradiation, residual orientation of both A_{CN} and P4VP increases with A_{CN} content from 40% to 80%. The opposite is found for P4VP/A_H, for which the residual orientation of A_H decreases with A_H content from 40% to 0%.

Those significant differences can be related to the different transition dipole moments of A_{CN} (larger) and A_H (smaller). Because of this, the predominant chromophore-chromophore interactions are dipole-dipole and π-$\pi*$ interaction in P4VP/A_{CN} and P4VP/A_H, respectively. The strong dipole-dipole interactions accelerate the rotational diffusion following ultrafast *trans-cis* or *cis-trans* isomerization, breaking the equilibrium of such interactions among A_{CN} in either photo-orientation or thermal relaxation processes. This further drives a cooperative angular reorientation of the azobenzenes, leading to higher photo-orientation and residual orientation. This strong rotational diffusion effect further induces the cooperative movement of P4VP, leading to the orientation of pyridine rings. However, no spectral evidence of such orientation of the P4VP main chain was observed in either complex, which indicates that the rotational diffusion of azobenzene is not strong enough to induce the cooperative movement of the main chains themselves.

Finally, these findings explain very well the trend of birefringence reported by Vapaavuori et al. on a molecular level. That is, both photo-orientation of pyridine rings and A_{CN} increase with A_{CN} content, contributing to the same trend for the overall anisotropy of P4VP/A_{CN}. In contrast, the overall photo-orientation of P4VP/A_H is only influenced by that of A_H, which decreases with increasing A_H content.

6.2 Perspectives

6.2.1 Effect of small crosslinkers to increase the electrospinnability of P4VP (5 kg/mol)

In this thesis, we illustrated the effect of small hydrogen-bond and metal ionic crosslinkers to improve the electrospinnability of P4VP. We also showed that stronger interactions between these crosslinkers and pyridine rings lead to better electrospinnability. Therefore, this strategy could be expanded to electrospin some non-electrospinnable polymers, whose molecular weight is below their critical entanglement molecular weight (M_c), by using crosslinkers which provide much more effective crosslinking to compensate for the lack of entanglements in solution of these polymers.

Future work extending this strategy can still rely on the use of P4VP as the model polymer. Although the M_c of P4VP has never been reported to my knowledge, it can be assumed that it is close to the M_c of polystyrene, which is 34 kg/mol according to Graessley,[7] due to the similar molecular structure of P4VP and PS. P4VP with a molecular weight of 5 kg/mol, which is commercially available, is far below this M_c, and it is therefore of high interest to investigate if it can be made electrospinnable by the addition of suitable small molecule crosslinkers. The selection of small crosslinkers should follow two criteria: 1) they should provide relatively strong interactions with the pyridine rings, so that the maximum increase of electrospinnability of P4VP can be obtained with a minimum amount of small molecules; 2) the strength and/or degree of interaction involved must avoid the gelation of P4VP. Interesting candidates to meet these criteria are cyclodextrins (CDs) as hydrogen-bond crosslinkers, and Zn^{2+}, Mg^{2+} and Ca^{2+} as metal ionic crosslinkers.

6.2.1.1 Cyclodextrins as crosslinkers

Cyclodextrins are a series of cyclic compounds composed of jointed sugar molecules, each of which have three hydroxyl groups, and they have very well known architectures in supramolecular chemistry. Typical representatives of the CD family are α, β and γ-CD, which are composed of 6, 7 and 8 sugars, respectively, as shown in Fig. 6.1a. As shown in Fig. 6.1b, the inner diameters of α, β and γ-CD are 0.57, 0.78 and 0.95 nm, respectively. Each CD can complex with 1 to 4 pyridine rings through hydrogen bonding with inner hydroxyl groups, considering that the size of the pyridine ring is only 0.23 nm. For example, it is reported that methylated β-CD can form an inclusion complex with two 4-vinyl pyridine molecules.[8]

Fig. 6.2 shows a possible scheme of P4VP chains effectively crosslinked by CD. It indicates that each CD can complex with two P4VP chains. The number of pyridine rings included depends on the inner size of the CD. The more pyridine rings included, the stronger the network is. However, too strong inclusion complexation can lead to P4VP gelation. To avoid this, CD substitutes can be tuned by replacing some OH groups by OR, where R is a short alkyl group, so that hydrogen bonding is decreased. Using a low concentration of CDs can also decrease the risk of gelation. In Chapter 4, we have shown that 4,4'-biphenol can be thermally removed at around 140 °C under vacuum without causing damage to the P4VP fibers. However, this method cannot be applied to fibers of low molecular weight P4VP (5 kg/mol), since their Tg should be much lower than about the 142 °C for high molecular weight P4VP. As an alternative, Saito et al. reported the removal of complexed methylated β-CD from P4VP using a water purification method.[8] This method can also be used to remove the CDs from P4VP/CD fibers, thereby yielding pure P4VP fibers in principle.

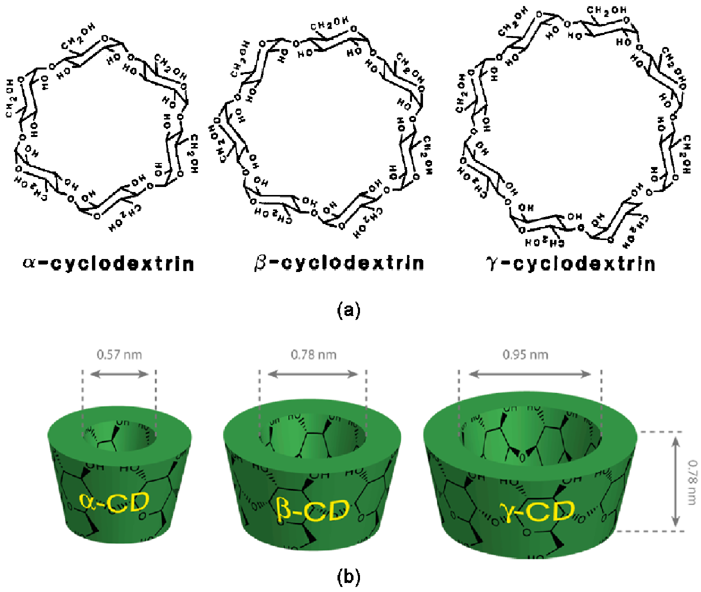

Figure 6.1. (a) Structures of α, β and γ-cyclodextrin (CD). Reproduced with permission from Ref. 9, © 1992 American Chemical Society. (b) geometric dimensions of CDs. Reproduced with permission from Ref. 10, © 2012 American Chemical Society.

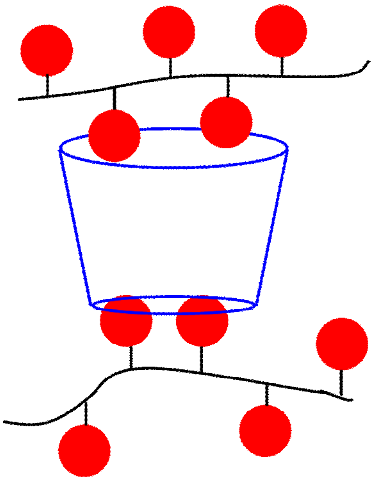

Figure 6.2. Representation of P4VP (black backbone and red pyridine rings) crosslinked by CD (blue).

6.2.1.2 Metal ions and organmetals as crosslinkers

In Chapter 4, we showed that Zn^{2+} could be used as a very effective crosslinker to facilitate the electrospinning of P4VP (50 kg/mol). Due to its strong metal coordination with pyridine rings, it is an ideal candidate as a crosslinker for P4VP (5 kg/mol). The preliminary results, as shown in Fig. 6.3, show that addition of $ZnCl_2$ leads to the formation of fibers, although the reproducibility was poor. Gelation of P4VP was observed for $ZnCl_2$ contents over 3 mol% of pyridine rings, suggesting difficulty in preparing homogenous solutions with increasing Zn^{2+} content and the challenge of reaching a suitable degree of crosslinking.

Using organozinc compounds, which are formed by a zinc ion and organic ligands, instead of pure Zn^{2+}, might be an option. Craig and coworkers have suggested that the dissociation rate of the bisfunctional Pd^{2+} and Pt^{2+} organometallic crosslinkers with P4VP varies with different ligands.[11-12] Therefore, we believe that, by selecting a suitable organozinc compound, the crosslinking extent of Zn^{2+} with P4VP could be tuned to form an appropriate P4VP network in solution without gel formation. Several such compounds, like zinc dodecyl benzene sulfonate,[13] and carboxylic acid-functionalized alkoxymethoxybiphenyl mesogen zinc salts,[14] have been reported to complex with P4VP and can be used as references for selecting potential organozinc compounds.

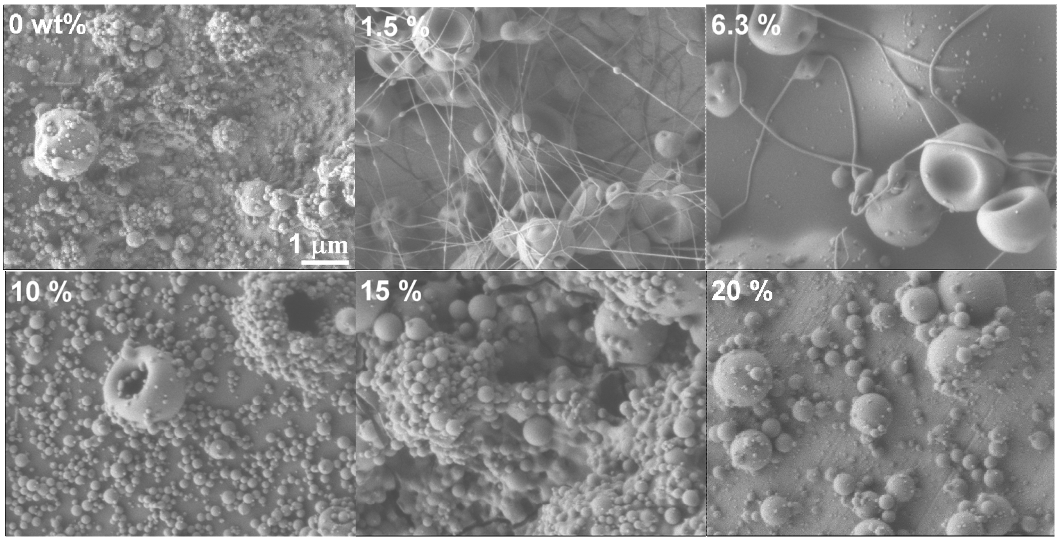

Figure 6.3. SEM images of electrospun products from P4VP-$ZnCl_2$/DMF solutions with different $ZnCl_2$ contents (molar percentage relative to pyridine rings) based on preliminary results. P4VP concentration is 20 wt%. All images have the same scale bar as shown in the first image.

Alternatively, the crosslinking extent can be tuned by use of other metal ions or their organometallic compounds; for example, other widely used colorless metals ions like Mg^{2+}, Al^{3+}, and Ca^{2+}. Compared with the tetrahedral coordination geometry between Zn^{2+} and pyridine rings, each Mg^{2+} and Ca^{2+} were reported to coordianate with 6 and 3-9 pyridine rings of P4VP, respectively,[15] suggesting that different metal ion species lead to different extents of crosslinking.

6.2.2 Photo-orientation of other P4VP/azobenzene complexes

In Chapter 5, we illustrated that polarization modulation infrared structural absorbance spectroscopy (PM-IRSAS) is a very informative tool to follow the dynamic photoinduced behavior in P4VP/azobenzene complexes. The results revealed the impact of the tails on the photo-orientation of P4VP/(monofunctional azobenzene derivative) complexes. It is of interest to extend these studies to other systems, such as other tails, other polymers, more complex azo molecules, and other interacting groups. Regarding the latter, the impact of the azobenzene "head" group on photo-orientation upon irradiation and on the residual orientation after the thermal relaxation can be investigated. Specifically, two groups of azobenzene derivatives can be used as model compounds for this study, notably the 4-phenylazophenol and 4-(phenylazo)benzoic acid group and the 4-cyano-4'-hydroxyl azobenzene and 4-cyanoazobenznene-4'-carboxylic acid group, as shown in Fig. 6.4. These compounds compare OH-pyridine interactions, which are relatively weak, and COOH-pyridine interactions, which are relatively stronger.[16] The difference in interaction strength of complexation induced by the two types of head groups leads to different performance for the inscription of surface-relief gratings (SRG), according to our preliminary results.

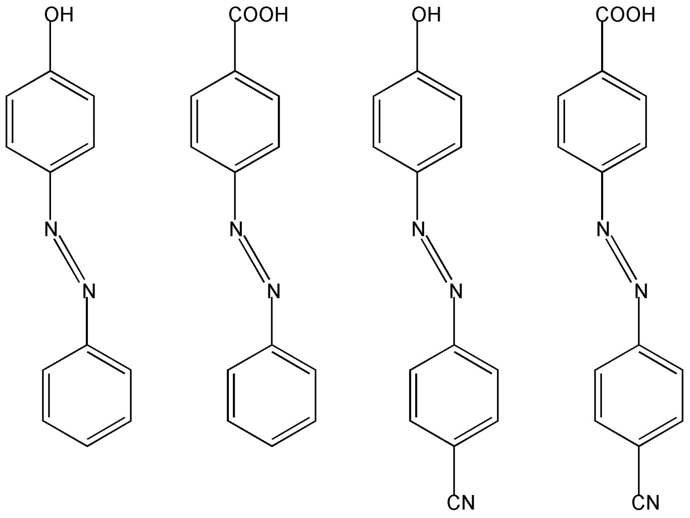

(a) (b) (c) (d)

Figure 6.4. Chemical structures of (a) 4-phenylazophenol, (b) 4-(phenylazo)benzoic acid, (c) 4-cyano-4'-hydroxyl azobenzene and (d) 4-cyanoazobenzene-4'-carboxylic acid.

Another interest is to investigate complexes of P4VP physically crosslinked by bifunctional azobenzene derivatives using PM-IRSAS. 4,4'-Dihydroxyazobenzene (HOAOH) and 4-hydoxyazobenzene-4’-carboxylic acid (HOACOOH), shown in Fig. 6.5, are two model compounds for such bifunctional azobenzene derivatives. In Chapter 2, we found that the percentage of hydrogen-bonded pyridine rings in P4VP/4,4’-biphenol complex is 76% when the molar amount of hydroxyl groups is the same as that of pyridine rings, indicating the formation of crosslinking.[17] Therefore, we believe such crosslinking will also exist in complexes of both P4VP/HOAOH and P4VP/HOACOOH.

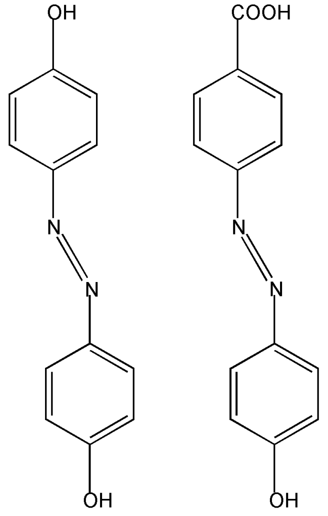

(a) (b)

Figure 6.5. Chemical structures of (a) 4,4’-dihydroxyazobenzene (HOAOH) and (b) 4-hydoxyazobenzene-4’-carboxylic acid (HOACOOH).

PM-IRSAS measurements can provide the desired information on photo-orientation and thermal relaxation, as observed from preliminary results for P4VP/HOAOH. Such measurements on P4VP/HOAOH and P4VP/HOACOOH are expected to help understand the effect of crosslinking on the photoactivity, including SRG inscription efficiency which is to be investigated in parallel, in comparison to P4VP/4-phenylazophenol and P4VP/4-(phenylazo)benzoic acid complexes. They will also help understand the effect of the head group (strength of complexation) for these two complexes. In addition, PM-IRSAS measurements can provide information on possible photoinduced breakage of the crosslinks.

This can lead to a decrease in the Tg of the crosslinked systems in the solid state and in the solution viscosity in response to irradiation.

6.3 References

1. Cesteros, L. C.; Meaurio, E.; Katime, I., *Macromolecules* **1993,** 26, 2323-2330.
2. Lee, J. Y.; Painter, P. C.; Coleman, M. M., *Macromolecules* **1988,** 21, 954-960.
3. Korhonen, J. T.; Verho, T.; Rannou, P.; Ikkala, O., *Macromolecules* **2010,** 43, 1507-1514.
4. Soininen, A. J.; Tanionou, I.; ten Brummelhuis, N.; Schlaad, H.; Hadjichristidis, N.; Ikkala, O.; Raula, J.; Mezzenga, R.; Ruokolainen, J., *Macromolecules* **2012,** 45, 7091-7097.
5. Kuo, S.-W.; Lin, C.-L.; Chang, F.-C., *Polymer* **2002,** 43, 3943-3949.
6. Vapaavuori, J.; Valtavirta, V.; Alasaarela, T.; Mamiya, J.-I.; Priimagi, A.; Shishido, A.; Kaivola, M., *Journal of Materials Chemistry* **2011,** 21, 15437-15441.
7. Graessley, W. W., *Advances in Polymer Science, Vol. 16: The Entanglement Concept in Polymer Rheology*. Springer: 1974; p 179 pp.
8. Saito, R.; Saito, Y.; Kamoshita, H.; Tokubuchi, Y., *J. Polym. Sci., Part A: Polym. Chem.* **2012,** 50, 3444-3451.
9. Li, S.; Purdy, W. C., *Chem. Rev.* **1992,** 92, 1457-1470.
10. Crini, G., *Chem. Rev.* **2014,** 114, 10940-10975.
11. Yount, W. C.; Loveless, D. M.; Craig, S. L., *J. Am. Chem. Soc.* **2005,** 127, 14488-14496.
12. Loveless, D. M.; Jeon, S. L.; Craig, S. L., *Macromolecules* **2005,** 38, 10171-10177.
13. Ruokolainen, J.; Tanner, J.; ten Brinke, G.; Ikkala, O.; Torkkeli, M.; Serimaa, R., *Macromolecules* **1995,** 28, 7779-7784.
14. Benouazzane, M.; Bravo-Grimaldo, E.; Bissessur, R.; Bazuin, C. G., *Macromolecules* **2006,** 39, 5364-5370.
15. Zander, N. E.; Orlicki, J. A.; Rawlett, A. M., *Polym. Prepr. (Am. Chem. Soc., Div. Polym. Chem.)* **2009,** 50, 710-711.
16. Gilli, P.; Pretto, L.; Bertolasi, V.; Gilli, G., *Acc. Chem. Res.* **2009,** 42, 33-44.

17. Wang, X.; Bazuin, C. G.; Pellerin, C., *Vib. Spectrosc.* **2014,** 71, 18-23.